APPROACHES FOR ASSESSING WHETHER THE HUMAN HAND EVOLVED BY NATURAL SELECTION IN ADAPTATION TO STONE TOOL USE

Ana Bucchi Morales

UNIVERSITAT ROVIRA I VIRGILI
APPROACHES FOR ASSESSING WHETHER THE HUMAN HAND EVOLVED BY NATURAL SELECTION IN ADAPTATION TO STONE TOOL USE
Ana Bucchi Morales

UNIVERSITAT ROVIRA i VIRGILI

BECAS CHILE

IPHES
Institut Català de Paleoecologia Humana i Evolució Social

Doctoral Thesis
Ana Bucchi

2020

UNIVERSITAT ROVIRA i VIRGILI

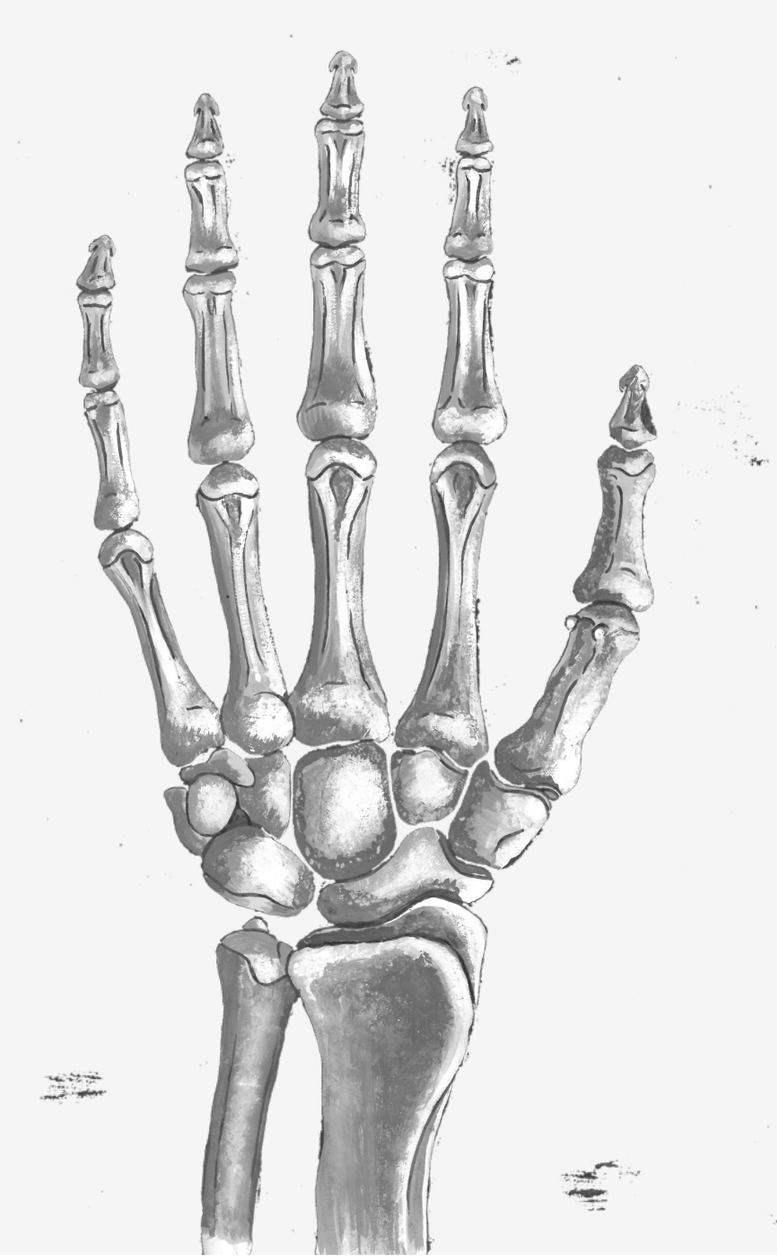

Approaches for assessing whether the human hand evolved by natural selection in adaptation to stone tool use

Ana Bucchi

PhD Thesis | 2020

UNIVERSITAT ROVIRA i VIRGILI

UNIVERSITAT ROVIRA I VIRGILI
APPROACHES FOR ASSESSING WHETHER THE HUMAN HAND EVOLVED BY NATURAL SELECTION IN ADAPTATION TO STONE TOOL USE
Ana Bucchi Morales

UNIVERSITAT ROVIRA I VIRGILI
APPROACHES FOR ASSESSING WHETHER THE HUMAN HAND EVOLVED BY NATURAL SELECTION IN ADAPTATION TO STONE TOOL USE
Ana Bucchi Morales

A mi mamá

UNIVERSITAT ROVIRA I VIRGILI
APPROACHES FOR ASSESSING WHETHER THE HUMAN HAND EVOLVED BY NATURAL SELECTION IN ADAPTATION TO STONE TOOL USE
Ana Bucchi Morales

Ana Bucchi Morales

Approaches for assessing whether the human hand evolved by natural selection in adaptation to stone tool use

Doctoral thesis

Directed by

Dr. Carlos Lorenzo Merino

Department of History and Art History

UNIVERSITAT ROVIRA i VIRGILI

Tarragona

2020

UNIVERSITAT ROVIRA I VIRGILI
APPROACHES FOR ASSESSING WHETHER THE HUMAN HAND EVOLVED BY NATURAL SELECTION IN ADAPTATION TO STONE TOOL USE
Ana Bucchi Morales

UNIVERSITAT ROVIRA i VIRGILI

I STATE that the present study, entitled “Approaches for assessing whether the human hand evolved by natural selection in adaptation to stone tool use”, presented by Ana Bucchi Morales for the award of the degree of Doctor, has been carried out under my supervision at the Department of History and Art History of this university.

Tarragona, 24th April 2020.

Doctoral Thesis Supervisor/s

Carlos Lorenzo Merino

UNIVERSITAT ROVIRA I VIRGILI
APPROACHES FOR ASSESSING WHETHER THE HUMAN HAND EVOLVED BY NATURAL SELECTION IN ADAPTATION TO STONE TOOL USE
Ana Bucchi Morales

Acknowledgements
Agradecimientos

Quiero expresar mi gratitud a las siguientes personas e instituciones:

A Carlos Lorenzo, mi director de tesis. Carlos, gracias por el apoyo y por darme la libertad, la independencia para investigar un tema tan interesante como este. El uso que di de todo ello resultó en esta tesis; es mi deseo que con ello haya aprendido a investigar mejor.

A Rosa Huguet, Josep Maria Vergès, Palmira Saladié y Gemma Chacón, algunos de los directores y coordinadores de los yacimientos en los que excavé esto años: Sima del Elefante, Cueva de El Mirador, El Barranc de la Boella y el Abric Romaní. He disfrutado mucho cada una de estas experiencias y aprendido excavando en yacimientos con una profundidad temporal que difícilmente volveré a ver, así que gracias por la oportunidad.

A los curadores que me abrieron amablemente las puertas de los museos a los que fui buscando material para esta tesis: Emmanuel Gilissen del AfricaMuseum (Bélgica), Anneke van Heteren del Zoologische Staatssammlung München y Javier Quezada del Museu de Ciències Naturals en Barcelona. Y a Juan Ignacio Morales y Javier Luengo por el tiempo que dedicaron a enseñarme a construir modelos 3D.

A los amigos que hice durante mi viaje de 6 años a España. A Lou primero. Lou, gracias por los dibujos científicos, el de la portada y el otro, el de la página 87. Y por ser tan auténtica y única. A Toni, mi primer amigo certificadamente catalán, que además me acompañó con sus consejos científicos y cuyo humor me hizo sentir más cerca de casa. A Edgar e Irene, por la sensibilidad. A todos, gracias por la amistad y las conversaciones antes y durante la

pandemia, han hecho la diferencia. Quiero mencionar también a Javier, Blanca y a Anna, a quienes me alegra haber conocido en este tiempo.

Esta tesis fue financiada con una Beca Chile Doctorado en el Extranjero (Agencia Nacional de Investigación y Desarrollo). Mis viajes a congresos y estancias dentro de Europa fueron apoyados por los proyectos de investigación financiados por la Generalitat de Catalunya (SGR2017-1040) y por el Gobierno de España (CGL2015-65387-C3-1-P y PGC2018-093925-B-C32).

Abbreviations

HA: Hamate

CA: Capitate

D1: *First dorsal interosseus* muscle

DP1-5: Distal phalanges 1-5

FEA: Finite element analysis

FDP: *Flexor digitorum profundus* muscle

FDS: *Flexor digitorum superficialis* muscle

FPB: *Flexor pollicis brevis* muscle

FPL: *Flexor pollicis longus* muscle

Kyr: Thousand years

LCA: Last common ancestor

LU: Lunate

Ma: Million years ago

MC1-5: Metacarpals 1-5

MP2-5: Middle phalanges 2-5

OP: *Opponens pollicis* muscle

PP1-5: Proximal phalanges 1-5

PS: Pisiform

PTA: Phalangeal total area

SC: Scaphoid

TQ: Triquetrum

TZD: Trapezoid

TZM: Trapezium

Key concepts

Acheulean: Technological mode ranging from 1.76 to 0.76 Ma. It represents the emergence of a complex behavior, expressed in the recurrent manufacture of large-sized tools, with standardized forms (Diez-Martín et al. 2015).

Digit: The chain of phalanges.

Exaptation: refers to traits whose benefits to an organism are unrelated to the reasons for their origination. They are features that enhanced fitness but were not built by natural selection for that role yet were later coopted for this purpose (Gould and Vrba, 1982).

Forceful precision grips/precision grip strength: Precision grip exerted with larger force (Marzke and Wullstein, 1996).

Pad-to-pad grip: Grip in which both the thumb and index distal interphalangeal joints are extended to bring the volar pads over the distal phalanges into opposition (Marzke, 1997).

Precision grips: Grips in which an object is pinched between the flexor aspects of the fingers and the opposing thumb (Napier, 1956).

Power grips: Grips in which objects are strongly squeezed by the fingers alone or squeezed by the fingers, thumb and actively by the palm (Napier, 1956).

Power squeeze: The relative ability to orient a cylindrical object so that it functions effectively as an extension of the forearm (Marzke and Wullstein, 1996).

Oldowan: Technological mode (2.6-1.7 Ma) characterized by simple core forms, usually made on cobbles or chunks, the resulting debitage struck from these cores, and the battered percussors (hammerstones or spheroids) used to produce the flaking blows (Toth and Schick, 2006).

Lomekwian: Technological mode of oldest stone tools (3.3 Ma). They are larger and heavier than those of the Oldowan (Harmand et al., 2015).

Opposition: Ability to turn the thumb so that it can touch each fingertip of the other digits of the same hand.

Ray: Metacarpal and the chain of phalanges.

Tip-to-tip grip: Grip for retrieving and holding small objects between distal volar tips of thumb and index finger (Marzke and Wullstein, 1996).

Tool-manufacture/Tool-production:
Any structural modification of an object or an existing tool so that the object serves, or serves more effectively, as a tool (Shumaker et al., 2011).

Tool use: Use of an object to alter the form, position or condition of another object, another organism, or the user itself when the user holds or carries the tool during or just prior to use (for a discussion, see Seed and Byrne, 2010).

Table of contents

List of Figures and Tables

UNIVERSITAT ROVIRA I VIRGILI
APPROACHES FOR ASSESSING WHETHER THE HUMAN HAND EVOLVED BY NATURAL SELECTION IN ADAPTATION TO STONE TOOL USE
Ana Bucchi Morales

Abstract

Stone tool use is a key component of the hominin behavioral repertoire. A unique configuration of musculoskeletal traits in the human hand is compatible with effective stone tool use, and the question remains as to how humans acquired this redefined manipulation capability. The most widespread hypothesis is that, once liberated from locomotion, the hominin hand evolved by natural selection to accommodate the functional demands of the use of stone tools. However, there is evidence that the hand could not have this adaptative origin, as derived morphologies were present in the hominin fossil record prior to the systematic use of stone tools. The aim of this thesis was to evaluate whether the human hand evolved by natural selection in adaptation to stone tool use. For this purpose, a comparative sample of hands of extant primates, mainly humans, chimpanzees and gorillas, were analyzed under different methods that relate biological form and function.

The first objective was to evaluate the performance of the thumb in terms of stress distribution during simulated hammerstone use. We expected our species to perform better than other primates based on the idea that, unlike apes, the human hand is adapted to the loads from tool-related behaviors. Using a finite element analysis, it is shown that the human first proximal phalanx (modern human and Neanderthal) unevenly distributes stresses and is one of the most fragile compared to apes (i.e., chimpanzee, gorilla and orangutan). These results indicate that great apes can withstand loads exerted during this activity more efficiently than humans. We conclude the human pollical phalanx did not evolve to withstand the stresses associated with hard hammer percussion.

Second, we hypothesize that if the human hand evolved to respond to selective pressures of tool-related behaviors, a distinctive pattern for modularity at the hand should have emerged. For this purpose, we evaluate whether humans have a different covariation structure at the wrist than that of chimpanzees and gorillas. Four carpals were analyzed (i.e., scaphoid, lunate, trapezium and capitate) through 3D geometric morphometrics and 15 different modular hypotheses were tested to find the optimal modular model. What sets humans apart from African apes is the degree of codependence between the trapezium and scaphoid, whereas in gorillas and chimpanzees both bones vary independently. This

suggests that covariation patterns may be shaping the evolution of the wrist in these primates. It remains to be tested whether function is a factor behind the formation of the wrist modules.

Finally, we tested whether entheseal size of ligaments and muscles is reliable for inferring activity patterns in the hand. First, we evaluated the attachment sites of the ligaments holding the *flexor digitorum superficialis* and *profundus* muscles at the proximal phalanges 2-5 (flexor ridges). The results indicate that these entheses at phalanges 2-4 are capable of distinguishing between taxa that use their hands for manipulation and locomotion (gorillas and chimpanzees) and taxa that use them exclusively for manipulation (humans). They also indicate that these entheses signal differences in manipulation capabilities across extant hominids at the fifth phalanx. Additionally, results on a cadaveric human sample suggest that the strength of the *abductor pollicis longus* muscle, but not the *opponens pollicis* muscle, is related to the size of the insertion sites. This is in line with previous analyses suggesting that the fibrocartilaginous entheses seem to be better correlated with activity levels than fibrous entheses. This result supports previous studies using fibrocartilaginous attachment sites as proxies for stone tool use in hominins and questions the conclusions on thumb dexterity based on the *opponens pollicis* attachment site.

In summary, these studies indicate that stress distribution in hand bones was unlikely to be a selective pressure strong enough to shape the hand of humans; however, the biomechanics of the wrist may have been so. They also indicate that stone tool use may be inferred in hominins by analyzing hand regions where tendons (with fibrocartilaginous entheses) and ligaments attach.

CHAPTER I

Introduction

Introduction

Studies in hand morphology have generally concluded that derived traits in humans facilitated stone tool-related behaviors (Hamrick et al., 1998; Nelson et al., 2011; Marzke, 2013; Key and Dunmore, 2015; Skinner et al., 2015) and made us a highly dexterous primate (Diogo et al., 2012; Kivell et al., 2016; Marchi et al., 2017). How humans acquired this unique configuration of musculoskeletal traits has profound implications for our understanding of human evolution overall, considering that stone technology is a key element defining culture in our species (e.g., Foley and Lahr, 2003). Some have asserted that a functional adaptation to tools mediated hand evolution, i.e., that our anatomy is a result of selective pressures related to stone tool behaviors (Hamrick et al., 1998; Key and Dunmore, 2015; Skinner et al., 2015). However, this cause-effect relationship is a biological problem that is not easy to address. This challenge is made clearer by other studies that have concluded that some derived traits leading towards *Homo* (i.e., finger proportions) are not the product of selective pressures acting directly on the hands, but rather acting on other regions of the skeleton (i.e., the foot), which were subsequently exapted for tool manipulation (Rolian et al., 2010).

That the current shape of human hands is an adaptation to the use of tools, specifically to the manufacture and use of stone tools, is the most widespread hypothesis for the evolution of the human hand (Hamrick et al., 1998; Young et al., 2010; Key and Dunmore, 2015; Kivell et al., 2015, 2016; Skinner et al., 2015). This hypothesis holds that, through the course of human evolution, natural selection favored traits to accommodate the functional demands of stone tool-related behaviors and shaped the hands of hominins up to the fully derived manual morphology of Neanderthals and modern humans. In all primates but hominins, hands are involved in locomotion, and they are functionally adapted to their locomotor modes (Richmond, 2007; Rein, 2011; Tsegai et al., 2013; Matarazzo, 2015). With the advent of bipedalism, the hands of hominins were able to evolve subject to other evolutive forces than locomotion, and the selective pressure related to manual dexterity, long present in our order, became the strongest one (Alba et al., 2003; Almécija et al., 2015).

However, hands being free to evolve by tool-related behaviors is a broad concept. Williams-Hatala et al. (2018) found that biomechanical pressures on the hand vary across stone tool behaviors. Specifically, hammerstone use during marrow acquisition and flake production

imposes higher stresses on the hand than other behaviors such as handaxe use, flake use and particularly nut-cracking. Thus, marrow acquisition and flake production were the most likely behaviors to influence the evolution of the hand, and they began early as the records on marrow and meat consumption mediated by stone tools in the human lineage date back to 3.39 Ma (McPherron et al., 2010), and the first record of hammerstone production is 3.3 Ma (Harmand et al., 2015).

Yet there is some evidence in the archaeological record which indicates that the evolutionary picture of the human hand does not fit with the above explanation. One is that fossils from basal hominins discovered in the last few decades, i.e., *Orrorin tugenensis* and *Ardipithecus ramidus*, suggest that some of the anatomical features traditionally related to manual dexterity in humans (and supposedly evolved as a consequence of tool-related behaviors) were indeed already present millions of years before the first record of lithic industry (Section 2.3) (Gommery and Senut, 2006; Lovejoy et al., 2009). Another is that hands and feet have a certain degree of morphological integration (Rolian, 2009; Rolian et al., 2010), which means that phenotypic traits of both structures are mutually dependent, and covary. This emerging evolutionary picture for hands postulates that the traits beneficial to the use of tools are a by-product of evolutionary changes to the foot. The selection in the feet was not only stronger but also occurred before that of the hands, as the locomotor shifts to habitual bipedalism in the human lineage may have occurred soon after the divergence with *Pan* (Pickford et al., 2002; Zollikofer et al., 2005; Lovejoy et al., 2009), preceding by millions of years the first record of stone tool use around 3.39 Ma (McPherron et al., 2010) and the intensification of the use of stone tools around 2.5 Ma (Fig. 2.11). This is different from saying that the use of hands for locomotion obscured the selective pressures from redefined manipulation prior to bipedalism, but rather that the modern human hand had a non-adaptative origin, which affected the morphological variation of hands through the feet, and that the hands were subsequently coopted for tool manipulation.

The studies presented in this thesis are intended to test the adaptative value of some of the anatomical traits traditionally linked to tool use proficiency or, stated another way, they aim to examine the extent to which human hand anatomy fits with the idea that it is functionally adapted to tool-related behaviors. This is done by trying to link form and function in a phylogenetically comparative context of extant primates, mainly humans, chimpanzees and gorillas. Examining extant hominid hands may reveal the combined effects of natural selection and the effects of long-term trends on the use of hands.

This thesis is structured in eight chapters. This chapter, **Chapter I,** introduces the current discussion in the paleoanthropological community on whether the human hand evolved by natural selection in adaptation to stone tool use.

Chapter II presents the key concepts referred to in the subsequent chapters. **Section 2.1** shows the hand bones and muscles attaching into the hand in Hominoidea. **Section 2.2** is a summary of what paleoanthropologists mean when they say humans exhibit a refined manipulation. **Section 2.3** is a summary the skeletal proxies for refined manipulation, defined in the context of the manual fossil record for the human lineage. There are many morphological features worthy of comment here, but this section is limited to those relevant for this thesis: intrinsic hand proportions, thumb robusticity, muscular properties and wrist morphology.

Chapter III presents the research objectives of this thesis. The primary focus is to assess whether the human hand is functionally adapted to stone tool-related behaviors, and this was achieved through four research objectives. Each one is the focus of one of the studies presented in the Results Section (Chapter V).

Chapter IV mainly describes the material used in this thesis. It summarizes all the material for the studies in the Results Section (Chapter V), plus part of the photogrammetric 3D models as well as the complete dissection database constructed during the course of this thesis but are not included in any of the studies from the Results Section. This chapter also presents a paper about simple recommendations for improving photo quality in close range photogrammetry that was written after constructing 780 3D models of hand bones. Descriptions of the other methods used in this work are given exclusively in the papers found in the Results Chapter.

Chapter V presents the studies conducted during the thesis. The first (**Section 5.1**) offers a finite element analysis of the pollical proximal phalanx of six Hominoidea (a modern human, a Neanderthal, a chimpanzee, a gorilla, an orangutan and a gibbon). A percussive activity is simulated in 48 different scenarios to evaluate the patterns of stress distribution of this bone at the moment of striking the core with the hammerstone. This paper has been accepted by the *Comptes Rendus Palevol* journal and is awaiting publication. A poster made with these results won the prize for the best student poster at the 8th Annual ESHE meeting held at Faro, Portugal in 2018 and is shown on page 177. **Section 5.2** presents a pre-print of a study on the patterns of modularity at the wrist in humans (*Homo sapiens*), chimpanzees (*Pan troglodytes*) and gorillas (*Gorilla gorilla* and *Gorila Beringei*). 3D models of four carpals (i.e., lunate, scaphoid, capitate and trapezium) were analyzed for this

purpose and the modularity was investigated through geometric morphometrics. This study is currently under review by the *Journal of Human Evolution*. **In Section 5.3** we studied the entheses in the hand of humans, gorillas and chimpanzees in order to evaluate whether they signal differences in locomotion and manipulation across these genera. This paper is currently under review by the *American Journal of Physical Anthropology*. A poster showing some of these results was presented at the 9th Annual ESHE meeting in Brussels, Belgium in 2019 and is shown on page 178. Finally, **Section 5.4** provides an analysis of the entheseal sizes of the muscles attaching to the first metacarpal in a sample of bodies donated to science. We study the metacarpal and the muscles inserted into this bone (*opponens pollicis* and *abductor pollicis longus* muscles). This is a conference proceeding published in the *Journal of the International Union of Prehistorical and Protohistorical Sciences* and corresponds to a presentation given at the XVIII UISPP congress in Paris in 2018.

Chapters VI and VII are the discussion and conclusion on whether the approaches used here fit with the hypothesis that the human hand evolved in adaptation to stone tool use. Future perspectives are also included here.

The last chapter (**Chapter VIII**) is the appendix, which includes the dissection database for the thumb muscles dissected in 23 forearms, and the Supplementary Material for the studies found in the Results Chapter.

CHAPTER II

Literature review

2.1 Anatomy of the hand

2.2 Prehensile abilities in humans

2.3 Evolutionary history of the hominin hand

2.1 Anatomy of the hand in Hominoidea

In this section some of the basic aspects of the anatomy of the hand in the extant members of our superfamily (genus *Homo, Pan, Gorilla, Pongo* and *Hylobates*) are described. As the human hand is by far the most studied, and available information decreases as we move away phylogenetically from humans, these data are based mainly on our species.

2.1.1 Anatomical position

The standard anatomical position serves to standardize any reference to location in the body, and thus facilitate anatomical comparisons among species. Although the positional behavior in non-human primates is mostly non-bipedal, the anatomical position is the same as for humans: the body is upright, directly facing the observer, feet are flat, and the hands face forward and with the fingers extended (Fig. 2.1). The anatomical plans and directional terms of the body (including the hand) are thus the same for all these taxa.
The anatomical plans hypothetically transect the body to divide it into left and right (sagittal), upper and lower (transverse) and backward and forward (coronal) sides. Directional terms describe the position of a structure relative to others in the body (i.e., superior, inferior, anterior, posterior, medial, lateral, proximal, distal. Fig. 2.1).
There is a set of synonyms to refer the directional terms in the hand:

- Anterior = palmar
- Posterior = dorsal
- Medial = ulnar = little finger side
- Lateral = radial = thumb side

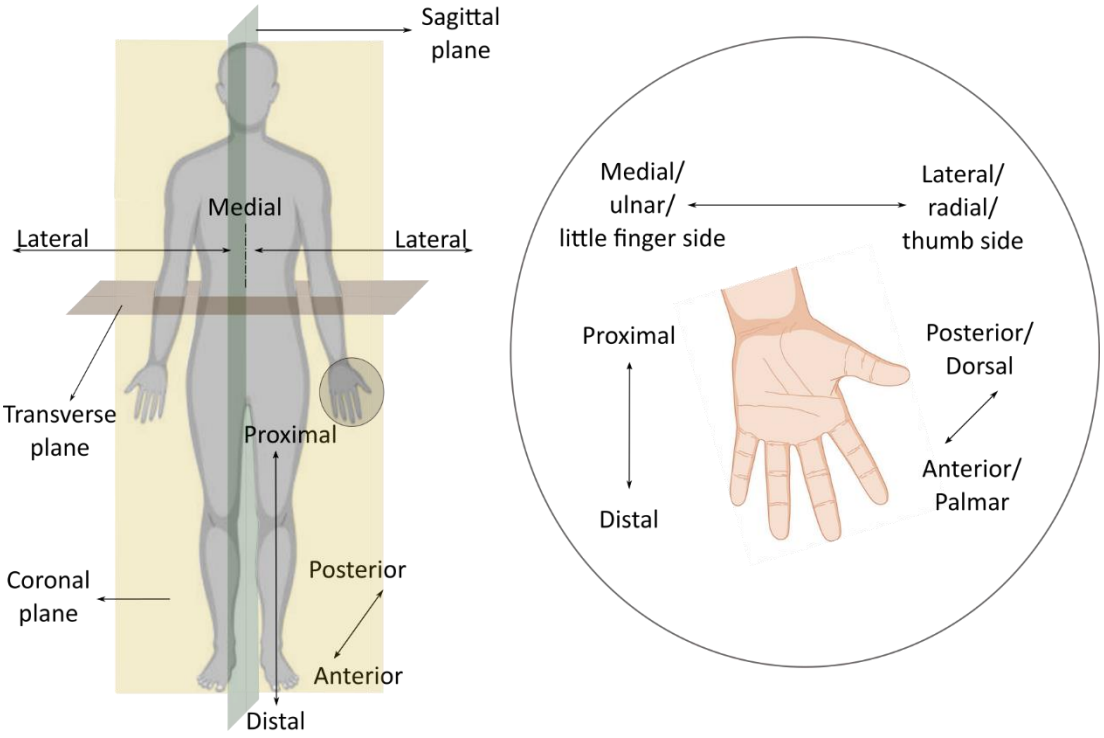

Figure 2.1 Standard anatomical position in humans. Figure shows the planes and directional terms.

2.1.2 Hand bones

Hand bones are one of the largest osseous groups in Hominoidea. Each one is composed by 27 elements in humans (Fig. 2.2-3) and African apes, and usually 28 in Asian apes. They are divided into three categories: carpals, metacarpals and phalanges.

Carpals (wrist) are irregular bones (Fig. 2.4-5). From the proximomedial to the distolateral side they are the pisiform (PS), triquetral (TQ), lunate (LU), hamate (HA), capitate (CA), scaphoid (SC), trapezoid (TZD) and trapezium (TZM). In humans and African apes, the scaphoid is fused to the os centrale (Fig. 2.4) and the former term is used, whereas in Asian suspensory taxa (orangutan and hylobatids) they are two separate bones (Kivell and Begun, 2007). Figures 2.4 and 2.5 show seven of the eight carpals (pisiform was not analyzed in this thesis) in living hominids.

Metacarpals (palm) are five long bones numbered from the pollex to the little finger as MC1 to MC5. The heads of the metacarpals (distal) articulate with the proximal phalanges, and the bases of the distal row of the carpals (TZM, TZD, CA and HA). Metacarpals in extant hominids are shown in Figure 2.6.

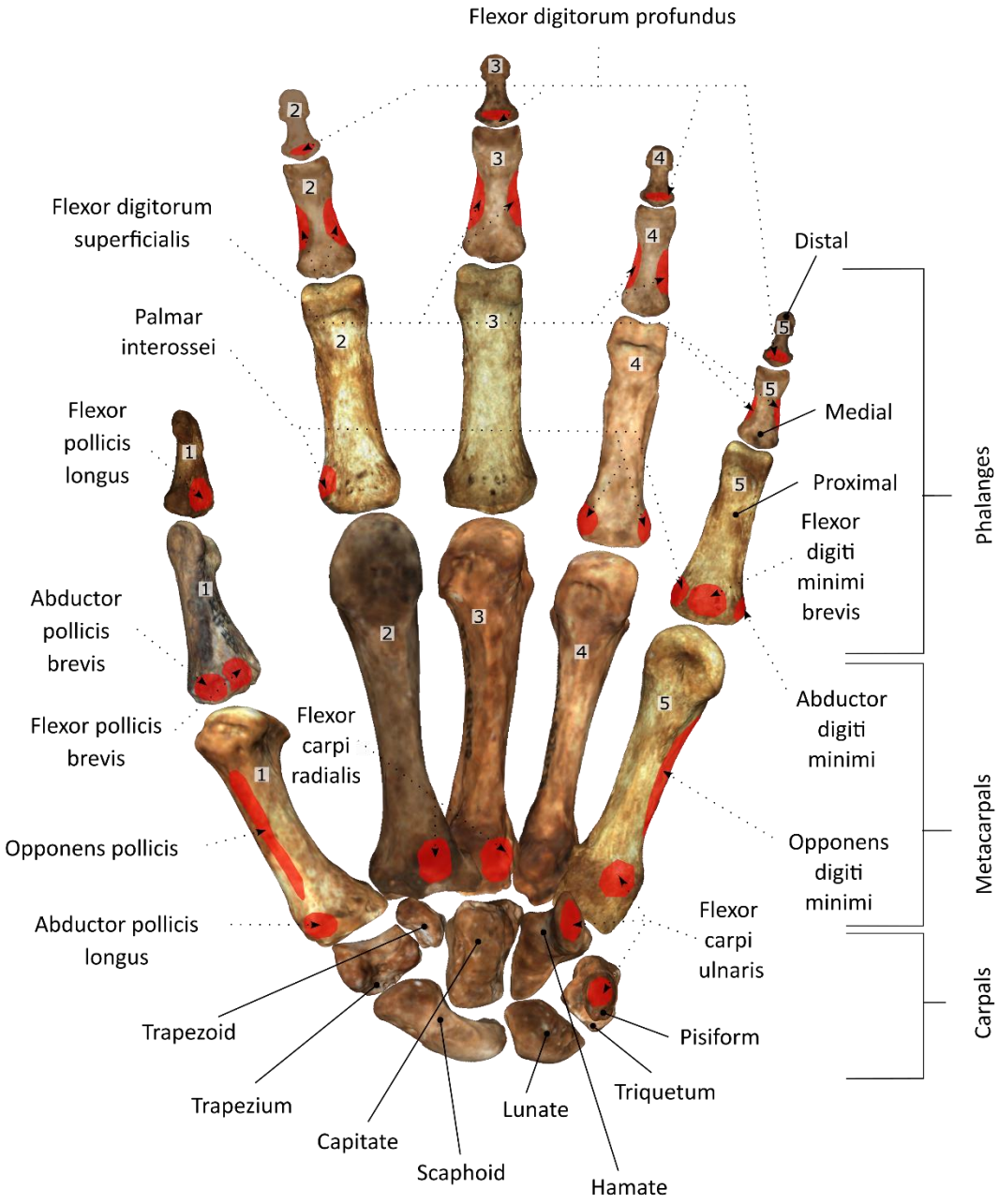

Figure 2.2 Palmar view of a human left hand. Bones are indicated in continuous lines and insertion sites of the muscles are shown in red. As in anthropology the insertion (and not the origin) of the muscles is studied to describe the activity patterns in the past, only insertion sites are shown in Figures 2.2 and 2.3.

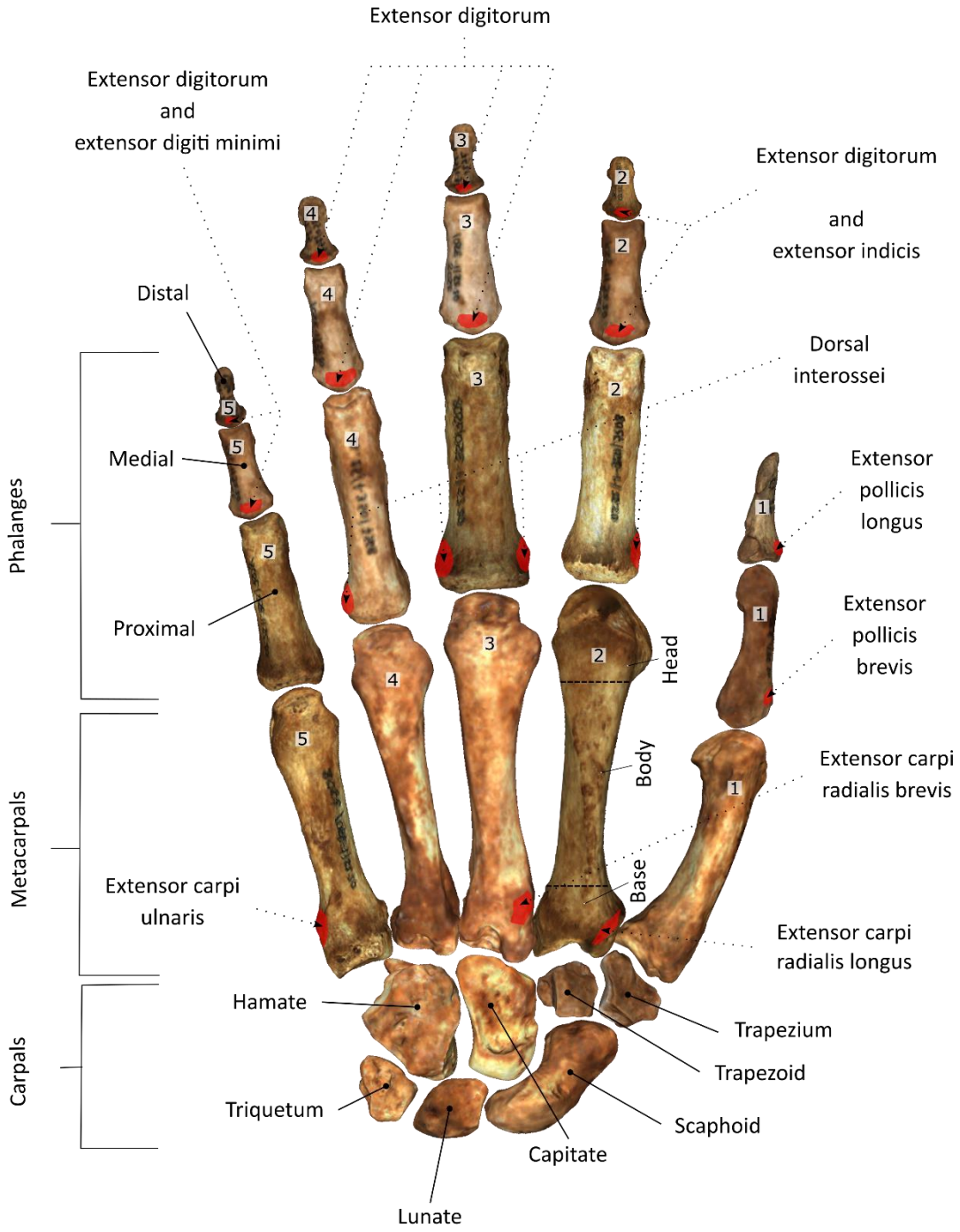

Figure 2.3 Dorsal view of a human left hand. Bones are indicated in continuous lines and insertion sites of the muscles are shown in red. Bone segments of rays are depicted in MC2. As in anthropology the insertion (not origin) of muscles is studied to describe the activity patterns in the past, only insertion sites are shown in Figures 2.2 and 2.3.

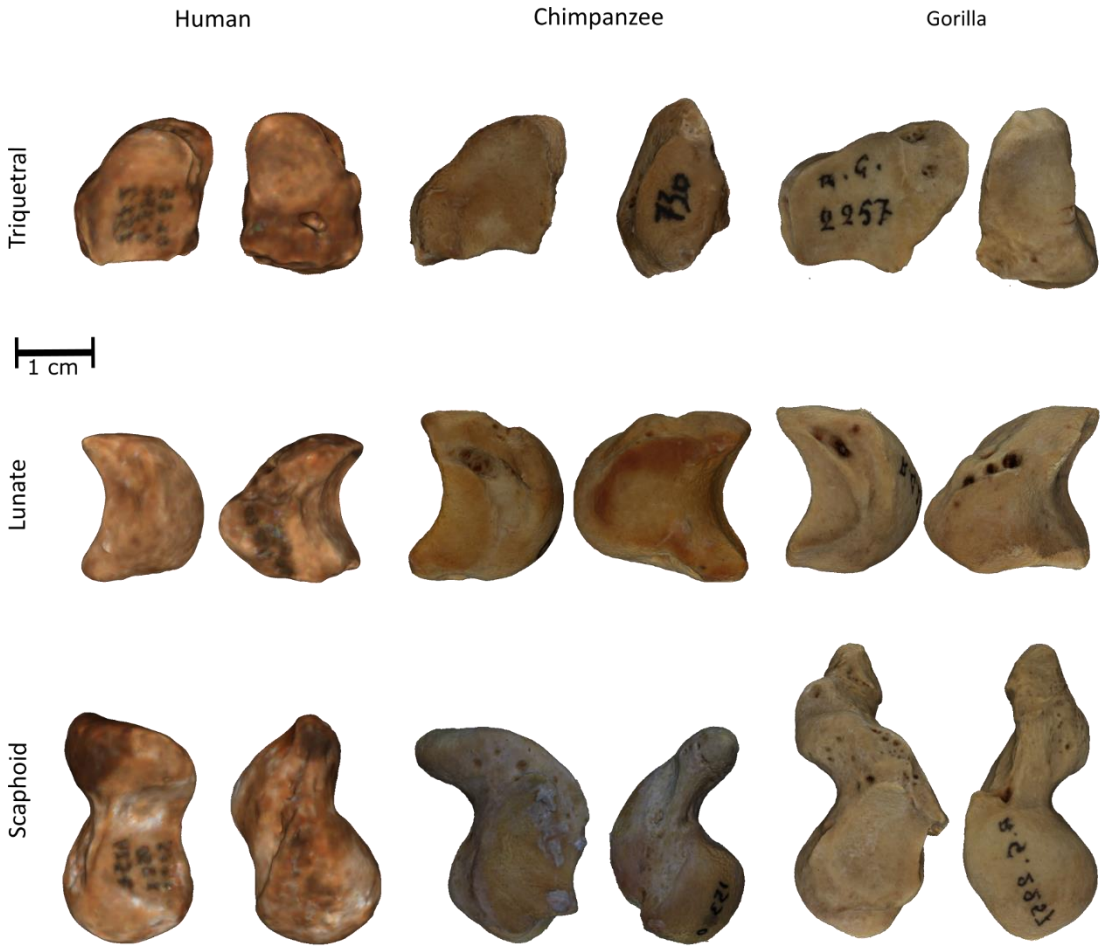

Figure 2.4 Proximal row of the left carpals in Hominidae (*Homo sapiens, Pan troglodytes* and *Gorilla beringei*) except for the pisiform. Triquetral is shown from the hamate and from the pisiform, respectively. Lunate is shown from the scaphoid and from the triquetral, respectively. Scaphoid is shown from the capitate and the radius, respectively. Scale = 1 cm.

Phalanges (fingers or digits) include, from radial to ulnar, the five proximal phalanges (PP1-PP5), four intermediate or medial phalanges (MP2-MP5 - the thumb does not have an intermediate phalanx), and five distal phalanges (DP1-DP5). Phalanges are long bones. Proximal phalanges of extant hominids are shown in Figure 2.7. No 3D models were obtained from middle and distal phalanges in the course of this thesis, so they are not shown in the image.

Collectively, metacarpals and fingers are called rays.

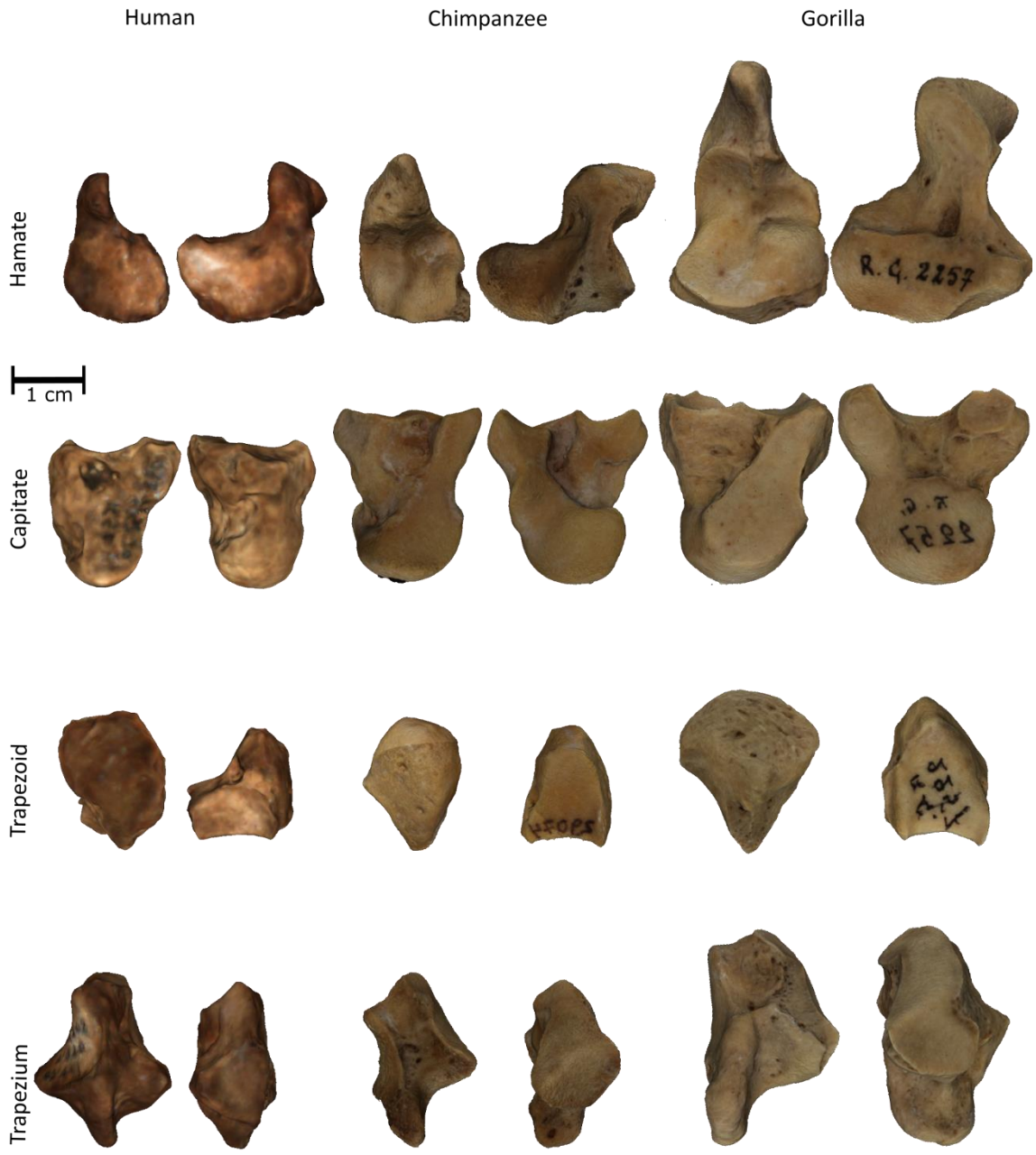

Figure 2.5 Distal row of left carpals in Hominidae (*Homo sapiens, Pan troglodytes* and *Gorilla beringei*). Hamate is shown from MC4 and MC5, and from the triquetral, respectively. Capitate is shown from the hamate and from the trapezoid, respectively. Trapezoid is shown from the dorsal surface, and from the trapezium, respectively. Trapezium is viewed from anterior view and from the scaphoid, respectively. Scale = 1 cm.

Figure 2.6 Left metacarpals in humans *(Homo sapiens),* chimpanzees *(Pan troglodytes)* and gorillas *(Gorilla beringei).* They are shown in palmar and lateral (MC1-2) or medial (MC3-5) view. From top to bottom: first to fifth metacarpal. Scale= 2cm.

Figure 2.7 Left proximal phalanges in palmar and medial view in humans *(Homo sapiens)*, chimpanzees *(Pan troglodytes)* and gorillas *(Gorilla beringei)*. From top to bottom: first proximal phalanx (PP1) to fifth proximal phalanx (PP5). Scale= 2cm.

2.1.3 Hand muscles

Although there are a few studies on muscles of the hand in non-human primates (Straus, 1942; Tuttle, 1969; Marzke et al., 1999; Diogo et al., 2011, 2012a, 2012b, 2013a, 2013b), most of the research on hands is focused on bones. Other soft tissue structures, such as sheaths, nerves and blood vessels, remain largely unexplored in non-human primates.

One of the most complete descriptions of the myology in primates is by Diogo et al. (2012b), both in terms of the diversity of taxa studied as well as for the sample size per taxon. According to this study, none of the muscles of the hand in modern humans is autapomorphic, yet more muscles (21, instead of 19) go into the human hand than in most other primates. Modern humans (and hylobatids) have an independent *flexor pollicis longus* muscle (Fig 2.2, Table 2.2), which is usually thin, vestigial and fused to the *flexor digitorum profundus* muscle in other primates. Modern humans (and hylobatids) also have an independent *extensor pollicis brevis* muscle (Fig. 2.3, Table 2.2), which is fused to the *abductor pollicis longus* muscle in other primates. As both of these muscles are inserted into the thumb, this reinforces the idea that this digit was subject to strong selective pressures in the past (see Section 2.3).

Tables 2.1 and 2.2 indicate all the muscles inserted into the hand in humans. The place of origin and insertion of these muscles vary in non-human primates but are largely similar to humans (Diogo et al., 2011, 2012b, 2012a, 2013a, 2013b).

Hand muscles are divided into intrinsic and extrinsic (Tables 2.1 and 2.2). Extrinsic muscles are those attached proximally to the arm or forearm and insert into the hand, and intrinsic muscles have their origin and insertion in the hand. As their names indicate, the functions of the intrinsic muscles are more variable than the extrinsic muscles (the functions of which are mainly extend and flex. Tables 2.1 and 2.2).

Table 2.1 Attachment sites of the intrinsic muscles in humans and their function at the hand, after Platzer (2003).

Muscle	Origin[1]	Insertion[1]	Main function
Opponens pollicis	TZM, flexor retinaculum	Lateral margin of MC1 at the body	Opposes the thumb and assists in adduction
Abductor pollicis brevis	Scaphoid tubercle and flexor retinaculum	Radial sesamoid and base of PP1 at the lateral side	Abducts the thumb
Flexor pollicis brevis	*Superficial head:* flexor retinaculum. *Deep head:* TZM, TZD, CA.	Radial sesamoid bone of the metacarpophalangeal thumb joint	Flexes, adducts and abducts the thumb and brings the thumb into opposition
Adductor pollicis	*Transverse head*: body of MC3. *Oblique head*: MC2, MC3, TZD and CA.	Ulnar sesamoid bone of the metacarpophalangeal thumb joint	Adducts, and assists in the opposition and flexion of the thumb
Flexor digiti minimi brevis	Hook of HA	Palmar side of the base of PP5	Flexes the fifth digit at the metacarpophalangeal joint
Opponens digiti minimi	Hook of HA and flexor retinaculum	Body of MC5 at the ulnar side	Flexes and rotates MC5 at the carpometacarpal joint
Abductor digiti minimi	PS, pisohamate ligament and flexor retinaculum	Ulnar margin of the base of PP5	Abducts the fifth finger
Palmar interossei (4)	MC2, MC4 and MC5	Bases of the corresponding proximal phalanges and the dorsal aponeurosis	Flex the metacarpophalangeal joints and extend at the interphalangeal joints
Dorsal interossei (4)	Bodies of the five metacarpal bones	Extensor expansions and base of PP2 (1), base of PP3 (2 and 3), base of PP4 (4)	Flex the metacarpophalangeal joints and extend at the interphalangeal joints
Lumbricals (4)	Tendons of FDP	Extensor aponeurosis and the metacarpophalangeal joint capsules	Flex the metacarpophalangeal joints and extend the interphalangeal joints
Palmaris brevis	Flexor retinaculium and palmar aponeurosis	Dermis of skin at the medial side	Puckering of the skin

[1]TZM=trapezium, TZD=trapezoid, CA=capitate, HA=hamate, MC1-5=metacarpals 1 to 5, FDP=*flexor digitorum profundus* muscle, PP1-5=proximal phalanges 1 to 5.

Table 2.2 Attachment sites of the extrinsic muscles in humans and their function at the hand, after Platzer (2003).

Muscle	Origin[1]	Insertion[1]	Main function
Extensor carpi radialis longus	Subcondylar ridge of the humerus	Base of MC2 at the dorsal surface	Extends and abducts the wrist
Extensor carpi radialis brevis	Lateral epicondyle of the humerus	Base of MC3	Extends and abducts the wrist
Extensor digitorum	Lateral epicondyle of the humerus	Dorsal surface of the base of MP2-5 and DP2-5	Extends and spreads the fingers 2-5, dorsiflexes the wrist and midcarpal joints
Extensor digiti minimi	Lateral epicondyle of the humerus	Dorsal surface of the base of PP5	Extends the fifth digit, and dorsiflexes and abducts the hand ulnary
Extensor carpi ulnaris	Humeral head and posterior surface of the ulna	Base of MC5, at the dorsal surface	Abducts medially the hand and flexes palmary the midcarpal joint
Extensor pollicis brevis	Ulna, radius and interosseous membrane	Base of PP1 at the dorsal surface	Extends and abducts the thumb at the metacarpophalangeal joint
Extensor pollicis longus	Dorsal surface of the ulna	Base of DP1 at the dorsal surface	Dorsiflexes and abducts the hand radially
Extensor indicis	Ulna and the interosseous membrane	Dorsal aponeurosis of MP2	Extends the index finger
Flexor pollicis longus	Anterior surface of the radius	Base of DP1 at the palmar surface	Flexes DP1 and abducts the thumb
Flexor carpi ulnaris	Humerus and ulna	PS, HA and base of MC5	Flexes and adducts the wrist
Flexor carpi radialis	Medial epicondyle of the humerus	TZM and base of MC2 and MC3	Flexes and abducts the wrist
Flexor digitorum profundus	Proximal two third of the ulna	Bases of DP2-5 at palmar surface	Flexes the wrist, midcarpal, metacarpophalangeal and phalangeal joints
Flexor digitorum superficialis	Humerus, radius and ulna	Bases of MP2-5 at the anterior side	Flexes (weakly) the elbow, the wrist and the metacarpophalangeal and phalangeal joints
Abductor pollicis longus	Ulna and radius	TZM and base of MC1 at the radial side	Flexes the hand toward the palm and abducts the thumb
Palmaris longus	Medial epicondyle of the humerus	Palmar aponeurosis	Flexes the hand towards the palm and tenses the palmar aponeurosis

[1]MC1-5: metacarpals from 1 to 5, PP1-5: proximal phalanges 1 to 5, MP1-5: middle phalanges 2-5, DP1-5: distal phalanges 1 to 5, PS= pisiform, HA=hamate, TZM=trapezium.

2.2 Prehensile abilities in humans

This chapter is an overview of the terms used by the anthropological literature to define the gripping capabilities of humans and apes, and their relationship with effective tool use. These abilities in fossils are inferred by using skeletal proxies, which are briefly referred to here and more extensively defined in the next chapter.

The fundamental definition for the prehensile movements of the hands, "the movements in which an object is seized and held partly or wholly within the compass of the hand", was postulated by Napier in 1956. He divided these movements into "power" and "precision" grips, and although further studies have redefined and widened these concepts, the use of "power" and "precision" grips has permeated research to date.

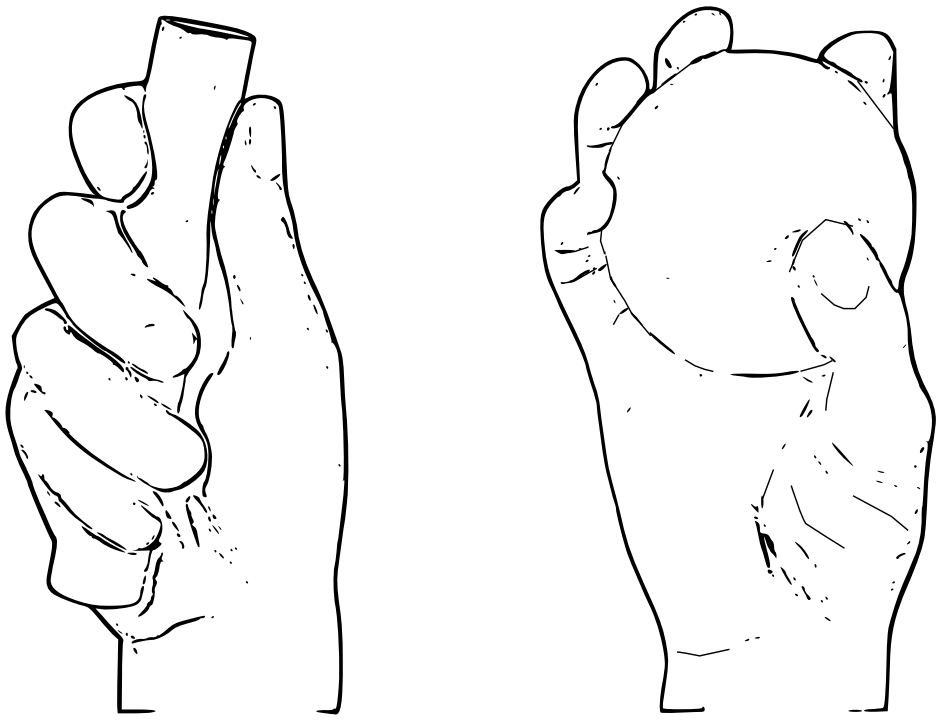

Figure 2.8 Power (left) and precision (right) grips. Drawn from Napier (1956).

Power grip (Fig. 2.8) occurs when "the object is held in a clamp formed by the partly flexed fingers and the palm, counter pressure being applied by the thumb lying more or less in the plane of the palm" (Napier, 1956). Precision grip occurs when "the object is pinched between the flexor aspects of the fingers and the opposing thumb" (Napier, 1956). Precision grip

"involves the thumb and one or more fingers, with or without the palm serving passively as a prop. It is distinguished from the term "power grip," in which objects are strongly squeezed by the fingers alone or squeezed by the fingers, thumb, and actively by the palm" (Marzke, 1997). Both basic grips are depicted in Figure 2.8.

Napier's classic paper pointed out that there was a discernible link between precision gripping and effective toolmaking. Although he recognized that other primates share both patterns of movements, these two grips differ profoundly in humans (Napier, 1960). Specifically, according to Napier (1960), during precision grip humans are characterized by "the ability to pick up small objects between thumb and index finger and hold them delicately yet securely between the opposed pulp surfaces. This posture demands perfect opposability of the thumb at the metacarpo-phalangeal joint as well as at the carpo-metacarpal joint. Young anthropoid apes are incapable of assuming this posture owing to the relative shortness of their thumbs". Indeed, it has been shown that humans are particularly well suited to manipulate small objects compared to other primates (Feix et al., 2015).

Later on, other studies (Marzke and Shackley, 1986; Marzke, 1997; Marzke and Pouydebat, 2009) postulated that the frequent use of the term "precision grip" restricted the number of postures and movements used to manipulate objects with precision among primates, as it only accounted for the manipulation of small objects with the opposition of the thumb's distal phalanx and one or more fingers. A diversity of grips used to hold an object, which can be categorized as types of precision grips or types of power grips, as well as grips that incorporate elements of both, has been identified in humans (Marzke and Shackley, 1986; Marzke, 1997; Key et al., 2018) as well in non-human primates, which, at least, includes apes (Christel et al., 1998; Pouydebat et al., 2009, 2011; Marzke et al., 2015; Bardo et al., 2016, 2017; Neufuss et al., 2016, 2019) and macaques (MacFarlane and Graziano, 2009; Pouydebat et al., 2009). Certainly, humans are not the only taxon capable of producing and using stone tools (e.g., Wynn and McGrew, 1989; Pruetz and Bertolani, 2007; Wynn et al., 2011; Gumert and Malaivijitnond, 2013; Visalberghi et al., 2015), nor are they the only ones with stone-tool culture fossil records, as behaviorally modified stones have been found at chimpanzee (Mercader et al., 2007) and macaque sites (Falótico et al., 2019) (Fig. 2.9).

Yet the grip repertoires of human and non-human primates partially overlap and are broader than traditionally thought, some grips are reported to be unique in humans, which may explain our comparatively more effective manipulative performance. One of these is the *forceful precision grip*, which Marzke and Wullstein (1996) identify when comparing

humans to chimpanzees. Although chimpanzees are capable of a precision grip, these authors claim it is weaker than that exerted by humans. Marzke and Wullstein (1996) propose that the larger palmar surfaces of the larger thumb of humans and proportionally shorter fingers help to accommodate irregular objects with one hand, such as the large stones needed for stone toolmaking and the removal of flakes by holding a hammerstone with the other. Another is the oblique power "squeeze" grips, in which a cylindrical object is secured by the palm and facilitates the use of an object as an extension of the arm; by contrast, in chimpanzees the cylindrical object or locomotor support is held diagonally across the fingers, with no active involvement of the palm (Marzke et al., 1992). Marzke and Wullstein (1996) mention that during this form of power grip the human thumb secures the object tightly and locks it into alignment with the forearm, facilitating its effective use as a tool by increasing the leverage of the forearm and applying force to the target.

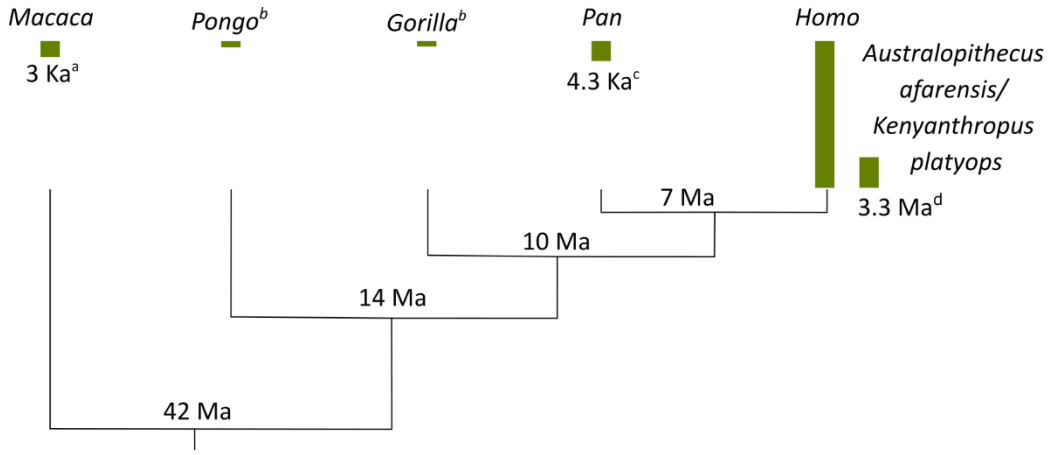

Figure 2.9 Fossil evidence of stone tool use in different primate species based on Carvalho et al. (2019). Green bars represent the time range of documented tool use in each taxon and the associated age indicates the oldest record of tool use. [a]Falótico et al. (2019), [b]No fossil evidence to date, [c]Mercader et al. (2006), [d]Harmand et al. (2015).

Because of the reductive use, in studies, of the various types of precision grips to a single one, Marzke (1997) points out that the discussion of the manipulative capabilities of extant primates and fossils hominins has been linked to one aspect of hand morphology, the relationship between the thumb length and the length of the other fingers (Hand proportions, see next section), for which humans present a high ratio. This ratio has been used as a proxy for opposability and for manual dexterity (e.g., Alba et al., 2003; Green and Gordon, 2008; Kivell et al., 2015).

Considering that a range of grips is recognized within primates, it follows that there are many proxies for effectiveness in tool manipulation other than relative thumb length. For example, some of these can be categorized in terms of hand myology (Marzke et al., 1999; Diogo et al., 2012), muscle activity (Hamrick et al., 1998; Marzke et al., 1998; Rolian et al., 2011), trabecular structure (Tsegai et al., 2013; Schilling et al., 2014; Stephens et al., 2018), hand pressure (Rolian et al., 2011; Key and Dunmore, 2018; Williams-Hatala et al., 2018) and behavioral comparisons during tool use (Pouydebat et al., 2009; Bardo et al., 2017). The next section deals with some of these traits, which are presented in the context of the fossil record of hominins.

2.3 The evolutionary history of the hominin hand

This section focuses on the fossil record of hands since the last common ancestor (LCA) of Pan and Homo, specifically those anatomical traits that are the subject of this thesis: thumb morphology, intrinsic and extrinsic musculature attaching into the fingers, and wrist morphology. Considering the topic of this chapter, hand proportions are also included in the summary, as they have been an important part of the discussion of hand evolution (Marzke, 1997), though they are not the focus of any of the studies presented here (for a discussion on the historical importance of hand proportions, see the previous section). Descriptions of each of these four traits, as well as the evolutionary interpretation researchers have given them are discussed here.

Information is provided on the basal hominins (*Ardipithecus* and *Orrorin*), followed by *Australopithecus* genera, then *Paranthropus* and early *Homo*, and finally on the most recent *Homo* fossils (Fig. 2.11). A brief description of the inferred ancestral morphotype between *Pan* and *Homo*, for which there is no physical evidence, is given at the beginning of each section. Note that although fossil descriptions are ordered from oldest to most recent, this does not mean they present either a single evolving lineage or that even if they do, evolution occurred in a linear, unified way. Indeed, it has been demonstrated that hand evolution in humans occurred in a heterogeneous and complex fashion (Kivell et al., 2011). Figure 2.11 shows the human fossil record for hands, and Tables 2.3 and 2.4 are a list of those osteological and myological features discussed in this section which are most likely

present in the hand of the *Pan-Homo* LCA. For a summary of other ancestral and derived traits not discussed in this thesis, see Tocheri et al. (2008).

Table 2.3 Character state definition of the traits used to examine the evolution of hominin hand morphology. Only traits relevant to this thesis are presented. The functional interpretation of these characters and their first appearance in the hominin fossil record are also provided.

Ancestral features in hominoids[1]		Derived features[1]	Functional significance of derived condition	First record of derived condition
Pan-like LCA	Long digits relative to the thumb	Fingers are short relative to thumb length	Refined manipulation: efficient pad-to-pad precision grasping[2]	*Ar. Ramidus*[3]
Ardipithecus-like LCA	Moderately short digits relative to the thumb	Fingers are long relative to thumb length	Specialized adaptation for below-branch suspension[4]	*Pan troglodytes*[4]
First metacarpal is gracile		First metacarpal is robust	Produces more force and tolerates higher joint stresses during tool use[5]	*P. robustus*/early *Homo*[6]
Distal phalanges have narrow apical tufts		Distal phalanges have broad apical tufts	Enhanced tip-weight support[7]	*O. tugenensis*[6]
Thumb is opposable with strongly curved first carpometacarpal joint surfaces		Thumb is opposable with less-curved first carpometacarpal joint surfaces	Reduced joint stress associated with forceful precision grip[8]	*P. robustus*[8]
The facet on MC2 for the trapezium faces radially and joint between MC2 and capitate is oriented more radio-ulnarly		The facet on MC2 for the trapezium faces proximally and for the capitate more proximo-distally	Increased mobility (pronation) of the MC2[9]. Effectively transmitting both axial and oblique loads[10]	*Au. afarensis*[9]
In the radius, a very prominent distally projecting dorsal ridge, a more dorsally oriented scaphoid notch, and a scaphoid notch and scaphoid-lunate angle that are small		Less prominent distally projecting dorsal ridge, a less dorsally oriented scaphoid notch, and a larger scaphoid notch and scaphoid-lunate angle	High degrees of wrist extension contribute to accuracy and high linear velocity of the hand[11]	*Au. africanus*[12]

[1] Taken from Tocheri et al. (2008), and Richmond and Strait (2000), [2]Marzke (1997), [3]Lovejoy et al. (2009), [4]Almécija et al. (2015b), [5]Rolian et al. (2011), [6]Susman (1994), [7]Almécija et al. (2010), [8]Susman et al. (1988), [9]Marzke (1983), Tocheri et al. (2003), [10] Niewoehner et al. (1997), Tocheri et al. (2003), [11]Williams et al. (2014), [12]Richmond and Strait (2000), inferred from radius.

Table 2.4 Character state definition for three myological features evolved in the human lineage, their functional significance and their first appearance in the hominin fossil record. Only relevant traits for this thesis are presented.

Ancestral features in hominoids[1]	Derived features[1]	Functional significance of the derived condition	First record of derived condition
Flexor pollicis longus absent, degenerate or ligament-like tendon slip with no separation from the *flexor digitorum profundus*	Independent, well-developed *flexor pollicis longus* muscle.	Powerful thumb flexion required to control the hammerstone[2]	*O. tugenensis*[3]
Poorly developed thenar musculature	Well-developed thenar musculature	Recruited at high force levels for strong precision pinch grips required to control the hammerstone and core[4]	*Au. africanus*[5]
Proximal phalangeal shafts are robust with marked flexor sheaths (PP2-5)	Proximal phalangeal shafts are gracile with weak flexor sheath ridges	Decrease in the frequency of activation of the flexor muscles, recruited during locomotion[6]	*H. antecessor*[7]

[1]Tocheri et al. (2008), [2]Hamrick et al. (1998), [3]Gommery and Senut (2006), [4]Marzke et al. (1998),[5]Ricklan (1987), [6]Susman (1979), [7]Lorenzo et al. (1999) however, development of flexor ridges is a matter of degree.

2.3.1 Hand proportions

The thumb-to-digit ratio is the length of the thumb relative to the length of the lateral digits, also called intrinsic hand proportions. This ratio is calculated by dividing the pollical metacarpal or phalangeal length by the length of the corresponding phalanx or metacarpal of one of the other fingers. Humans exhibit a high ratio for intrinsic hand proportions compared to apes, meaning a long thumb relative to the fingers (Napier, 1960; Green and Gordon, 2008; Almécija et al., 2015b; Feix et al., 2015) (Fig. 2.10).

As discussed in Section 2.2, intrinsic hand proportions are used as a proxy for thumb opposability and manual dexterity (Napier, 1960; Alba et al., 2003; Almécija et al., 2015b; Feix et al., 2015). This trait has been fundamental to arguing that effective precision grip is an ability that characterizes humans (Napier, 1960; Feix et al., 2015).

According to the traditional view, the hands of the *Pan-Homo* LCA resemble those of a modern chimpanzee in proportions as well as in general morphology (Richmond and Strait, 2000; Tocheri et al., 2008). As in chimpanzees, the *Pan-Homo* LCA is inferred to have short thumbs relative to the other digits. The human lineage presents a progressive lengthening of the thumb relative to the other digits and/or a progressive shortening of the other digits, which ensures the efficient pad-to-pad precision grasping that characterize humans

(Tocheri et al., 2008) (Figure 2.10). According to this model, the human hand is derived, whereas the hands of chimpanzees (and other apes) are largely plesiomorphic.

However, this model for LCA was created by parsimony with comparisons with non-human taxa, as well as relatively recent hominin fossils (from *Australopithecus* on). Until 2005, no chimpanzee fossils had been reported (McBrearty and Jablonski, 2005) and no fossil exists to date on the hand of chimpanzee ancestors. Similarly, only recently have anatomical descriptions from basal hominins been published (two fragmentary phalanges of *Ardipithecus kadabba* in 2001, two phalanges from *Orrorin tugenesis* in 2006 and a nearly complete hand for *Ardipithecus ramidus* in 2009 – see below).

Although initially the expectation was that pre-*Australopithecus* hands would be increasingly chimpanzee-like (Table 2.3), new analyses including *Ar. ramidus* fossils indicate that the chimpanzee hand is highly derived in terms of digit proportions (White et al., 2009; Almécija et al., 2015b), thus contradicting a *Pan*-like ancestor based on parsimony. *Ar. ramidus* exhibits a moderate condition of thumb-to-digit ratio, which would be the ancestral condition in the Catarrhini clade according to Almécija et al. (2015b). This means that no chimpanzees, but *Ar. ramidus* would be the best current model for the *Pan-Homo* LCA (White et al., 2009). However, note that this proposition is made for hand proportions only. For other traits, such as wrist morphology (Kivell et al., 2013), *Ar. ramidus* possesses a derived morphology. This means that the ape-like model for the LCA is not entirely dismissed (see below).

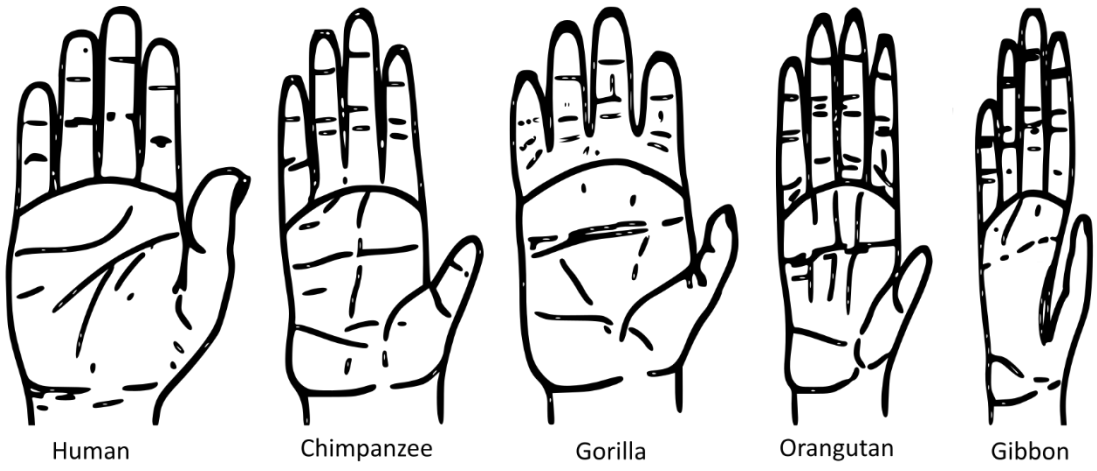

Figure 2.10 Schematic figure showing thumb-to-digit proportion in Hominoidea. Drawn from Straus (1942).

Although not to the extent of modern humans, the grasping capabilities of *Ar. ramidus* suggest that high dexterity was acquired much earlier than the systematic use of stone tools and is shared with other anthropoids (Fig. 2.11) (Almécija et al., 2015b). It also indicates that the opposability in humans was acquired by the shortening of the digits instead of the lengthening of the thumb (Almécija et al., 2015b). Hominins have only slightly reduced their digital lengths and modestly increased their thumb length through the course of human evolution.

Later hominin fossils (*Australopithecus afarensis, Australopithecus africanus* and *Paranthropus boisei*) also indicate finger proportions close to the modern human configuration (Green and Gordon, 2008; Rolian and Gordon, 2013; Feix et al., 2015; Richmond et al., 2020) or even fully human (Alba et al., 2003; Almécija and Alba, 2014), but either way capable of producing the types of tip-to-tip precision grips employed in fine manipulation. The earliest direct evidence of stone tools use (3.39 Ma, McPherron et al., 2010) is contemporaneous with this *Au. afarensis* and *Kenyantropus platyops,* of which there are no hand fossils (Fig. 2.11).

Curiously, the only other *Australopithecus* species with sufficient fossil preservation to estimate this trait, 2 Ma *Australopithecus sebida*, present higher thumb-to-digit ratio than later hominins and even modern humans (Kivell et al., 2011). For *Homo neanderthalensis*, results in Almécija et al. (2015b) indicate a similar proportion to *Au. sediba* (Almécija et al., 2015b), while similar to *Homo sapiens* in Feix et al. (2015), but either way with a high manual dexterity. Finally, 230 Kya *Homo naledi* hand proportions are lower than in *Au. sediba* and within the range of modern humans (Kivell et al., 2015)

There is not enough fossil evidence or published reports to estimate intrinsic hand proportions for fossils between *Au. sediba* and *H. neanderthalensis* (Fig. 2.11).

2.3.2 Thumb robusticity

Gracility of the thumb is another inferred condition of the LCA (Tocheri et al., 2008), as chimpanzees and other primates exhibit (Table 2.3). According to the chimpanzee like-model for the LCA, the LCA would have had a slender thumb in relation to the other fingers, while during human evolution, robusticity of the thumb increased. This section includes the robusticity changes in the bones composing the thumb in humans (first metacarpal (MC1), first proximal phalanx (PP1) and first distal phalanx (DP1), Section 2.1) compared to those of fossil hominins, modern apes and the inferred LCA condition.

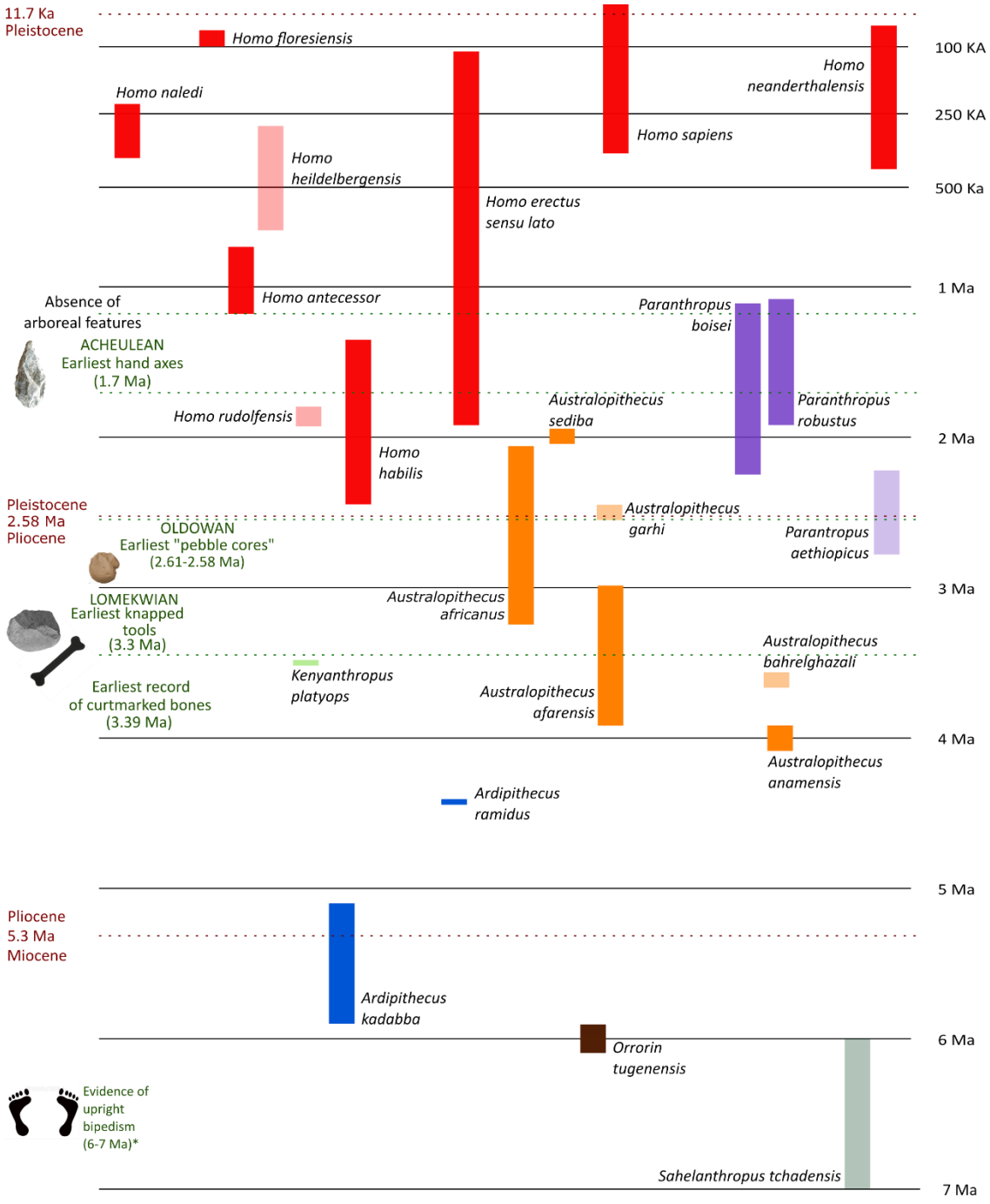

Figure 2.11 Hominin taxonomy showing the hand fossil record and major changes in locomotion and stone-tool culture. Translucent bars indicate that there is no manual evidence to date for *S. tchadensis, K. platyops, Au. Bahrelghazali, P. aethipicus, Au. garhi, H. rudolfensis, H. heildelbengensis*. Each genus is depicted in a different color. *Although see Wolpoff et al. (2002).

Traits used to refer to the human thumb as robust include a broad ungular tuft in the DP1 (Marzke, 1997), for MC1 a radial palmar condyle that is larger and more palmarly pronounced than the ulnar one (Susman, 1994; Galletta et al., 2019), several linear dimensions (Green and Gordon, 2008) and, more recently, the relatively greater trabecular bone volume for this bone (Dunmore et al., 2020). Due to the several traits used to refer to robusticity, not all studies are directly comparable, but they are all used to infer greater recruitment of the thumb during tool-related behaviors.

Robusticity of the thumb allowed our species to produce greater force and tolerate higher stresses during tool use (Rolian et al., 2011), and this is used as a proxy for effective precision grips in humans (Susman, 1994; Marzke, 1997; Green and Gordon, 2008; Rolian et al., 2011; Marchi et al., 2017). The thumb in both dominant and non-dominant hands experiences greater pressure than the other fingers during a variety of stone tool behaviors (Key and Dunmore, 2015; Williams-Hatala et al., 2018. Although see Williams et al., 2012). Pressures in the thumb would have been greater during the late Acheulean, as the preparation of flake platforms, a technological behavior associated with the production of late Acheulean handaxes, required more forceful precision grips than those needed during Oldowan and the Oldowan-Acheulean transition (Key and Dunmore, 2018). The pressures experienced by the thumb during tool-related activities has led to the conclusion that they were an important selective pressure for the hand (Key and Dunmore, 2015, 2018).

The single DP1 found for *O. tugenensis* (ca. 6 Ma), the oldest hominin species with a manual record, possesses all the features related to refined manipulation in modern humans (Gommery and Senut, 2006; Almécija et al., 2010), including a broad apical tuft. The features presented in this bone led researchers to propose human-like precision grip abilities several million years prior to the establishment of a systematized stone-tool culture (Fig. 2.11) (Gommery and Senut, 2006). Similarly, the *Ar. ramidus* thumb has larger interphalangeal joints than in apes, which would be consistent with the use of stone tools (Lovejoy et al., 2009).

Au. afarensis, *Au. africanus* and *P. boisei* are reported to be more similar to chimpanzees in the degree of the MC1 robusticity (Green and Gordon, 2008; Marchi et al., 2017; Galletta et al., 2019; Richmond et al., 2020). These features lead Galletta et al. (2019) to propose that if *Au. afarensis* was using stone tools, they were not using them in the same way as modern humans do. However, *Au. africanus* shows a human-like trabecular bone patterning indicative of forceful precision grip and “squeeze” gripping (Stephens et al., 2018, yet see Almécija et al., 2015a), which is an example of how different lines of evidence

point to different hominin capabilities for the use of tools. A robust metacarpal has also been reported for *H. erectus* (Richmond et al., 2020).
The paper in Section 5.1 deals with this subject. It is a test of whether human PP1 is more efficient at distributing stress during simulated stone tool use than extant apes.

2.3.3 Muscle properties

Ligament and tendon insertion sites (also called entheses, musculoskeletal stress markers, or attachment sites) are used as a proxy for actual hominin behavior with the hands, instead of the potential manipulative capacities they may have had, which are inferred from thumb robusticity, hand proportions (see above) and wrist morphology (see below). They thus provide a different type of information.
Insertion sites are the place on the bone where tendons or ligaments attach (Hawkey and Merbs, 1995; Villotte et al., 2010). They are supposed to reflect both the relaxation in locomotor demands on hands in the human lineage and the increase in manipulative behaviors. Considering the purpose of this thesis, only insertion sites for the ligaments holding the tendons of the *flexor digitorum profundus* and *superficialis* muscles (called "flexor ridges") and the insertion sites from the muscles attaching into the thumb (Fig. 2.1-2, Tables 2.1-2) are summarized here. The analysis of insertion sites of these muscles is presented in Sections 5.3-4.

2.3.3.1 Flexor ridges

In non-human apes, proximal and middle phalangeal shafts of fingers 2-5 exhibit marked flexor ridges (Susman, 1979), and this is also the most likely condition of the LCA (Tocheri et al., 2008) for both the *Pan*-like and *Ardipithecus*-like models (Table 2.4). The flexor ridges are a reaction of bone to the ligaments holding the main flexor muscles of the hand *(flexor digitorum profundus and superficialis)* being pulled during locomotion, and they are used as a proxy for it. During suspension and climbing both muscles are strongly recruited (Susman and Stern, 1979) and slightly active during knuckle-walking (Tuttle et al., 1972; Susman and Stern, 1979).
Flexor ridges of *Ardipithecus, Australopithecus, Paranthropus*/Early *Homo* genera retain the inferred primitive condition for the *Pan-Homo* LCA (Susman and Creel, 1979; Bush et al., 1982; Ricklan, 1987; Ward et al., 1999, 2012; Susman et al., 2001; Tocheri et al., 2008; Kivell et al., 2011; Richmond et al., 2020), although there are some differences of degree (the flexor ridges of *Ar. kadabba* are less developed than those of *Au. afarensis* according

to Haile-Selassie (2001), and the latter more than *Au. africanus* according to Ricklan, 1987). Functionally, this trait, along with others such as curvature of the phalanges, has been used to infer that grasping and climbing capabilities were retained until the Middle Pleistocene. Kivell et al. (2011) mentions that the absence of arboreal features (such as a developed flexor apparatus) and the appearance of an essentially modern human-like hand was the latest stage of human hand evolution. *Homo antecessor* (0.8 Ma) shows the suite of these traits, exhibiting a hand morphology that remained more or less stable during the Middle and Late Pleistocene (Lorenzo et al., 1999). *H. antecessor*, Neanderthals and modern humans hand morphology is to a large extent fully derived, and although flexor ridges are marked in *H. antecessor*, they are less so than in australopithecines and *H. habilis*. Additionally, this development has not been associated with arboreality (Lorenzo et al., 1999). The development of flexor ridges in fully biped species depends on the intensity/frequency of the use of hands for labor, and are far less developed than those of great apes and older hominins.

An exception to this decline in development of flexor ridges over time is 250 Kya *H. naledi*, whose long, curved phalanges and marked flexor ridges indicate a significant degree of climbing and suspension (Kivell et al., 2015).

2.3.3.2 Muscles attaching into the thumb

Humans have larger intrinsic thumb muscles relative to the intrinsic musculature of the hand than apes (Tuttle, 1969). Among primates, humans also have more muscles attaching into the thumb than most primates (Diogo et al., 2012).

Diogo et al. (2012) mention that humans have three derived structures in the hand: an independent *flexor pollicis longus* (FPL) and *extensor pollicis brevis* (EPB) muscles, and an additional muscle called *"adductor pollicis accessorius"*. They all involve the thumb, and "this is consistent with the hypothesis that movements of the thumb played an important role in human evolution" (pp. 75).

The FPL muscle enables powerful thumb flexion and enhances opposition of the thumb necessary for stone tool manipulation (Shrewsbury et al., 2003) and it has been reported to be highly activated during the production of Oldowan tools (Hamrick et al., 1998; Marzke et al., 1998), as well as other muscles attaching into the thumb (*flexor pollicis brevis* (FPB), *opponens pollicis* (OP) and *first dorsal interosseus* (D1), see Marzke et al., 1998).

Under the *Pan*-like LCA model it was supposed that there was an evolutionary trend from less developed thumb muscles to more developed muscles. However, the discovery of early

hominins *Ar. ramidus* (Lovejoy et al., 2009) and *O. tugenensis* (Gommery and Senut, 2006) revealed that they share a condition similar to the human FPL muscle, and they could exert strong distal phalanx flexion. The same is true for Early Pleistocene hominins *Au. africanus* (Ricklan, 1987), *Au. sediba* (Kivell et al., 2011), *P. robustus*/early *Homo* (Susman, 1998) and for Late Pleistocene hominins *H. naledi* and *H. neanderthalensis* (Marzke and Shackley, 1986). Exceptions to this condition are *Au. afarensis* (Marzke and Shackley, 1986) and *H. habilis* (Almécija et al., 2010). This leads Kivell *et al.* (2011) to suggest that a well-developed FPL is not a derived trait in humans but rather the primitive condition of the hominin clade or that it was convengently acquired by different hominin taxa for tool and non-tool related behaviors.

The other muscles inserting into the thumb that have been identified as activated during the control of the hammerstone and core are the FPB, OP and D1 (Marzke et al., 1998). Development of these muscles in australopithecines exemplified the belief that the hand evolved in a mosaic fashion (Kivell et al., 2011; Hamrick, 2012). This is because although thumb-to-digit ratio and the greater development of some muscles like the FPB indicates that they were able to perform precision grip as effectively as humans, this is not the case for the poorly developed OP and D1 muscles in *Au. sediba* (Kivell et al., 2011), *Au. Afarensis* (Bush et al., 1982) and *P. boisei* (Richmond et al., 2020), closer to the chimpanzee condition (Marzke et al., 1999).

The full suite of entheseal properties for the muscles most intensively recruited during tool use (Hamrick et al., 1998; Marzke et al., 1998) are present in later Swartkrans hominids (SK 84 and SKX 5020, attributed to either *P. robustus* or early *Homo*) (Susman, 1988) as well as *H. naledi* (Kivell et al., 2015) and Neanderthals (Maki and Trinkaus, 2011; Karakostis et al., 2018).

2.3.4 Wrist morphology

Eight bones make up the hominoid wrist (for details see Section 2.1.2). Studies of wrist morphology and manipulative capabilities have focused mainly on the size, orientation and curvature of carpal articular surfaces. These traits are a good proxy for a range of movements at the wrist, and among primates they are adapted to the functional demands of locomotion (Kivell et al., 2016, and references therein) or manipulation (Table 2.3).

Due to the number and complex morphology of carpals, part of the research is limited to specific joint surfaces (e.g., Richmond and Strait, 2000; Tocheri et al., 2003, 2005), but there is also a search for a suite of functional traits that may be informative of locomotory

modes. For instance, studies have discussed whether there is a specialized knuckle-walking complex in the wrist of African apes that allows a distinction with other modes of locomotion (e.g., Corruccini, 1978; Richmond and Strait, 2000; Kivell and Schmitt, 2009; Williams, 2010); this makes for an interesting discussion about whether bipedal hominids evolved from a knuckle-walking ancestor or a more generalized arboreal ancestor.

As for a manipulative complex, which is a covariation of multiple traits at the wrist that enhance manual dexterity, there is less research. With the exception of a case study suggesting a high integration between hamate and capitate in hominids (Peña et al., 2018), no patterns of morphological integration or modularity have been proposed for the wrist, and research has mainly focused on specific articular facets (e.g., Tocheri et al., 2003, 2005; Marzke et al., 2010), with modern human-like traits associated with enhanced dexterity (Table 2.3). Our study in Section 5.2 deals with the patterns of modularity in the hominid wrist.

In relation to hominins, the wrist of *Ar. ramidus* allows a degree of extension greater than the limited condition of knuckle-walkers, and more similar to Miocene apes (Lovejoy et al., 2009). Latter australopithecines *Au. anamensis* and *Au. afarensis* retain the primitive condition of African apes (Richmond and Strait, 2000) in which direction of the joint surfaces of the radius with the scaphoid and lunate bones allows a limited extension capability (Table 2.3). This in turn helps to stabilize the wrist during knuckle-walking (however, see Kivell and Schmitt, 2009). *Au. africanus* is closer to the modern human condition in this regard, according to Richmond and Strait (2000), with a higher degree of extension at the wrist probably related to greater accuracy and strength in effective tool-use (Williams et al., 2010, 2014). This derived condition for the radiocarpal morphology in *Au. africanus* is inferred for the radius, yet the first derived scaphoid in the hominin record is the one from 2 Ma *Au. sediba* which, besides modern humans, is only also found in *H. neanderthalensis* (Kivell et al., 2011).

H. habilis shows a morphology that resembles African apes in the scaphoid (Susman and Creel, 1979). The fossils for this species also exhibit other ape-like characteristics, such as curved phalanges with a developed flexor apparatus (Susman and Creel, 1979), poorly developed FPL (Almécija et al., 2010) and carpal articulation for the MC2 with limited pronation capabilities (unlike those of humans, see below). The hand remains of *Homo habilis*, whose name originally emphasized the tool-making capabilities of the oldest species in the genus *Homo*, has been called into question regarding the taxonomical attribution of the remains, as they may belong to the *Paranthropus* genus that appears in the fossil

records at nearly the same period (Robinson, 1972; Moyà-Solà et al., 2008) (Fig. 2.11). This discussion was especially important because at the time of the definition of *H. habilis* as a new species (Leakey et al., 1964), one of the features defining the genus *Homo* was the full opposition of the thumb, capable not only of the power grip but also of the precision grip as defined by Napier in 1956; however, the characters mentioned above cast doubt on how effectively *H. habilis* may have been using stone tools.

Back to *Au. sediba*, unlike the derived radiocarpal morphology (Kivell et al., 2013), the joint of the MC1 for the trapezium remains primitive for this hominin, similar to African apes, *A. afarensis* (Bush et al., 1982) and *P. boisei* (Richmond et al., 2020). *P. robustus* [SKX 5020] represents the first report of derived morphology for this articulation in hominins, which is flatter and broader and functionally advantageous for resisting the elevated loads associated with forceful precision gripping (Table 2.3) (Susman, 1988).

Another change in the joint surfaces has also been related to effective tool use. For articulation of MC2 with the capitate and trapezium (Fig. 2.1-2), *Au. afarensis* exhibits surface orientation that allows MC2 to pronate and supinate more, a feature shared with modern humans (Marzke, 1983; Tocheri et al., 2003), while this capability would be more limited in later *H. habilis* fossils as it occurs in African apes (Tocheri et al., 2003).

CHAPTER III

Research aim and objectives

Research aim and objectives

Major objective

- To assess whether the modern human hand is functionally adapted to stone tool-related behaviors.

Research aims

- To evaluate whether the human thumb performs better than that of apes in terms of stress distribution on the proximal phalanx under simulated scenarios of hammerstone use (Section 5.1).

- To study the patterns of bone covariation at the wrist (i.e., scaphoid, lunate, trapezium and capitate) in humans and African apes (Section 5.2).

- To test whether the insertion sites of the ligaments holding the flexor muscles (*flexor digitorum profundus* and *superficialis*) in proximal phalanges signal known differences in locomotor and manipulation capabilities in extant hominids (Section 5.3).

- To assess whether the variation in muscle properties of some of the muscles most strongly recruited during stone tool use in modern humans (*opponens pollicis* and *abductor pollicis longus*) can be linked to the variation in their insertion site sizes (Section 5.4).

CHAPTER IV

Materials and Methods

4.1 Digital models

4.2 Recommendations for improving photo quality in close range photogrammetry, exemplified in hand bones of chimpanzees and gorillas

4.3 Dissection material

Materials and Methods

This chapter provides a summary of all the 3D models of hand bones constructed or accessed during the three years of this thesis. These models greatly correspond to carpals (except pisiform), metacarpals and proximal phalanges from hominoids, mainly humans, chimpanzees and gorillas. Three categories of 3D models were analyzed: photogrammetric, surface scanner and microCT/CT scanner models. This chapter also includes the database of muscles attaching into the thumb of 23 forearms dissected during this thesis. The materials can thus be divided into two: digital models from hand bones and dissected soft tissue attaching into the thumb.

Except for the photogrammetric paper (Section 4.2), no details are provided about the methods in this chapter. Each study in the Results Section has a different method and they are described there.

4.1 Digital models

Digital models include material from surface models (from a scanner and photogrammetry) and microCT and CT scans from hand bones. This entire sample is in Table 4.1.

Most of the human material corresponds to hand bones from 50 individuals from the medieval San Pablo cemetery (Burgos, Spain) (Casillas and Adán, 2005), which belongs to the Universidad de Burgos, although it is currently held at the Institut Català de Paleoecologia Humana i Evolució Social (IPHES, Tarragona, Spain). The 3D models from this human sample were obtained from other researchers through a Breuckmann SmartSCAN structured light scanner (Breuckmann Inc.) with 125 fields of view, which according to the manufacturer provides a resolution of 9 μm. Another part of the human sample corresponds to the dissected thumbs of 23 hands from bodies donated to science (see below). I scanned the thumb bones (first metacarpal, first proximal phalanx and distal phalanx) of these individuals with the same surface scanner and the same field of view

described above. 29 bones of this cadaveric sample were uploaded to the Morphosource repository and can be downloaded from "Thumb bones of modern humans" project (https://www.morphosource.org/Detail/ProjectDetail/Show/project_id/993). A single microCT from one of the dissected thumbs (belonging to the right forearm of individual 1 in Table S1 at Section 8.1) was also obtained. Finally, a microCT scan from a Neanderthal (Vi 202) was downloaded from the NESPOS digital database (https://www.nespos.org/display/openspace/Home).

The hands of 48 chimpanzees (*Pan troglodytes*), 22 mountain gorillas (*Gorilla beringei*), 20 western gorillas (*Gorilla gorilla*), one orangutan (*Pongo pymaeus*) and one gibbon (*Hylobates lar*) were analyzed (Table 4.1). The African ape material belongs mainly to collections held at the AfricaMuseum in Tervuren (AM, Belgium), Zoologischen Staatsammlung München (ZSC, Germany), Museu de Ciències Naturals de Barcelona in Barcelona (MCN, Spain) and the Institut Català de Paleoecologia Humana i Evolució Social (IPHES, Spain). The material on 26 apes was downloaded from digital repositories. They include eight CT scans from chimpanzees belonging to the Center for Academic research and Training in Anthropogeny (CARTA, https://carta.anthropogeny.org/), two chimpanzees (*Pan troglodytes*) digitized by the American Museum of Natural History in New York and accessed via the Morphosource webpage (https://www.morphosource.org/), and one from the KUPRI digital database: http://dmm.pri.kyoto-u.ac.jp/dmm/WebGallery/index.html. As for gorillas, eight western gorillas (*Gorilla gorilla*) were digitized by the American Museum of Natural History in New York and accessed via the Morphosource webpage, four (one *Gorilla gorilla* and three *Gorilla beringei*) came from the Smithsonian database (https://www.si.edu/openaccess) and one specimen from the KUPRI digital database. One gibbon was also downloaded from the KUPRI database. Finally, a microCT scan from an orangutan held at the Senckenberg Museum in Frankfurt (SMF 74303) was provided by Dr. Tracy L. Kivell.

The African ape sample at AM and ZSC (46 and 11 individuals, respectively) came from a different provenance: wild-shot, captive and of unknown origin, and received by these institutions during the 20th century. The MCN apes (n=10) were captive, as well as the two chimpanzees held by the IPHES and those from the digital repositories.

Most of the African ape digital sample was constructed through photogrammetry during this thesis (66 out of 90 individuals, 1007 of the 1084 3D models). The procedure for taking the photos is described in the paper at the end of this chapter. This paper endeavors to offer simple guidelines for beginners in the technique to take better photos and thus improve the

quality of the 3D models. The resolution of these photogrammetric models is comparable to those of the Breuckmann scanner, as demonstrated in the study in Section 5.3.

Table 4.1 Number of hand bones per species analyzed in this thesis.

	Homo sapiens	*Pan troglodytes*	*Gorilla beringei*	*Gorilla gorilla*	*Pongo pygmaeus*	*Hylobates lar*	Total
Lunate	42	41	21	18	-	-	122
Scaphoid	39	45	22	18	-	-	124
Triquetral	-	30	18	9	-	-	57
Trapezium	40	39	22	17	-	-	118
Trapezoid	-	40	19	11	-	-	70
Capitate	41	41	22	19	-	-	123
Hamate	-	35	18	10	-	-	63
First metacarpal	23	36	19	10	-	-	88
Second metacarpal	-	27	16	9	-	-	52
Third metacarpal	-	36	14	10	-	-	60
Fourth metacarpal	-	32	16	9	-	-	57
Fifth metacarpal	-	29	17	10	-	-	56
First proximal phalanx	24	23	14	10	1	1	73
Second proximal phalanx	35	30	17	11	-	-	93
Third proximal phalanx	36	31	19	12	-	-	98
Fourth proximal phalanx	36	28	18	9	-	-	91
Fifth proximal phalanx	33	30	18	9	-	-	90
First distal phalanx	23	-	-	-	-	-	23
Total	372	573	310	201	1	1	1458

4.2 Recommendations for improving photo quality in close range photogrammetry, exemplified in hand bones of chimpanzees and gorillas (paper)

Int. J. Morphol.,
38(2):348-355, 2020.

Recommendations for Improving Photo Quality in Close Range Photogrammetry, Exemplified in Hand Bones of Chimpanzees and Gorillas

Recomendaciones para Mejorar la Calidad de las Fotos en Fotogrametría de Corto Alcance, Ejemplificado en Huesos de las Manos de Chimpancés y Gorillas

Ana Bucchi[1,2]; Javier Luengo[1,2]; Ramón Fuentes[3]; Manuel Arellano-Villalón[3] & Carlos Lorenzo[1,2]

BUCCHI, A.; LUENGO, J.; FUENTES, R.; ARELLANO-VILLALÓN, M. & LORENZO, C. Recommendations for improving photo quality in close range photogrammetry, exemplified in hand bones of chimpanzees and gorillas. *Int. J. Morphol., 38(2)*:348-355, 2020.

SUMMARY: Photogrammetry is becoming increasingly popular in morphological research and teaching due to its portability, ability to reliably render 3D models, and quality-to-price relationship relative to some popular surface scanners. Compared to surface scanners, however, the learning process in photogrammetry can be very time consuming. Here we describe common mistakes of photo capture in close-range photogrammetry that greatly affect 3D output and tips to improve them. Problems were identified after the 3D model construction of 780 hand bones of chimpanzees and gorillas from museum collections. Their hands are composed of 27 bones which vary in length and complexity. We show how lighting, object position and orientation, camera angle, and background affect the 3D output. By taking these factors into account, time and error rates for beginners can be greatly reduced and 3D model quality can be considerably improved.

KEY WORDS: Close range photogrammetry; Proof of concept ; Primates; Hands.

INTRODUCTION

Photogrammetry is a technique for building three-dimensional models of an object based upon photographs. It is growing in popularity in anthropology and related fields as it can produce high-quality and reliable virtual renderings of an object (Olson *et al*., 2013; Katz & Friess, 2014; Evin *et al*., 2016). It is also cost-effective compared to some popular commercial surface scanners (Porter *et al*., 2016) and portable, which is convenient when researchers do not have access to other equipment.

Broadly, the photogrammetric process can be divided in two steps: image acquisition and image processing to obtain 3D models using software (the most popular software is Agisoft Photoscan, although there are open-source options available as well, such as VisualSFM and Multiview Environment [MVE]). Regarding the first point, photogrammetry requires a very specific kind of image, which has a tremendous impact on the 3D output. It is sometimes easier and more efficient to repeat the photo session than to try to build 3D models with poor-quality pictures. Specifications for image acquisition vary greatly depending on the preferences of the researcher, the conditions in which the object is set; for example if there is no electricity in the location where the object has been accessed, as in Porter *et al*., or if the object is static, as in Mitchell & Chadwick (2008) or Mallison & Wings (2014), and the characteristics of the object to be modeled (such as whether it is refractive or translucent (Nicolae *et al*., 2014; Porter *et al*.).

Our objects were relatively small, opaque, movable, and were rotated on a turntable inside a photocube to obtain the photos instead of being photographed using the walk-around method (Fig. 1). There are a handful of

[1] Institut Català de Paleoecologia Humana i Evolució Social (IPHES), Zona Educacional 4, Campus Sescelades URV, Tarragona, 43007, Spain.
[2] Universitat Rovira i Virgili (URV), Area de Prehistòria, Avinguda Catalunya 35, Tarragona, 43002, Spain.
[3] Department of Integral Dentistry, CICO-Research Centre in Dental Sciences, Dental School, Universidad de La Frontera, Chile.
Sources of fouding: This study was funded by the research projects AGAUR 2017 SGR 1040 and MINECO [PGC2018-093925-B-C32]. A.B. would like to acknowledge financial support from Becas Chile (Conicyt, Chile).

BUCCHI, A.; LUENGO, J.; FUENTES, R.; ARELLANO-VILLALÓN, M. & LORENZO, C. Recommendations for improving photo quality in close range photogrammetry, exemplified in hand bones of chimpanzees and gorillas. *Int. J. Morphol., 38(2)*:348-355, 2020.

recommendations in articles and webpages for photo capture regarding the types of objects to be photographed, although there is still a lack of comprehensive guidelines with examples to help beginners acquire photos that guarantee the scientific quality of the 3D models. This is important considering that most researchers are not experts in photography or photogrammetry.

We used photogrammetry (Fig. 1) to create 3D models from hand bones of African apes. Hands in the family Hominidae are composed of 27 bones that range from 1 to 10 centimeters long and have variable shapes, from small and complex to long and simple. Hundreds of bones (N=780) were photographed in order to obtain 3D models, and several problems regarding image characteristics were addressed. In cases where no model or a poor-quality model was obtained from the photos, the photo sessions were redone, which allowed us to identify repetitive mistakes that resulted in higher quality models once solved. Considering the number of models, the equipment (Fig. 2, Table I) and photography instructions described below speed up the photo capture and the construction of the 3D model in the AgiSoft PhotoScan Professional Software (version 1.2.6).

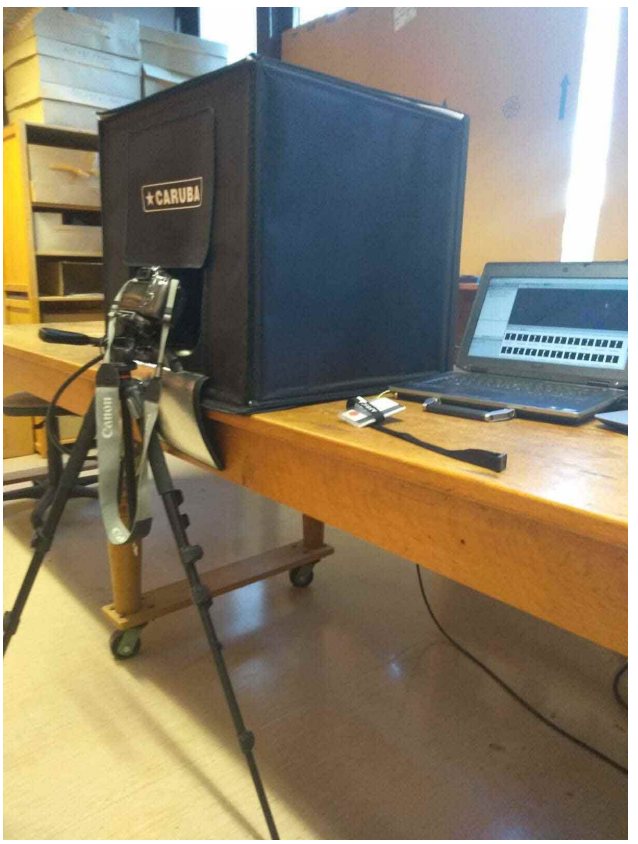

Fig. 1. Setup of the equipment.

Table I. Brand and price of the equipment.

Equipment	Brand and model	Cost (euros)
Camera	Cannon EOS 1200D	999 (includes lens
Remote control	RS-60 E3	19.84
Tripod	AmazonBasics	23.49
Photo cube	Caruba LED 50x50x50	139.90
Mastic	Blu-tack	1.90
Turntable	RamPro	7.99
Scale	Strati-Arqueolag	3.24
Total		1195.36

Fig. 2. Equipment used to take the photos.

MATERIAL AND METHOD

Materials and setup. Table I and Figures 1-2 show the equipment used here in the photo capture process. Hand bones were accessed from the primate collections of the Royal Museum for Central Africa, the Zoological State Collection in Munich, and the Zoological Museum in Barcelona.

We placed the phototube on a table, near an electrical outlet. The camera was connected to the remote control and mounted in a tripod (Fig. 1). The tripod and the remote control help prevent blurry images, and the remote control can be more comfortable for the operator when a large number of photos are taken.

BUCCHI, A.; LUENGO, J.; FUENTES, R.; ARELLANO-VILLALÓN, M. & LORENZO, C. Recommendations for improving photo quality in close range photogrammetry, exemplified in hand bones of chimpanzees and gorillas. *Int. J. Morphol., 38(2)*:348-355, 2020.

The photocube controlled the amount and evenness of the light on the object due to its reflective interior and the diffuse canvas; this is particularly important for complexly-shaped objects and when the photo capture is carried out in a poorly-lit place. One of the walls of the photocube (Table I) had small LED lights (the light source, which could be covered with a diffuser); three were reflective, and the remaining two were covered with a canvas. Because the canvas comprised the background in the final photo, we chose a color that contrasted with the bones (which was white in most cases).

The turntable was the same color as the background and was placed in the center of the cube. Marks were placed at 20-degree intervals on the side of the turntable, shown in Figure 2.

The bones were fixed to the turntable using a mastic the same color as the background and checked to ensure they remained fixed during rotation. Finally, we placed the scale next to the object.

Camera settings. Photos were taken with a Canon EOS 1200D camera mounted on a tripod. The lens was an EFS 18-55 mm macro 0.25/0.8ft and image size was 18 Mp. All the parameters were set to obtain the best quality photos and avoid different adverse situations which could have affected the 3D output. High focal length was used (50-55 mm) to increase magnification of the object relative to the whole picture. Though borders can be affected by optic distortion when using high focal length, the details at the center of the image are sharper. We used a high Depth of Field (DoF) (f/29) to avoid blurriness. Similarly, the ISO was reduced to a minimum level of 100 to avoid grainy images. The shutter speed was not fixed, and varied depending on the object. Photos were captured within a distance of 25 ± 10 cm .

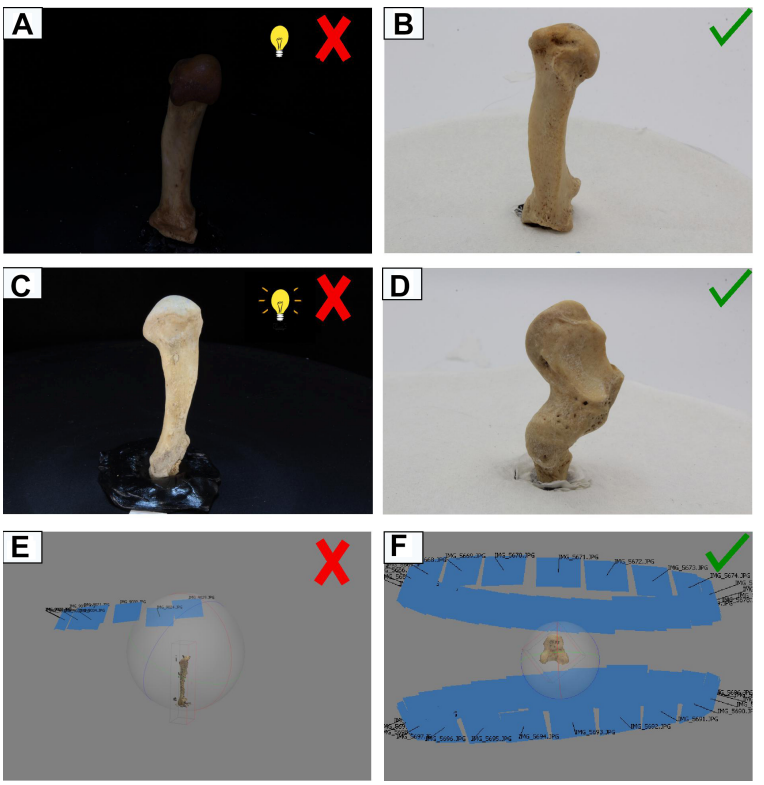

Fig. 3. Showing a dark (a) and over-exposed photo (c), while images b and d show adequately lit bones. Image e shows a dense cloud constructed incorrectly with overexposed photos; in most of these images (in which camera positions are represented by blue rectangles) there is not enough information to facilitate alignment and they cannot be used by the software to build the point cloud. In contrast, image f shows a dense cloud constructed with all the photos.

Images were saved in JPG format, which does not affect the quality of the final model (Mallison & Wings) and occupies less disk space than uncompressed formats such as RAW.

The photographic steps

1. A photo of each bone's label was taken to facilitate identification of the final pool of photographs.
2. The object was placed in the center of the turntable and the scale next to it.
3. The turntable was placed with the zero-degree mark facing the camera.
4. The camera was positioned at an approximately 45-degree angle relative to the object (see Fig. 8h) so that the surface of the bone facing upwards could be captured in the photos. The angle should be such that there is no need to raise or lower the tripod to accommodate the different portions of the object being captured.
5. A photo was taken and checked to ensure it was correctly taken (see below).
6. The turntable was rotated every 20 degrees, until the zero-degree mark faced the camera again, resulting in 18 photos.
7. The bones were flipped 180 degrees so that the surface that had been facing the turntable was facing the upwards.
8. The scale was removed.
9. Pictures were taken every 20 degrees, until the zero-degree mark was facing the camera again. In total, 36 photos were taken of the bones.

Photographic tips

Amount of light: Too little or too much light can make the object look featureless (Figs. 3a,c), which can result in erroneous image alignment or even prevent alignment altogether (Fig. 3e, in

BUCCHI, A.; LUENGO, J.; FUENTES, R.; ARELLANO-VILLALÓN, M. & LORENZO, C. Recommendations for improving photo quality in close range photogrammetry, exemplified in hand bones of chimpanzees and gorillas. *Int. J. Morphol., 38(2)*:348-355, 2020.

contrast to Fig. 3f). Photogrammetry works by aligning common points photographed from at least two positions, so these reference points must be recognizable. Exposure time should be increased or decreased so the smallest surface details are visible (Figs. 3b,d).

Light distribution: Uneven lighting on the object can produce strong shadows on some parts of the bone (Figs. 4a,c,e). This is a problem when using a turntable; while rotating the object the shadows move as well, and complicate the alignment of photos in the software (e.g., Fig. 3e), as explained in the first point. We used a photocube (Fig. 2, Table I) to ensure the bones were evenly lit and note that a white background produced better results than a black one.

Object relative to the background: The object should be easily distinguishable from the background and the background should be featureless and homogeneous (unlike Fig. 5a). A color that contrasts with the object should be chosen (not as in Figure 5b, but as in Figures 5c and 5d). In our case, we used the canvases available in the photocube and white proved better than black, as it reflects light better and because some bones were labeled in back (Figs. 5a,b). The background were then removed along with the background in the masking step.

Mastic should be invisible in the photos (Fig. 6b) or it will complicate alignment (Figs. 6a,e) and it will take more time to clean the model in the software. The mastic is used to fix the bone to the turntable. If the object remains still on its own, as the mandible shown in Figure 9b, it is not necessary to use mastic to affix it to the turntable.

When using the "moving around the object method" and using a single chunk in the software, as here, the background should be removed prior to the alignment of photos, which can be done by automatically masking the background in the Agisoft Photoscan Software, as shown in Figures 6c and 6d. This process takes around 2 minutes and allows the software to ignore the background in the subsequent steps. Other methods use the background to help with the alignment process and so it is not removed prior to alignment, but note that in this case two chunks must be used instead of a single one (see below).

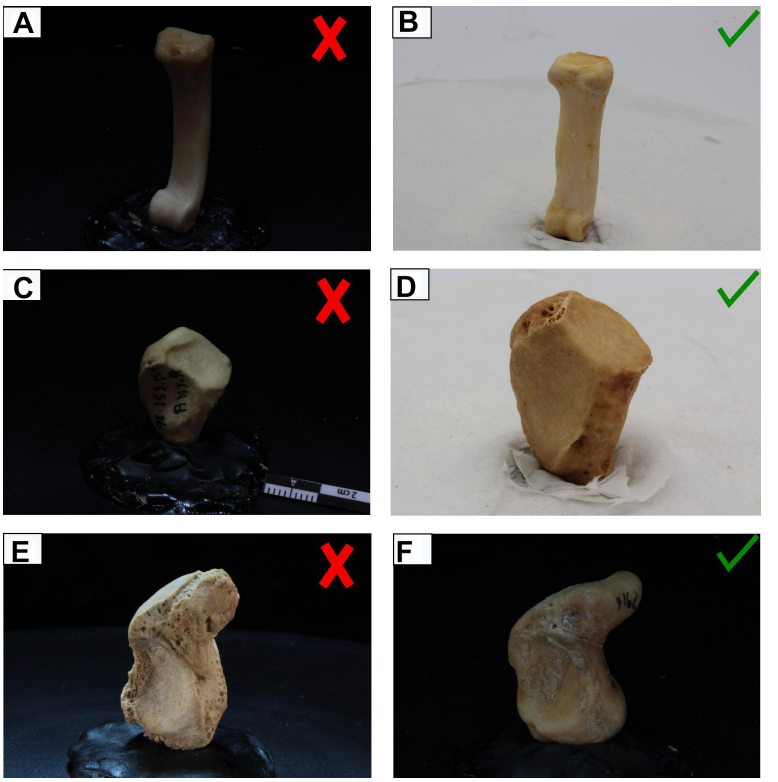

Fig. 4. Showing bone with harsh bone lightening (left column) and evenly lit (right column).

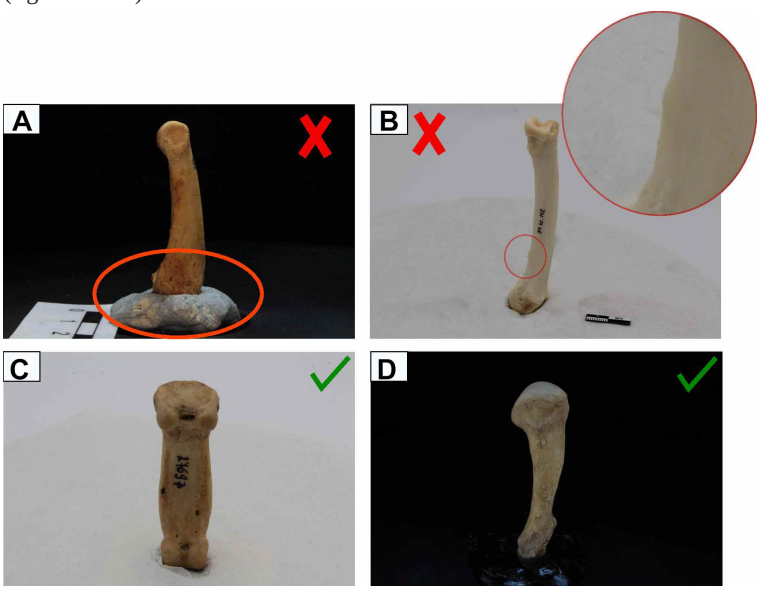

Fig. 5. The background. Image a is inadequate because the color of the mastic (light blue) is different from the background (black). Image b is inadequate because the bone is too white to use a background of the same color. Good contrast of the object relative to the background can be seen in images c and d.

Frame the object so it occupies most of the photo. This will ensure the background occupies as little space in the picture as possible. In Figure 7b the metacarpal is position vertically relative to the screen, but

BUCCHI, A.; LUENGO, J.; FUENTES, R.; ARELLANO-VILLALÓN, M. & LORENZO, C. Recommendations for improving photo quality in close range photogrammetry, exemplified in hand bones of chimpanzees and gorillas. *Int. J. Morphol., 38(2)*:348-355, 2020.

the camera can also be turned 90 degrees so that the long axis of the bone matches the long axis of the screen (Fig. 7d). This is preferable to flipping the bone, because then a larger part of the bone will not be visible in the photos (Fig. 7c). Note that the difference between Figures 7c and 7d is that in c the long axis of the bone is facing the turntable while in 7d it is not.

Camera lenses can be configured at a specific distance from the camera to control the magnification of the object and how much of the environment is going to be captured. Here we used a relatively long focal length (55 mm) so the object looks big relative to the whole picture. This work well with phalanges and metacarpals, but note that small bones, such as some carpals (trapezoid, triquetral, and lunate, 1.5 to 3.5 cm), occupy a smaller area relative to the whole image regardless.

Focus: The focus of the object should be as sharp as possible (Fig. 8b).

Use a tripod and a remote control (Table I) or the exposure-delay mode of the camera to prevent blurry images (Fig. 8a).

A high depth of field (f/29) was used to ensure that as much of the object got into proper focus.

In order for the object to remain in focus throughout the photo session, it must be facing the center of the camera screen (Fig. 8d) and be in the center of the turntable (Fig. 8f). Otherwise it will be out of focus during part or all of the photo session.

Avoid sharp angles of the object relative to the camera, as in Figure 8g. Otherwise the inferior part of the bone will remain out of focus. In this case the tripod should be lowered.

Check the position of the object relative to the vertical axis of the screen. Put the longer axis of the object as straight and close to the vertical axis of the screen as possible (Fig. 8f). The metacarpal in Figure 8i is inclined and the base of the bone (which is facing upwards) remains out of focus when rotating the turntable.

Scale: Place the scale near the object as in Figure 9a and take it out in step 8 (Section The photographic steps). This way half of the photos are taken with the scale and the other half without it. As such, all pictures can be put in the Agisoft Photoscan software in a single

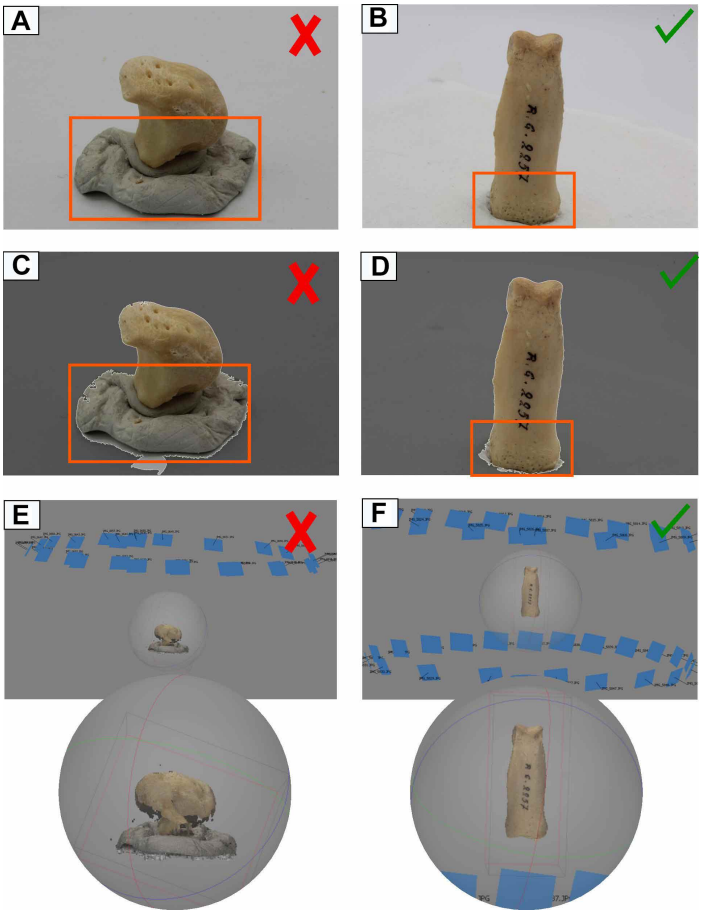

Fig. 6. The effect of the visible (a) and hidden mastic (b) in the alignment of the photos when using a single chunk in the software. If it is visible, mastic may not be masked (c) and instead might be used by the software for alignment rather than the bone, resulting in a wrong dense cloud as shown in image e. In contrast, if the mastic is not visible, the masking step is more efficient (d) and so is the alignment of photos.

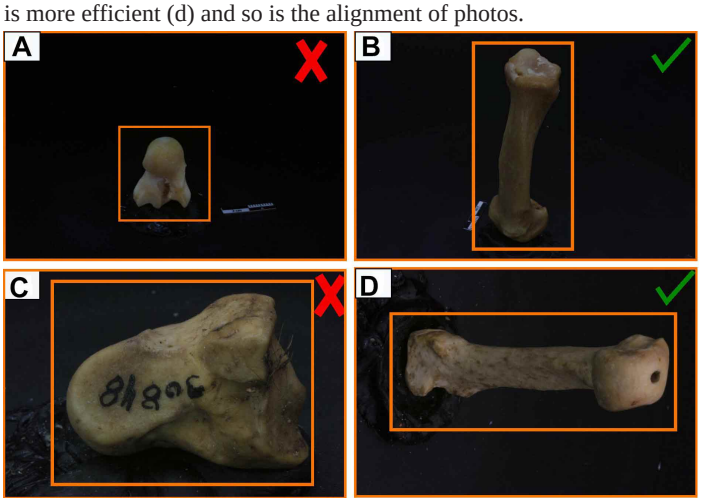

Fig. 7. Size of the bone relative to the whole picture. The camera is far from the object in image a, making it look small, while in image c most of the bone is facing the turntable. Images b and d are correctly framed bones. In d the camera is turned in 90 degrees.

BUCCHI, A.; LUENGO, J.; FUENTES, R.; ARELLANO-VILLALÓN, M. & LORENZO, C. Recommendations for improving photo quality in close range photogrammetry, exemplified in hand bones of chimpanzees and gorillas. *Int. J. Morphol., 38(2)*:348-355, 2020.

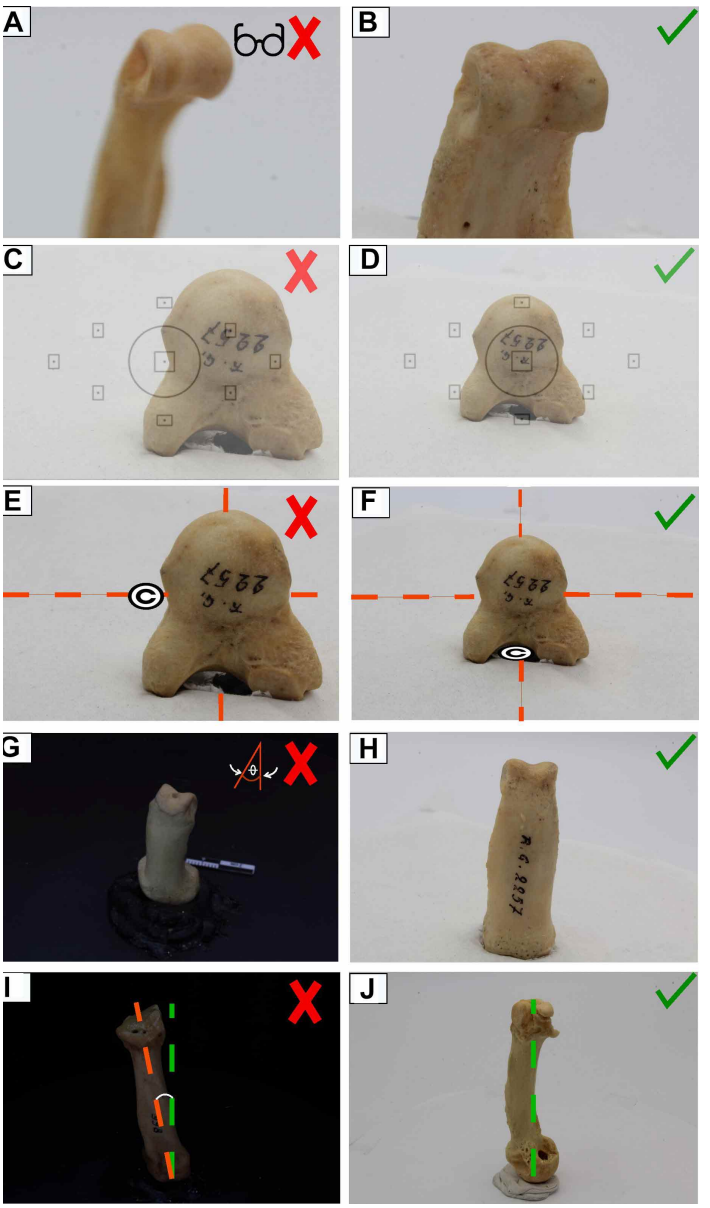

Fig. 8. Factors affecting focus. Image a: bone is blurry because the turntable was rotated too quickly. Using a tripod and delaying photo capture once the shutter is pressed prevents blurry images. Image b: sharp image. Image c: bone far from the center of the camera screen. Image d: bone facing the center of the camera screen. Image e: a bone located far from the center of the turntable. Image f: bone in the center of the turntable. Image g: sharp angle of the camera relative to the bone. Image h: correct angle between the bone and the camera. Image i: inclined metacarpal. Image j: straight metacarpal.

chunk, which speeds up the process of 3D model creation. If the scale is in every photo (Fig. 9b), two chunks will be needed, which will add a step in the model creation process (alignment of the chunks). If only one chunk is used the software may align the photos by the scale and not by the bone, which occurred with the mastic in Figure 6e. A scale such as the one used by Porter *et al*. can also be used to help align the photos (Fig. 9b). Another option is not to use scale at all (Fig. 9c) and scale the model by using a known length of the bone (as in Fig. 10).

Number of photos: Every area of the bones must be visible in at least two photos (Fig. 10) so the software can identify reference points. A high percentage of overlap (70-80 %) is needed in all photos. Take more photos than are strictly necessary. Here 30 photos were generally enough to build most of the models, but because some bones have more homogeneous textures or some photos were taken incorrectly, 36 photos—and in some cases more—were taken to ensure a successful 3D model. When deciding on the number of photos to take, it should be taken into account that that the number of photos affects the time required by the software to build the 3D models, as the more photos there are the slower the model is built.

RESULTS AND DISCUSSION

The Table II shows parameters describing the quality of some of the 3D models constructed here. They were obtained from the photographs captured following the recommendations described below. Four bones were chosen for this purpose; a small, simple one (trapezoid of chimpanzees), a medium-sized complex one (scaphoid), a medium-sized simple one (third proximal phalanx), and a long relatively complex one (third metacarpal). The mean maximum lengths of the bones were also calculated to indicate their size.

Initially, a large number of errors (poorly constructed models or failure to build models at all) occurred. The repetition of photo session this time fixing the aspects described in this paper greatly improve model quality, the probability of success (in here, in 6 of the 780 cases failed to construct a 3D model after the second attempt) and the time needed to build the model in the software. Figures 11 and 12 show two 3D models, one from a carpal bone (gorilla), and the other from a fourth metacarpal (chimpanzee). These 3D models are avaliable upon request.

It should be noted that after this second attempt the 3D model included holes in a few cases. We believe this is due to the very smooth texture of some bones, especially in the joint areas. The guidelines described here did not fix this problem. Previous studies have tested dusting featureless surfaces of

BUCCHI, A.; LUENGO, J.; FUENTES, R.; ARELLANO-VILLALÓN, M. & LORENZO, C. Recommendations for improving photo quality in close range photogrammetry, exemplified in hand bones of chimpanzees and gorillas. *Int. J. Morphol., 38(2)*:348-355, 2020.

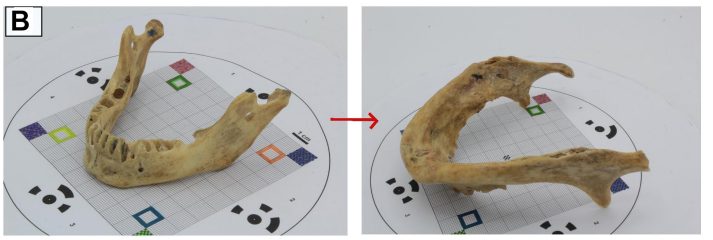

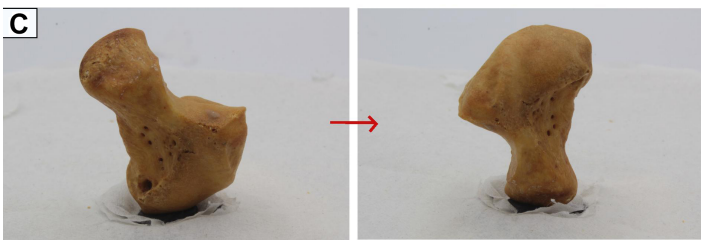

Fig. 9. Scale in the photo session. Image a represents the same photo session in which the scale was placed (left), and then removed once the bone was flipped (right) (one chunk method). Image b shows a photogrammetric scale that helps with the alignment and scale of the models (two chunk method), similar to the one that can be accessed in Porter *et al*. Image c shows a photo session in which no scale was used (one chunk method).

archaeological material with powder (Porter *et al*.) or using textured light pattern projections (Galantucci *et al*., 2008; Koutsoudis *et al*., 2015; Santosˇi *et al*., 2019) to increase alignment and dense reconstruction quality, but this was not tested here.

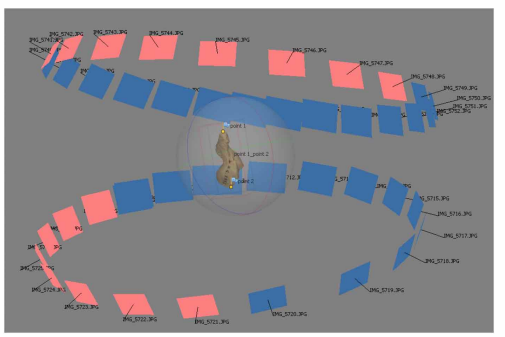

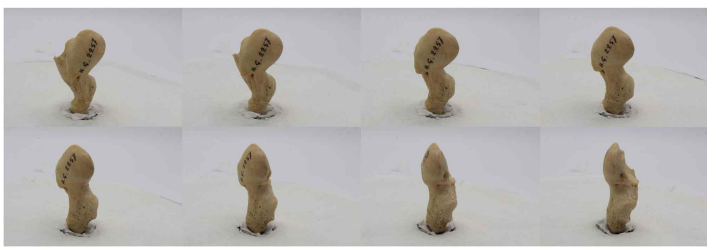

Fig. 10. A 3D model of a scaphoid from a gorilla (central image) in Agisoft Photoscan software. Top photos were taken approximately every 20 degrees, and the position of the camera for each photo is highlighted in pink at the top of the central image. Bottom photos were taken when the bone was flipped and the position of the camera for each photo is shown in pink at the bottom of the central image.

Fig. 11. 3D model of a scaphoid from a male gorilla (Gorilla beringei beringei) held at the Royal Museum of Central Africa (Tervuren). Number of triangles: 519.480. Number of photos: 46.

Fig. 12. 3D model for a fourth metacarpal of a chimpanzee held at the Royal Museum of Central Africa (Tervuren). Number of triangles: 279.024. Number of Photos: 30.

Table II. Parameters describing the quality of the 3D models of four hand bones obtained with the method described in the text. Triangles are of uniform size.

Bone	Taxon	Number of 3D models	Mean number of triangles	Standard deviation	Mean maximum length (cm)
Trapezoid	Chimpanzee	10	230.387	64.553	1.88
Scaphoid	Gorilla	22	562.250	137.420	3.97
Third metacarpal	Gorilla	18	370.590	130.331	7.99
Third proximal phalanx	Chimpanzee	26	438.542	161.908	5.59

CONCLUSIONS

Here were describe simple, effective criteria to facilitate taking good photos in close-range photogrammetry using relatively small, opaque objects such as the hand bones of African apes. We think these recommendations are also appropriate for a variety of objects that might fit in a photocube (except objects with difficult optical properties, such as brightness or transparency). With few exceptions, 3D models constructed following these guidelines are high quality and appropriate for scientific purposes.

ACKNOWLEDGEMENTS

We are grateful to the institutions holding the material we analyzed; the Royal Museum for Central (Belgium), Museu de Ciències Naturals de Barcelona (Spain) and Zoologische Staatssammlung München (Germany), and to the people who kindly helped us there, especially to Emmanuel Gilissen, Javier Quesada, Anneke van Heteren and Michael Hiermeier. To Juan Ignacio Morales and Antonietta Del Bove for their photogrammetric guidelines.

BUCCHI, A.; LUENGO, J.; FUENTES, R.; ARELLANO-VILLALÓN, M. & LORENZO, C. Recomendaciones para mejorar la calidad de las fotos en fotogrametría de corto alcance, ejemplificado en huesos de las manos de chimpancés y gorillas. *Int. J. Morphol., 38(2)*:348-355, 2019.

RESUMEN: La fotogrametría está siendo cada vez más popular en la investigación y enseñanza morfológica. Esto debido a su portabilidad, confiabilidad de los modelos 3D y buena relación calidad-precio. Comparada con los escáneres de superficie, sin embargo, el proceso de aprendizaje de la fotogrametría puede llevar mucho tiempo. Aquí se describen errores comunes en la toma de fotos para fotogrametería que afectan de manera importante la creación de los modelos 3D, así como consejos para superarlos. Los problemas descritos fueron identificados luego de la construcción de 780 modelos 3D de huesos de la mano de chimpancés y gorillas depositados en distintas colecciones de museos. Las manos de estas especies están compuestas por 27 huesos que varían en tamaño y complejidad. En este artículo mostramos como la luz, la posición y orientación del objeto, el ángulo de la cámara y el fondo de la imagen afectan el resultado en 3D. Considerando estos factores, personas que están aprendiendo esta técnica pueden reducir de manera importante el tiempo y la probabilidad de error, y mejorar considerablemente la calidad de los modelos 3D.

PALABRAS CLAVE: Fotogrametría de corto alcance; Prueba de concepto; Primates; Manos.

REFERENCES

Evin, A.; Souter, T.; Hulme-Beaman, A.; Ameen, C.; Allen, R.; Viacava, P.; Larson, G.; Cucchi, T. & Dobney, K. The use of close-range photogrammetry in zooarchaeology: Creating accurate 3D models of wolf crania to study dog domestication. *J. Archaeol. Sci. Rep., 9*:87-93, 2016.

Galantucci, L. M.; Percoco, G. & Dal Maso, U. Coded targets and hybrid grids for photogrammetric 3D digitisation of human faces. *Virtual Phys. Prototyp., 3(3)*:167-76, 2008.

Katz, D. & Friess, M. Technical note: 3D from standard digital photography of human crania - A preliminary assessment. *Am. J. Phys. Anthropol., 154(1)*:152-8, 2014.

Koutsoudis, A.; Ioannakis, G.; Vidmar, B.; Arnaoutoglou, F. & Chamzas, C. Using noise function-based patterns to enhance photogrammetric 3D reconstruction performance of featureless surfaces. *J. Cult. Herit., 16(5)*:664-70, 2015.

Mallison, H. & Wings, O. Photogrammetry in paleontology – a practical guide. *J. Paleontol. Tech., 12*:1-31, 2014.

Micheletti, N.; Lane, S. N. & Chandler, J. H. Application of archival aerial photogrammetry to quantify climate forcing of alpine landscapes. *Photogramm. Rec., 30(150)*:143-65, 2015.

Mitchell, H. L. & Chadwick, R. G. Challenges of photogrammetric intra-oral tooth measurement. *Int. Arch. Photogramm. Remote Sens. Spat. Inf. Sci., 37 Part B5*:779-82, 2008.

Nicolae, C.; Nocerino, E.; Menna, F. & Remondino, F. Photogrammetry applied to problematic artefacts. *Int. Arch. Photogramm. Remote Sens. Spat. Inf. Sci., 40*:451-6, 2014.

Olson, B. R.; Placchetti, R. A.; Quartermaine, J. & Killebrew, A. E. The Tel Akko total archaeology project (Akko, Israel): Assessing the suitability of multi-scale 3d field recording in archaeology. *J. Field Archaeol., 38(3)*:244-62, 2013.

Porter, S. T.; Roussel, M. & Soressi, M. A Simple Photogrammetry Rig for the Reliable Creation of 3D Artifact Models in the Field: Lithic Examples from the Early Upper Paleolithic Sequence of Les Cottés (France). *Adv. Archaeol. Pract., 4(1)*:71-86, 2016.

Santosi, Z.; Budak, I.; Sokac, M.; Puskar, T.; Vukelic, & Trifkovic, B. 3D digitization of featureless dental models using close range photogrammetry aided by noise based patterns. *Facta Univ. Ser. Mech. Eng., 16(3)*:297-305, 2019.

Tiano, P.; Tapete, D.; Matteini, M. & Ceccaroni, F. *The Microphotogrammetry: A New Diagnostic Tool for On Site Monitoring of Monumental Surfaces.* Florence, Proceedings of the International Workshop SMW08, 2008. pp.27-9.

Corresponding author:
Ana Bucchi
4 Zona Educacional
Campus Sescelades URV
43007 Tarragona - SPAIN

Email: anabuchi@gmail.com

Received: 24-07-2019
Accepted: 15-10-2019

4.3 Dissected material

Tables S1 and S2 at Section 8.1 detail the dissection information of 23 forearms from 17 individuals donated to the Human Donation Service at the University of Barcelona (http://www.ub.edu/bellvitge/donacion.htm). The legislation in Spain regarding bodies donated to sciences allows researchers to know only the sex and age-at-death of individuals, and this information is provided in Table S1. These bodies were donated in 2017 and 2018 and frozen until analysis. As usually occurs with bodies donated to science, age-at-death of the sample is high in most cases (median is 79 years).

All muscles attaching into the thumb were dissected in 12 forearms and fewer muscles in the remaining forearms. Table S2 describes the dissected sample and muscle variables measured. As stated above, some of the bones to which these muscles attached were scanned and are available for download in Morphosource.

CHAPTER V
Results

5.1 Finite element analysis of the proximal phalanx of the thumb in Hominoidea during simulated stone tool use

5.2 Modularity of the wrist in extant hominids

5.3 Insertion sites in manual proximal phalanges of African apes and modern humans

5.4 Muscle strength and entheseal size in human thumbs: testing the relationship with a cadaveric model

Finite element analysis of the proximal phalanx of the thumb in Hominoidea during simulated stone tool use

Ana Bucchi[a,b,*], Thomas A. Püschel[c], Carlos Lorenzo[a,b], Jordi Marcé-Nogué[d,e]

[a] Institut Català de Paleoecologia Humana i Evolució Social (IPHES), Tarragona, Spain
[b] Area de Prehistòria, Universitat Rovira i Virgili (URV), Tarragona, Spain
[c] Primate Models for Behavioural Evolution Lab, Institute of Cognitive and Evolutionary Anthropology, University of Oxford, Oxford, United Kingdom
[d] Center of Natural History, University of Hamburg, Hamburg, Germany
[e] Institut Català de Paleontologia M. Crusafont, Universitat Autònoma de Barcelona, Barcelona, Spain

Corresponding author: Institut Català de Paleoecologia Humana i Evolució Social (IPHES), Tarragona, and Area de Prehistòria, Universitat Rovira i Virgili (URV), Tarragona, Spain.
E-mail address: anabucchi@gmail.com (A. Bucchi)

Abstract

Finite element analysis was applied to analyze six individuals from different primate species (*Homo sapiens, Homo sapiens neanderthalensis, Pan troglodytes, Gorilla gorilla, Pongo pygmaeus* and *Hylobates lar*) to identify stress distribution patterns on the pollical proximal phalanx during simulated hammerstone use. We expected the stress to be better distributed in our species than in other hominids based on the idea that, unlike apes, the human hand is adapted to tool-related behaviors. Our results indicate that the human phalanx unevenly distributes stresses and is one of the most fragile of all, especially when a small hammerstone is simulated. Tool orientation relative to the phalanx did not have a substantial effect on average stress or distribution. We conclude that great apes can resist loads exerted during this activity more efficiently than humans and that there were probably other evolutionary factors acting on this bone in our species.
Keywords: Functional morphology; Hand evolution; Primates; Stress.

Introduction

There is a widespread idea that the derived manual anatomy of humans is a result of selective pressures related to manipulative behaviors (e.g., Hamrick et al., 1998; Key and Dunmore, 2015; Kivell et al., 2016; Skinner et al., 2015; Young, 2003) as, among primates, humans exert unique, more efficient precision and power grips (e.g., Bardo et al., 2017; Key and Dunmore, 2015; Marzke, 2013; Niewoehner, 2001; Rolian et al., 2011; Shrewsbury et al., 2003; Tocheri et al., 2003). Unlike humans, locomotion constitutes the primarily selective pressure on the hand for most primates (e.g., Jouffroy et al., 1991; Tuttle, 1969). This is not to say that non-humans primates are unable of performing tool-based activities, as they have been reported in other primates (Gumert and Malaivijitnond, 2013; Pruetz and Bertolani, 2007; Visalberghi et al., 2015; Wynn et al., 2011), and some of their tools, including stone hammers, and the behaviors involved (e.g., direct hard hammer knapping) are very similar or indistinguishable from Oldowan culture (Wynn and McGrew, 1989; Wynn et al., 2011). However, the manual pressures and high muscle activities experienced by the hand during travel (Matarazzo, 2013; Samuel et al., 2018; Susman and Stern, 1979; Wunderlich and Jungers, 2009) play a more important role.

The selective pressures related to stone tool use supposedly started early in the human lineage. The intrinsic muscles of the thumb show high level forces during hard hammer percussion manufacture of Oldowan tools (Hamrick, 1998; Marzke et al., 1998). The thumb also experiences significant pressures during stone tool production (Key and Dunmore, 2015; Williams-Hatala et al., 2018). In addition, some derived morphology facilitating manipulation of stone tools, as the expanded apical tuft of the distal thumb phalanx, were already present in *Orrorin* (Gommery and Senut, 2006), although numerous derived conditions evolved later in a mosaic fashion until the fully-derived hand of Neanderthals and modern humans (for a review, see Tocheri et al., 2008, and also Key and Dunmore, 2018). Changes in hominins in the shortening of the fingers relative to thumb length, which ensures the human-like precision grip capability, occurred in *Australopithecus* (Alba, 2003; Green and Gordon, 2008; Tocheri et al., 2008). Robust first metacarpals have been identified in early *Homo/Paranthropus* (Susman, 1988), which helps to produce stronger, efficient grips and tolerate higher joint stresses (Key and Dunmore, 2015; Key and Lycett, 2018; Rolian et al., 2011).

Even though most of the paleoanthropological literature agrees that hands of humans and non-human primates are adapted to different functions (i.e., manipulation vs. locomotion), recent studies have concluded that some derived traits leading towards *Homo* (e.g., finger proportions) are not the product of selective pressures acting directly on the hands but on other region of the skeleton (i.e., the foot) (Rolian et al., 2010) which are related to terrestriality (Bardo et al., 2017; Heldstab et al., 2016) and were subsequently exapted for tool manipulation. This can explain why skillful hands were present long before the first record of lithic industry (Alba et al., 2003; Almécija et al., 2010).

How humans acquired this unique configuration of musculoskeletal traits in the hand which facilitates tool related behaviors has profound implications in our understanding of human evolution overall, considering that stone technology is a key element defining culture in our species (e.g., Foley and Lahr, 2003). However, testing biological causality is hard to address and we may never be absolutely certain on the evolutionary mechanisms having shaped the human hand. Consequently, we think that new insights are needed to better assess whether the evolution of the human hand is driven by tool-related behaviors.

Here we use finite element analysis (FEA) to evaluate if stress on the human pollical proximal phalanx (PP1) fits with the functional adaptation (to tool use) hypothesis for the evolution of our hand. This method makes it possible to control and repeat biomechanical scenarios under modifiable conditions (for a review, see Rayfield, 2007) making it suitable for morpho-functional problems such as this. To our knowledge, no study has applied FEA to evaluate the effect of stone tool use on the hand.

The stress distribution in the PP1 was analyzed in six Hominoidea taxa (*Homo sapiens, Homo sapiens neanderthalensis, Pan troglodytes, Gorilla gorilla, Pongo pygmaeus* and *Hylobates lar*) (Table 1) under loading conditions related to hard hammer percussion to describe stress patterns on PP1s during the same task. We expect to find that the human PP1s distribute stresses differently than apes, as hands in humans and apes show morphologically commitment to different functions - manipulation and locomotion (Table 2) - and the loading condition simulated here are related to stone tool use. In particular, we expect that the human phalanges distribute stresses more efficiently and can withstand the stresses related to hammerstone use better than our closest living relatives.

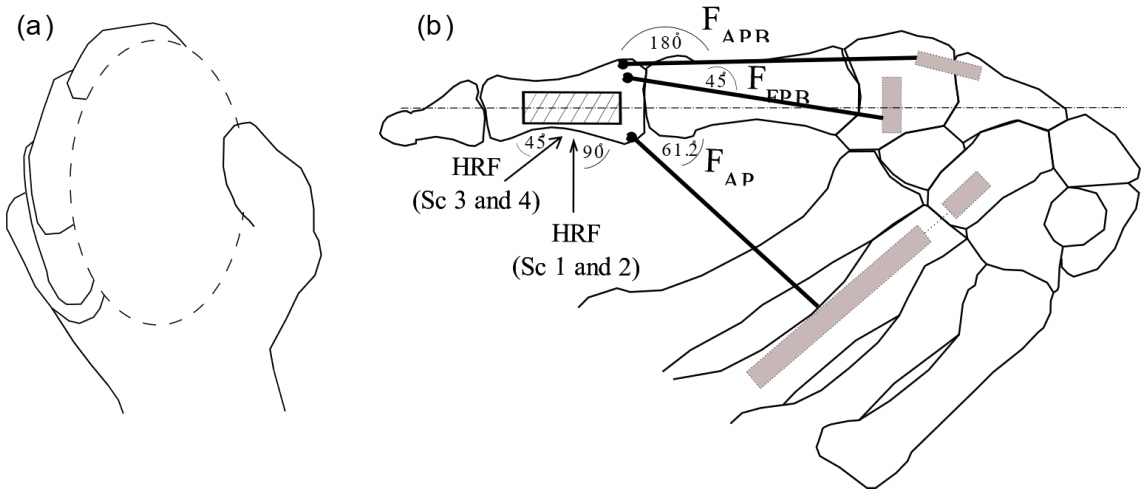

Figure 1. Biomechanical model of hammerstone use. (b) corresponds to a zoom in palmar view of the area of interest during (a) the grip of a human individual (based on Marzke et al., 1998). (b) shows the angles of the muscular forces acting on the PP1. HRF is in 90° relative to the horizontal line for scenarios 1 and 2 and in 45° for scenarios 2 and 4. This force was applied on the entire palmar surface of the PP1 except in the joint areas and is represented with a hatched rectangle. Angles of the muscle forces are shown relative to the horizontal line. F_{AP}: Adductor Pollicis Force; F_{APB}: Abductor Pollicis Brevis Force; F_{FPB}: Flexor Pollicis Brevis Force. EPB direction force was applied in 16.7° and is not showed here as it attached on the dorsal surface of the PP1. Grey rectangles represent the origin areas of the muscles.

Material and methods

Sample and digitalization

A recent modern human, a Neanderthal from Krapina (Vi 202) and four extant non-human hominoids were analyzed: chimpanzee, gorilla, orangutan and gibbon. All specimens were adults with no evident pathologies (Table 1).

The PP1 from the human individual was obtained from a fresh cadaver and scanned with a micro-CT (Perkin Elmer, model Quantum Fx, Hopkinton MA, USA). The orangutan PP1 is from the Senckenberg Museum in Frankfurt, Germany (SMF 74303) and was scanned on a BIR ACTIS 225/330 micro-CT scanner at the Department of Human Evolution, Max Planck Institute for Evolutionary Anthropology (Leipzig, Germany). The remaining specimens were obtained from digital databases; the micro-CT of the Neanderthal PP1 from NESPOS (https://www.nespos.org/display/PublicNesposSpace/Human+Fossils), whereas the CT scans from the rest of the non-human sample were downloaded from the Digital

Morphology Museum, Kyoto University, Japan (KUPRI; http://dmm.pri.kyoto-u.ac.jp/dmm/WebGallery/index.html). Even though KUPRI CT scans have a relative low resolution (Table 1) and do not allow to observe bone segments in high detail, they can still provide relevant morphological information, as it has been shown that even medium-resolution scans can accurately quantify shape (Slizewski et al., 2010; McCurry et al., 2015). In fact, it has been shown that this resolution is sufficiently accurate to even identify intra-specific differences of relatively small specimens (Marcy et al., 2018).

Table 1 The sample.

Taxon	Common name	Age[a]	Sex[b]	Side[c]	Digital database/ nº	CT/microCT resolution (mm)
Homo sapiens	Extant human	59	M	R	None	0.08
Homo sapiens neanderthalensis	Neanderthal	unk	unk	R	NESPOS/ Krapina 202	0.03
Pan troglodytes	Chimpanzee	29	M	L	KURPI/345	0.219
Gorilla gorilla	Gorilla	38	M	R	KUPRI/1353	0.500
Pongo pygmaeus	Orangutan	32	F	R	None	0.03
Hylobates lar	Gibbon	33	M	R	KUPRI/465	0.250

[a] Age in years of the individual; unk: unknown.
[b] M: male; F: female; unk: unknown.
[c] R= right, L= left.

In order to make models from different resolution scans comparable, trabecular bone was enclosed using the "Convex Hull" tool in Meshlab v.2016.12 (Cignoni et al., 2008) and the same mechanical properties were defined for all the specimens. Elements were then converted to CAD models. During this last step, irregularities in the surface caused by segmentation were repaired using refinement and smoothing tools (Lautenschlager, 2016) in Geomagic Studio® (3D Systems, v. 12, Rock Hill, SC, USA). All scans were segmented using Seg3D software (CIBC, v. 2.4.0, 2017). The medullary cavity, trabeculae and compact bone were segmented on the specimens by applying a combination of case-specific thresholding values and manual painting techniques. Models of left PP1's (Table 1) were reflected to enable meaningful comparisons.

To avoid possible problems when aligning different individuals (due to inter-specific morphological differences), we selected one individual as a reference (i.e., the chimpanzee representative) to perform a best-fit alignment to align all the models

according to a common reference plane. This procedure was carried out in Geomagic Studio® (3D Systems, v. 12, Rock Hill, SC, USA) prior to FEA to align all the models, so that loads could be applied in the same axis and allow an easier interpretation of the results.

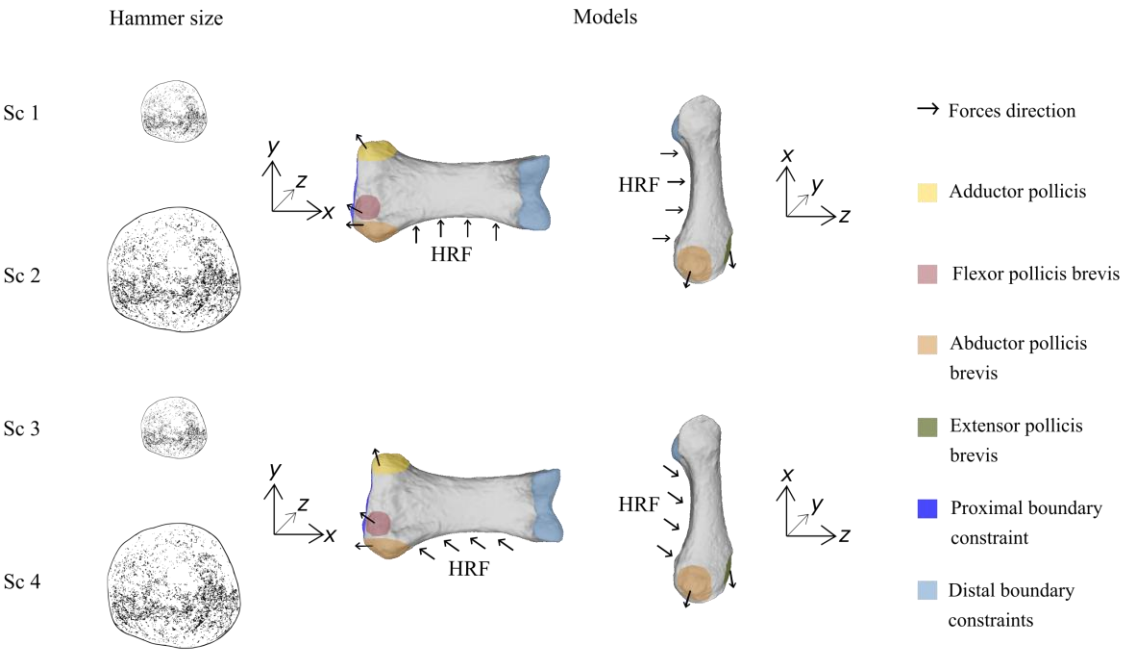

Figure 2. Free-body diagram of the phalanx in the different scenarios. This figure depicts the boundary conditions, areas of insertion of muscles, and direction of forces. For all loading configurations, joint reaction forces resulted from the rigid boundary constraints that were fixed at the distal joint in X, Y and Z-axes (light blue area), and at the proximal joint in the X-axis (dark blue area). The hammer reaction force (HRF) was applied to the entire palmar surface of the bone. 3.29 N for the HRF was simulated for Sc 1 and 3, and 7.65 N for Sc 2 and 4. Phalanges are shown in palmar (right) and radial (left) views.

Model properties

Structural static analysis was performed to evaluate the biomechanical behavior of the PP1s using the Finite Element Package ANSYS 17.1 in a Dell Precision™ Workstation T5500 with 48 GB and 5.33 GHz. Elastic, linear and homogeneous material properties were assumed for the cortical bone using the values of E (Young's modulus) 18.6 GPa and v (Poisson's ratio) 0.3, while for trabecular bone values of E 0.75 GPa and v 0.3 were assumed (Butz et al., 2012).

Table 2 Percentage (%) of main locomotor behaviors of the non-human sample, according to Hunt (2004).

Taxon	Climb	Braquiate	Clamber	Walk
Chimpanzee	6.5	0.8	0.0	89.9
Gorilla	19.7	3.6	0.0	64.4
Orangutan	31.3	15.5	40.7	12.0
Gibbon	34.2	51.2	0.0	0.0

In this study, the focus in the comparison of the models is primarily on the von Mises stress distribution. Bone can be modeled as a brittle (Doblaré et al., 2004) or ductile (Dumont et al., 2009) material. According to Doblaré et al. (2004), the von Mises criterion is the most commonly applied and useful criterion for predicting the yield and fracture location in bone when ductile and isotropic material properties are assumed in cortical bone. The PP1 models were meshed using an adaptive hexahedral mesh and ANSYS® (Marcé-Nogué et al., 2015). The model meshes ranged between 200,000 and 320,000 elements depending on the particular specimen and loading scenario (Table 3).

Loading scenarios and boundary conditions

The hands were modeled using a free-body diagram approach in a precision three-jaw chuck grip (Fig. 1), following Marzke et al. (1998), since we obtained the applied muscle recruitment data from their study.

Forty-eight loading cases were generated. These included two hammerstone orientations relative to the PP1 and two muscle activity patterns associated with differences in hammerstone mass for the six individuals under study (Figs 1 and 2). We also generated two different scaling scenarios for muscular data considering that for only two species (*Homo sapiens* and *Pan troglodytes*) there is enough muscular information to perform the simulations.

In the first scaling scenario, we scaled the forces of the Neanderthal, chimpanzee, gorilla, orangutan and gibbon using the extant human data as a reference, whereas in the second one, we used the chimpanzee muscular data as a reference to scale the forces of all the other representatives. In each of these two settings, the loads of the remaining specimens were scaled relative to the individuals of reference to yield identical force, i.e., the volume ratios (Supplementary data Table S1). This way differences in stress distribution can be interpreted entirely as result of shape

differences (Dumont et al., 2009). These values of muscular contraction pressure were calculated according to the method developed by Marcé-Nogué et al. (2013) and rearranged for 3D models by Fortuny et al. (2015). Equation for this is $F_A = \left(\sqrt[3]{\frac{V_A}{V_B}}\right)^2 F_B$, where F_A is the scaled force, F_B the reference force, and V_A and V_B the respective volumes for CB.

For the human, muscle forces were calculated by means of the physiological cross-sectional area (PCSA) collected from the forearm of a fresh cadaver of a 59-year-old man. All muscles attached at the PP1 were dissected: abductor pollicis brevis (APB), extensor pollicis brevis (EPB), flexor pollicis brevis (FPB), and adductor pollicis (AP) (cf. Sacks and Roy, 1982). The PCSA obtained from the human cadaver were the following: FPB (0.6612 cm^2), ADP (1.429 cm^2), EPB (0.2121 cm^2), and APB (0.2587 cm^2). The insertion areas of the muscles involved were defined in the model to apply the forces of muscular contraction. The angles of the muscle tendons were estimated *in situ*. For the remaining specimens, tendon angles were assumed to be the same as for the human (Table S1), as areas of the bone in which muscles attached are similar between them (Diogo et al., 2011; Diogo et al., 2012a, Diogo et al., 2013a, b). PCSAs for chimpanzees were obtained from Marzke et al. (1999) for the APB, FPB and AD muscles, and from Kikuchi (2010) for EPB. The PCSA for the chimpanzee was: FPB (1.40 cm^2), ADP (2.50 cm^2), EPB (1.44 cm^2), and APB (1.80 cm^2) (Kikuchi, 2010; Marzke et al., 1999).

Table 3 Mesh characteristics for each specimens.

Specimen	Volume CB (mm^3)[a]	Volume TB (mm^3)[b]	N elements[c]
Extant human	1012.8	651.1	225729
Neanderthal	733.3	662.6	240469
Chimpanzee	1046.1	178.6	160103
Gorilla	1642.9	577.9	225710
Orangutan	610.1	542.8	199857
Gibbon	250.7	65.9	311431

[a] Volume of the cortical bone.
[B] Volume of the trabecular bone.
[c] Number of elements used to create the mesh for each FE model.

The PCSA for FPB, APB, and EPB muscles was then adjusted to the levels of muscle activity described in the electromyography (EMG) study of Marzke et al. (1998). These

data correspond to the active (i.e., dominant) hand and were recorded at the strike, so all scenarios were simulated at that specific moment. Following Maier and Hepp-Reymond (1995), we assumed that the activity for the APB, not monitored in Marzke et al. (1998), was similar to EPB.

Muscle activity was considered during the use of two hammerstone sizes (400 g and 780 g, respectively, which are equivalent to 3.92 N and 7.65 N and represent the HRF). Although it would be interesting to include the loads from the core, they can significantly vary in size, as well as during the reduction sequence. More importantly, the reaction force corresponding to the core would need to be considerably higher than the hammerstone reaction force to alter the stress distribution on the PP1, which is the focus of the present study.

We simulated two tool orientations relative to the PP1: one with the long axis of the bone parallel to horizontal line (Sc 1 and 2), and the other at 45° (Sc 3 and 4), as shown in Figures 1 and 2.

The hands were modeled using a free-body diagram approach. A biomechanical model (Fig. 1b) was constructed based on data about hand posture, muscles active during hammerstone use, the reaction forces from the hammerstone (HRF), and the joint reaction forces from metacarpal and distal phalanx (JRF_{mc} and $JRF_{d,}$ respectively). Details of all loads involved are in Table S1.

Boundary conditions were defined to represent the fixed displacements that the models of PP1 experience during the loading scenarios. Once the models were solved, the joint reaction forces from the metacarpal (JRF_{mc}) and from the distal phalanx (JRF_{d}) were obtained. As boundary conditions have a great impact in the solution of the model, we intended to reproduce biological meaningful conditions for the PP1 to constrain the movements of the FEA models. The proximal part of the bone was fixed in the X dimension, and the distal part fixed in the X, Y and Z-axes (Fig. 2). All analyses were performed under these conditions (Table S1).

Analysis of von Mises stress

We applied the recently-proposed quasi-ideal mesh (QIM) and its percentile values (M25, M50, M75, and M95) as a basis for our analysis (Marcé-Nogué et al., 2016). The use of a QIM mesh, corresponding to a mesh in which all the elements have practically the same size, facilitated between model comparisons, thus allowing the stress values obtained to be displayed as boxplots. Because the maximum value cannot be properly analyzed since it corresponds to artificially inflated values (Marcé-Nogué et al., 2015),

here the M95 percentile is assumed as the peak value of stress following the concept introduced by Walmsley et al. (2013).

In addition, a quantitative single measurement of the relative strength of the structure under study was used to summarize the strength of the whole phalanx as the mesh-weighted arithmetic mean (MWAM) and the mesh-weighted median (MWM). These last values are also required to estimate the percentage error of the arithmetic mean (PEofAM) and the percentage error of the median (PEofM), which are statistics used to ensure that our models were reliable QIMs as described in Marcé-Nogué et al. (2016). This information can be found in Supplementary data Tables S2 and S3.

Results

The distribution of von Mises stress for each phalanx and scenario is shown in Figures 3 and 4. The specimen with the highest peak stress level was the gibbon, followed by the extant human, the Neanderthal, the orangutan, the gorilla and the chimpanzee representatives. This order was the same for all analyzed loading and scaling scenarios, except for the chimpanzee and gorilla, with the former having higher peak stresses than the gorilla in the first and second loading scenario (*Homo*-scaled), but lower in the remaining ones (Fig. 5).

Maximum von Mises stress values in the gibbon, extant human, Neanderthal and gorilla models were located in the center of the palmar surface of the phalanx body, decreasing towards the dorsal surface and the distal and proximal portions (Figs 3 and 4). In these specimens, the lowest stress values were found in the joint areas and dorsal part, where the bone was not significantly affected by stress. Stress for the orangutan, chimpanzee and gorilla specimens were lower and more evenly distributed over the bone and, similarly to the humans and gibbon, did not affect the joint areas. In most cases, median stress values (MWM) for the extant human and Neanderthal representatives (Fig. 5) were lower and more focused than measured in chimpanzee, gorilla and orangutan (Figs 3 and 4).

Peak and mean stress levels were considerably higher when the smaller hammerstone was simulated in all species (Fig. 5), while the effect of hammerstone orientation was less important. Overall, the effect of the hammerstone size was even greater than that related to the morphological differences between species (Fig. 5). Of all the scenarios,

that showing the highest mean and peak values for all species was the one with the smaller hammerstone and the second bone orientation (SC 3).

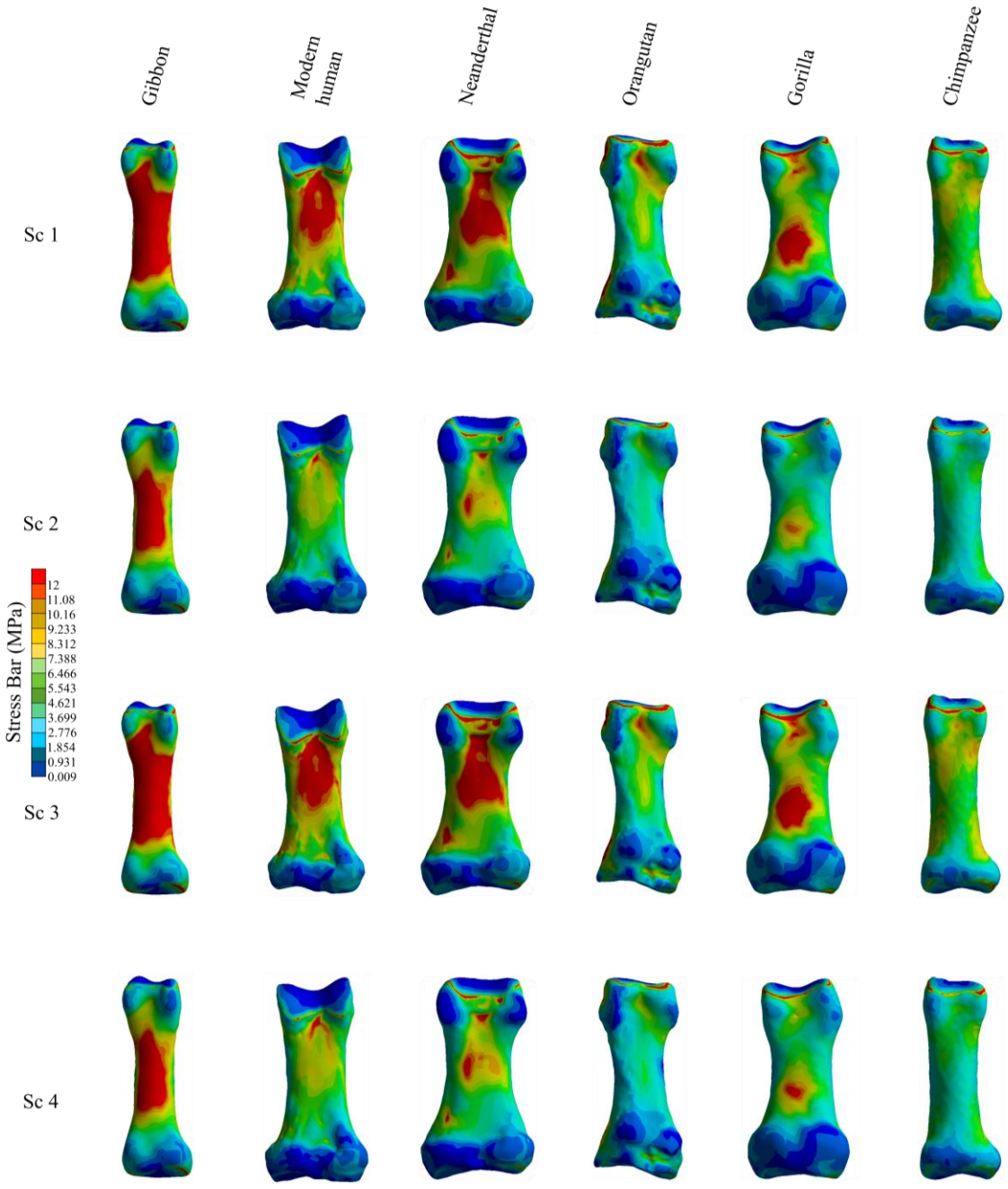

Figure 3 Von Mises stress maps for all analyzed species under different loading scenarios using the extant human as reference to scale the simulated muscular forces in all other specimens. Species are ordered from higher to lower peak stresses values. Phalanges are shown at the same length. MPa bar is set at 12 MPa.

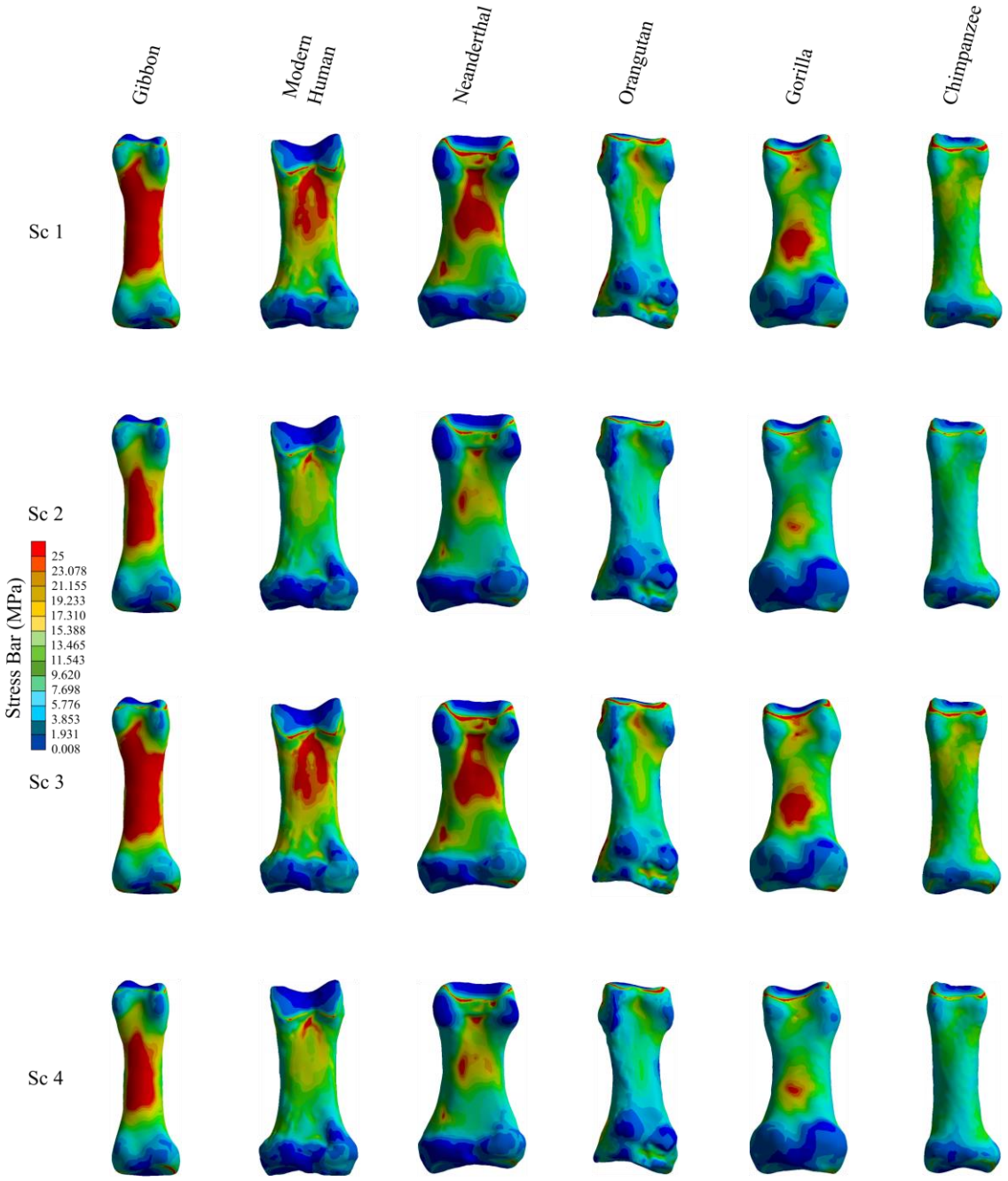

Figure 4 Von Mises stress maps for all analyzed species under different loading scenarios using the chimpanzee as reference to scale the simulated muscular forces in all other specimens. Species are ordered from higher to lower peak stresses values. Images are not scaled. MPa is set at 25 MPa.

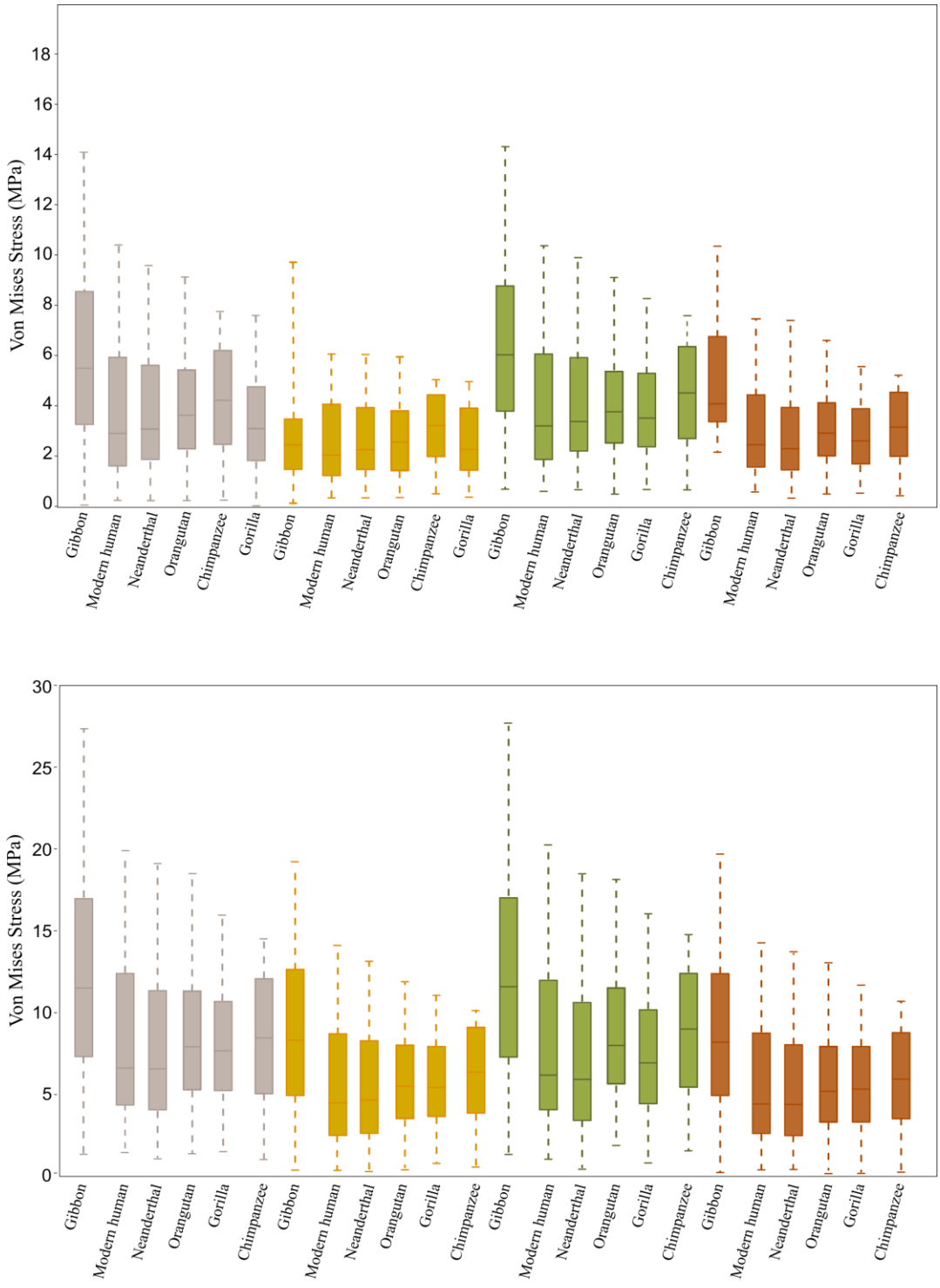

Figure 5 Box-plots of von Mises stress (MPa) distribution for all species under different scenarios, until Q95. The first row shows stress distribution of the models using the extant human as a reference to scale muscular forces in all other specimens, whereas the second one shows the results when the chimpanzee is+ used as a reference. Species are ordered from higher to lower peak stresses.

Discussion

The objective of this study was to assess stress distribution in the pollical proximal phalanx (PP1) of the active hand during the simulated use of hammerstones in different Hominoidea species. In the analyses, we varied the size of the hammerstone, the orientation of the tool relative to the hand, and the muscular properties to see their effects in stress distribution over the bone. We expected human PP1 to behave more efficiently in every scenario, as we assumed its greater adaptation to tool-related behaviors. However, we found that, in all cases, the human phalanx behaved as one among the most fragile bones, second only to the gibbon (Figs 3-5). Stress distribution in the human PP1 was uneven and its concentration at the center of the shaft indicates that it is less resistant to loads during forceful precision grip and is more prone to structural failure. These results indicate that non-human hominids (i.e., gorilla, chimpanzee and orangutan) can better withstand loads exerted during this activity as compared to humans, although other key anatomical characteristics, for instance finger proportions, facilitate this activity in the later (Napier, 1960; Rolian et al., 2011).

Our results suggest that stresses in the PP1 during tool-related behaviors were not the main driving force explaining the morphology of this bone, otherwise a different stress distribution would have very likely been observed in the human PP1. It is possible that the selective pressures acting on the thumb during stone tool production were not as consistently high to affect the morphology of this bone. Although other studies have found that the biomechanical stresses experienced by the thumb are high during this activity (Hamrick et al., 1998; Key and Dunmore, 2015; Marzke et al., 1998; Williams-Hatala et al., 2018), there is a noticeably high variability between individuals in the observed kinematics (Rein et al., 2014), muscle activity (Marzke et al., 1998), and manual pressures (Williams et al., 2012; Williams-Hatala et al., 2018). These results raise the possibility that there were other stronger selective pressures acting on the PP1 that may not be related to stone-tool use. The argument that the evolution of the human hand was driven by selective pressures other than manipulative capabilities has been introduced in some previous studies (Alba et al., 2003; Almécija et al., 2010; Heldstab et al., 2016; Rolian et al., 2010). Specifically, the concept that the evolution of thumbs is linked to the evolution of toes (Rolian, 2009; Rolian et al., 2010), thus to locomotor functions, which imply higher biomechanical demands than manipulation.

Accordingly, locomotor functions would represent the primarily selective pressures shaping feet and hands in primates, including humans.

Even though the mean (MWM) and median (MWAM) stress values of humans were found relatively similar to those of non-human hominoids (i.e., gorilla, chimpanzee and orangutan) (Fig. 5), the poor stress distribution observed on the human representative resulted in a more fragile PP1. The variation in the distribution of stress among the specimens is probably related to differences in the morphology of the PP1 (Figs 3 and 4). Future analyses deepen the relation between PP1 morphology and stress distribution under stone tool use conditions might shed some light into this link. Previous studies provide some guidance to this problem, as anatomical variations in hand morphology and structure within and among primates has been described, notably with respect to cortices thickness (Susman, 1979; Tsegai et al., 2017), trabecular bone organisation (Chirchir et al., 2015; Lazenby et al., 2011; Matarazzo; 2015; Skinner et al., 2015; Stephens et al., 2016), external dimensions and proportions (Key and Lycett, 2018; Napier, 1962; Susman, 1979), and joint surface shape (Marchi et al., 2017; Tocheri et al., 2003, 2005).

Does the force scaling of the non-human sample affect these results? While comprehensive knowledge is available about human muscles (e.g., Diogo et al., 2012b; Marzke et al., 1998; Tuttle, 1969) and, to a lesser extent, in chimpanzees (Kikuchi, 2010; Marzke et al, 1999), there are no analogous studies about the levels of muscular forces and activation patterns during the use of hammerstones for the other primate taxa considered here. To solve this problem, following Marcé-Nogué et al. (2013) and Fortuny et al. (2015), we scaled the muscular forces in the non-human hominins using the human and chimpanzee data as a reference, which allowed us to compare the behaviors of the PP1 from species that differ in size and morphology. In spite of this assumption, what makes the human (and gibbon) PP1 fragile is the stress distribution along the bone, which in this comparative analysis is not affected by the level of activation of the muscles. This becomes apparent when results from the two muscle scaling scenarios (human and chimpanzee) are compared: while stress values increase when using the chimpanzee muscles as reference, the stress distribution was very similar to the human scaling reference (Figs 3-5).

A validation of FEA results against experimental data to see how precisely and accurately they reflect reality was not performed. Assumptions in our study for the non-human sample are related to muscle properties (tendon angles and forces), muscle activation patterns, and muscle function. Although detailed scenarios for each

non-human representative would be ideal in such kind of analyses, these simplifications were necessary to evaluate the performance of each specimen which are difficult to access, such as muscle activation patterns during hammer use. Therefore, simulations were used to extract general patterns between species and should be interpreted in a comparative framework. This comparative approach has been successfully applied in several other studies using FEA (e.g., Marcé-Nogué et al., 2017; Püschel and Sellers, 2016; Serrano-Fochs et al., 2015).

Conclusions

Non-human hominids (i.e., gorilla, chimpanzee and orangutan) can better withstand loads exerted during simulations of hard hammer percussion than humans. Among extant Hominoidea, the human PP1s were relatively fragile at the moment of strike. Our results suggest that in humans the forces exerted during forceful precision gripping did not act as a strong selective pressure affecting the morphology of the first pollical phalanx.

Supplementary data

Supplementary data (Tables S1-S3) associated with this article can be found in the Appendix.

Acknowledgements

We want to thank the University of Barcelona's body donation service, especially Cristina Manzanares, Juan Antonio Camara, José Luis Ramón Cayuela, and Gemma Ramón Cayuela for their assistance. We are grateful to Dr. Tracy Kivell who gave us the micro-CT data of the orangutan phalanx and to the Senckenberg Museum in Frankfurt, where this specimen is housed. We are also grateful to Clément Zanolli for the translation into French. We acknowledge NESPOS, and KUPRI for the CT scans of the non-human primates used in this study and the original providers of the material: Tennoji Zoo, Fukuoka City Zoo and the Fukuchiyama City Zoo. This work was supported by the General Directorate of Research of the Spanish Ministry of Science and Technology (MICINN-FEDER: grant number PGC2018-093925-B-C32); the

Government of Catalonia (AGAUR: grant number 2017SGR 1040); the URV Project 2016 PFR-URV-B2-17; the Becas Chile Program of the Chilean National Commission for Scientific and Technological Research (CONICYT); the DFG, German Research Foundation (grant number KA 1525/9-2); and the Government of Catalonia's CERCA program. T.A.P was funded by the Leverhulme Trust Early Career Fellowship (grant number ECF-2018-264).

References

Alba, D.M., Moyà-Solà, S., Köhler, M., 2003. Morphological affinities of the *Australopithecus afarensis* hand on the basis of manual proportions and relative thumb length. J. Hum. Evol. 44, 225-254.

Almécija, S., Moyà-Solà, S., Alba, D.M., 2010. Early origin for human-like precision grasping: A comparative study of pollical distal phalanges in fossil hominins. PLoS One 5, e11727.

Bardo, A., Cornette, R., Borel, A., Pouydebat, E., 2017. Manual function and performance in humans, gorillas, and orangutans during the same tool use task. Am. J. Phys. Anthropol. 164, 1-16.

Butz, K.D., Merrell, G., Nauman, E.A., 2012. A three-dimensional finite element analysis of finger joint stresses in the MCP joint while performing common tasks. Hand, 7, 341-345.

Chirchir, H., Kivell, T.L., Ruff, C.B., Hublin, J.J., Carlson, K.J., Zipfel, B., Richmond, B.G., 2015. Recent origin of low trabecular bone density in modern humans. Proc. Natl. Acad. Sci. USA 112, 366-371.

Cignoni, P., Callieri, M., Corsini, M., Dellepiane, M., Ganovelli, F., Ranzuglia, G., 2008. Meshlab: An open-source mesh processing tool. Version 1.3.2. Meshlab Visual Computing Lab, Pisa.

Diogo, R., Potau, J.M., Pastor, J.F., de Paz, F.J., Ferrero, E.M., Bello, G., Barbosa, M., Wood, B.A., 2011. Photographic and descriptive musculoskeletal atlas of Gorilla: With notes on the attachments, variations, innervation, synonymy and weight of the muscles. Science Publishers, Enfield.

Diogo, R., Potau, J.M., Pastor, J.F., de Paz, F.J., Ferrero, E.M., Bello, G., Barbosa, M., Aziz, M.A., Burrows, A.M., Arias-Martorell, J., Wood, B.A., 2012a. Photographic and descriptive musculoskeletal atlas of Gibbons and Siamangs (*Hylobates*): With notes on the attachments, variations, innervation, synonymy and weight of the muscles. CRC Press, St. Helier.

Diogo, R., Potau, J.M., Pastor, J.F., de Paz, F.J., Ferrero, E.M., Bello, G., Barbosa, M., Aziz, M.A., Burrows, A.M., Arias-Martorell, J., Wood, B., 2013a. Photographic and Descriptive Musculoskeltal Atlas of Chimpanzees: With notes on the attachments, variations, innervation, synonymy and weight of the muscles. CRC Press, Boca Raton.

Diogo, R., Potau, J.M., Pastor, J.F., de Paz, F.J., Ferrero, E.M., Bello, G., Barbosa, M., Aziz,

M.A., Arias-Martorell, J., Wood, B.A., 2013b. Photographic and Descriptive Musculoskeltal Atlas of Orangutans: With notes on the attachments, variations, innervation, synonymy and weight of the muscles. CRC Press, Boca Raton.

Diogo, R., Richmond, B.G., Wood, B., 2012b. Evolution and homologies of primate and modern human hand and forearm muscles, with notes on thumb movements and tool use. J. Hum. Evol. 63, 64-78.

Doblaré, M., Garcı´a, J.M., Gómez, M.J.J., 2004. Modelling bone tissue fracture and healing: A review. Eng. Fract. Mech. 71, 1809-1840.

Dumont, E.R., Grosse, I.R., Slater, G.J., 2009. Requirements for comparing the performance of finite element models of biological structures. J. Theor. Biol. 256, 96-103.

Foley, R., Lahr, M.M., 2003. On stony ground: Lithic technology, human evolution, and the emergence of culture. Evol. Anthropol. 12, 109-122.

Fortuny, J., Marcé-Nogué, J., Heiss, E., Sanchez, M., Gil, L., Galobart, À., 2015. 3D bite modeling and feeding mechanics of the largest living amphibian, the Chinese giant salamander *Andrias davidianus* (Amphibia: Urodela). PLoS One 10, e0121885.

Gommery, D., Senut, B., 2006. The terminal thumb phalanx of *Orrorin tugenensis* (Upper Miocene of Kenya). Geobios 39, 372-384.

Green, D.J., Gordon, A.D., 2008. Metacarpal proportions in *Australopithecus africanus*. J. Hum. Evol. 54, 705-719.

Gumert, M.D., Malaivijitnond, S., 2013. Long-tailed macaques select mass of stone tools according to food type. Philos. Trans. Royal Soc. B 368, 20120413.

Hamrick, M.W., Churchill, S.E., Schmitt, D., Hylander, W.L., 1998. EMG of the human flexor pollicis longus muscle: Implications for the evolution of hominid tool use. J. Hum. Evol. 34, 123-136.

Heldstab, S.A., Kosonen, Z.K., Koski, S.E., Burkart, J.M., Van Schaik, C.P., Isler, K., 2016. Manipulation complexity in primates coevolved with brain size and terrestriality. Sci. Rep. 6, 24528.

Hunt, K.D., 2004. The special demands of great ape locomotion and posture. In: Russon, A.E., Begun, D.R. (Eds), The evolution of thought: Evolutionary origins of great ape intelligence. Cambridge University Press, Cambridge, pp. 172-189.

Jouffroy, F.K., Godinot, M., Nakano, Y., 1991. Biometrical characteristics of primate hands. In: Preuschoft, H. (Ed.), Hands of primates. Springer-Verlag, Wien, pp. 133-171.

Key, A.J.M., Dunmore, C.J., 2015. The evolution of the hominin thumb and the influence exerted by the non-dominant hand during stone tool production. J. Hum. Evol. 78, 60-69.

Key, A.J., Dunmore, C.J., 2018. Manual restrictions on Palaeolithic technological behaviours. PeerJ 6, e5399.

Key, A.J., Lycett, S.J., 2018. Investigating interrelationships between Lower Palaeolithic stone

tool effectiveness and tool user biometric variation: Implications for technological and evolutionary changes. Archaeol. Anthrop. Sci. 10, 989-1006.

Kikuchi, Y., 2010. Comparative analysis of muscle architecture in primate arm and forearm. J. Vet. Med. 39, 93-106.

Kivell, T.L., Lemelin, P., Richmond, B.G., Schmitt D., (Eds), 2016. The evolution of the primate hand: Anatomical, developmental, functional and paleontological evidence. Springer, New York.

Lautenschlager, S., 2016. Reconstructing the past: Methods and techniques for the digital restoration of fossils. Roy. Soc. Open Sci. 3, 160342.

Lazenby, R.A., Skinner, M.M., Hublin, J.J., Boesch, C., 2011. Metacarpal trabecular architecture variation in the chimpanzee (*Pan troglodytes*): Evidence for locomotion and tool-use? Am. J. Phys. Anthropol. 144, 215-225.

Maier, M.A., Hepp-Reymond, M.C., 1995. EMG activation patterns during force production in precision grip - II. Muscular synergies in the spatial and temporal domain. Exp. Brain Res. 103, 123-136.

Marcé-Nogué, J., DeMiguel, D., Fortuny, J., de Esteban-Trivigno, S., Gil, L., 2013. Quasi-homothetic transformation for comparing the mechanical performance of planar models in biological research. Palaeontol. Electron. 16, 1-15.

Marcé-Nogué, J., De Esteban-Trivigno, S., Escrig, C., Gil, L., 2016. Accounting for differences in element size and homogeneity when comparing Finite Element models: Armadillos as a case study. Palaeontol. Electron. 19, 1-22.

Marcé-Nogué, J., Fortuny, J., Gil, L., Sánchez, M., 2015. Improving mesh generation in finite element analysis for functional morphology approaches. Spanish J. Palaeo. 30, 117-132.

Marcé-Nogué, J., Püschel, T.A., Kaiser, T.M., 2017. A biomechanical approach to understand the ecomorphological relationship between primate mandibles and diet. Sci. Rep. 7, 8364.

Marchi, D., Proctor, D.J., Huston, E., Nicholas, C.L., Fischer, F., 2017. Morphological correlates of the first metacarpal proximal articular surface with manipulative capabilities in apes, humans and South African early hominins. Comptes Rendus Palevol 16, 645-654.

Marcy, A.E., Fruciano, C., Phillips, M.J., Mardon, K., Weisbecker, V., 2018. Low resolution scans can provide a sufficiently accurate, cost-and time-effective alternative to high resolution scans for 3D shape analyses. PeerJ 6, e5032.

Marzke, M.W., 2013. Tool making, hand morphology and fossil hominins. Philos. Trans. Royal Soc. B 368, 20120414.

Marzke, M.W., Marzke, R.F., Linscheid, R.L., Smutz, P., Steinberg, B., Reece, S., An, K.N., 1999. Chimpanzee thumb muscle cross sections, moment arms and potential torques, and comparisons with humans. Am. J. Phys. Anthropol. 110, 163-178.

Marzke, M.W., Toth, N., Schick, K., Reece, S., 1998. EMG study of hand muscle recruitment during hard hammer percussion manufacture of Oldowan tools. Am. J. Phys. Anthropol.

105, 315-332.

Matarazzo, S., 2013. Manual pressure distribution patterns of knuckle-walking apes. Am. J. Phys. Anthropol. 152, 44-50.

Matarazzo, S.A., 2015. Trabecular architecture of the manual elements reflects locomotor patterns in primates. PLoS One 10, e0120436.

McCurry, M.R., Evans, A.R., McHenry, C.R., 2015. The sensitivity of biological finite element models to the resolution of surface geometry: a case study of crocodilian crania. PeerJ 3, e988.

Napier, J.R., 1960. Studies of the hands of living primates. Proc. Zool. Soc. Lond. 134, 647-657.

Napier, J.R., 1962. Fossil hand bones from Olduvai Gorge. Nature 196, 952-953.

Niewoehner, W.A., 2001. Behavioral inferences from the Skhul/Qafzeh early modern human hand remains. Proc. Natl. Acad. Sci. USA 98, 2979-2984.

Pruetz, J.D., Bertolani, P., 2007. Savanna chimpanzees, *Pan troglodytes verus*, hunt with tools. Curr. Biol. 17, 412-417.

Püschel, T.A., Sellers, W.I., 2016. Standing on the shoulders of apes: Analyzing the form and function of the hominoid scapula using geometric morphometrics and finite element analysis. Am. J. Phys. Anthropol. 159, 325-341.

Rayfield, E., 2007. Finite element analysis and understanding the biomechanics and evolution of living and fossil organisms. Annu. Rev. Earth Planet. Sci. 35, 541-576.

Rein, R., Nonaka, T., Bril, B., 2014. Movement pattern variability in stone knapping: implications for the development of percussive technologies. PLoS One 9, e113567.

Rolian, C., 2009. Integration and evolvability in primate hands and feet. Evol. Bio. 3536, 100-117.

Rolian, C., Lieberman, D.E., Hallgrímsson, B., 2010. The coevolution of human hands and feet. Evolution 64, 1558-1568.

Rolian, C., Lieberman, D.E., Zermeno, J.P., 2011. Hand biomechanics during simulated stone tool use. J. Hum. Evol. 61, 26-41.

Sacks, R.D., Roy, R.R., 1982. Architecture of the hind limb muscles of cats: Functional significance. J. Morphol. 173, 185-195.

Samuel, D.S., Nauwelaerts, S., Stevens, J.M., Kivell, T.L., 2018. Hand pressures during arboreal locomotion in captive bonobos (*Pan paniscus*). J. Exp. Biol. 221, jeb170910.

Serrano-Fochs, S., De Esteban-Trivigno, S., Marcé-Nogué, J., Fortuny, J., Fariña, R.A. 2015., Finite element analysis of the Cingulata jaw: An ecomorphological approach to armadillo's diets. PloS One 10, e0120653.

Shrewsbury, M.M., Marzke, M.W., Linscheid, R.L., Reece, S.P., 2003. Comparative morphology of the pollical distal phalanx. Am. J. Phys. Anthropol. 121, 30-47.

Skinner, M.M., Stephens, N.B., Tsegai, Z.J., Foote, A.C., Nguyen, N.H., Gross, T., Pahr, D.H., Hublin, J.-J., Kivell, T.L., 2015. Human-like hand use in *Australopithecus africanus*. Science 347, 395-399.

Slizewski, A., Friess, M., Semal, P., 2010. Surface scanning of anthropological specimens: Nominal-actual comparison with low cost laser scanner and high end fringe light projection surface scanning systems. Quartär 57, 179-187.

Stephens, N.B., Kivell, T.L., Gross, T., Pahr, D.H., Lazenby, R.A., Hublin, J.J., Hershkovitz, I., Skinner, M.M., 2016. Trabecular architecture in the thumb of *Pan* and *Homo*: implications for investigating hand use, loading, and hand preference in the fossil record. Am. J. Phys. Anthropol. 161, 603-619.

Susman, R.L., 1979. Comparative and functional morphology of hominoid fingers. Am. J. Phys. Anthropol. 50, 215-236.

Susman, R.L., 1988. New postcranial remains from Swartkrans and their bearing on the functional morphology and behavior of *Paranthropus robustus*. In: Grine, F.E. (Ed.), The evolutionary history of the "robust" australopithecines. Aldine de Gruyter, New York, pp. 149-172.

Susman, R.L., Stern, J.T., 1979. Telemetered electromyography of flexor digitorum profundus and flexor digitorum superficialis in *Pan troglodytes* and implications for interpretation of the O. H. 7 hand. Am. J. Phys. Anthropol. 50, 565-574.

Tocheri, M.W., Marzke, M.W., Liu, D., Bae, M., Jones, G.P., Williams, R.C., Razdan, A., 2003. Functional capabilities of modern and fossil hominid hands: Three-dimensional analysis of trapezia. Am. J. Phys. Anthropol. 122, 101-112.

Tocheri, M.W., Orr, C.M., Jacofsky, M.C., Marzke, M.W., 2008. The evolutionary history of the hominin hand since the last common ancestor of *Pan* and *Homo*. J. Anat. 212, 544-562.

Tocheri, M.W., Razdan, A., Williams, R.C., Marzke, M.W., 2005. A 3D quantitative comparison of trapezium and trapezoid relative articular and nonarticular surface areas in modern humans and great apes. J. Hum. Evol. 49, 570-586.

Tsegai, Z.J., Stephens, N.B., Treece, G.M., Skinner, M.M., Kivell, T.L., Gee, A.H., 2017. Cortical bone mapping: an application to hand and foot bones in hominoids. Comptes Rendus Palevol 16, 690-701.

Tuttle, R.H., 1969. Quantitative and functional studies on the hands of the Anthropoidea. J. Morphol. 128, 309-363.

Visalberghi, E., Sirianni, G., Fragaszy, D., Boesch, C., 2015. Percussive tool use by Taï Western chimpanzees and Fazenda Boa Vista bearded capuchin monkeys: A comparison. Philos. Trans. Royal Soc. B 370, 20140351.

Walmsley, C.W., Smits, P.D., Quayle, M.R., McCurry, M.R., Richards, H.S., Oldfield, C.C., Wroe, S., Clausen, P.D., McHenry, C.R., 2013. Why the long face? The mechanics of mandibular symphysis proportions in crocodiles. PLoS One 8, e53873.

Williams, E.M., Gordon, A.D., Richmond, B.G., 2012. Hand pressure distribution during Oldowan stone tool production. J. Hum. Evol. 62, 520-532.

Williams-Hatala, E.M., Hatala, K.G., Gordon, M., Key, A., Kasper, M., Kivell, T.L., 2018. The manual pressures of stone tool behaviors and their implications for the evolution of the human hand. J. Hum. Evol. 119, 14-26.

Wunderlich, R.E., Jungers, W.L., 2009. Manual digital pressures during knuckle-walking in chimpanzees (*Pan troglodytes*). Am. J. Phys. Anthropol. 139, 394-403.

Wynn, T., Hernandez-Aguilar, R.A., Marchant, L.F., McGrew, W.C., 2011. "An ape's view of the Oldowan" revisited. Evol. Anthropol. 20, 181-197.

Wynn, T., McGrew, W.C., 1989. An ape's view of the Oldowan. Man 24, 383-398.

Young, R.W., 2003. Evolution of the human hand: The role of throwing and clubbing. J. Anat. 202, 165-174.

Preprints (www.preprints.org) | NOT PEER-REVIEWED | Posted: 27 April 2020 doi:10.20944/preprints202004.0474.v1

Modularity of the Wrist in Extant Hominids

Ana Bucchi[1,2], Thomas A. Püschel[3], Antonio Profico[4], Carlos Lorenzo[1,2]

[1]Universitat Rovira i Virgili, Departament d'Història i Història de l'Art, Avinguda de Catalunya 35, 43002 Tarragona, Spain.

[2]Institut Català de Paleoecologia Humana i Evolució Social (IPHES), Zona Educacional 4, Campus Sescelades URV (Edifici W3), 43007 Tarragona, Spain

[3]Primate Models for Behavioural Evolution Lab, Institute of Cognitive and Evolutionary Anthropology, School of Anthropology, University of Oxford, 64 Banbury Road, OX2 6PN, Oxford, United Kingdom.

[4]PaleoHub, University of York, Wentworth Way Heslington, YO10 5NG York, United Kingdom

Correspondence: Ana Bucchi, Universitat Rovira i Virgili, Departament d'Història i Història de l'Art, Tarragona, Spain. email: anabucchi@gmail.com

Abstract

Wrist shape varies greatly across primates and previous studies indicate that the numerous morphological differences among them are related to a complex mixture of phylogeny and function. However, little is known about whether the variation in these various anatomical differences is linked and to what extent the wrist bones vary independently. Here, we used 3D geometric morphometrics on a sample of extant hominids (*Homo sapiens, Pan troglodytes, Gorilla gorilla,* and *Gorilla beringei*), to find the model that best describes the covariation patterns among four of the eight carpals (i.e., capitate, lunate, scaphoid, and trapezium). For this purpose, 15 modular hypotheses were tested using the Covariation Coefficient. Results indicate that there is a covariation structure common to all hominids, which corresponds to stronger covariation within each carpal as compared to the covariation between carpals. However, the results also indicate that that there is a degree of codependence in the variation of some carpals, which is unique in humans, chimpanzees, and gorillas, respectively. In humans there is evidence of associated shape changes between the lunate and capitate, and between the scaphoid and trapezium. This covariation between lunate and capitate is also apparent in gorillas, while chimpanzees display the greatest disassociation among carpals, showing low covariation values in all pairwise comparisons. Our analyses indicate that carpals have an important level of variational independence which might suggest a high degree of independent evolvability in the wrists of hominids, and that although weak, the structure of associated changes of these four carpals varies across genera. To our knowledge this is the first report on the patterns of modularity between these four wrist bones in the Homininae and future studies might attempt to investigate whether the anatomical shape associations among carpals are functionally related to locomotion and manipulation.

Key words: modularity; trait covariation; wrist; hominids

Introduction

The wrist in hominids is composed of eight bones with complex shapes and numerous joint surfaces, which allow the hand to move along multiple axes (Kivell et al., 2016). Genetically, a common Hox gene expression regulates the development of the hand in anthropoids (Reno et al., 2008), yet carpals also have a degree of functional and evolutionary independence (Tocheri et al., 2003; Kivell et al., 2013). This functional and evolutionary independence may explain why carpal morphology varies so greatly across taxa (Tocheri et al., 2005; Marzke et al., 2010; Orr, 2017).

Among primates, humans exhibit a derived carpal morphology (Kivell et al., 2016), which previous studies suggest evolved as a consequence of relaxed locomotor pressures with the advent of bipedalism and as an adaptation to tool making and use (Hamrick et al., 1998; Williams et al., 2010; Key and Dunmore, 2015; Skinner et al., 2015; Kivell et al., 2016). Wrist morphology in humans contributes significantly to stone tool-making performance (Tocheri et al., 2003; Marzke et al., 2010; Williams et al., 2010, 2014), and some carpal features in humans that have been thought to be beneficial for this activity include the size, orientation, and degree of curvature of joint surfaces at the trapezium, capitate, and radiocarpal joints (Marzke, 1983, 1997; Niewoehner et al., 1997; Richmond and Strait, 2000; Tocheri et al., 2003, 2005; Marzke et al., 2010; Williams et al., 2010, 2014; Orr, 2017). The characteristic joint surfaces in the human wrist allow for increased accuracy (Williams et al., 2014) and mechanical work at the joint during stone tool production (Williams et al., 2010). They also allow toolmakers to effectively resist and transmit both axial and oblique joint reaction forces generated by power and precision grips as compared to the rest of the extant apes (Marzke, 1983; Niewoehner et al., 1997). Conversely, the wrist in chimpanzees and gorillas seems better adapted to locomotor demands, by contributing to better stabilization at the joint (Tuttle, 1967; Richmond and Strait, 2000) and by allowing the joint to better withstand the stresses imposed by knuckle walking (Püschel et al., 2020).

Several previous studies have analyzed single bones and specific joint surfaces with the aim of inferring the functional capabilities that set apart hominins from non-human primates (e.g., Tocheri et al., 2003, 2005; Marzke et al., 2010; Kivell, 2011). However, with some exceptions (Williams, 2010; Peña, 2018), there are almost no studies analyzing whether the numerous shape variations in wrist bones are associated or independent with respect to each other. Peña (2018) proposes that the level of integration of the wrist is higher in some primate genera (i.e., *Pongo*) than others, suggesting that specific covariation patterns may be shaping the evolution of this structure in primates. For humans, previous studies indicate that the morphological integration of autopods is lower than in quadrupeds, making the human hand more evolvable (Rolian, 2009; Rolian et al., 2010; Young et al., 2010). However, Williams (2010) indicates that the patterns of integration of the capitate and third metacarpal are more similar between humans and gorillas than between gorillas and chimpanzees, and that knuckle-walkers are not characterized by highly integrated morphologies.

 doi:10.20944/preprints202004.0474.v1

The mutual relationships between bony elements of a single structure are best studied within the framework of modularity as they allow us to know how flexible the evolution of this anatomical region is under differing functional demands. If all carpals behave as a single entity that is tightly integrated by strong interactions, they should comprise a module (Klingenberg, 2008; Esteve-Altava, 2017), thus causing wrist bones to covary strongly. Conversely, if more than one module is present in the wrist, this should cause carpals in different modules to vary independently. It is currently unknown how many modules there are in the primate wrist, and how strong the modular signal is.

Our analysis intends to address the question of how independent the variation within the wrist is by analyzing the modularity pattern of four carpals in extant hominids (i.e., the capitate, trapezium, lunate, and scaphoid). As far as we know, this is the first time that the covariation structure for these bones has been reported for modern humans (*Homo sapiens*), chimpanzees (*Pan troglodytes*), and gorillas (*Gorilla gorilla* and *Gorilla beringei*). 3D models and geometric morphometrics were used for this purpose, and modularity was investigated through the testing procedure proposed by Adams and Collyer (2019), known as the covariance ratio effect sizes (Z_{CR} and $\hat{Z}12$). We tested 15 different modular hypotheses combining all possible partitions of the wrist bones and selected the one that best describes the covariation structure in hominids as a whole, and in humans, chimpanzees, and gorillas in particular. In doing so, we try to answer two main questions: a) what is the modularity pattern of these four bones in living hominids? and b) is the observed covariation pattern shared across the analyzed taxa? We hypothesize that humans exhibit a pattern of covariation that distinguishes them from African apes, based on previous studies suggesting that manipulation has driven the evolution of the wrist in humans (e.g., Williams et al., 2010; Key and Dunmore, 2015; Skinner et al., 2015), while in apes its better adapted for locomotion (e.g., Richmond and Strait, 2000; Püschel et al., 2020).

Materials and methods

Primate sample

The sample comprises 478 bones from three primate genera: 50 modern humans (*Homo sapiens*), 41 chimpanzees *(Pan troglodytes)*, and 41 gorillas (19 *Gorilla gorilla* and 22 *Gorilla beringei*) (Table 1). 3D models came from different sources. All human surface models were obtained using a Breuckmann SmartSCAN structured light scanner (Breuckmann Inc.). Most non-human primate surface models were generated via photogrammetry (further details can be found in Bucchi et al., 2020), while CT scans of 23 ape hands were accessed from two different digital repositories: Morphosource (www.morphosource.org) and the Museum of Primatology (https://carta.anthropogeny.org/).

The resolutions of micro-CT, surface scanner, and photogrammetric models have been previously tested and found to be comparable (Giacomini et al., 2019) thus allowing us to combine these data types in our analyses. The human hands belonged to a medieval cemetery (Burgos, Spain) (Casillas García and

Preprints (www.preprints.org) | NOT PEER-REVIEWED | Posted: 27 April 2020 doi:10.20944/preprints202004.0474.v1

Adán Álvarez, 2005) and the non-human sample were of different origins (wild shot, in captivity, and of unknown provenance). Right hands were preferred. Most of the wrists included the four carpals under analysis, and when there were some missing bones, their antimeres, when present, were reflected using the 'Flip and/or Swap axis' and 'Invert faces orientation' tools in Meshlab software (v. 2020.02) (Cignoni et al., 2008).

We analyzed the morphology of four carpals (i.e., the capitate, trapezium, lunate, and scaphoid), although not all individuals had all of these bones (some elements were missing in some cases; further details can be found in Table 1 and in Supp. Table S1).

Table 1 The study sample. UBU: Universidad de Burgos, AM: AfricaMuseum, IPHES: Catalan Institute of Human Palaeoecology and Social Evolution, MZB: Natural Sciences Museum in Barcelona, and ZSM: Zoological State Collection in Munich.

Species	Specimens	Carpal bones				Sex			Collection
		TM	SC	CA	LU	Male	Female	Unknown	
Homo sapiens	50	40	39	41	42	25	25	0	UBU
Pan troglodytes	41	38	41	40	38	16	14	11	AM, ZMB, ZCM, Morphosource, Museum of Primatology
Gorilla beringei	22	22	22	22	21	10	9	3	
Gorilla gorilla	19	17	18	19	18	5	5	9	
Total	110	117	120	122	119	56	53	24	

Landmark configuration

We acquired five fixed landmarks per bone (Fig. 1 and Table 2). Landmark coordinates were imported into R using the *Arothron* package version 1.1.1 (Profico et al., 2018) in R 1.2.5019 (R Core Team, 2019). A generalized Procrustes analysis (GPA) was then performed separately for each bone in order to normalize for location, rotation, and scale. Corrected coordinates were then compiled into a new dataframe, and hypotheses of modularity were tested (see below).

Allometry

Taxonomic differences in size can affect the pattern and magnitude of modularity (Klingenberg and Marugán-Lobón, 2013). Therefore, we tested for allometric signals in the data by using a regression of Procrustes shape variables on centroid size. This test was performed with the *procD.lm()* function of

 doi:10.20944/preprints202004.0474.v1

the *geomorph* package, version 3.2.1 (Adams et al., 2019). Note that in order to have balanced sample sizes, this and all further statistical analyses were carried out by pooling both gorilla species together.

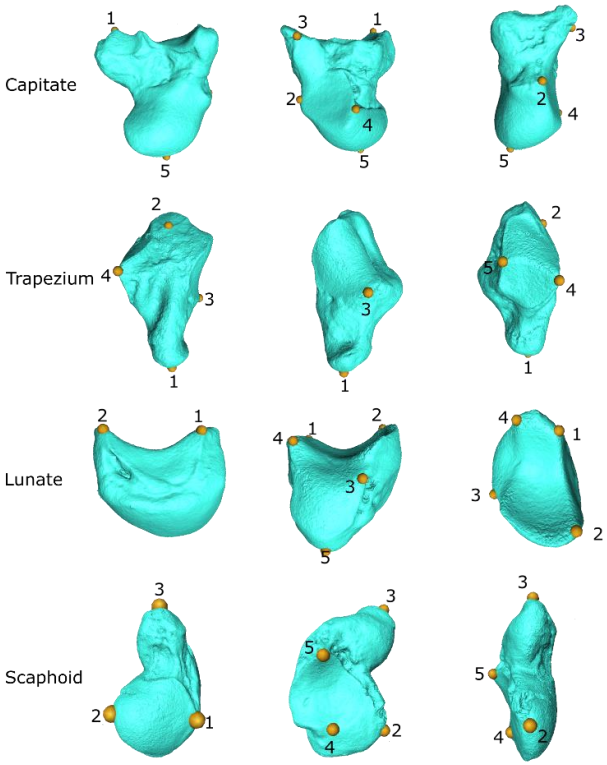

Figure 1 The landmark configuration shown on specimen AM 998 (*Gorilla beringei*) for the capitate, trapezium, lunate, and scaphoid bones. Landmark definitions are provided in Table 2.

Modular hypotheses

We tested 15 different hypotheses of modularity corresponding to all possible partitions of the sample (Table 3). We defined one four-module model (H1), seven two-module models (H2-8), six three-module models (H9-H14), and one single-module model. The optimal modular hypothesis for the wrist was assessed by measuring the strength of covariation for each modular hypothesis with the covariance ratio (CR) (Adams, 2016) and then statistically comparing alternative modular hypotheses with the covariance ratio effect sizes *(Z_{CR} and $\hat{Z}12$)* (Adams and Collyer, 2019).

Covariance ratio (CR)

The covariance ratio (CR) (Adams, 2016) was computed to measure the degree of modular signal in two or more *a priori* modules of Procrustes shape variables. The CR coefficient calculates the ratio of the overall covariation between modules relative to the overall covariation within modules (Adams,

 doi:10.20944/preprints202004.0474.v1

2016). The CR coefficient ranges from 0 to positive values. CR values lower than 1 indicate low covariation between modules, and strong covariation otherwise. The significance of the CR coefficient is assessed via permutations. At each repetition, landmarks are randomly assigned to different modules and the CR coefficient is calculated. The original CR value is then compared to the CR distribution (Adams, 2016).

Table 2 Definitions of landmarks digitalized in this study.

Bone	Landmark	Position
Capitate	1	Most anterior point of the union between the facets for the second and third metacarpals.
	2	Most distal and posterior point of the union of the facets for the hamate and the lunate.
	3	Most distal point of the facet for the hamate.
	4	Most inferior and anterior point of the union of facets for the hamate and the lunate.
	5	Point of maximum curvature of the lunate-scaphoid facet.
Trapezium	1	Point of maximum curvature of the ridge of the trapezium.
	2	Most anterior point of the facet for the second metacarpal.
	3	Most lateral and proximal point of the facet for the first metacarpal.
	4	Most anterior point of the union between the facets for the trapezoid and the scaphoid.
	5	Most posterior point of the union between the facets for the trapezoid and the scaphoid.
Lunate	1	Most posterior and distal point of the facet for the scaphoid.
	2	Most anterior and distal point of the facet for the scaphoid.
	3	Most anterior point of the intersection between the facets for the triquetral and the hamate.
	4	Most posterior point of the intersection between the facets for the hamate and capitate.
	5	Point of maximum curvature of the facet for the radius.
Scaphoid	1	Most posterior point of the facet for the radius.
	2	Most anterior point for the facet for the radius.
	3	Point of maximum curvature of the tubercle of the scaphoid.
	4	Most medial point of the facet for the capitate.
	5	Most lateral point of the facet for the capitate.

Table 3 The 15 modular hypotheses tested in this study. CA=capitate, LU=lunate, SC=scaphoid, and TZM= trapezium.

Model hypotheses	Modules	Description
H1	CA-LU-SC-TZM	All carpals belong to different modules.
H2	CALU-SCTZM	The capitate and lunate belong to one module and the scaphoid and trapezium to another.
H3	CASC-LUTZM	The capitate and scaphoid belong to one module and the lunate and trapezium to another.
H4	CATZM-LUSC	The capitate and trapezium belong to one module and the lunate and scaphoid to another.
H5	CA-LUSCTZM	The capitate belongs to one module and the lunate, scaphoid, and trapezium to another.
H6	LU-CASCTZM	The lunate belongs to one module and the capitate, scaphoid, and trapezium to another.
H7	SC-CALUTZM	The scaphoid belongs to one module and the capitate, lunate, and trapezium to another.
H8	TZM-CALUSC	The trapezium belongs to one module and the capitate, lunate, and scaphoid to another.
H9	CALU-SC-TZM	There are three modules: one includes the capitate and lunate, the second includes the scaphoid, and the third includes the trapezium.
H10	CASC-LU-TZM	There are three modules: one includes the capitate and scaphoid, the second includes the lunate, and the third includes the trapezium.
H11	CATZM-LU-SC	There are three modules: one includes the capitate and trapezium, the second includes the lunate, and the third includes the scaphoid.
H12	LUSC-CA-TZM	There are three modules: one includes the lunate and scaphoid, the second includes the capitate, and the third includes the trapezium.
H13	LUTZM-CA-SC	There are three modules: one includes the lunate and trapezium, the second includes the capitate, and the third includes the scaphoid.
H14	SCTZM-CA-LU	There are three modules: one includes scaphoid and trapezium, the second includes the capitate, and the third includes the lunate.
H15	CALUSCTZM	All carpals belong to one module

Comparing the strengths of the modular signals (Z_{CR} and $\hat{Z}12$)

The covariance ratios effect size (Z_{CR}) is derived from the CR and is a standardized test statistic which ensures statistical compatibility with the CR (Adams and Collyer, 2019) (Table 1). When the observed CR is larger than expected under the null hypothesis of no modularity, the Z_{CR} exhibits greater negative values which indicates a stronger modular signal. Here, whether Z_{CR} values are statistically different from each other was evaluated using a two sample Z-score for comparing modular signals ($\hat{Z}_{12}$). Both metrics are needed to compare alternative modular hypotheses. Z_{CR} was calculated for all modular hypotheses and the model presenting the strongest modular signal (i.e., the lowest Z_{CR}) was selected as

Preprints (www.preprints.org) | NOT PEER-REVIEWED | Posted: 27 April 2020 doi:10.20944/preprints202004.0474.v1

the optimal modular hypothesis for all samples, and for each genus separately. Once the best hypothesis was identified, we also tested whether some genera displayed a greater degree of modularity than others. The CR, Z_{CR}, and $\hat{Z}_{12}$ were also calculated using the *modularity.test()* and *compare.CR()* functions of the *geomorph* R package (Adams et al., 2019).

All the data used in this study are available in Supplementary Material 1 (Table S1). These data comprise the landmark coordinates after Procrustes superimposition.

Results

Allometry

Regression analyses of Procrustes coordinates on centroid size produced non-significant results in all cases ($p>0.05$). Therefore, we excluded size as a factor contributing to variation in shape among the taxa studied here, and the following analyses were carried out using Procrustes coordinates and not 'size-corrected' variables (i.e., the residuals from the regressions of shape on centroid size).

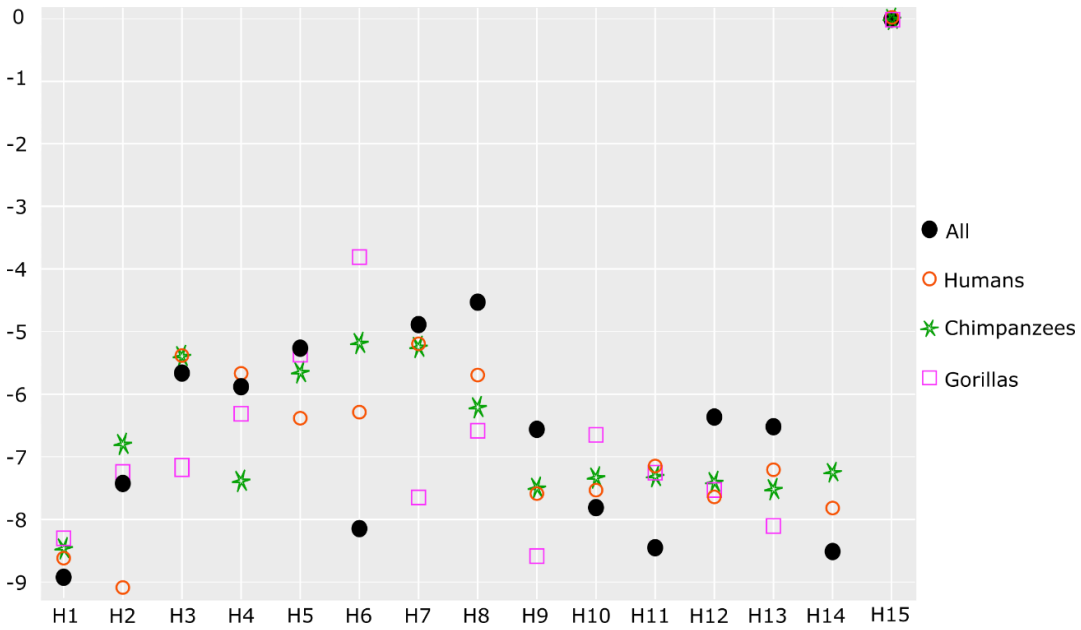

Figure 2 Effect sizes (Z_{CR}) for the covariance ratio (CR) for the 15 modular hypotheses for all samples, and for each genus separately. Hypotheses are described in Table 3. The exact Z_{CR} values are in Table 4 and the pairwise differences in ZCR ($\hat{Z}_{12}$) are in Tables S3-6.

 doi:10.20944/preprints202004.0474.v1

Optimal modular hypotheses for hominids.

The CRs of all hypotheses were significantly less than 1 (Table 4), indicating that regardless of how the bones are combined to create the alternative modular hypotheses there is a strong modular signal in the sample. When comparing all hypotheses, H1 for the whole sample exhibited the largest negative Z_{CR} (Fig. 2, Table 4) which was significantly different ($p<0.05$) from all the remaining hypotheses (Fig. 2, Table S6). H1 was thus selected as the best modularity model for hominids, which implies that each carpal represented is its own modular unit. However, except in chimpanzees (Fig. 2 and 3, Table 4), H1 was not the best modular model for each genus individually. In humans, H2 showed a larger negative Z_{CR} than H1 (Fig. 2, Table 4), although this difference was not significant ($\hat{Z}_{12}$=0.63, p=0.53) (Table S3). Model H2 implies that the capitate and lunate form a different module than that of the scaphoid and trapezium. In gorillas, H9 yielded a larger negative Z_{CR} than H1 (Fig. 2, Table 4), yet this difference was not statistically significant either ($\hat{Z}_{12}$=0.43, p=0.67) (Table S5). H9 groups the capitate and lunate in the same module, while the scaphoid and trapezium each belong to their own modules. Figure 3 depicts the optimal modular hypothesis for each genus.

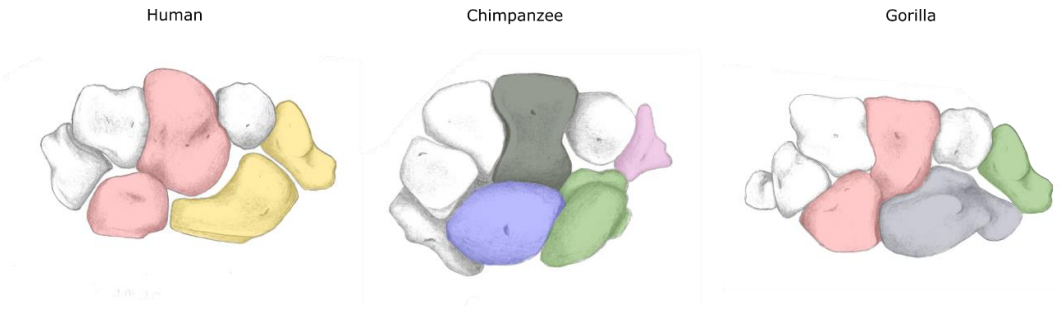

Figure 3 Illustration of the dorsal view of a left wrist showing the optimal modular hypothesis for humans (H2), chimpanzees (H1) and gorillas (H9). They were selected as they have the largest negative Z_{CR} values (Table 4). Hypotheses are described in Table 3.

To further explore the previous finding indicating possible variation in the modularity structure across taxa (Fig. 2), a pairwise modularity score ($\hat{Z}_{12}$) was calculated for every pair of carpals within each genus (Fig. 4). In humans, the modular signals between capitate and lunate, and between trapezium and scaphoid, was significantly lower ($p<0.05$) than those of the remaining pairs of carpals (capitate and trapezium, and lunate and trapezium). This might suggest that the lunate and capitate have a degree of morphological integration, as do the trapezium and scaphoid. Additionally, the modular signals between capitate and lunate in one module, and trapezium and scaphoid in another, were statistically similar ($\hat{Z}_{12}$=0.26, p=0.28) (Fig. 4). These findings are consistent with H2 being the model with the best fit for humans (Fig. 2 and 3). In chimpanzees, no pair of carpals exhibits a greater Z_{CR} than any other, which is also expected given that H1 is the optimal modular hypothesis for this genus. As for gorillas, the

capitate and trapezium show a significantly higher modular signal than the lunate and scaphoid ($\hat{Z}_{12}$= 2.14, p=0.03), which is consistent with the capitate belonging to a different module than the trapezium, as indicated by the hypothesis with the most negative Z_{CR} value (H9). Similarly, the only other significantly different modular signal in gorillas was between the capitate and trapezium, which is higher than that found for the capitate and lunate ($\hat{Z}_{12}$=1.90, p=0.05). Both results for gorillas are consistent with H9 being the best model for this genus. However, these results for gorillas do not exclude other hypotheses from being the best modular hypothesis (H1, H8, H10, H12, and H13, Table S5).

Table 4 Covariance ratio (CR) and effect sizes (Z_{CR}) for the modularity hypotheses in the hominid wrist. All CR are statistically significant at p<0.01. The Z_{CR} values are depicted in Figure 2 and the pairwise differences in ZCR ($\hat{Z}_{12}$) are in Tables S3-6. Hypotheses are described in Table 3.

Hypothess	All		Human		Chimpanzees		Gorillas	
	CR	Z_{CR}	CR	Z_{CR}	CR	Z_{CR}	CR	Z_{CR}
H1	0.64	-8.9	0.55	-8.6	0.57	-8.5	0.53	-8.3
H2	0.75	-7.4	0.56	-9.1	0.7	-6.9	0.63	-7.3
H3	0.81	-5.8	0.76	-5.4	0.76	-5.6	0.63	-7.2
H4	0.80	-5.9	0.74	-5.9	0.66	-7.4	0.64	-7.2
H5	0.75	-5.2	0.61	-6.3	0.67	-5.8	0.66	-5.3
H6	0.60	-8.1	0.62	-6.2	0.71	-5.2	0.76	-3.9
H7	0.77	-4.9	0.7	-5.1	0.71	-5.2	0.48	-7.7
H8	0.81	-4.5	0.66	-5.7	0.65	-6.1	0.56	-6.7
H9	0.81	-6.6	0.57	-7.7	0.6	-7.6	0.48	-8.6
H10	0.73	-7.9	0.59	-7.6	0.63	-7.3	0.61	-6.7
H11	0.65	-8.4	0.6	-7.1	0.61	-7.3	0.57	-7.3
H12	0.63	-6.2	0.59	-7.6	0.6	-7.4	0.56	-7.4
H13	0.74	-6.5	0.6	-7.1	0.61	-7.5	0.51	-8.1
H14	0.63	-8.4	0.58	-7.8	0.63	-7.2	0.66	-6
H15	0	0	0	0	0	0	0	0

Discussion

In this study we aimed to describe the modular pattern in the wrist of hominids and determine whether the pattern and strength of covariation across carpals is shared in humans, chimpanzees, and gorillas. To do this, we used the covariance ratio (CR) (Adams, 2016; Adams and Collyer, 2019) to test the degree to which changes in the capitate, lunate, scaphoid, and trapezium are associated with changes in each of the other bones. Our results indicate that the best fit for the covariation patterns in the wrist of hominids is the hypothesis that indicates that each carpal is its own modular unit (H1), as the level of

Preprints (www.preprints.org) | NOT PEER-REVIEWED | Posted: 27 April 2020 doi:10.20944/preprints202004.0474.v1

covariation between carpals was always smaller than the covariation within carpals (CR in Table 4). This supports previous evidence demonstrating great variability in the shape of carpals across primates (Lewis, 1972; Corruccini, 1978; Kivell et al., 2013). It also indicates that although the hands of humans have become less integrated with the feet in comparison to species with functionally similar use of both structures (Rolian, 2009), it may not mean that the strength of reciprocal relationships across carpals is lower than in apes (H1 in Fig. 2).

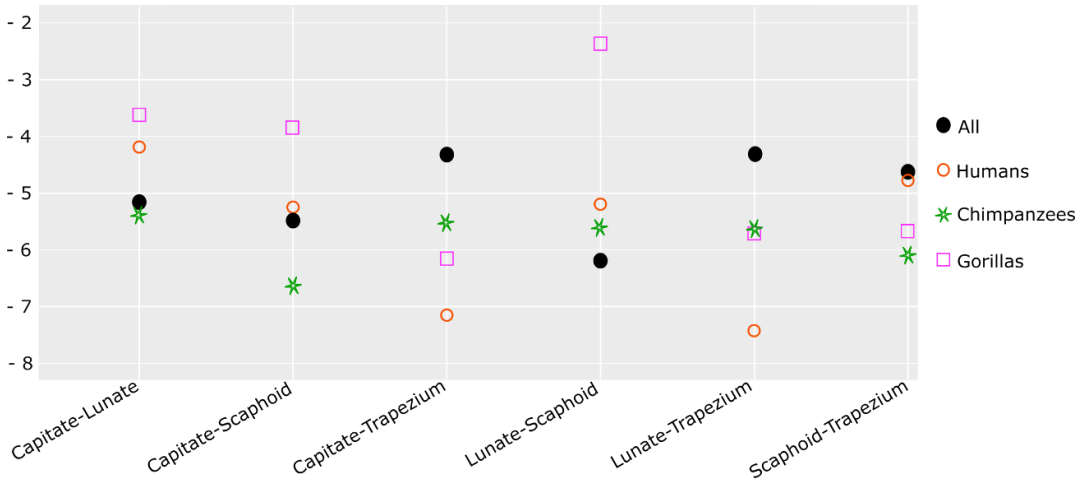

Figure 4 Effect sizes (Z_{CR}) for the optimal modular hypothesis for the wrist in hominids (H1), and for each genus separately.

However, the high level of autonomy of these four carpals indicated by our results requires some caution. First, the generalized Procrustes superimposition procedure, in which each bone was subject to a separate GPA, reduces the possible inflation of the covariance pattern between bones, as compared to the approach that uses one common superimposition and then splits the dataset to assess modularity hypotheses (Cardini, 2019). However, the applied approach (i.e., separate superimpositions) may overestimate modularity, as it discards information related to the relative size and position of the modules (Cardini, 2019). Second, it is also probable that the different covariation structure in the wrist found in some of our analyses for humans, chimpanzees, and gorillas (Fig. 2 and 3, Table 4), favors the simplest of all available hypotheses (H1), particularly when the entire sample is pooled (in terms that suggest no covariation between any of the carpals). In relation to the latter, although H1 was selected as the best model explaining the covariation structure of hominids, the different behavior of the genera when analyzed separately (Fig. 2) and the Z_{CR} comparison between carpal pairs indicate otherwise: that the level of association between some of them vary across taxa. This is true for the levels of covariation between the capitate and lunate, and the trapezium and scaphoid, which are higher for humans when compared to other pairs of carpals (Fig. 4), while for chimpanzees carpal pairs do not present different strengths of covariation. This makes H1 the optimal modular hypothesis for chimpanzees (in which

Preprints (www.preprints.org) | NOT PEER-REVIEWED | Posted: 27 April 2020 doi:10.20944/preprints202004.0474.v1

each carpal corresponds to its own modular unit), while in the case of humans H2 is a better fit (i.e., the capitate and lunate belong to the same modular unit, and the trapezium to another) (Fig. 2 and 3). Gorillas share with humans that the capitate and lunate exhibit a degree of covariation and that the capitate and trapezium belong to different modules (as indicated by H9). However, results were less conclusive for this genus than for the others, as H9 presented the lowest Z_{CR}; however, these results could not be confirmed when a pairwise modularity score ($\hat{Z}_{12}$) was calculated for every pair of carpals (Table S5).

According to our analysis, what separates humans from African apes is a stronger degree of covariation between the trapezium and the scaphoid. It is interesting that the radial side of the wrist separates these two groups, as a large proportion of studies dealing with manual differences between apes and humans have focused on the thumb, including the trapeziometacarpal joint, and point to enhanced manipulative capabilities in the former (Hamrick et al., 1998; Marzke et al., 1999, 2010; Tocheri et al., 2008; Feix et al., 2015; Key and Dunmore, 2015). Also, the radio-carpal joint (which involves the scaphoid) has been related to mechanical advantages in accuracy and force generation for the use of tools in humans (Williams et al., 2010, 2014). Further analyses should estimate whether the associated changes of these bones are functionally linked to fine manipulation of objects in humans relative to African apes (Tocheri et al., 2005, 2008; Marzke et al., 2010; Feix et al., 2015). This would require a more detailed landmark configuration and a different statistical approach than the one presented here, as CR cannot be used to describe specific associated shape changes, as principal component analysis and/or partial least squares analysis might (although see Cardini, 2019).

The presence of different modular strengths in the wrist bones of gorillas and chimpanzees (higher modular strength in the latter) is also noteworthy, as the presence of a knuckle-walking complex, common to chimpanzees and gorillas, has long been discussed (Corruccini, 1978; Begun, 1992; Richmond and Strait, 2000; Kivell and Schmitt, 2009; Williams, 2010; Püschel et al., 2020). For instance, Richmond and Strait (2000) proposed that African apes have a unique suite of skeletal traits involving the radiocarpal joint, which is adapted to stabilize the wrist during knuckle-walking, yet others argue that this type of locomotion is not the same biomechanical phenomenon in chimpanzees and gorillas (Inouye, 1994; Kivell and Schmitt, 2009). Our analysis does not indicate that there is a common covariation pattern for chimpanzees and gorillas, different from that of humans, that could allow us to define a potential knuckle-walking complex. This is in line with Williams' (2010) conclusion that there is not a unique pattern of integration between the capitate and third metacarpal that distinguishes knuckle-walkers from non-knuckle-walking taxa.

 doi:10.20944/preprints202004.0474.v1

Conclusions.

Hominids have in common that each carpal covaries mainly with itself (scaphoid, lunate, trapezium and capitate) and with other carpals to a lesser extent. However, there are differences in the covariation strength that they exhibit with other wrist bones. In humans, the trapezium and scaphoid present a significantly lower modular signal with one another than with the remaining bones, and this also occurs with the capitate and lunate. This suggests that there may be associated shape changes between the scaphoid and trapezium, and between the capitate and lunate in humans. In gorillas there are also significant differences in the covariation structure across carpals, which indicates that the capitate and trapezium vary more independently than other pairs of carpals, and that the capitate and lunate covary as they do in humans. Of the three genera, chimpanzees presented the lowest interaction among carpals.

ORCID

Ana Bucchi https://orcid.org/0000-0002-1247-230X

Thomas A. Püschel https://orcid.org/0000-0002-2231-2297

Antonio Profico https://orcid.org/0000-0003-2884-7118

Carlos Lorenzo https://orcid.org/0000-0001-5706-293X

Acknowledgements

We are thankful to Alessio Veneziano for his advice on using R. The illustration depicted in Figure 3 was made by the palaeoartist Lou-Octavia Mørch, we really appreciate her help. We are also grateful to the following curators and institutions for the access to the ape specimens: Emmanuel Gilissen (AfricaMuseum), Anneke H. van Heteren and Michael Hiermeier (Zoologische Staatssammlung München), Javier Quesada (Museu de Ciències Naturals de Barcelona), José Miguel Carretero (Universidad de Burgos), and Sergio Almécija (American Museum of Natural History). AB was partially funded by a Becas Chile scholarship, whilst TP was funded by the Leverhulme Trust Early Career Fellowship, ECF-2018-264. This study was funded by research projects AGAUR 2017 SGR 1040 and MICINN-FEDER PGC2018-093925-B-C32.

References

Adams, D.C., 2016. Evaluating modularity in morphometric data: Challenges with the RV coefficient and a new test measure. Methods in Ecology and Evolution. 7, 565–572.

Adams, D.C., Collyer, M.L., 2019., Comparing the strength of modular signal, and evaluating alternative modular hypotheses, using covariance ratio effect sizes with morphometric data. Evolution. 73, 2352-2367.

Adams, D.C., Collyer, M.L., Kaliontzopoulou, A., 2019. Geomorph: Software for geometric morphometric analysis. R package version 3.0. 6.

Begun, D.R., 1992. Miocene fossil hominids and the chimp-human clade. Science. 257, 1929–1933.

Bucchi, A., Luengo, J., Fuentes, R., Arellano-Villalón, M., Lorenzo, C., 2020. Recommendations for improving photo quality in close range photogrammetry, exemplified in hand bones of chimpanzees and gorillas. International Journal of Morphology. 38, 348–355.

Cardini, A., 2019. Integration and modularity in Procrustes shape data: is there a risk of spurious results? Evolutionary Biology. 46, 90–105.

CARTA Subject IDs: 3991, 4001, 4003, 4007, 4010, 4073, 4076, 4182. Courtesy of the Center for Academic Research and Training in Anthropogeny/Museum of Primatology at UC San Diego. Retrieved February 11, 2020 from http://carta.anthropogeny.org.

Casillas García, J.A., Adán Álvarez, G.E., 2005. Rescatando la memoria: La actuación arqueológica en el Solar de Caballería y el Convento de San Pablo de Burgos. Instituto Municipal de Cultura del Ayuntamiento de Burgos, Burgos.

Cignoni, P., Callieri, M., Corsini, M., Dellepiane, M., Ganovelli, F., Ranzuglia, G., (2008, July). Meshlab: an open-source mesh processing tool. In Eurographics Italian chapter conference (pp. 129-136).

Corruccini, R.S., 1978. Comparative osteometrics of the hominoid wrist joint, with special reference to knuckle-walking. Journal of Human Evolution. 7, 307–321.

Esteve-Altava, B., 2017. In search of morphological modules: a systematic review. Biological Reviews. 92, 1332–1347.

Feix, T., Kivell, T.L., Pouydebat, E., Dollar, A.M., 2015. Estimating thumb-index finger precision grip and manipulation potential in extant and fossil primates. Journal of the Royal Society Interface. 12, 20150176.

 doi:10.20944/preprints202004.0474.v1

Giacomini, G., Scaravelli, D., Herrel, A., Veneziano, A., Russo, D., Brown, R.P., Meloro, C., 2019. 3D photogrammetry of bat skulls: Perspectives for macro-evolutionary analyses. Evolutionary Biology. 46, 249-259.

Hamrick, M.W., Churchill, S.E., Schmitt, D., Hylander, W.L., 1998. EMG of the human flexor pollicis longus muscle: Implications for the evolution of hominid tool use. Journal of Human Evolution. 34, 123–136.

Inouye, S.E., 1994. Ontogeny of knuckle-walking hand postures in African apes. Journal of Human Evolution. 26, 459-485.

Key, A.J.M., Dunmore, C.J., 2015. The evolution of the hominin thumb and the influence exerted by the non-dominant hand during stone tool production. Journal of Human Evolution. 78, 60–69.

Kivell, T.L., 2011. A comparative analysis of the hominin triquetrum (SKX 3498) from Swartkrans, South Africa. South African Journal of Science. 107, 60-69.

Kivell, T., Lemelin, P., Richmond, B.G., Schimtt, D., 2016. The evolution of the primate hand. Springer, New York.

Kivell, T.L., Barros, A.P., Smaers, J.B., 2013. Different evolutionary pathways underlie the morphology of wrist bones in hominoids. BMC Evolutionary Biology. 13, 229.

Kivell, T.L., Schmitt, D., 2009. Independent evolution of knuckle-walking in African apes shows that humans did not evolve from a knuckle-walking ancestor. Proceedings of the National Academy of Sciences. 106, 14241–14246.

Klingenberg, C.P. 2008. Morphological integration and developmental modularity. Annual Review of Ecology, Evolution, and Systematics. 39, 115-132.

Klingenberg, C.P., Marugán-Lobón, J., 2013. Evolutionary covariation in geometric morphometric data: Analyzing integration, modularity, and allometry in a phylogenetic context. Systematic Biology. 62, 591–610.

Lewis, O.J., 1972. Osteological features characterizing the wrists of monkeys and apes, with a reconsideration of this region in *Dryopithecus (Proconsul) africanus*. American Journal of Physical Anthropology. 36, 45–58.

Marzke, M.W., 1983. Joint functions and grips of the *Australopithecus afarensis* hand, with special reference to the region of the capitate. Journal of Human Evolution. 12, 197–211.

Marzke, M.W., 1997. Precision grips, hand morphology, and tools. American Journal of Physical

Anthropology. 102, 91–110.

Marzke, M.W., Marzke, R.F., Linscheid, R.L., Smutz, P., Steinberg, B., Reece, S., An, K.N., 1999. Chimpanzee thumb muscle cross sections, moment arms and potential torques, and comparisons with humans. American Journal of Physical Anthropology. 110, 163–178.

Marzke, M.W., Tocheri, M.W., Steinberg, B., Femiani, J.D., Reece, S.P., Linscheid, R.L., Orr, C.M., Marzke, R.F., 2010. Comparative 3D quantitative analyses of trapeziometacarpal joint surface curvatures among living catarrhines and fossil hominins. American Journal of Physical Anthropology. 141, 38–51.

Niewoehner, W.A., Weaver, A.H., Trinkaus, E., 1997. Neandertal capitate-metacarpal articular morphology. American Journal of Physical Anthropology. 103, 219–233.

Orr, C.M., 2017. Locomotor hand postures, carpal kinematics during wrist extension, and associated morphology in anthropoid primates. Anatomical Record. 300, 382–401.

Peña, A., 2018. Patterns of integration and modularity in the hominoid wrist (MSc thesis). Retrieved from https://scholarspace.library.gwu.edu/concern/gw_etds/ms35t8905

Profico, A., Schlager, S., Valoriani, V., Buzi, C., Melchionna, M., Veneziano, A., Raia, P., Moggi-Cecchi, J., Manzi, G., 2018. Package 'Arothron.' American Journal of Physical Anthropology. 166, 979–986.

Püschel, T.A., Marcé-Nogué, J., Chamberlain, A.T., Yoxall, A., Sellers, W.I., 2020. The biomechanical importance of the scaphoid-centrale fusion during simulated knuckle-walking and its implications for human locomotor evolution. Scientific Reports. 10, 3526.

Reno, P.L., Mccollum, M.A., Cohn, M.J., Meindl, R.S., Hamrick, M., Lovejoy, C.O., 2008. Patterns of correlation and covariation of anthropoid distal forelimb segments correspond to hoxd expression territories. Journal of Experimental Zoology Part B: Molecular and Developmental Evolution. 310, 240–258.

Richmond, B.G., Strait, D.S., 2000. Evidence that humans evolved from a knuckle-walking ancestor. Nature. 404, 382–385.

Rolian, C., 2009. Integration and evolvability in primate hands and feet. Evolutionary Biology. 36, 100–117.

Rolian, C., Lieberman, D.E., Hallgrímsson, B., 2010. The coevolution of human hands and feet. Evolution. 64, 1558–1568.

Skinner, M.M., Stephens, N.B., Tsegai, Z.J., Foote, A.C., Nguyen, N.H., Gross, T., Pahr, D.H., Hublin, J.-J., Kivell, T.L., 2015. Human-like hand use in *Australopithecus africanus*. Science. 347, 395–399.

Tocheri, M.W., Marzke, M.W., Liu, D., Bae, M., Jones, G.P., Williams, R.C., Razdan, A., 2003. Functional capabilities of modern and fossil hominid hands: Three-dimensional analysis of trapezia. American Journal of Physical Anthropology. 122, 101–112.

Tocheri, M.W., Orr, C.M., Jacofsky, M.C., Marzke, M.W., 2008. The evolutionary history of the hominin hand since the last common ancestor of *Pan* and *Homo*. Journal of Anatomy. 212, 544–562.

Tocheri, M.W., Razdan, A., Williams, R.C., Marzke, M.W., 2005. A 3D quantitative comparison of trapezium and trapezoid relative articular and nonarticular surface areas in modern humans and great apes. Journal of Human Evolution. 49, 570–586.

Tuttle, R.H., 1967. Knuckle-walking and the evolution of hominoid hands. American Journal of Physical Anthropology. 26, 171–206.

Williams, E.M., Gordon, A.D., Richmond, B.G., 2010. Upper limb kinematics and the role of the wrist during stone tool production. American Journal of Physical Anthropology. 143, 134–145.

Williams, E.M., Gordon, A.D., Richmond, B.G., 2014. Biomechanical strategies for accuracy and force generation during stone tool production. Journal of Human Evolution. 72, 52–63.

Williams, S.A., 2010. Morphological integration and the evolution of knuckle-walking. Journal of Human Evolution. 58, 432–440.

Young, N.M., Wagner, G.P., Hallgrimsson, B., 2010. Development and the evolvability of human limbs. Proceedings of the National Academy of Sciences. 107, 3400–3405.

Insertion sites in manual proximal phalanges of African apes and modern humans.

Looking for behavioral traces in phalanges.

Ana Bucchi[1,2], Javier Luengo[1,2], Antonietta del Bove[1,2], Carlos Lorenzo[1,2]

[1] Institut Català de Paleoecologia Humana i Evolució Social (IPHES), 4 Zona Educacional Campus Sescelades URV, Tarragona, 43007, Spain.

[2] Area de Prehistòria, Universitat Rovira i Virgili (URV), 35 Avinguda Catalunya, Tarragona, 43002, Spain.

Corresponding author: Ana Bucchi, anabucchi@gmail.com

Abstract

Objectives:

To describe the insertion sites of the ligaments holding the *flexor digitorum profundus* and *superficialis* muscles (flexor ridges) in proximal phalanges 2-5 of African apes and modern humans. To interpret differences in flexor ridge development based on known behavioral differences among taxa.

Materials and Methods:

We analyzed 3D models of proximal phalanges 2-5 from 29 hands from gorillas (*Gorilla beringei* and *Gorilla gorilla*), 30 from chimpanzees (*Pan troglodytes)* and 36 from recent modern humans. Flexor ridges (mm^2) were compared within and across genera.

Results:

Gorillas and chimpanzees have larger flexor ridges for phalanges 2-4 than humans and this difference subsists when controlling for body size. Each genus has a unique insertion pattern across the digits, with the most homogeneous pattern found in gorillas, followed by humans, and lastly chimpanzees. These patterns correspond strongly to the differences in the size of the phalanges within each genus, with the exception of phalanx 5 in humans, which has a larger flexor ridge than expected.

Discussion:

When comparing these genera, the flexor ridges signal differences between taxa that use their hands for manipulation and locomotion (gorillas and chimpanzees) and taxa that use

them exclusively for manipulation (humans). This functional signal is also apparent in the PP5 of humans, whose larger FR may be indicating the high recruitment of this digit during forceful precision grip characteristic of humans.
Keywords: A2 pulley; functional morphology; locomotion; insertion areas.

Introduction

The flexor ridges are the insertion areas of the annular ligaments of the fingers which hold the synovial sheaths of the tendons of both the *flexor digitorum profundus* (FDP) and *superficialis* (FDS) muscles, the main flexors of the digits. During climbing and suspension both muscles are strongly recruited (Susman & Stern, 1979) and are also slightly active during knuckle-walking (Susman & Stern, 1979; Tuttle, Shine, Basmajian & Regenos, 1972), the most frequent form of locomotion in African apes (Table 1).

Here we analyzed the areas of the flexor ridges (FR, in mm^2) in the proximal phalanges of adult gorillas (*Gorilla beringei* and *Gorilla gorilla*), chimpanzees (*Pan troglodytes*), and recent modern humans (*Homo sapiens*) (Table 2). We did this in order to (i) compare the FR of proximal phalanges 2-5 (PP2-PP5) between African apes and modern humans, and (ii) determine whether variation in the FR patterns indicates functional differences in the use of the hands.

Humans use their hands exclusively for manipulation while African apes use them for manipulation and travel, which may have an effect on FR development. We expect that African apes will have more highly developed FR than humans in all phalanges, since locomotion and manipulation require generation of higher manual forces than manipulation alone. This expectation is founded on previous electromyographic research that showed that *flexor digitorum profundus* and *superficialis* muscles are active during manipulation of objects and during the most frequent modes of locomotion of African apes (Susman & Stern, 1979; Tuttle, Shine, Basmajian & Regenos, 1972). During the onset of the swing phase of knuckle-walking, both muscles are slightly active in chimpanzees (Susman & Stern, 1979) while for gorillas moderate to marked potentials were recorded for *flexor digitorum superficialis* (Tuttle et al. 1972). This was interpreted by Tuttle et al. (1972) as a response to the propellant flexion of metacarpophalangeal joints when the hand is lifted from the ground. Also, a burst of potential for the latter muscle occurs during rapid progression in gorillas (Tuttle et al. 1972) and for both muscles in chimpanzees when the hand is parallel to the line of progression, which serves to counter the effect of the opposing

extensor muscles and thus enhance support of the hyperextended metacarpophalangeal joints (Tuttle et al. 1972; Susman & Stern, 1979). In both vertical climb and suspension a significant part of the body weight is borne by the forelimbs (Hunt et al. 1996), and large forces are required to propell the body upwards, which probably explains why the activity of the flexor muscles is maximum when climbing a vertical trunk or ropes, and during suspension from a horizontal rope and ladder (Susman & Stern, 1979). Hand-gripping for manipulative purposes requires an activation for the flexor muscles as well, and its activation level depends on the magnitude of the task (Susman and Stern 1979; Danion et al. 2002; Forman et al. 2019).

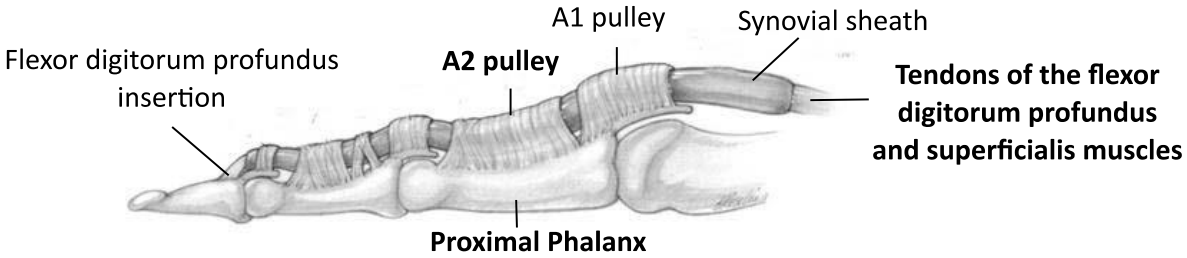

Figure 1 Depiction of some of the annular ligaments of the fingers (A2 and A1 pulleys), tendons from the *flexor digitorum profundus* and *superficialis* muscles, and their attachment to bones. Modified from Doyle (1988).

It is to be expected that the activity of the flexor muscles leaves a skeletal trace in the hands. It has been extensively proposed in the anthropological literature that the insertion areas of tendons and ligaments reflect their activity level during life (e.g. Villotte et al. 2010; Karakostis et al. 2018) (although see below). Indeed, previous descriptions of these insertion sites conclude they are marked in African apes and absent in humans (Susman 1979). However, in that study body size was not taken into account when measuring FR, thus complicating the comparison of FR across species. For this reason, we have studied the scaling relationship of the FR with the size of individuals (using first metacarpal length (McL) as a proxy for body size, see Methods). We have also studied the scaling relationship of FR with phalangeal size to investigate whether they are related to the different FR patterns across digits found among the taxa studied here.

A methodological aspect must be considered to achieve these aims. The insertion areas (also called entheses) of the bones to which connective tissue is attached (e.g. tendons, ligaments), have commonly been used to infer activity patterns in the past (e.g. Eshed, Gopher, Galili, & Hershkovitz, 2004; Hawkey & Merbs, 1995; Karakostis, Hotz, Tourloukis,

& Harvati, 2018; Villotte *et al.,* 2010), but there is debate regarding the extent to which they can provide such information and the degree to which they are dependent on the biological profile of individuals, including differences in sex, age, and body size (Janssen, Heymsfield, Wang, & Ross, 2000; Weiss, Corona, & Schultz, 2012; Weiss, 2004; Foster *et al.,* 2012; Milella, 2014). Furthermore, data from experiments on animals (Rabey *et al.,* 2015; Zumwalt, 2006; Wallace et al., 2017) and dissected human material (Williams-Hatala, Hiles, & Rabey, 2016) indicate that there is no causal relationship between the intensity or frequency of muscle recruitment and entheseal properties.

Studying taxa which we know *a priori* use their hands differently allows us to test whether insertion sites actually reflect these functional differences. If entheses signal behavior, the higher forces African apes apply on their hands should leave larger insertion sites than in humans. This may help to elucidate the suitability of entheses to inform on the use of the hands in taxa with unknown activity patterns (e.g. human past populations), yet this kind of study is relatively scarce (Zumwalt, 2006; Drapeau, 2008; Milella, 2014; Rabey *et al.,* 2015; Casado *et al.,* 2019).

Table 1 Overall locomotion (in percentage of locomotory categories) and mean body mass per subspecies.

Taxon	Main locomotor modes		Mean body mass (kg)	
	Females	Males	Females	Males
Gorilla beringei beringei	Quadrupedalism (95.6%), quadrumanous climbing and scrambling (2.7%), biped (1.4%), Suspension (0.2%)[a]	Quadrupedalism (97.3%), quadrumanous climbing and scrambling (0.7%), biped (1.7%)[a]	97.7[d]	159.2[d]
Gorilla beringei graueri	Knuckle-walking, suspension, climbing[b]		80[d]	175.2[d]
Gorilla gorilla gorilla			71.5[d]	169.5[d]
Pan troglodytes schweinfurthii	Quadrupedalism (90.4%), quadrumanous climbing and scrambling (8.3%), suspension (0.9%), biped (0.2%)[c]	Quadrupedalism (94.5 %), quadrumanous climbing and scrambling (4.3%), suspension (0.8%), biped (0.3%)[c]	33.7[e]	42.7[e]
Homo sapiens	Bipedalism (100%)		54.4[f]	62.2[f]

[a] Doran (1997).
[b] Remis (1995) and Tuttle and Watts (1985), unknown percentages.
[c] Doran and Hunt (1994). Data is averaged for multiple sites.
[d] Jungers & Susman (1984).
[e] Smith & Jungers (1997).
[f] Siegmund & Papageorgopoulou (2011).

Materials and methods

Sample.

The proximal phalanges (PP) 2-5 of the hand were analyzed in a sample of African apes (29 *Gorilla beringei* and *Gorilla gorilla,* 30 *Pan troglodytes)* and 36 modern humans belonging to a medieval population (Karakostis & Lorenzo, 2016 and references therein) (Tables 2 and 3). Only adult individuals were included in the analysis (all specimens with a fully erupted third molar were considered adults). Apes were mostly wild-shot (30), some of them were captive (12) and 17 were of unknown origin. Pathological phalanges involving trauma or osteoarthritis were excluded from analysis.

As the ape sample came from different origins which may affect locomotion and finally FR development, no statistical tests were carried out between chimpanzees and gorillas, nor between subspecies or sexes, although males and females are shown separately in Figure 3 and Table 3. Comparisons were thus limited to humans, on the one side, and chimpanzees and gorillas on the other.

Table 2 The sample. Samples were obtained from the RMCA (Royal Museum for Central Africa, Tervuren), MZB (Museu de Ciències Naturals, Barcelona), ZSC (Zoologische Staatssammlung München, Munich), IPHES (Catalan Institut the Human Palaoecology and Social Evolution, Tarragona), UBU (Universidad de Burgos).

Subspecies	Common name	Number	Male: Female: Unknown	Collection
Gorilla beringei beringei	Mountain gorilla	3	1:2	RMCA
Gorilla beringei graueri	Eastern lowland gorilla	16	9:7	RMCA
Gorilla gorilla gorilla	Western lowland gorilla	10	5:5	RMCA, MZB, ZSC
Pan troglodytes schweinfurthii	Eastern chimpanzee	10	4:1:5	RMCA
Pan troglodytes (unknown subspecies)	Common chimpanzee	20	10:6:4	RMCA, MZB, ZSC, IPHES
Homo sapiens	Modern Human	36	18:18	UBU

Right hands were preferred, but in cases where some bones or the complete right hand was missing their antimeres were used. We have assumed that the difference between the manual forces required for locomotion and for manipulation is greater than any difference

due to right or left-handedness. We think this is a safe assumption, given the difficulties of assessing hand preference based upon skeletal traces (see Cashmore, 2009).

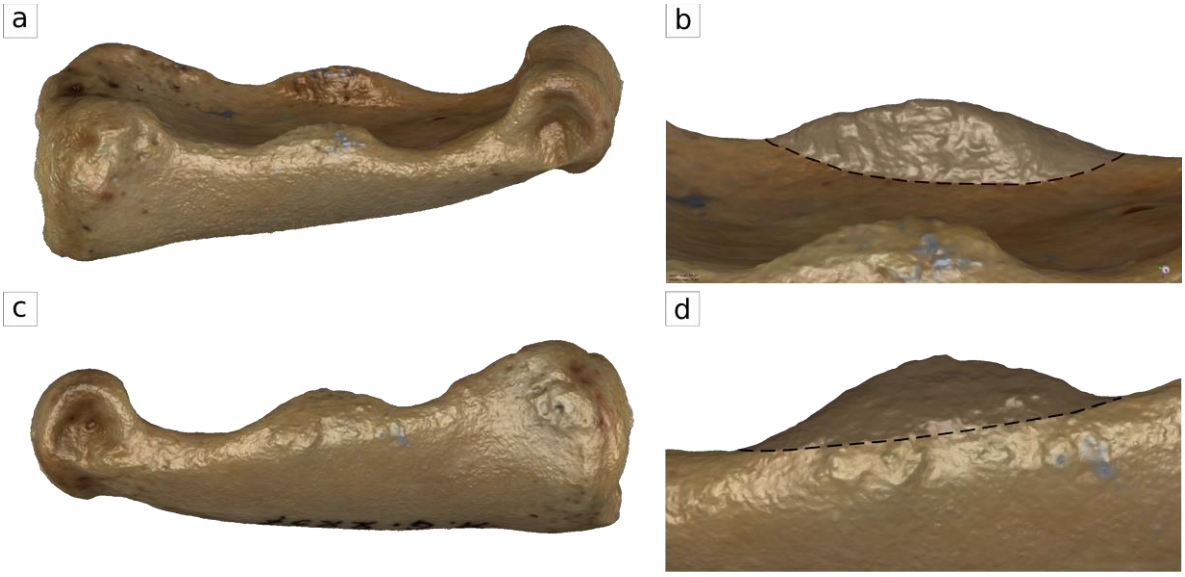

Figure 2 Selection of ulnar and radial insertion areas of the sheath in a PP4 of a male gorilla (*Gorilla beringei*). Images a and c show the position in which phalanges were set in order to select this area, b shows the selection of the internal part, and d the selection of the external part of the phalanx.

Digital models

3D models of 364 proximal phalanges were analyzed (Table 2). For humans, they were obtained from a surface scanner (Breuckmann SmartSCAN structured light scanner, Breuckmann Inc.), while for apes they were built in AgiSoft PhotoScan Professional Software (version 1.2.6) through photogrammetry. Both techniques provide high-resolution surface models; those from the surface scanner were obtained using a resolution of 0.125 mm, while most of the photogrammetric models ranged from 300.000 to 600.000 triangles of uniform size.

To test whether the quality of scanner and photogrammetric models is comparable, a subsample of 30 human phalanges (which had the smallest FR, see Results) were randomly selected and both types of models were obtained from them. FR was then measured in the 60 models and paired *t*-tests showed that there are no significant differences in FR measurement between both types of models (t=0.16, p=0.87), indicating that scanner and photogrammetric models are of similar resolution.

Table 3 Summary statistics of phalanges per sex and genus.

Genera	Phalanx[a]	N	Mean FR and standard deviation (mm^2)			Mean PTA and standard deviation (mm^2)[c]		
			all	Male	Female	all	Male	Female
Gorilla	PP2	28	191 ± 75	232 ± 72	150 ± 52	2478 ± 664	3060 ± 501	2096 ± 405
	PP3	28	281 ± 99	336 ± 96	127 ± 59	3320 ± 713	2860 ± 427	2697 ± 214
	PP4	29	246 ± 90	300 ± 81	188 ± 58	2908 ± 656	3465 ± 327	2311 ± 280
	PP5	25	155 ± 55	182 ± 82	125 ± 58	2173 ± 534	2545 ± 387	1770 ± 343
Chimpanzee	PP2	29	99 ± 36	105 ± 33	92 ± 39	2154 ± 429	2270 ± 449	2012 ± 371
	PP3	29	129 ± 51	131 ± 55	127 ± 59	2772 ± 486	2932 ± 537	2575 ± 340
	PP4	29	109 ± 46	121 ± 45	97 ± 45	2329 ± 501	2588 ± 496	2070 ± 363
	PP5	27	48 ± 34	48 ± 15	46 ± 15	1443 ± 315	1253 ± 285	1573 ± 264
Human	PP2	35	46 ± 16	50 ± 18	42 ± 13	1419 ± 152	1498 ± 124	1330 ± 132
	PP3	36	66 ± 23	75 ± 24	57 ± 17	1600 ± 213	1702 ± 187	1498 ± 189
	PP4	36	56 ± 19	65 ± 21	47 ± 11	1348 ± 183	1445 ± 154	1257 ± 164
	PP5	33	38 ± 17	46 ± 15	29 ± 15	997 ± 138	1094 ± 120	1253 ± 59

[b]PP2= second proximal phalanx, PP3= third proximal phalanx, PP4= fourth proximal phalanx, and PP5= fifth proximal phalanx.

[c]Phalangeal total area (PTA), see text.

Measurements

The insertion site of the A2 pulley was measured in each bone. The A2 pulley is the annular ligament of the fingers inserted into the shaft of proximal phalanges (Fig. 1). Although a similar analysis can be done on the middle and distal phalanges, we only studied proximal phalanges as they are more common in museum collections than middle and distal phalanges. Selected insertion areas can be observed in Figure 2. Attachment sites analyzed here include the radial and ulnar sides of the flexor ridges at the proximal phalanges. Both areas (mm^2) were added and this single value per phalanx was used (FR), as no significant differences were found between ulnar and radial sides of the insertion (t-test, $p>0.05$ for all phalanges).

Some conditions were defined in order to standardize measurements. All measurements were carried out by the same person (A.B.). Secondly, 3D models were imported in Geomagic Studio® (3D Systems, v. 12, Rock Hill, SC, USA) and FR were quantified as follows. The external and internal margins of the insertion were delimited differently using the Lasso Selection Tool (Fig. 2 b, d). We found the internal border of the ridges easier to observe, as there were differences in the elevation and texture of the insertion area and the surrounding bone (Fig. 2a, b). The external surface of the bone is relatively homogeneous in coloration and texture between the insertion area and the surrounding bone (Fig. 2c, d). Therefore, in order to minimize errors, the external border

was defined by placing the bone in the medial view and drawing a continuous line from the natural (not altered by the insertion) contour of the bone at both ends of the body, and selecting the upper area, as shown in Figure 2d. As previously stated, there are some characteristics of the bone surface that help delineate entheses (e.g. Hawkey & Mebs, 1995; Zumwalt, 2005; Karakostis & Lorenzo, 2016): the cortical surface in the insertion areas is uneven, and it is more elevated or robust than the surrounding surface (Fig. 2). The area also presents characteristic irregularities (pitting, ridges, and color) in comparison with unaffected bone surface.

Statistical analysis

Intra-observer error test

The intra-observer reliability test in the measurement of FR was assessed in a randomly selected subsample of 30 surface models of human phalanges. The FR were calculated and repeated twice by the same researcher (A. B.) in a span of two months each. Significant differences among these three measurements were looked for by means of an ANOVA test, which showed that the repeated measurements of FR are not significantly different from each other ($F_{2,81}$= 0.0018, p>0.99). We thus conclude that our simple method of insertion delimitation in 3D models is reproducible.

After confirming there were no significant differences in the quality of both types of 3D models (see above) and that the error in the observer's measurements was negligible, the following tests were carried out to achieve our objectives.

Insertion sites across different genera

ANOVA tests were performed to detect differences in FR across genera (Table 3). This test was followed by post hoc paired comparisons using Tukey's Honest Significant Difference test (Tukey's HSD) to check which specific genera differ in FR. All variables were *log*-transformed to approximately conform to normality for this and following tests.

Insertion sites and body size

The above analysis should inform us whether the FR are larger in African apes than in humans. However, it is also reasonable to think that body size affects insertion sites sizes (FR), and this is especially important when comparing genera that vary greatly in mean body weight (Table 1). For this reason, we studied the relationship between FR and body size of the individuals. This variable was unknown for most of the sample and we did not

have data on the femoral superoinferior diameter, which is the best proxy for it (Ruff, 2003). Instead, we used the first metacarpal length (McL) of the corresponding hand as it has been shown to be a good proxy for body size in anthropoids (Lovejoy et al. 2009). In the two individuals with missing Mc1, this metric was assumed to be the mean length for its species and sex.

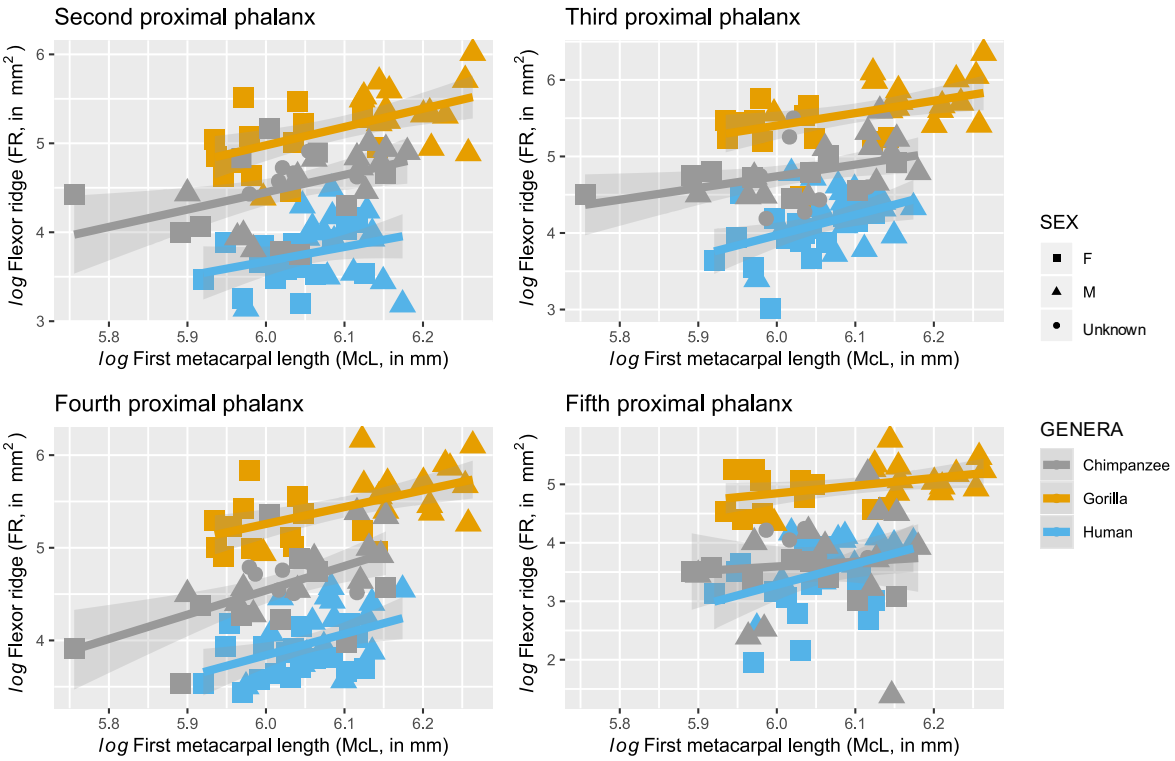

Figure 3 Scaling relationship between the size of the insertion sites (FR) and the first metacarpal length (McL) among taxa. The figures are bivariate plots of *log* McL vs *log* FR among genera for PP2-5. Fitting method: ordinary least squares. Slopes are shown separately per each phalanx with a 95% confidence interval.

To assess how FR scaled with McL in each genus, we computed the strength and direction of the correlations by using the Pearson's correlation coefficient (r), which will be hereafter referred to as the *correlation within each genus*. As it is possible that the *correlation within each genus* differs from the correlation of the entire sample, we also studied the strength and direction of the *total correlation* by combining all the sample and seeing whether a linear relationship exists between FR and McL. We also estimate whether the scaling

relationship between FR and McL differed from isometry. *Log* squared root of FR was regressed on *log* McL using ordinary least squares (OLS). Thus, isometry is indicated by a slope of 1, while slopes significantly lower or greater than 1 indicate negative and positive allometry, respectively.

In those cases where a significant correlation between the variables was found, an ANCOVA was used to determine whether there are significant differences in FR between the genera while adjusting for McL.

Insertion sites and phalange size

We also study the correlation of FR with the phalangeal total area (PTA) in order to estimate the relationship of each FR with the size of its corresponding bone, and thus see how the pattern of FR across the digits match the patterns of the size of phalanges in each genus. PTA represents the whole surface of the bone, and it was calculated in square millimeters (mm^2) using the Calculate Area tool in Geomagic Studio.

The *log* FR were used to study the scaling relationship with *log* PTA in a similar manner as described above for *log* McL.

To study how FR of one finger related to the FR of the others, ANOVAs with Tukey post-hoc tests were carried out to see if there were significant differences in the FR of the four digits in each of the genera. These tests were repeated using PTA instead of FR as the dependent variable.

The data used in this study is available in Supplementary Material 1.

Results

Insertion sites across different genera

ANOVA tests showed there is a statistically significant difference between humans, chimpanzees and gorillas in the FR of PP2 ($F_{2,88}$=106.1, $p<0.01$), PP3 ($F_{2,87}$=114.7, $p<0.01$), PP4 ($F_{2,89}$=130.6, $p<0.01$) and PP5 ($F_{2,82}$=52.81, $p<0.01$) (Table 3). Pairwise comparisons (Tukey's HSD) indicate that in all cases, gorillas and chimpanzees have greater FR ($p<0.05$) than humans, with the only exception being FR in PP5 between chimpanzees and humans, which were not significantly different ($p= 0.61$).

Table 4 Scaling relationship between the *log* square root of the insertion sites (FR) and the *log* first metacarpal length (McL)[a]

Phalanx [b]	Group	n	r[c]	p (corr)	Intercept	Slope	95% CI	p (slope) [d]	Scaling relationship
PP2	Gorilla	27	0.64	**<0.01**	-4.8	1.21	0.61, 1.81	0.48	Isometry
	Chimpanzee	27	0.41	**0.04**	-2.7	0.82	0.06, 1.58	0.63	Isometry
	Humans	30	0.22	0.22	-1.9	0.63	-0.4, 1.65	0.46	No correlation
PP3	Gorilla	27	0.47	**0.01**	-2.2	0.82	0.19, 1.45	0.56	Isometry
	Chimpanzee	28	0.39	**0.04**	-2.9	0.87	0.04, 1.7	0.75	Isometry
	Humans	33	0.38	**0.02**	-5.5	1.26	0.18, 2.33	0.63	Isometry
PP4	Gorilla	29	0.56	**<0.01**	-2.8	0.91	0.38, 1.44	0.91	Isometry
	Chimpanzee	26	0.59	**<0.01**	-5.8	1.34	0.57, 2.1	0.37	Isometry
	Humans	30	0.41	**0.02**	-4.6	1.08	0.19, 1.97	0.86	Isometry
PP5	Gorilla	20	0.38	0.1	-1.5	0.65	-0.15, 1.44	0.36	No correlation
	Chimpanzee	24	0.11	0.62	-1.4	0.54	-1.67, 2.78	0.68	No correlation
	Humans	27	0.35	0.08	-8.9	1.77	-0.2, 3.7	0.43	No correlation

[a]Computed by ordinary least squares (OLS).

[b]PP2= second proximal phalanx, PP3= third proximal phalanx, PP4= fourth proximal phalanx, and PP5= fifth proximal phalanx.

[c]Pearson's correlation coefficient.

[d]A slope of 1.0 indicates isometry. Significant values indicate the slope differs from isometry.

Insertion sites and body size

Total correlations per each phalanx were significant at $p<0.01$ and show that the insertion sites sizes (FR) bear a moderate and positive correlation with size of individuals (indicated by McL) for PP2 (r=0.36,), PP3 (r=0.4), PP4 (r=0.44), and PP5 (r=0.35) (Fig. 3). Similarly, within each genus there was a linear relationship between FR and McL in most cases for phalanges PP2-PP4, and they scaled isometrically (Table 4, Fig 4). For the FR of PP5, none of the genera showed a correlation with McL.

ANCOVA tests were carried out in those phalanges in which FR was correlated with McL in every genus (PP3 and PP4, Table 4). The results indicate there is a significant effect of the genera on the FR of PP3 after controlling for the body size of individuals (using McL as

proxy), ($F_{2,79}$=13.3, p<0.01). This was also true for the FR of PP4 ($F_{2,78}$=9.07, p=0.01). Therefore, gorillas and chimpanzees have larger adjusted means than humans for these two FR (p<0.01).

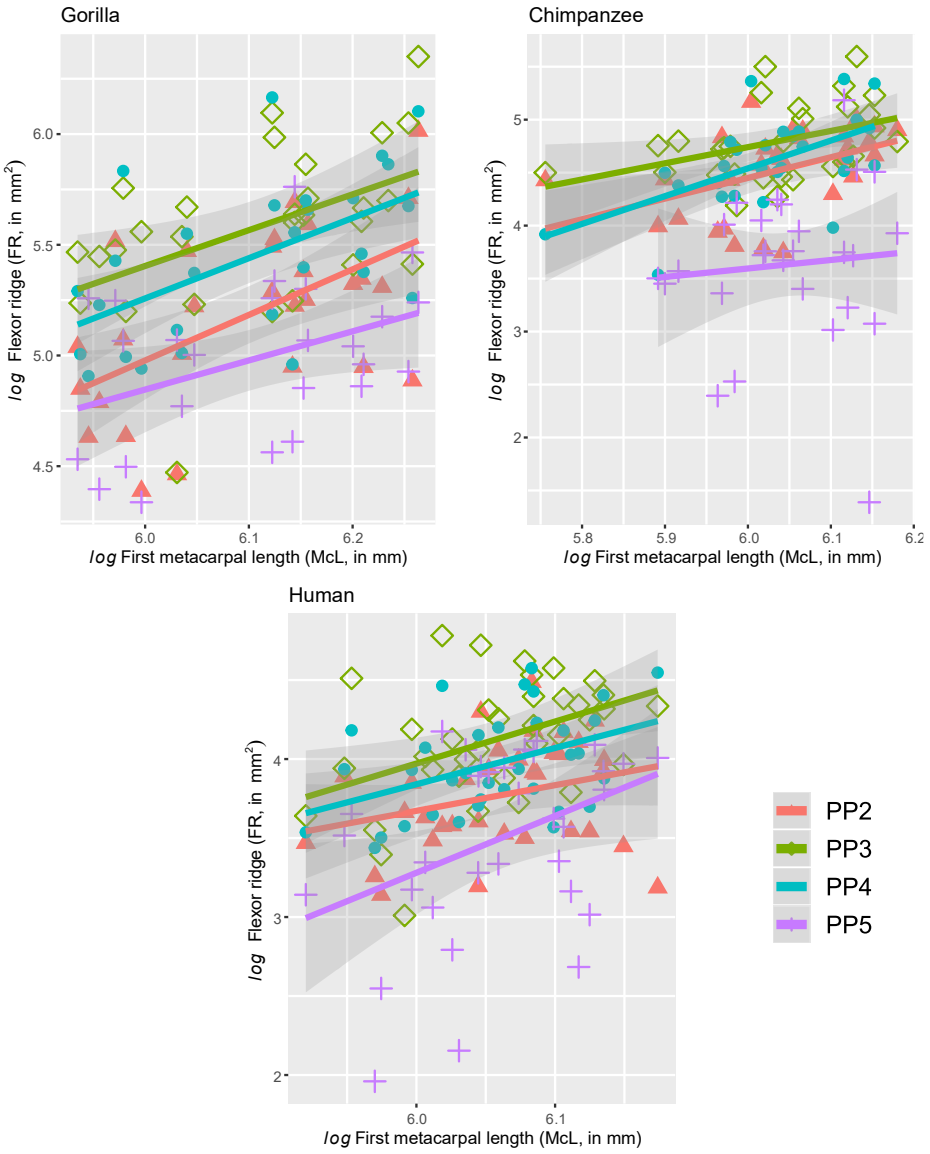

Figure 4 Bivariate plots of *log* first metacarpal length (McL) vs *log* flexor ridges areas (FR) among the phalanges of gorillas, chimpanzees, and humans. Fitting method: ordinary least squares. Slopes are shown separately per each phalanx with a 95% confidence interval. PP2= second proximal phalanx, PP3= third proximal phalanx, PP4= fourth proximal phalanx, and PP5= fifth proximal phalanx.

Insertion sites and phalanx sizes

In gorillas and chimpanzees there is a significant and strong positive correlation between PTA and FR for all phalanges (Table 5), while the correlation is moderately strong and positive for all phalanges in humans, but for PP2 ($p=0.06$). In most cases FR scaled isometrically with PTA, except in PP4 in chimpanzees and PP5 in humans, which show a positive allometry ($p<0.05$) (Table 5).

Table 5 Scaling relationship between the *log* insertion sites (FR) and the *log* phalangeal total area (PTA)[a]

Group	Phalanx[b]	n	r[c]	p (corr)	Intercept	Slope	95% CI	p (slope) [d]	Scaling relationship
Gorilla	PP2	28	0.87	**<0.01**	-2.4	1.29	0.99, 1.59	0.06	Isometry
	PP3	28	0.72	**<0.01**	-2.1	1.2	0.73, 1.66	0.39	Isometry
	PP4	29	0.76	**<0.01**	-1.9	1.16	0.77, 1.55	0.41	Isometry
	PP5	25	0.85	**<0.01**	-1.9	1.17	0.85, 1.49	0.28	Isometry
Chimpanzee	PP2	29	0.60	**<0.01**	-2.8	1.24	0.58, 1.90	0.47	Isometry
	PP3	29	0.68	**<0.01**	-2.8	1.43	0.80, 2.06	0.17	Isometry
	PP4	29	0.80	**<0.01**	-3.8	1.57	1.1, 2.04	**0.02**	Positive allometry
	PP5	27	0.51	**0.01**	-4.6	1.7	0.51, 2.89	0.23	Isometry
Human	PP2	35	0.33	0.06	0.8	1.04	-0.02, 2.1	0.94	No correlation
	PP3	36	0.58	**<0.01**	-3.8	1.63	0.83, 2.42	0.12	Isometry
	PP4	36	0.58	**<0.01**	-2.7	1.29	0.64, 1.94	0.37	Isometry
	PP5	33	0.55	**<0.01**	-6.9	2.34	1.05, 3.64	**0.04**	Positive allometry

[a]Computed by ordinary least squares (OLS).

[b]PP2= second proximal phalanx, PP3= third proximal phalanx, PP4= fourth proximal phalanx, and PP5= fifth proximal phalanx.

[c]Pearson's correlation coefficient.

[d]A slope of 1.0 indicates isometry. Significant values indicate the slope differ from isometry.

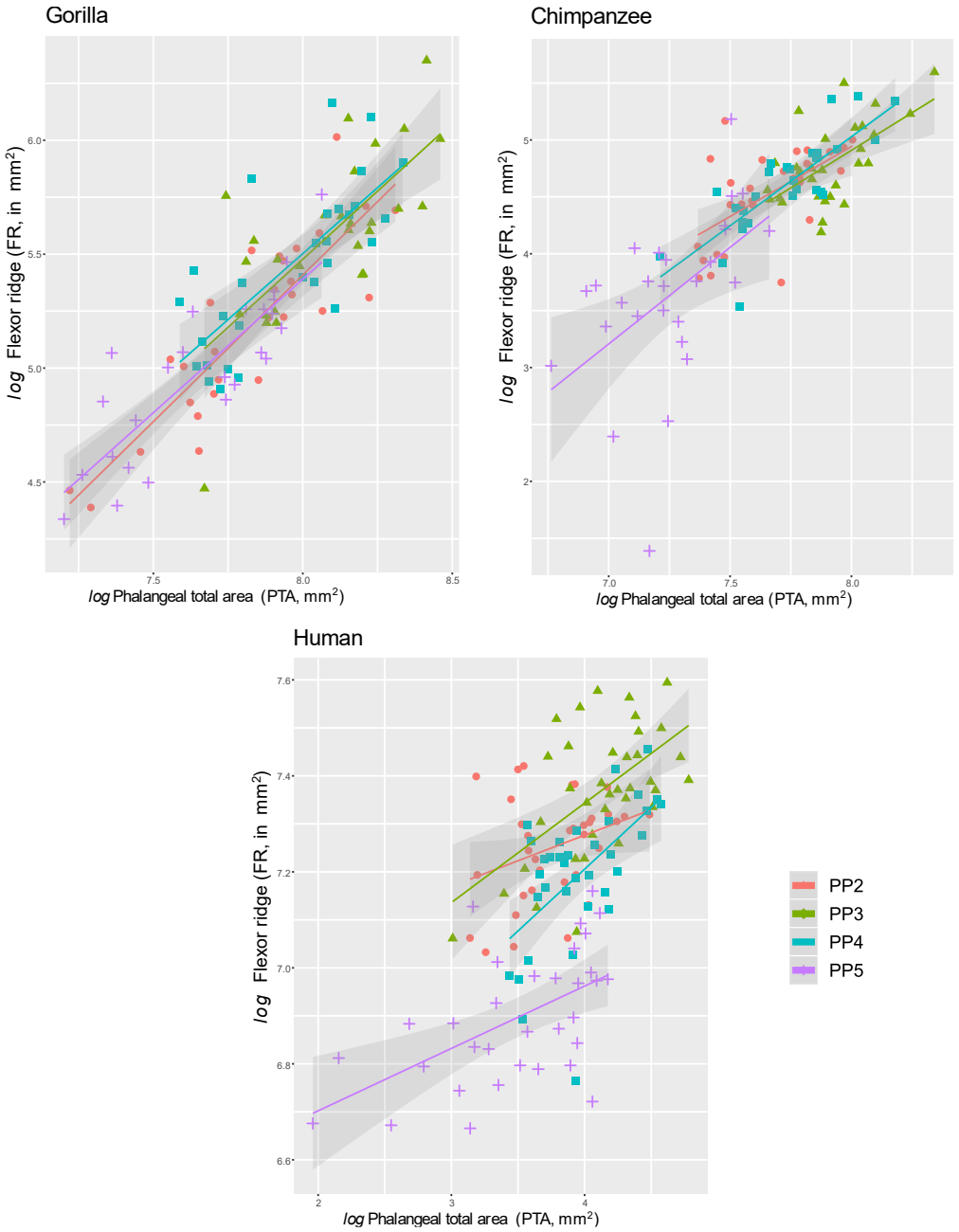

Figure 5 Bivariate plots of *log* phalangeal total area (PTA) vs *log* flexor ridges areas (FR) among the phalanges of gorillas, chimpanzees, and humans. Fitting method: ordinary least squares. Slopes are shown separately per each phalanx with a 95% confidence interval. PP2= second proximal phalanx, PP3= third proximal phalanx, PP4= fourth proximal phalanx, and PP5= fifth proximal phalanx.

The ANOVA tests showed that mean FR vary significantly across fingers in gorillas ($F_{3,106}$=12.6, p<0.01), chimpanzees ($F_{3,109}$=18.6, p<0.01) and humans ($F_{3,136}$=13.5, p<0.01).

Results were similar when using PTA as a dependent variable in gorillas ($F_{3,107}$=15.1, p<0.01), chimpanzees ($F_{3,109}$=43.8, p<0.01) and humans ($F_{3,136}$=71.2, p<0.01). All pairwise comparisons (Tukey HSD test) between FR are given in Table 6, and in Table 7 for PTA.
Each genus has a unique FR pattern across digits (Table 6). In gorillas this pattern is FR PP3 = FR PP4 > FR PP5, FR PP2 = FR PP4 and FR PP5; this pattern is the same for PTA. In chimpanzees the pattern is FR PP3 > FR PP4 = FR PP2 > FR PP5, and the pattern is the same for PTA. In humans, the gradient for FR is PP3 > PP4 > PP5, and PP2 = PP4 and PP5, while for PTA it is PP3 > PP4 = PP2 > PP5. This means either that FR in PP2 is smaller, or the FR of PP5 greater, than one would expect for the PTA of the corresponding phalanx in humans. As FR and PTA in humans scale with positive allometry (Table 5, Fig. 5), it is the latter.

Table 6 ANOVA Post-hoc pairwise comparisons (Tukey's HSD) of the insertion areas (FR, in mm²) across phalanges in gorillas, chimpanzees and humans. P-values are adjusted for multiple comparisons.

FR comparison	Gorillas	Chimpanzees	Humans
PP2-PP3	<0.01	<0.01	<0.01
PP2-PP4	ns	ns	ns
PP2-PP5	ns	<0.01	ns
PP3-PP4	ns	<0.01	<0.01
PP3-PP5	<0.01	<0.01	<0.01
PP4-PP5	<0.01	<0.01	<0.01

[b]PP2= second proximal phalanx, PP3= third proximal phalanx, PP4= fourth proximal phalanx, and PP5= fifth proximal phalanx.

Table 7 ANOVA Post-hoc pairwise comparisons (Tukey's HSD) of the phalangeal total area (PTA, in mm²) across phalanges in gorillas, chimpanzees and humans. P-values are adjusted for multiple comparisons.

PTA comparison	Gorillas	Chimpanzees	Humans
PP2-PP3	<0.01	<0.01	<0.01
PP2-PP4	ns	ns	ns
PP2-PP5	ns	<0.01	<0.01
PP3-PP4	ns	<0.01	<0.01
PP3-PP5	<0.01	<0.01	<0.01
PP4-PP5	<0.01	<0.01	<0.01

[b]PP2= second proximal phalanx, PP3= third proximal phalanx, PP4= fourth proximal phalanx, and PP5= fifth proximal phalanx.

Discussion

We attempted to test the ability of flexor ridges (FR) to reveal information on the use of the hands in gorillas, chimpanzees, and humans. To do this, we compared the FR of PP2-5 within and among taxa (Tables 3-7, Fig. 3-5), and evaluated whether the differences in these insertion patterns could be linked to differences in behavior.

When genera are compared, results for PP2-PP4 support our expectation than African apes would show larger FR than humans. However, this is not the case for PP5 (see below). This indicates that when comparing either gorillas and humans or chimpanzees and humans, FR in PP2-4 may act as functional markers by separating African apes from humans. This is in keeping with Drapeau (2008) and Casado *et al.* (2019) who found that entheses in limbs do indicate functional differences between African apes and humans. Interestingly, although previous research shows that body size is a significant predictor of insertion site variability (e.g. Zumwalt, 2006; Nolte & Wilczak, 2013) and our results suggest that body size exerts an influence on FR (Fig. 3 and Table 4), this cannot explain differences in FR when comparing humans to chimpanzees. Chimpanzees have smaller mean body size than humans (Jungers & Susman, 1984; Siegmund & Papageorgopoulou, 2011), yet have relatively larger FR (Table 3) before and after adjustment for body size (indicated by McL). We thus think FR reflect the greater manual forces chimpanzees place on their hands during locomotion and manipulation compared to humans, who use their hands for manipulation only. The exceptional strength of chimpanzees and their higher muscle mass in the forelimbs compared to humans have been linked to locomotion (Thorpe et al., 1999; Walker, 2009; O'Neill et al., 2017), so our results on FR development are not surprising in that regard.

However, one must be careful when attempting to make FR comparisons between other groups than the ones presented here (humans and chimpanzees, and humans and gorillas), as the influence of body size on FR is not completely clear. Gorillas show larger FR than chimpanzees (Table 3 and Fig. 3), yet, if insertion sites do reflect behavior, there is some evidence in the literature that would lead one to expect otherwise. Chimpanzees climb and engage in more frequent suspensory behavior than gorillas (Hunt, 1991; 1992; Doran, 1996; Remis, 1995), which impose higher activation of the flexor muscles than knuckle-walking (Susman & Stern, 1979; Tuttle et al., 1972; Remis, 1995; 2000; Masi, Cipolletta, & Robbins, 2009). Gorillas' large body mass acts as a constraint to the arboreal behavior, and they spend less time in trees than small-bodied chimpanzees (Doran, 1996; Remis, 1999), thus

the opposite pattern for FR than the one presented here might be expected. However, other studies point out that during vertical climbing both captive (Isler, 2002) and wild (Neufuss et al., 2018) gorillas, compared to chimpanzees, show a more prolonged cycle duration (the time between two initial contacts with the substrate by the same limb) and increased fraction of the cycle duration that a particular limb contacts the substrate, which in turn is a climbing strategy to accommodate their large body size (Neufuss et al., 2018). All of this might explain the larger FR of gorillas relative to chimpanzees. In this case, body mass would be so tightly linked to behavior that it would not be a confounding factor, unrelated to activity patterns. It would therefore be advisable to discuss whether body mass needs to be controlled for before analyzing the insertion sites patters, as studies on insertion sites usually do for humans (e.g Weiss, 2004; Weiss et al., 2012). This observation remains to be tested, as we did not directly compare chimpanzees and gorillas in this study due to the artificial environment in which part of the ape sample lived, which may affect the frequency of locomotor modes, and thus prevent the identification of meaningful functional signals between these two genera. Samples with clear functional patterns are needed for this purpose.

We also evaluated whether the patterns for FR within genera correlate with the interphalangeal sizes. Our FR results (Table 6) match those found for the PTA (Table 7) in most cases, except for PP5 in humans (see below), and positive correlations were found between both variables for most phalanges (Table 5). This resulted in chimpanzees showing relatively higher variation in FR (as well in PTA) relative to gorillas and humans. This is in agreement with previous findings indicating less interphalangeal length variation in gorillas than in chimpanzees (Inouye, 1992), which in turn affects the different way apes load their hands during knuckle-walking (Inouye, 1992; 1994; Matarazzo, 2013).

Throughout the analysis presented here, the FR of PP5 represented several exceptions. It was the single exception to the rule of African apes showing larger FR than humans (Table 3, Fig. 3), as differences were not statistically significant in the case of chimpanzee-human comparisons, and the only phalanx in which FR did not bear a correlation with body size in any of the genera studied here (Table 4). It was also the only phalanx in humans with larger FR than expected for its PTA (Table 5, Fig. 5). The fifth digit is recruited in some of the grips used for grasping objects in gorillas (Neufuss, Robbins, Baeumer, Humle, & Kivell, 2019) and chimpanzees (Pouydebat, Reghem, Borel, & Gorce, 2011). However, the articulations at the base and head of the fifth metacarpal in humans allows this digit to rotate towards the thumb during flexion and better oppose this digits towards the palm than in apes (Marzke

et al., 1992; Dapreau, 2015) which is relevant to effectivelly use tools (Marzke, 1992; 1997; Marzke *et al.,* 1998). This finger is heavily and frequently recruited during forceful precision grip in humans (Key, Dunmore & Marzke, 2019; Marzke, 1997; Marzke et al., 1992; 1998) and sometimes bears even more pressure than the thumb during tool use (Key, Dunmore & Marzke, 2019), which in turn is highly active during the use of tools (Hamrick et al., 1998; Marzke et al., 1998; Williams-Hatala et al., 2018). In chimpanzes, also, this ray is remarkavely short (Inouye, 1992) which also affects the hand position and the weight bearing during knuckle-walking (Inouye, 1992; 1994; Matarazzo, 2013; Wunderlich & Jungers, 2009), yet they bear weight with all four fingers during suspension (Susman and Stern 1979), which also occurs during ascent and descent climbing in both chimpanzees and gorillas (Neufuss et al. 2017), and also in bonobos during vertical climbing, clambering and suspension (Samuel, Nauwelaerts, Stevens, & Kivell, 2018).

Conclusions

Differences in FR for PP2-PP4 among taxa can be related to the overall amount of force that the taxa place on their hands. FR are more developed in groups which use their hands for traveling and manipulation (gorillas and chimpanzees) in comparison with humans, who use them exclusively for manipulation.

Each genus has a unique insertion pattern across digits, with FR variability being most homogeneous in gorillas, less so in humans, and least homogenous in chimpanzees. These patterns strongly correspond to differences in phalangeal size across digits, with the exception of PP5 in humans. This human phalanx also has FR that is as large as that of chimpanzees, which may be related to the forceful precision grips characteristic of humans.

Supplementary data

Supplementary data (Tables S1-S3) associated with this article can be found in the Appendix.

Acknowledgements

We are grateful to the institutions holding the material we analyzed: the Royal Museum for Central (Belgium), Museu de Ciències Naturals de Barcelona (Spain), Zoologische Staatssammlung München (Germany), Universidad de Burgos (Spain), and to the people who kindly helped us there, especially to Emmanuel Gilissen, Javier Quesada, Anneke H. van Heteren, Michael Hiermeier and José Miguel Carretero. To Juan Ignacio Morales, Valerie Deschênes and Alexandros Karakostis for the scanning of the human sample. This study was funded by the research projects AGAUR 2017 SGR 1040 and MINECO PGC2018-093925-B-C32. A.B. would like to acknowledge financial support from Becas Chile (Conicyt, Chile).

References

Casado, A., Punsola, V., Gómez, M., de Diego, M., Barbosa, M., de Paz, F. J., & Potau, J. M. (2019). Three-dimensional geometric morphometric analysis of the distal radius insertion sites of the palmar radiocarpal ligaments in hominoid primates. *American Journal of Physical Anthropology*, 170, 24-36.

Cashmore, L. (2009). Can hominin 'handedness' be accurately assessed? *Annals of Human Biology*, 36, 624-641.

Danion, F., Li, S., Zatsiorsky, V. M., & Latash, M. L. (2002). Relations between surface EMG of extrinsic flexors and individual finger forces support the notion of muscle compartments. *European Journal of Applied Physiology*, 88, 185–88.

Doran, D.M., & Hunt, K.D. (1994). Comparative locomotor behavior of chimpanzees and bonobos. In: *Chimpanzee cultures*. Cambridge: Harvard University Press. Pp 93-108.

Doran, D. M. (1996). Comparative positional behavior of the African apes. In: *Great ape societies*. Cambridge: Cambridge University Press. Pp 213–224.

Doran, D. M. (1997). Ontogeny of locomotion in mountain. *Journal of Human Evolution,* 33, 323-344.

Doyle, J. R. (1988). Anatomy of the finger flexor tendon sheath and pulley system. *The Journal of Hand Surgery*, 13, 473-484.

Drapeau, M. S. M. (2008). Enthesis bilateral asymmetry in humans and African apes. *HOMO-Journal of Comparative Human Biology*, *59*, 93–109.

Eshed, V., Gopher, A., Galili, E., & Hershkovitz, I. (2004). Musculoskeletal stress markers in Natufian

hunter-gatherers and Neolithic farmers in the Levant : The upper limb. *American Journal of Physical Anthropology*, 315, 303–315.

Foster, A., Buckley, H., & Tayles, N. (2014). Using enthesis robusticity to infer activity in the past: a review. *Journal of Archaeological Method and Theory*, 21, 511-533.

Hamrick, M. W., Churchill, S. E., Schmitt, D., & Hylander, W. L. (1998). EMG of the human flexor pollicis longus muscle: Implications for the evolution of hominid tool use. *Journal of Human Evolution*, 34, 123–136.

Hawkey, D. E., & Merbs, C. F. (1995). Activity-induced musculoskeletal stress markers (MSM) and subsistence strategy changes among ancient Hudson Bay Eskimos. *International Journal of Osteoarchaeology*, 5, 324–338.

Hunt, K. D. (1991). Positional behavior in the Hominoidea. *International Journal of Primatology*, 12, 95–118.

Hunt, K. D. (1992). Positional behavior in *Pan troglodytes* at the Mahale Mountains and the Gombe Stream National Park, Tanzania. American Journal of Physical Anthropology, 87, 83–105.

Hunt, K. D., Cant, J. G., Gebo, D. L., Rose, M. D., Walker, S. E., & Youlatos, D. (1996). Standardized descriptions of primate locomotor and postural modes. *Primates,* 37, 363-387.

Inouye, S. E. (1992). Ontogeny and allometry of African ape manual rays. *Journal of Human Evolution*, 23, 107–138.

Inouye, S. E. (1994). Ontogeny of knuckle-walking hand postures in African apes. *Journal of Human Evolution*, *26*, 459-485.

Isler, K. (2002). Characteristics of vertical climbing in African apes. *Senckenbergiana Lethaea*, 82, 115–124.

Janssen, I., Heymsfield, S. B., Wang, Z., & Ross, R. (2000). Skeletal muscle mass and distribution in 468 men and women aged 18–88 yr. *Journal of Applied Physiology*, 89, 81–88.

Jungers, W. L., & Susman, R. L. (1984). Body size and skeletal allometry in African apes. In *The Pygmy Chimpanzee*. Springer, Boston. Pp 131-177.

Karakostis, F. A., Hotz, G., Tourloukis, V., & Harvati, K. (2018). Evidence for precision grasping in Neandertal daily activities. *Science Advances,* 4, eaat2369.

Karakostis, F. A., & Lorenzo, C. (2016). Morphometric patterns among the 3D surface areas of human hand entheses. *American Journal of Physical Anthropology*, 160, 694–707.

Key, A. J. M., Dunmore, C. J., & Marzke, M. W. (2019). The unexpected importance of the fifth digit during stone tool production. Scientific Reports, 9, 16724.

Lovejoy, C. O., Suwa, G., Simpson, S. W., Matternes, J. H. & White, T. D. (2009). The great divides: *Ardipithecus ramidus* reveals the postcrania of our last common ancestors with african apes. *Science,* 326, 100–106.

Marzke, M.W., Toth, N., Schick, K., & Reece, S. (1998). EMG study of hand muscle recruitment during hard hammer percussion manufacture of Oldowan tools. *American Journal of Physical Anthropology*, 105, 315–332.

Marzke, M. W., Wullstein, K. L., & Viegas, S. F. (1992). Evolution of the power ("squeeze") grip and its morphological correlates in hominids. *American Journal of Physical Anthropology,* 89(3), 283–298.

Marzke, M. W. (1997). Precision grips, hand morphology, and tools. *American Journal of Physical Anthropology,* 102, 91–110.

Masi, S., Cipolletta, C., & Robbins, M. M. (2009). Western lowland gorillas (*Gorilla gorilla gorilla*) change their activity patterns in response to frugivory. *American Journal of Primatology*, 71(2), 91–100.

Matarazzo, S. (2013). Manual pressure distribution patterns of knuckle-walking apes. *American Journal of Physical Anthropology*, 152, 44–50.

Milella, M. (2014). The influence of life history and sexual dimorphism on entheseal changes in modern humans and african great apes. *PLoS ONE,* 9, e107963.

Neufuss, J., Robbins, M. M., Baeumer, J., Humle, T., & Kivell, T. L. (2017). Comparison of hand use and forelimb posture during vertical climbing in mountain gorillas (*Gorilla beringei beringei*) and chimpanzees *(Pan troglodytes). American journal of physical anthropology*, 164, 651-664.

Neufuss, J., Robbins, M. M., Baeumer, J., Humle, T., & Kivell, T. L. (2018). Gait characteristics of vertical climbing in mountain gorillas and chimpanzees. *Journal of Zoology,* 306, 129–138.

Neufuss, J., Robbins, M. M., Baeumer, J., Humle, T., & Kivell, T. L. (2019). Manual skills for food processing by mountain gorillas (*Gorilla beringei beringei*) in Bwindi Impenetrable National Park, Uganda. *Biological Journal of the Linnean Society,* 127, 543-562.

Nolte, M., & Wilczak, C. (2013). Three-dimensional surface area of the distal biceps enthesis, relationship to body size, sex, age and secular changes in a 20th century American sample. *International Journal of Osteoarchaeology*, 23, 163–174.

O'Neill, M. C., Umberger, B. R., Holowka, N. B., Larson, S. G., & Reiser, P. J. (2017). Chimpanzee super strength and human skeletal muscle evolution. *Proceedings of the National Academy of Sciences,* 114, 7343-7348.

Pouydebat, E., Reghem, E., Borel, A., & Gorce, P. (2011). Diversity of grip in adults and young humans and chimpanzees *(Pan troglodytes). Behavioural Brain Research,* 218, 21-28.

Rabey, K. N., Green, D. J., Taylor, A. B., Begun, D. R., Richmond, B. G., & McFarlin, S. C. (2015). Locomotor activity influences muscle architecture and bone growth but not muscle attachment site morphology. *Journal of Human Evolution*, 78, 91–102.

Remis, M. (1995). Effects of body size and social context on the arboreal activities of lowland gorilla Central African Republic. *American Journal of Physical Anthropology*, *97*, 413–433.

Remis, M. (1999). Tree structure and sex differences in arboreality among western lowland gorillas (*Gorilla gorilla gorilla*) at Bai Hokou, Central African Republic. Primates, 40, 383.

Remis, M. (2000). The gorilla paradox. The effects of body size and habitat on the positional behavior of lowland and mountain gorillas. In: *Primate Locomotion Recent Advances*. New york: Springer Science+Business MedAL New. Pp 95-106.

Samuel, D. S., Nauwelaerts, S., Stevens, J. M. G., & Kivell, T. L. (2018). Hand pressures during arboreal locomotion in captive bonobos (*Pan paniscus*). *Journal of Experimental Biology*, 221, jeb.170910.

Siegmund, F., & Papageorgopoulou, C. (2011). Body mass and body mass index estimation in medieval Switzerland. *Bulletin Der Schweizerischen Gesellschaft Für Anthropologie*, 17, 35–44.

Smith, R. J., & Jungers, W. L. (1997). Body mass in comparative primatology. *Journal of Human Evolution*, 32, 523-559.

Susman, R. L. (1979). Comparative and functional morphology of hominoid fingers. *American Journal of Physical Anthropology*, 50, 215–236.

Susman, R. L., & Stern, J. T. (1979). Telemetered electromyography of *flexor digitorum profundus* and *flexor digitorum superfi*cialis in *Pan troglodytes* and implications for interpretation of the 0.H. 7 hand. *American Journal of Physical Anthropology*, 50, 565–574.

Thorpe, S. K., Crompton, R. H., Guenther, M. M., Ker, R. F., & McNeill Alexander, R. (1999). Dimensions and moment arms of the hind and forelimb muscles of common chimpanzees (*Pan troglodytes*). *American Journal of Physical Anthropology*, 110, 179-199.

Tuttle, R., Shine, G., Basmajian, & Regenos, E. (1972). Electromyography of knuckle-walking: results of four experiments on the forearm of *Pan gorilla*. *American Journal of Physical Anthropology*, 37, 255-265.

Tuttle, R.H. & Watts, D. P. (1985). The positional behavior and adaptive complexes of *Pan gorilla*. In: Primate morphophysiology, locomotor analyses and human bipedalism. Tokyo: University of Tokyo Press. Pp 261–288.

Villotte, S., Castex, D., Couallier, V., Dutour, O., Knu, C. J., & Henry-gambier, D. (2010). Enthesopathies as occupational stress markers: Evidence from the upper limb. *Journal of Physical Anthropology,* 234, 224–234.

Wallace, I. J., Winchester, J. M., Su, A., Boyer, D. M., & Konow, N. (2017). Physical activity alters limb bone structure but not entheseal morphology. *Journal of human evolution*, 107, 14-18.

Walker, A. (2009). The strength of great apes and the speed of humans. *Current Anthropology*, 50(2), 229-234.

Weiss, E., Corona, L., & Schultz, B. (2012). Sex differences in musculoskeletal stress markers: Problems with activity pattern reconstructions. *International Journal of Osteoarchaeology, 22,* 70-80.

Weiss, E. (2004). Understanding muscle markers: Lower limbs. *American Journal of Physical* Anthropology, 238, 232–238.

Williams-Hatala, E. M., Hatala, K. G., Gordon, M., Key, A., Kasper, M., & Kivell, T. L. (2018). The manual pressures of stone tool behaviors and their implications for the evolution of the human hand. *Journal of Human Evolution,* 119, 14-26.

Williams-Hatala, K. G., Hiles, S., & Rabey, K. N. (2016). Morphology of muscle attachment sites in the modern human hand does not reflect muscle architecture. *Scientific Reports*, 6, 28353.

Wunderlich, R. E., & Jungers, W. L. (2009). Manual digital pressures during knuckle-walking in chimpanzees (*Pan troglodytes*). *American Journal of Physical Anthropology,* 139, 394–403.

Zumwalt, A. (2005). A new method for quantifying the complexity of muscle attachment sites. *The Anatomical Record,* 286, 21-28.

Zumwalt, A. (2006). The effect of endurance exercise on the morphology of muscle attachment sites. *Journal of Experimental Biology*, 209, 444–454.

MUSCLE STRENGTH AND ENTHESEAL SIZE IN HUMAN THUMBS: TESTING THE RELATIONSHIP WITH A CADAVERIC MODEL

Ana BUCCHI[1,2]

Maria Cristina MANZANARES[3]

Javier LUENGO[1,2]

Cristina BUCCHI[3,4]

Carlos LORENZO[1,2]

INTRODUCTION

In this study we analyze the relationship between strength and the entheseal area of the *opponens pollicis* (OP) and *abductor pollicis longus* (APL) muscles, two muscles of the hand whose main function is to oppose the thumb and move the thumb anteriorly, respectively.

We were interested in this link for two reasons: (1) to determine if muscular strength is related to entheseal size, and (2) to evaluate the predictive power of enthesis, age, sex and body size on muscular strength. With the latter objective we attempt to discuss whether it is reasonable to infer behaviour from entheses in the archaeological record. To figure out if the recruitment of muscles leaves a distinctive mark on the bone is a key component for understanding human hand evolution. This is because manipulative activities, like tool-related behaviours, could contribute to the anatomical changes in the hand of our lineage as well as explain the high dexterity we have (e.g. Hamrick et al. 1998; Key & Dunmore 2015; Kivell et al. 2015).

The ability of entheses to provide information on activity patterns has a long history of debate. Briefly, there are studies concluding that manual labour has an effect on entheseal morphology (Karakostis & Lorenzo 2016; Karakostis et al. 2017), and others stating that entheseal anatomy is strongly dependant on the biological profile of individuals (e.g. age and body size) which makes them poor behavioural indicators (Zumwalt 2006; Williams-Hatala et al. 2016; Djukic et al. 2015).

[1]Institut Català de Paleoecologia Humana i Evolució Social, Zona Educacional 4, Campus Sescelades URV, 43007, Tarragona, Spain
anabucchi@gmail.com

[2]Universitat Rovira i Virgili, Àrea de Prehistòria, Avinguda de Catalunya 35, 43002 Tarragona, Spain

[3]Unitat d'Anatomia i Embriologia Humana. Departament de Patologia i Terapèutica Experimental, Universitat de Barcelona, Barcelona, Spain

[4]CICO Research Centre, Facultad de Odontología, Universidad de la Frontera, Av. Francisco Salazar 01145, Temuco, Chile

KEY WORDS:
Metacarpal
Physiological cross-sectional area
Hand evolution

UISPP
The Journal of the International Union for Prehistoric and Protohistoric Sciences

Vol. 2
Special issue 2
September 2019

UISPP
The Journal of the International Union for Prehistoric and Protohistoric Sciences
Muscle strength and entheseal size in human thumbs
Vol 2-2: 38-42

MATERIAL AND METHODS

To investigate these issues, we have dissected 20 hands and forearms from fresh human cadavers of known sex and age at death held at the Human Donation Service of the Universitat de Barcelona (for details of the dissection procedures see Sacks and Roy 1982). The sample was composed by 15 different individuals (five of them were represented by their left and right hands and forearms). The mean age at death was 73.63 ± 10.29 years, 12 hands and forearms were from the right side, and eight were from the left side. We measured the physiological cross-sectional area (PCSA) of the OP and APL (Figure 1), which is proportional to muscular strength (Alexander 1975).

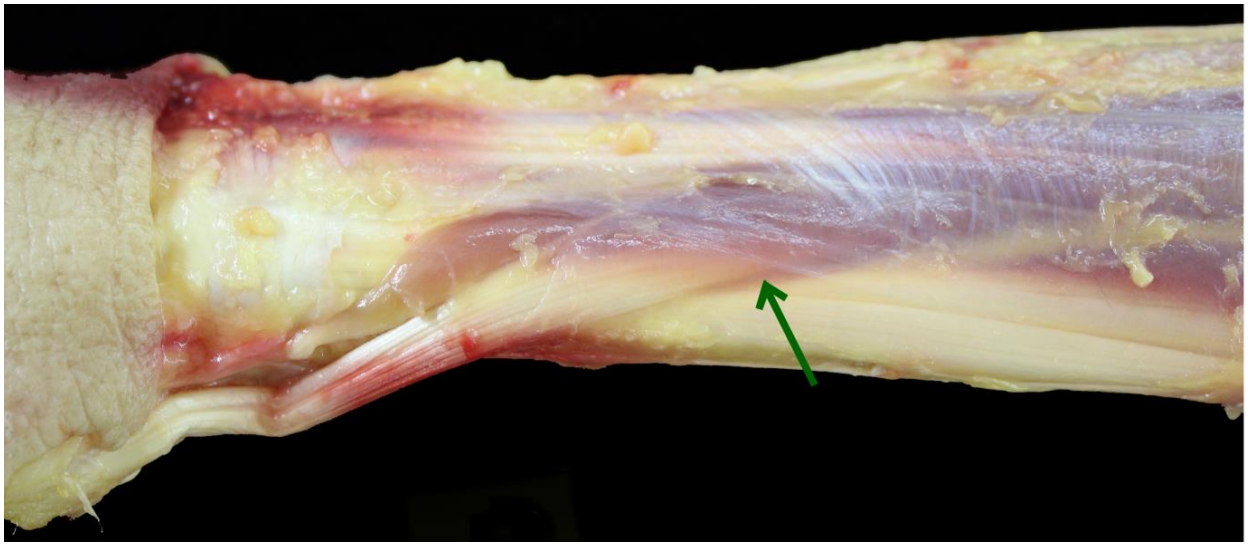

Fig. 1: Photograph of one of the individuals dissected in this study (lateral view). Green arrow shows the *abductor pollicis longus* muscle (APL).

To analyze the entheseal area we used the recent methodology proposed by Karakostis and Lorenzo (2016). High resolution 3D models of the bones were obtained using Breuckmann SmartScan structured-light scanner (Breuckmann Inc., Baden, Germany) and the absolute area (in mm2) of the entheses of the OP and APL were measured.

We also measured the length of the radius as an estimation of body size (mm).

A Pearson correlation test between entheseal area, PCSA, age and body size were performed, while the association between sex and entheseal area and PCSA was evaluated through an independent t-test. We then made simple and multiple linear regression of enthesis area on all other variables (PCSA, age, body size and sex) to evaluate their relative contribution, and the same test was carried out with PCSA as the dependent variable. Data analyses were performed in R Studio (R Development Core Team 2018).

Two out of the 20 individuals dissected presented evidence of osteoarthritis and were excluded from further analysis.

RESULTS

For the APL, entheseal area show a significant and relatively strong correlation with PCSA (0.61, $p<0.01$) (Figure 2), and with sex: on average females presented 23.63 mm^2 of entheseal area less than males ($t17= -7.9556$, $p<0.01$). There was also a significant average difference

UISPP
The Journal of the International Union for Prehistoric and Protohistoric Sciences
Muscle strength and entheseal size in human thumbs
Vol 2-2: 38-42

between males and females in PCSA, with females having less muscular strength (t17= -3.8833, p<0.01). Age and body size did not show a correlation with entheseal area of the APL. Interestingly, in the multiple regression analysis of insertion area on sex and PCSA of this muscle, PCSA was the only significant predictor of the size of the enthesis (p<0.01), $F(2,15)=4.609$, $p<0.05$, $R^2=0.38$. In turn, age and entheseal size significantly predicted PCSA, $F(2,15)=6.094$, $p<0.05$, $R^2=0.45$, and entheseal size alone predicted the 37% of the variance of the PCSA: $F(1,16)=9.25$, $p<0.01$, $R^2=0.366$.

OP only correlated significantly with the length of the radius (0.57, p<0.05), which significantly predicted 32% of the variance of the PCSA: $F(1,16)=7.605$, $p<0.05$.

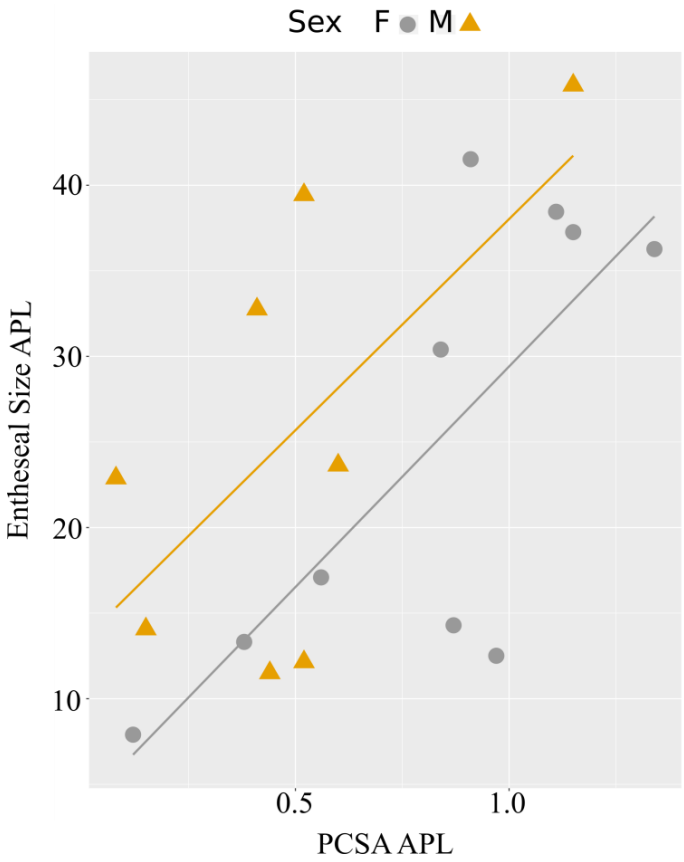

Fig. 2: Scatter plot of the entheseal area (mm^2) and the physiological cross-sectional area (cm^2) of the APL. Regression line is shown for males and females separately.

DISCUSSION AND CONCLUSION

These results mean that in the case of APL, muscular strength can be inferred from the size of the enthesis alone (and vice versa), in a relatively strong manner (Pearson's r between both variables was 0.61, p<0.01), validating a useful, simple way to infer muscular strength in paleoanthropological record. However, our results also indicate that strength of the muscles is dependent on the body size of individuals and their age, which is in line with previous studies showing a positive relationship with body size (Nedeljkovic et al. 2008) and a decrease in this muscular property with aging (for a review see Doherty 2003); R-squared raised from 37% to 45% when this last variable was added to the regression analysis.

Even so, there is a considerable proportion of the variance that is not explained by the biological profile of the individuals (sex, age and body size), which indicates that other relevant predictors were not studied here. We believe that it is reasonable to expect that activity patterns may have a potentially large influence on muscular properties and entheseal size as

UISPP
The Journal of the International Union for Prehistoric and Protohistoric Sciences

suggested in previous studies (e.g. Villotte et al. 2010; Karakostis et al. 2017), but this proposition remains to be further tested on material in which soft tissue is present. Sadly, no information about activity was available for the individuals dissected in this work, and therefore, it was not possible to evaluate its effect on muscle strength and entheseal size.

For OP, we found an analogous result than Williams-Hatala et al. (2016), who in a methodologically similar study found that entheseal size does not reflect architectural measurements (including PCSA) of the OP and *opponens digiti minimi* muscles.

The different results we obtain between APL and OP may be due to the histological composition of the tissue in the bone-tendon interface; APL has a fibrocartilaginous insertion, while OP has a fibrous attachment. Fibrous attachments dissipate stress over a relatively greater, but less-defined, area (Benjamin et al. 2006; Zumwalt 2006). Previous studies also proposed that fibrocartilaginous attachments are better indicators of general level of activities (Villotte et al. 2010).

There are few studies using dissected material with the aim of relating soft and hard tissue of hands (Shrewsbury et al. 2003; Marzke et al. 2007; Williams-Hatala et al. 2016) and, to our knowledge, ours provides the first promising results on the ability of bone features to provide information on muscular properties of this anatomical segment using this type of material. Further studies on other muscles of the hand would serve as corroborative data on this problem and may improve our knowledge on activity patterns and human hand evolution.

AKNOWLEDGMENTS

We want to thank the Human Body Donation Service at the University of Barcelona. We are also grateful to John Willman, Juan Ignacio Morales and Ester Lopez for their comments on this work. This work was supported by the General Directorate of Research of the Spanish Ministry of Science and Technology (MINECO/FEDER) [grant number CGL2015-65387-C3-1-P/2-P]; the Government of Catalonia, AGAUR, 2017 SGR 1040 Research Group; URV Project 2016PFR-URV-B2-17. A. B. and C. B. would like to acknowledge the support of the Becas Chile Program of the Comisión Nacional de Investigación Científica y Tecnológica (CONICYT, Chile).

BIBLIOGRAPHY

Alexander, R., 1975. The dimension of knee and muscles and the forces they exert. *Journal of Human Movement Studies,*1, pp.115-123.

Benjamin, M. et al., 2006. Where tendons and ligaments meet bone: Attachment sites ('entheses') in relation to exercise and/or mechanical load. *Journal of Anatomy*, 208(4), pp.471–490.

Djukic, K. et al., 2015. Bone microarchitecture at muscle attachment sites: The relationship between macroscopic scores of entheses and their cortical and trabecular microstructural design. *American Journal of Physical Anthropology*, 157(1), pp.81–93.

Doherty, T.J., 2003. Invited Review : Aging and sarcopenia. *Journal of Applied Physiology*, 95, pp.1717–1727.

Hamrick, M.W. et al., 1998. EMG of the human flexor pollicis longus muscle: Implications for the evolution of hominid tool use. *Journal of Human Evolution*, 34(2), pp.123–136.

Karakostis, F.A. & Lorenzo, C., 2016. Morphometric patterns among the 3D surface areas of human hand entheses. *American Journal of Physical Anthropology*, 160(4), pp.694–707.

Karakostis, F.A. et al., 2017. Occupational manual activity is reflected on the patterns among hand entheses. *American Journal of Physical Anthropology*, 164(1), pp.1–11.

Key, A.J.M. & Dunmore, C.J., 2015. The evolution of the hominin thumb and the influence exerted by the non-dominant hand during stone tool production. *Journal of Human Evolution*, 78, pp.60–69.

Kivell, T.L. et al., 2015. The hand of Homo naledi. *Nature Communications*, 6, pp.1–9.

UISPP
The Journal of the International Union for Prehistoric and Protohistoric Sciences
Muscle strength and entheseal size in human thumbs
Vol 2-2: 38-42

Marzke, M.W., Shrewsbury, M.M., & Horner, K.E., 2007. Middle Phalanx Skeletal Morphology in the Hand : Can it Predict Flexor Tendon Size and Attachments? *American Journal of Physical Anthropology* 151, pp.141-151.

Marzke, M.W., 2013. Tool making, hand morphology and fossil hominins. *Philosophical Transactions of the Royal Society B: Biological Sciences*, 368(1630), p.20120414.

Nedeljkovic, A. et al., 2008. Tests of Muscle Power Output: The Role of Body Size. *International journal of sports medicine*, 30(02), pp.100-106.

R Development Core Team., 2008. *R: A language and environment for statistical computing*. Viena: R Foundation for Statistical Computing.

Sacks, R.D. & Roy, R.R., 1982. Architecture of the hind limb muscles of cats: Functional significance. *Journal of Morphology*, 173(2), pp.185–195.

Shrewsbury, M.M. et al., 2003. Comparative morphology of the pollical distal phalanx. *American Journal of Physical Anthropology*, 121(1), pp.30–47.

Villotte, S. et al., 2010. Enthesopathies as Occupational Stress Markers: Evidence From the Upper Limb. *American Journal of Physical Anthropology*, 234(12), pp.224–234.

Williams-Hatala, K.G., Hiles, S. & Rabey, K.N., 2016. Morphology of muscle attachment sites in the modern human hand does not reflect muscle architecture. *Scientific Reports*, 6, pp.1–8.

Zumwalt, A., 2006. The effect of endurance exercise on the morphology of muscle attachment sites. *Journal of Experimental Biology*, 209(3), pp.444–454.

CHAPTER VI

Discussion and future perspectives

6.1 Evolutionary interpretations from bone shape

6.2 The signal on bone of activity patterns

Discussion and future perspectives

The studies conducted during this thesis present evidence both supporting and not supporting the widespread hypothesis that the human hand evolved to withstand stresses derived from tool-related behaviors. These analyses were made by examining extant hominid hands, which can reveal the skeletal traces of behavior during an individual's lifetime as well as the combined effects of natural selection and the long-term trends in the use of hands.

In summary, the study in Section 5.1 reveals that the pollical proximal phalanx in humans may not have evolved to accommodate the functional demands of the use of stone tools, as humans inefficiently distribute stress on these bones compared to great apes. The study in Section 5.2 does provide some support for the expectation that modern humans show a unique modular structure at the wrist, different from that of African apes. This might indicate that specific covariation patterns are shaping the evolution of the wrist in some primates and it remains to be seen whether these differences are associated with the use of stone tools. The analyses in sections 5.3 and 5.4 validate the study of entheses for making inferences on manual behaviors related to stone tool use in humans. They suggest that inferences on soft tissue recruitment are also possible in fossil hominins, particularly for muscles with fibrocartilaginous attachments and for ligaments. Below the main findings and limitations of these analysis are discussed as well as future venues of research.

6.1 Evolutionary interpretations from bone shape

The first research objective was to test whether the human thumb performs better than apes in terms of stress distribution on the proximal phalanx under simulated scenarios of hammerstone use (Chapter III). This study is presented in Section 5.1.

What motivated this analysis was that the thumb in humans is said to be highly derived and functionally adapted to the use of stone tools. The loads borne by this digit during stone tool-related behaviors are inferred to produce the evolution of the thumb in humans

(Williams et al., 2012; Key, 2016; Stephens et al., 2016; Williams-Hatala et al., 2018; Dunmore et al., 2020), yet it is currently unknown if the stresses associated with the use of stone tools were sufficient to produce such a strong selective pressure. The conclusion that it was a strong selective pressure is based on the thumb experiencing high manual stresses *relative* to other fingers during certain tool behaviors (Key et al., 2018; Williams-Hatala et al., 2018), not relative to the amount of load needed to drive an evolutionary change. Estimating this level would be very difficult, especially since we cannot observe fossil hominins using tools. In our study, using finite element analysis we assumed that if the thumb evolved to withstand the stresses associated with stone tool use, the modern human thumb should behave better in terms of stress distribution in a percussive activity when compared to our closest living relatives.

This analysis was made in CT and microCT scans of the proximal pollical phalanx in 6 specimens: four apes (a chimpanzee, a gorilla, an orangutan and a gibbon) and two humans (a modern human and a Neanderthal). We simulated a hammerstone striking into a core in 48 different scenarios by varying the muscle properties of the specimens, the weight of the hammerstone and the orientation of the hammerstone relative to the thumb. The results indicate the human phalanges (those of the modern human and Neanderthal) concentrate the stress in the center of the shaft, while great apes distribute stresses evenly on the bone. This makes the human phalanx more fragile and more prone to fracture than expected under the hypothesis that the human thumb evolved as an adaptation to withstand the stresses associated with stone tool use. These results led us to conclude that other selective pressures not related to the stress produced by percussive activities shaped this bone in humans. Note that this study does not imply necessarily that the thumb did not evolve as an adaptation to the use of tools, but rather that it did not specifically evolve to withstand the stresses associated with hard hammer percussion. Additionally, the results indicate that regardless of the muscle properties, how big the hammerstone was and how the thumb was oriented relative to the tool, the stress distribution was very similar across the different scenarios, yet the amount of stress increased when simulating the smaller hammerstone (480 g vs 700 g).

The conclusions of this work suggest other courses of analysis. One of them is to discover which anatomical characteristics explain the pattern of stress distribution found across species. The worst performing specimen under our scenarios was the gibbon, with the most apparent differences with the remaining phalanges being its very long, thin phalanx (see Almécija et al., 2015). One possibility is that robusticity plays a role in explaining the results

of the finite element analysis. However, the modern human thumb is said to be robust in comparison with those of great apes and hominins (Napier, 1962; Marzke, 1997; Green and Gordon, 2008; Galletta et al., 2019), and also that the human thumb's robusticity is an evolutionary effect of the loads associated with stone tool use (Rolian et al., 2011; Williams et al., 2012; Key and Dunmore, 2015).

There are several factors to be considered regarding robusticity in thumbs. The first is that in general the studies on robusticity in the thumb are based on external dimensions of the bone relative to either the same metrics in apes or that of another finger in the same species (Napier, 1962; Marzke, 1997; Green and Gordon, 2008; Galletta et al., 2019). To the best of my knowledge, cortical thickness in phalanges, which may affect stress distribution, has not been compared within primates. It is possible that compared to the thumb in apes, humans have a relatively bigger thumb phalanx but with thin cortices, and this remains to be investigated further.

Second, it is also possible that the bone adaptation to locomotion in apes makes these taxa more resistant to the simulated use of a hammerstone. The thumb does not touch the substrate during knuckle-walking and brachiation (Straus, 1940; Van Horn, 1972; Wunderlich and Jungers, 2009; Matarazzo, 2013), but it does during climbing and suspension (McClure et al., 2012; Neufuss et al., 2017, 2018; Samuel et al., 2018). If great apes have adapted the thumb in response to habitual loading of the thumb during the later locomotor modes, it may also explain why great apes can also resist the loads exerted during simulation of hammerstone use more efficiently than humans. However, if this is the case, there would be no point in saying that the human thumb is robust (relative to those of apes), and that it evolved as an adaptation to the loads exerted during the use of stone tools. It remains to be seen whether the thumb performs better than in apes compared to fingers 2-5, yet the weight bearing loads that fingers 2-5 support during all modes of locomotion make this supposition unlikely.

An important area of future research would also be to investigate the stress distribution across different stone tool behaviors; in particular in hammerstone use during marrow acquisition and flake production, as these have been postulated as those with the greatest loads across digits and the most likely candidates for the functional evolution of hands (Williams-Hatala et al., 2018). Is there a stress pattern during these behaviors in the hands of humans that is more efficient than those of other primates?

As is usually done in a finite element analysis, a single element (a phalanx in this case) is tested to evaluate the relationship between form and function. However, there are benefits

in studying groups of several bones to evaluate how the variation of one is dependent on the variation of the others. Knowing the degree to which the variation of a bone is independent from the variation in another bone gives clues as to the evolvability and plasticity of an anatomical unit (Klingenberg, 2009; Esteve-Altava, 2017), and is thus important to understanding the evolution of complex structures. In Section 5.2, we analyzed the covariance structure of four wrist bones in humans, chimpanzees and gorillas (i.e., capitate, lunate, scaphoid and trapezium). Using no *a priori* modules, we tested 15 modular hypotheses. We inferred that there would be a linkage between these four bones which would set humans apart from African apes. This inference was based on traits dependent on one another and strongly linked (i.e., a module) eventually coevolved due to their coordinated response to selection (Olson and Miller, 1958; Klingenberg, 2009; Rolian et al., 2010), thus providing a line of evidence to discuss whether natural selection for efficient tool-related behaviors shaped the human wrist.

Function is a factor behind the formation of modules, as it can integrate parts that perform a common task (Cheverud, 1996; Esteve-Altava, 2017). Our study is based on this fundamental idea. We hypothesize that if the human hand evolved to respond to selective pressures related to tool behaviors, a distinctive pattern for modularity should emerge. On the other hand, the wrist of African apes is mainly loaded during locomotion (i.e., primary knuckle-walking, suspension, climbing, etc. See Doran (1996) for frequency on locomotor modes of African apes). Previous studies have debated whether there is a knuckle-walking complex in the chimpanzee's and gorilla's wrist (Corruccini, 1978; Richmond and Strait, 2000; Kivell and Schmitt, 2009; Williams, 2010); however, there is a lack of research into whether there is a covariance structure related to manipulation capabilities, such as those of humans.

Our results indicate that carpals have a high level of morphological independence, and in this respect, humans, chimpanzees and gorillas are similar. However, our analyses also show that the strength of the modular signal varies across carpals in these three taxa. For humans, we found evidence for two modules in these four bones; one composed of the capitate and lunate and the other including the scaphoid and trapezium. That the variation of the scaphoid is dependent on the variation of the trapezium, and vice versa, was only found for humans, whereas for chimpanzees and gorillas the two bones vary more independently. As discussed in the paper, it is noteworthy that the radial side of the carpals distinguish humans from African apes, as a considerable amount of the research on the wrist related to the enhanced manipulation abilities of humans mention the range of motion

allowed by the trapezium or trapezium-metacarpal joint (Susman and Creel, 1979; Tocheri et al., 2003, 2005; Drapeau, 2015; Marchi et al., 2017) and also at the radiocarpal joint, which involves the scaphoid (Williams et al., 2010, 2014).

Our results are consistent with the initial reports on the morphological changes in the trapezium and scaphoid for the paleoanthropological record (both around the Plio-Pleistocene transition), and also relative to the appearance of biomechanically more demanding technological behaviors. Previous reports indicate that a derived morphology of both the trapezium and scaphoid in hominins appeared around 2 Ma. The morphological changes in the trapezium that allow this bone to resist the axial forces involved in a forceful precision grip are reported for *Paranthropus*/early *Homo* (Marzke et al., 2010), and the derived human-like scaphoid is first reported for *Au. sediba* (Kivell et al., 2011) (details in Section 2.3.4). The changes in both the trapezium and scaphoid occurred a little before the origin of the Acheulean (1.7 Ma, Diez-Martín et al., 2015). In turn, the Acheulean would have been possible after the emergence of more forceful precision-manipulation in hominins (Key and Dunmore, 2018).

Yet in our study we show that the scaphoid and trapezium belong to the same module in humans, whether these two bones evolved in a coordinated manner as a response to selection for dexterity in hominins remains to be tested. Hominin fossils are necessary for this purpose, as is a more detailed landmark configuration than the simple one chosen in our study, so specific anatomical changes in the trapezium may be associated with other regions in the scaphoid, and vice versa. The simple landmark map of our study ensures statistical power of the analysis and is an exploratory analysis aimed at distinguishing covariance patterns across hominids. The results of the study fulfill our second research objective (Chapter III), which was to know whether African apes and humans differ in the modularity patterns at the wrist.

Although not directly related to the problem of this thesis, the results found for chimpanzees relative to gorillas are puzzling, as no common pattern was found between them. Previous studies suggest that the wrist morphology in African apes is functionally adapted to knuckle-walking (Richmond and Strait, 2000; Orr, 2005, 2017; Püschel et al., 2020). This putative complex would help to accommodate the heavy weight-bearing loads transmitted from digits 2-5 to the forearms during knuckle-walking. Thus, it is striking that although the importance of the wrist during locomotion, chimpanzees and gorillas do not share a common modularity pattern that distinguishes them from humans. A possible explanation for this might be that, although the primary locomotor mode of chimpanzees and gorillas is

knuckle-walking, this is not the same phenomenon in terms of biomechanics (Inouye, 1994; Kivell and Schmitt, 2009; Matarazzo, 2013). For instance, gorillas and chimpanzees differ in their relative digital length, thus affecting the manual pressure distribution across the hand (Matarazzo, 2013).

6.2 The signal on bone of activity patterns

The studies in the previous section are focused over an evolutionary timescale, not the individual's lifetime. The next two studies, presented in chapters 5.3 and 5.4, have in common that they test whether entheses signal the actual behavior individuals experience throughout their life.

There are important methodological limitations in the study of entheses that prevent looking directly at an entheseal pattern related to stone tool use. There is currently an important discussion in the anthropology community on whether changes in size and complexity of insertion sites signal behavior or whether the influence of variables such as sex is so great that it obscures any functional interpretation (Zumwalt, 2006; Rabey et al., 2015; Williams-Hatala et al., 2016). Therefore, this method needs to be validated before it can be applied to fossils of unknown tool repertoires. If entheses do signal behavior, this would validate the previous functional interpretation of the use of hand in hominins. This was what motivated our analyses in sections 5.3 and 5.4.

In Section 5.3 we modified the common type of entheseal analysis; in general, anthropologists quantify the size or complexity of insertion sites of past human populations having unknown activity patterns and try to infer behavior from the insertion sites (for a review see Foster et al., 2014), whereas we studied species about which we know *a priori* that they vary in terms of the systematic use of the hand, to test whether this known difference is reflected in the insertion sites. For this purpose, we study the areas of insertion of ligaments holding the *flexor digitorum superficialis* and *profundus* muscles at proximal phalanges 2-5 (flexor ridges). These muscles are active during the most frequent forms of locomotion of chimpanzees and gorillas (Tuttle et al., 1972; Susman and Stern, 1979) and also during manipulation activities that involve flexing the fingers (Mohideen and Sidek,

2011), including the use of tools (Marzke et al., 1998). Therefore, larger flexor ridges were expected in African apes under the assumption that entheses signal the frequency and level of recruitment of these muscles for both locomotion and manipulation. We attempted to perform this analysis as objectively as possible, so we measured the area of the flexor ridges in 3D models of proximal phalanges. Using 3D models to score insertion site development (Zumwalt, 2005; Noldner and Edgar, 2013; Sanchez et al., 2013; Karakostis and Lorenzo, 2016) reduces the inter-observer error of previous approaches based on visual scoring (Hawkey and Merbs, 1995; Henderson et al., 2016).

A significant difference in the size of the flexor ridges of phalanges 2 to 4 was found between humans and African apes, and this difference remains when controlled for body size. We concluded that the greater manual loading of hands in gorillas and chimpanzees, for both the manipulation of objects and locomotion, explains the larger size relative to humans. This may imply that once the hands of hominins were liberated from locomotion, it became more likely that an insertion site pattern related to manual dexterity would have emerged. Kivell et al. (2011) mentions that this moment would be from *H. antecessor* on, as this species had smaller flexor ridges than early hominins and apes (Lorenzo et al., 1999).

However, it should be noted that differences in locomotion between African apes and humans are large differences in behavior. One may think that while locomotion leaves bigger entheses in African apes relative to humans, this does not necessarily mean that muscle activities that impose lower mechanical loadings, for example the use of stone tools, will leave a distinctive entheseal pattern on the hand as well. Our results for the fifth phalanx in humans, however, indicate that the special morphology of the metacarpophalangeal joint in humans, related to the greater recruitment of this finger relative to the other fingers during a forceful precision grip (Key et al., 2019), may affect the development of the flexor ridges of the fifth phalanx. The flexor ridges were larger than expected given the size of the fifth phalanx and as large as those of chimpanzees. This provides evidence that manipulation capabilities might be observed in the entheseal patterns of the hand.

In summary, the previous results indicate that large known differences in behavior between African apes and humans are reflected in the size of the flexor ridges. They also indicate that entheses may signal manipulation capabilities, as suggested for the flexor ridges of phalanx 5 in humans. These results fulfill the third research objective (Chapter III).

It remains to be tested whether the muscle activation pattern associated with a grip category leaves a specific entheseal pattern. This is a difficult challenge considering there is a substantial diversity in gripping repertoires in primates (MacFarlane and Graziano, 2009;

Pouydebat et al., 2009; Bardo et al., 2016; Key et al., 2018; Neufuss et al., 2019) (Section 2.2), and that all of these might affect entheseal development, which probably prevents an association with a specific grip type. In particular, information is missing on whether the few grip categories that are unique to humans (forceful precision and power "squeeze" Marzke and Wullstein, 1996) and associated with the effective use of tools, leave a specific entheseal pattern on the hand. An electromyographic study in Marzke et al. (1998) defined the muscle activation pattern for 17 muscles of the hand during the unique forceful precision grip capability in humans. Future analysis may build on that study by analyzing if this muscle activation pattern is correlated with an entheseal pattern. If this distinctive pattern does exist, it would enable discussion on how earlier hominins were using tools in a way similar to modern humans.

The conference proceeding presented in Section 5.4 builds on this problem. It analyzes two active muscles during a forceful precision grip, the *opponent pollicis* and the *abductor pollicis longus* muscle, in a sample of cadaveric human hands of known sex and age to evaluate their relation with their insertion sites.

The proportionately well-developed intrinsic muscles of the thumb, and their greater torque are features distinguishing humans from apes (Tuttle, 1969; Marzke et al., 1999) and are predictive of effective precision grip repertoires in hominins (Marzke, 1997; Marzke et al., 1998) (Section 2.3.3.2). According to Marzke et al. (1999), the *opponens pollicis* muscle in humans has a larger physiological cross-sectional area (PCSA) and moment arm for movements in the abduction/adduction and flexion/extension planes, improving the ability to hold large objects on one hand. Although the activity of the *abductor pollicis longus* muscle was not measured in the electromyographic study by Marzke et al. (1998), this muscle plays an important role in stabilizing the trapeziometacarpal joint during a forceful pinch (Marzke et al., 1999).

The results of the analysis indicate that there is a correlation between the strength of the muscle (PCSA) and the size of the entheses of the *abductor pollicis longus* muscle. The size of its enthesis can predict the PCSA of this muscle, as it explains 37% of the variance. This indicates that muscle strength can be inferred from this osseous counterpart. After controlling for the effects of confounding factors (sex, age and body size), an important proportion of the variance of entheseal size and muscle strength remains to be explained. The variable(s) behind this could be variation in activity patterns, and further research is needed along this line. According to Lovejoy et al. (2009), prominent attachment for this muscle would already be present in *Ar. ramidus* as in later hominins, which is in line with

this muscle improving thumb dexterity in humans (Marzke et al., 1999). Interestingly, *Ar. ramidus* fossils are much older than the first record of the systematic use of stone tools (Fig. 2.11), which highlights the possibility that the *abductor pollicis longus* muscle was recruited for non-tool use behaviors, or at least not for stone tool use.

Unlike the *abductor pollicis longus*, the strength of the *opponens pollicis* muscle only correlated with the size of individuals but not with its corresponding attachment site. No inferences on muscle strength for this muscle could thus be made based on the size of its insertion sites. Our results therefore argue against the functional interpretations of manipulation capabilities and stone tool behaviors in hominins formulated on the basis of the degree of development of this muscle's insertion sites (Susman, 1988; Kivell et al., 2011; Maki and Trinkaus, 2011). In particular, a poorly developed attachment site for *Au. sediba* (Kivell et al., 2011), *Au. Afarensis* (Bush et al., 1982) and *P. boisei* (Richmond et al., 2020) has been proposed to argue that they were not opposing the thumb and holding and manipulating large objects as effectively as modern humans, contrary to later hominins such as *P. robustus*/early *Homo* (Susman, 1988), *H. naledi* (Kivell et al., 2015) and Neanderthals (Maki and Trinkaus, 2011; Karakostis et al., 2018).

The above results account for the fourth objective of this thesis, i.e., to assess if the variation in muscle properties of these muscles can be linked to the variation in their insertion site sizes (Chapter III).

The different results found for the *opponens pollicis* and *abductor pollicis longus* muscles may be due to the fibrous attachment of the first muscle to the bone. This type of attachment dissipates stress over a relatively greater but less-defined area than the fibrocartilaginous attachments (Benjamin et al. 2006; Zumwalt 2006), which in the case of the *opponens* muscle is the whole length of the diaphysis at the first metacarpal on the radial side (Fig. 2.2). By contrast, the fibrocartilaginous attachments, like those of the *abductor pollicis longus* muscle, have proven to be better indicators of general activity level (Villotte et al., 2010; Henderson et al., 2016). If the type of attachment affects entheseal development as previous studies also suggest (Benjamin et al., 2002; Villotte et al., 2010; Henderson et al., 2016), this would imply for the case of stone tool use that only those muscles with fibrocartilaginous attachments may be in the position of reflecting gripping repertoires.

However, it should be noted that the type of material used in this study has limitations. The most important is arguably the high mean age at death of the sample (73.63 ± 10.29). This implies not only a decrease in some architectural measurements such as PCSA with aging (Doherty, 2003), but also that the variability in architectural parameters is probably

reduced relative to a younger sample. This narrows the chances of finding a behavioral trace in the entheseal development, in the case that they do signal behavior. Although these are important factors to consider, they do not explain why, in the same sample, different results were found between the *opponens pollicis* and *abductor pollicis longus* muscles. It is also worth noting that in such an old sample it is possible to find a relationship between muscle strength and entheseal size (for the *abductor pollicis longus* muscle).

Chapter VII

Conclusions

Conclusions

The aim of this doctoral thesis was to assess if the modern human hand is functionally adapted to stone tool-related behaviors. The main conclusions are the following:

Section 5.1 Finite element analysis of the proximal phalanx of the thumb in Hominoidea during simulated stone tool use.

- Compared to apes, the human first proximal phalanx appears to be one of the most fragile bones when scenarios of hammerstone use were simulated through a finite element analysis. In humans, the stress on the phalanx at the moment of striking is concentrated in the center of the shaft, while in great apes it is evenly distributed over the bone. This runs counter to the expectation that the stress would be better distributed in our species than in other hominids because, unlike apes, the human hand is supposed to be adapted to tool-related behaviors. We concluded that the evolution of this bone in humans was not driven by better adaptation to the loads of hammerstone use.
- Peak and mean stress levels were considerably higher when the smaller hammerstone (i.e., 400 vs 780 grams) was simulated in all species, while the effect of hammerstone orientation relative to the thumb was less important.
- Variation in the shape of the phalanges across taxa explains the difference in performance of specimens in terms of stress distribution, yet it remains to be seen which specific morphological features are behind this pattern.

Section 5.2 Modularity of the wrist in extant hominoids.

- Carpals (i.e., capitate, lunate, scaphoid and trapezium) show a high degree of morphological independence in hominoids.
- The degree to which some carpals covary is not the same for humans, chimpanzees and gorillas. In humans, there is a degree of covariation between the lunate and capitate, and between the scaphoid and trapezium. In gorillas, lunate and capitate

also covary, yet unlike in humans, scaphoid and trapezium are more independent. Chimpanzees exhibit the highest level of independence across carpals. No common modularity pattern was found for knuckle-walkers.

- The level of covariation between the trapezium and scaphoid is what sets humans apart from African apes. Thus, among these four carpals, the scaphoid and trapezium are the most likely candidates for testing the hypothesis that there is a functional modularity in humans related to manual dexterity. These results may be in line with the hypothesis that stone tool use drives the covariation structure of the human wrist, yet it remains to be confirmed that it is linked to a particular functional performance.

Section 5.3. Insertion sites in manual proximal phalanges of African apes and modern humans.

- The flexor ridges reflect differences in locomotion and manipulation between African apes and humans, and they also indicate that specific manipulation capabilities may leave a skeletal signal as to the size of insertion sites.
- Chimpanzees and gorillas exhibit larger flexor ridges than humans for proximal phalanges 2 to 4, and this difference remains after controlling for body size. This difference is probably linked to the recruitment of the flexor muscles (*flexor digitorum profundus* and *superficialis*) during knuckle-walking, climbing and suspension.
- Each genus has a unique pattern of flexor ridges across digits, and these patterns highly correspond to the size of the corresponding phalanges. The only exception is phalanx 5 in humans, which has larger flexor ridges than expected for the size of this phalanx, and similar to those of chimpanzees. The flexor ridges of the fifth human proximal phalanx may signal the forceful precision grip capabilities of humans, in which this finger is greatly and frequently recruited.
- This analysis, in which taxa with known behavioral differences was studied, indicates that entheseal sizes are suitable for informing on the use of the hands in taxa with unknown activity patterns, such as hominins. Specifically, this is in line with the assumption that stone tool use could produce a bone adaptation to habitual loading during an individual's lifetime. Future studies could discover whether the unique forceful precision grip of humans leaves a specific entheseal pattern.

Section 5.4. Muscle strength and entheseal size in human thumbs: testing the relationship with a cadaveric model.

- Stronger (i.e., larger physiological cross-sectional area) *opponens pollicis* muscle is not correlated with larger insertion site for this muscle. Enthesis for this muscle has been largely studied in hominins as indicative of stone tool use, but the results of our study recommend caution. Conversely, the strength of *abductor pollicis longus* muscle can be predicted to some extent based on the size of the enthesis of this muscle. The fibrocartilaginous attachment of this last muscle may explain this difference.
- Part of the variance of the *abductor pollicis longus* muscle's strength is not explained by sex, age or body size. This might be explained by behavioral differences across individuals.
- Future perspectives for Section 5.3 (see above), in that the unique grips indicative of effective tool use in humans might leave a specific entheseal pattern, are conditioned by the results of this study. They indicate that the entheseal pattern should specifically be sought in hand muscles with fibrocartilaginous attachments.

References

Adams, D.C., Collyer, M.L., 2019. Comparing the strength of modular signal, and evaluating alternative modular hypotheses, using covariance ratio effect sizes with morphometric data. Evolution. 73, 2352–2367.

Alba, D.M., Moyà-Solà, S., Köhler, M., 2003. Morphological affinities of the *Australopithecus afarensis* hand on the basis of manual proportions and relative thumb length. Journal of Human Evolution. 44, 225–254.

Almécija, S., Alba, D.M., 2014. On manual proportions and pad-to-pad precision grasping in *Australopithecus afarensis*. Journal of Human Evolution. 73, 88–92.

Almécija, S., J.Wallace, I., Judex, S., Alba, D.M., Moyà-Solà, S., 2015a. Comment on "Human-like hand use in *Australopithecus africanus*." Science. 347, 395–399.

Almécija, S., Moyà-Solà, S., Alba, D.M., 2010. Early origin for human-like precision grasping: A comparative study of pollical distal phalanges in fossil hominins. PLoS ONE. 5, e11727.

Almécija, S., Smaers, J.B., Jungers, W.L., 2015b. The evolution of human and ape hand proportions. Nature Communications. 6, 7717.

Bardo, A., Borel, A., Meunier, H., Guéry, J.P., Pouydebat, E., 2016. Behavioral and functional strategies during tool use tasks in bonobos. American Journal of Physical Anthropology. 161, 125–140.

Bardo, A., Cornette, R., Borel, A., Pouydebat, E., 2017. Manual function and performance in humans, gorillas, and orangutans during the same tool use task. American Journal of Physical Anthropology. 164, 821–836.

Benjamin, M., Kumai, T., Milz, S., Boszczyk, B.M., Boszczyk, A.A., Ralphs, J.R., 2002. The skeletal attachment of tendons-tendon "entheses." Comparative Biochemistry and Physiology - A. 133, 931–945.

Bush, M.E., Lovejoy, C.O., Johanson, D.C., Coppens, Y., 1982. Hominid carpal, metacarpal, and phalangeal bones recovered from the Hadar formation: 1974–1977 collections. American Journal of Physical Anthropology. 57, 651–677.

Carvalho, S., Braun, D.R., Kaplan, R., Beardmore-Herd, M., Plummer, T., Biro, D., Matsuzawa, T., 2019. Stone selection by chimpanzees reveals parallel patterns to Oldowan hominins. In: 9th European Society for the Study of Human Evolution meeting, 24-26 September, Brussels.

Casillas, J.A., Adán, G.E., 2005. Rescatando la memoria: La actuación arqueológica en el Solar de Caballería y el Convento de San Pablo de Burgos. Instituto Municipal de Cultura del Ayuntamiento de Burgos, Burgos.

Cheverud, J.M., 1996. Developmental integration and the evolution of pleiotropy. American

Zoologist. 36, 44–50.

Christel, M.I., Kitzel, S., Niemitz, C., 1998. How precisely do bonobos (*Pan paniscus*) grasp small objects? International Journal of Primatology. 19, 165–194.

Corruccini, R.S., 1978. Comparative osteometrics of the hominoid wrist joint, with special reference to knuckle-walking. Journal of Human Evolution. 7, 307–321.

Diez-Martín, F., Sánchez Yustos, P., Uribelarrea, D., Baquedano, E., Mark, D.F., Mabulla, A., Fraile, C., Duque, J., Diáz, I., Pérez-González, A., Yravedra, J., Egeland, C.P., Organista, E., Domínguez-Rodrigo, M., 2015. The origin of the Acheulean: The 1.7 million-year-old site of FLK West, Olduvai Gorge (Tanzania). Scientific Reports. 5, 17839.

Diogo, R., Pastor, J.F., Ferrero, E., Barbosa, M., Potau, J., de Paz, F., Bello, G., Wood, B., 2011. Photographic and descriptive musculoskeletal atlas of *Gorilla*. With notes on the attachments, variations, innervation, synonymy and weight of the muscles. Science Publishers, New Hampshire.

Diogo, R., Pastor, J.F., Ferrero, E.M., Burrows, A., Wood, B., Potau, J.M., de Paz, F., Aziz, M.A., Arias-Martorell, J., 2012a. Photographic and descriptive musculoskeletal atlas of Gibbons and Siamangs (*Hylobates*). With notes on the attachments, variations, innervation, function and synonymy and weight of the muscles. Science Publishers, New Hampshire.

Diogo, R., Potau, J.M., Pastor, J.F., de Paz, F.J., Ferrero, E.M., Bello, G., Barbosa, M., Aziz, M.A., Arias-Martorell, J., & Wood, B., 2013a. Photographic and descriptive musculoskeletal atlas of orangutans. With notes on the attachments, variations, innervation, function and synonymy and weight of the muscles. Science Publishers, Boca Raton.

Diogo, R., Potau, J.M., Pastor, J.F., Paz, F.J. De, Ferrero, E.M., Bello, G., Barbosa, M., Aziz, M.A., Burrows, A.M., Arias-Martorell, J., Wood, B.A., 2013b. Photographic and descriptive musculoskeltal atlas of Chimpanzees. With notes on the attachments, variations, innervation, function and synonymy and weight of the muscles. Science Publishers, Boca Raton.

Diogo, R., Richmond, B.G., Wood, B., 2012b. Evolution and homologies of primate and modern human hand and forearm muscles, with notes on thumb movements and tool use. Journal of Human Evolution. 63, 64–78.

Doherty, T.J., 2003. Invited Review : Aging and sarcopenia. Journal of Applied Physiology. 95, 1717–1727.

Doran, D. M. (1996). Comparative positional behavior of the African apes. In: *Great ape societies*. Cambridge: Cambridge University Press.

Drapeau, M.S.M., 2015. Metacarpal torsion in apes, humans, and early *Australopithecus*: implications for manipulatory abilities. PeerJ. 3, e1311.

Dunmore, C.J., Bardo, A., Skinner, M.M., Kivell, T.L., 2020. Trabecular variation in the first metacarpal and manipulation in hominids. American Journal of Physical Anthropology. 171, 219–241.

Esteve-Altava, B., 2017. In search of morphological modules: A systematic review. Biological Reviews. 92, 1332–1347.

Falótico, T., Proffitt, T., Ottoni, E.B., Staff, R.A., Haslam, M., 2019. Three thousand years of wild capuchin stone tool use. Nature Ecology and Evolution. 3, 1034–1038.

Feix, T., Kivell, T.L., Pouydebat, E., Dollar, A.M., 2015. Estimating thumb-index finger precision grip and manipulation potential in extant and fossil primates. Journal of the Royal Society Interface. 12, 20150176.

Foley, R., Lahr, M.M., 2003. On stony ground: Lithic technology, human evolution, and the emergence of culture. Evolutionary Anthropology. 12, 109–122.

Foster, A., Buckley, H., Tayles, N., 2014. Using enthesis robusticity to infer activity in the past: a review. Journal of Archaeological Method and Theory. 21, 511–533.

Galletta, L., Stephens, N.B., Bardo, A., Kivell, T.L., Marchi, D., 2019. Three-dimensional geometric morphometric analysis of the first metacarpal distal articular surface in humans, great apes and fossil hominins. Journal of Human Evolution. 132, 119–136.

Gommery, D., Senut, B., 2006. La phalange distale du pouce d'*Orrorin tugenensis* (Miocène supérieur du Kenya). Geobios. 39, 372–384.

Gould, S.J., Vrba, E.S., 1982. Exaptation-A missing term in the science of form. Paleobiology. 8, 4–15.

Green, D.J., Gordon, A.D., 2008. Metacarpal proportions in *Australopithecus africanus*. Journal of Human Evolution. 54, 705–719.

Gumert, M.D., Malaivijitnond, S., 2013. Long-tailed macaques select mass of stone tools according to food type. Philosophical Transactions of the Royal Society B: Biological Sciences. 368, 20120413.

Haile-Selassie, Y., 2001. Late Miocene hominids from the Middle Awash, Ethiopia. Nature. 412, 178–181.

Hamrick, M.W., 2012. The developmental origins of mosaic evolution in the primate limb skeleton. Evolutionary Biology. 39, 447–455.

Hamrick, M.W., Churchill, S.E., Schmitt, D., Hylander, W.L., 1998. EMG of the human flexor pollicis longus muscle: Implications for the evolution of hominid tool use. Journal of Human Evolution. 34, 123–136.

Harmand, S., Lewis, J.E., Feibel, C.S., Lepre, C.J., Prat, S., Lenoble, A., Boës, X., Quinn, R.L., Brenet, M., Arroyo, A., Taylor, N., Clément, S., Daver, G., Brugal, J.-P., Leakey, L., Mortlock, R.A., Wright, J.D., Lokorodi, S., Kirwa, C., Kent, D. V., Roche, H., 2015. 3.3-million-year-old stone tools from Lomekwi 3, West Turkana, Kenya. Nature. 521, 310–315.

Hawkey, D.E., Merbs, C.F., 1995. Activity-induced musculoskeletal stress markers (MSM) and subsistence strategy changes among ancient Hudson Bay Eskimos. International Journal of Osteoarchaeology. 5, 324–338.

Henderson, C.Y., Mariotti, V., Pany-Kucera, D., Villotte, S., Wilczak, C., 2016. The new 'Coimbra Method': a biologically appropriate method for recording specific features of fibrocartilaginous entheseal changes. International Journal of Osteoarchaeology. 26, 925–932.

Inouye, S.E., 1994. Ontogeny of knuckle-walking hand postures in African apes. Journal of Human Evolution. 26, 459-485.

Karakostis, F.A., Hotz, G., Tourloukis, V., Harvati, K., 2018. Evidence for precision grasping in Neandertal daily activities. Science Advances. 4, eaat2369.

Karakostis, F.A., Lorenzo, C., 2016. Morphometric patterns among the 3D surface areas of human hand entheses. American Journal of Physical Anthropology. 160, 694–707.

Key, A.J.M., Merritt, S.R., Kivell, T.L., 2018. Hand grip diversity and frequency during the use of Lower Palaeolithic stone cutting-tools. Journal of Human Evolution. 125, 137–158.

Key, A.J.M., 2016. Manual loading distribution during carrying behaviors: Implications for the evolution of the hominin hand. PLoS ONE. 11, e0163801.

Key, A.J.M., Dunmore, C.J., 2015. The evolution of the hominin thumb and the influence exerted by the non-dominant hand during stone tool production. Journal of Human Evolution. 78, 60–69.

Key, A.J.M., Dunmore, C.J., 2018. Manual restrictions on Palaeolithic technological behaviours. PeerJ. 6, e5399.

Key, A.J.M., Dunmore, C.J., Marzke, M.W., 2019. The unexpected importance of the fifth digit during stone tool production. Scientific Reports. 9, 16724.

Kivell, T.L., Deane, A.S., Tocheri, M.W., Orr, C.M., Schmid, P., Hawks, J., Berger, L.R., Churchill, S.E., 2015. The hand of *Homo naledi*. Nature Communications. 6, 8431.

Kivell, T.L., Lemelin, P., Richmond, B.G., Schimtt, D., 2016. The primate wrist. In: The Evolution of the Primate Hand. Springer, New York.

Kivell, T.L., Barros, A.P., Smaers, J.B., 2013. Different evolutionary pathways underlie the morphology of wrist bones in hominoids. BMC Evolutionary Biology. 13, 229.

Kivell, T.L., Begun, D.R., 2007. Frequency and timing of scaphoid-centrale fusion in hominoids. Journal of Human Evolution. 52, 321–340.

Kivell, T.L., Kibii, J.M., Churchill, S.E., Schmid, P., Berger, L.R., 2011. *Australopithecus sediba* hand demonstrates mosaic evolution of locomotor and manipulative abilities. Science. 333, 1411–1417.

Kivell, T.L., Schmitt, D., 2009. Independent evolution of knuckle-walking in African apes shows that humans did not evolve from a knuckle-walking ancestor. Proceedings of the National Academy of Sciences. 106, 14241–14246.

Klingenberg, C.P., 2009. Morphometric integration and modularity in configurations of landmarks: Tools for evaluating a priori hypotheses. Evolution and Development. 11, 405–421.

Leakey, L.S.B., Tobias, P. V., Napier, J.R., 1964. A new species of the genus *Homo* from Olduvai Gorge. Nature. 202, 7–9.

Lorenzo, C., Arsuaga, J.L., Carretero, J.M., 1999. Hand and foot remains from the Gran Dolina Early Pleistocene site (Sierra de Atapuerca, Spain). Journal of Human Evolution. 37, 501–522.

Lovejoy, C. O., Simpson, S.W., White, T.D., Asfaw, B., Suwa, G., 2009. Careful climbing in the Miocene: the forelimbs of *Ardipithecus ramidus* and humans are primitive. Science. 326, 70-70e8.

Lovejoy, C.O., Suwa, G., Simpson, S.W., Matternes, J.H., White, T.D., 2009. The great divides: *Ardipithecus ramidus* reveals the postcrania of our last common ancestors with African apes. Science. 326, 100–106.

MacFarlane, N.B.W., Graziano, M.S.A., 2009. Diversity of grip in *Macaca mulatta*. Experimental Brain Research. 197, 255–268.

Maki, J., Trinkaus, E., 2011. Opponens pollicis mechanical effectiveness in Neandertals and early modern humans. PaleoAnthropology. 2011, 62–71.

Marchi, D., Proctor, D.J., Huston, E., Nicholas, C.L., Fischer, F., 2017. Morphological correlates of the first metacarpal proximal articular surface with manipulative capabilities in apes, humans and South African early hominins. Comptes Rendus Palevol. 16, 645–654.

Marzke, M.W., Toth, N., Schick, K., Reece, S., 1998. EMG study of hand muscle recruitment during hard hammer percussion manufacture of Oldowan tools. American Journal of Physical Anthropology. 105, 315–332.

Marzke, M.W., 1983. Joint functions and grips of the *Australopithecus afarensis* hand, with special reference to the region of the capitate. Journal of Human Evolution. 12, 197–211.

Marzke, M.W., 1997. Precision grips, hand morphology, and tools. American Journal of Physical Anthropology. 102, 91–110.

Marzke, M.W., 2013. Tool making, hand morphology and fossil hominins. Philosophical Transactions of the Royal Society B. 368, 20120414.

Marzke, M.W., Marchant, L.F., McGrew, W.C., Reece, S.P., 2015. Grips and hand movements of chimpanzees during feeding in Mahale Mountains National Park, Tanzania. American Journal of Physical Anthropology. 156, 317–326.

Marzke, M.W., Marzke, R.F., Linscheid, R.L., Smutz, P., Steinberg, B., Reece, S., An, K.N., 1999. Chimpanzee thumb muscle cross sections, moment arms and potential torques, and comparisons with humans. American Journal of Physical Anthropology. 110, 163–178.

Marzke, M.W., Pouydebat, E., 2009. Comments on E. Pouydebat, P. Gorce, Y. Coppens, V. Bels, 2009. Biomechanical study of grasping according to the volume of the object: Human versus non-human primates. J. Biomech. 42, 266-272. Journal of Biomechanics. 42, 2628–2629.

Marzke, M.W., Shackley, M.S., 1986. Hominid hand use in the Pliocene and Pleistocene - Evidence from experimental archeology and comparative morphology. Journal of Human Evolution. 15, 439–460.

Marzke, M.W., Tocheri, M.W., Steinberg, B., Femiani, J.D., Reece, S.P., Linscheid, R.L., Orr, C.M., Marzke, R.F., 2010. Comparative 3D quantitative analyses of trapeziometacarpal joint surface curvatures among living catarrhines and fossil hominins. American Journal of Physical Anthropology. 141, 38–51.

Marzke, M.W., Wullstein, K.L., 1996. Chimpanzee and human grips: A new classification with a focus

on evolutionary morphology. International Journal of Primatology. 17, 117–139.

Marzke, M.W., Wullstein, K.L., Viegas, S.F., 1992. Evolution of the power ("squeeze") grip and its morphological correlates in hominids. American Journal of Physical Anthropology. 89, 283–298.

Matarazzo, S., 2013. Manual pressure distribution patterns of knuckle-walking apes. American Journal of Physical Anthropology. 152, 44–50.

Matarazzo, S.A., 2015. Trabecular architecture of the manual elements reflects locomotor patterns in primates. PLoS ONE. 10, e0120436.

McBrearty, S., Jablonski, N.G., 2005. First fossil chimpanzee. Nature. 437, 105–108.

McClure, N., Phillips, A., Vogel ER, Tocheri, M., 2012. Unexpected pollex and hallux use in wild *Pongo pygmaeus wurmbii*. American Journal of Physical Anthropology. 147, S54–S208.

McPherron, S.P., Alemseged, Z., Marean, C.W., Wynn, J.G., Reed, D., Geraads, D., Bobe, R., Béarat, H.A., 2010. Evidence for stone-tool-assisted consumption of animal tissues before 3.39 million years ago at Dikika, Ethiopia. Nature. 466, 857–860.

Mercader, J., Barton, H., Gillespie, J., Harris, J., Kuhn, S., Tyler, R., Boesch, C., 2007. 4,300-Year-old chimpanzee sites and the origins of percussive stone technology. Proceedings of the National Academy of Sciences. 104, 3043–3048.

Mohideen, A.J.H., Sidek, S.N., 2011. Development of EMG circuit to study the relationship between flexor digitorum superficialis muscle activity and hand grip strength. In: 4th International Conference on Mechatronics, 17-19 May, Kuala Lumpur.

Moyà-Solà, S., Köhler, M., Alba, D.M., Almécija, S., 2008. Taxonomic attribution of the Olduvai Hominid 7 manual remains and the functional interpretation of hand morphology in robust australopithecines. Folia Primatologica. 79, 215–250.

Napier, J., 1962. The evolution of the hand. Scientific American. 207, 56–65.

Napier, J.R., 1956. The prehensile movements of the human hand. The Journal of Bone and Joint Surgery. 38, 902–913.

Napier, J.R., 1960. Studies of the hands of living primates. Proceedings of the Zoological Society of London. 134, 647–657.

Nelson, E., Rolian, C., Cashmore, L., Shultz, S., 2011. Digit ratios predict polygyny in early apes, *Ardipithecus*, Neanderthals and early modern humans but not in *Australopithecus*. Proceedings of the Royal Society B. 278, 1556–1563.

Neufuss, J., Humle, T., Cremaschi, A., Kivell, T.L., 2016. Nut-cracking behaviour in wild-born, rehabilitated bonobos (*Pan paniscus*): A comprehensive study of hand-preference, hand grips and efficiency. American Journal of Primatology. 79, e22589.

Neufuss, J., Robbins, M.M., Baeumer, J., Humle, T., Kivell, T.L., 2017. Comparison of hand use and forelimb posture during vertical climbing in mountain gorillas (*Gorilla beringei beringei*) and chimpanzees (*Pan troglodytes*). American Journal of Physical Anthropology. 164, 651–664.

Neufuss, J., Robbins, M.M., Baeumer, J., Humle, T., Kivell, T.L., 2018. Gait characteristics of vertical climbing in mountain gorillas and chimpanzees. Journal of Zoology. 306, 129–138.

Neufuss, J., Robbins, M.M., Baeumer, J., Humle, T., Kivell, T.L., 2019. Manual skills for food processing by mountain gorillas (*Gorilla beringei beringei*) in Bwindi Impenetrable National Park, Uganda. Biological Journal of the Linnean Society. 127, 543–562.

Niewoehner, W.A., Weaver, A.H., Trinkaus, E., 1997. Neandertal capitate-metacarpal articular morphology. American Journal of Physical Anthropology. 103, 219–233.

Noldner, L.K., Edgar, H.J.H., 2013. 3D representation and analysis of enthesis morphology. American Journal of Physical Anthropology. 152, 417–424.

Olson, E., Miller, R., 1958. *Morphological Integration*. University of Chicago Press, Chicago.

Orr, C.M., 2005. Knuckle-walking anteater: A convergence test of adaptation for purported knuckle-walking features of African hominidae. American Journal of Physical Anthropology. 128, 639–658.

Orr, C.M., 2017. Locomotor hand postures, carpal kinematics during wrist extension, and associated morphology in anthropoid primates. Anatomical Record. 300, 382–401.

Peña, A., 2018. Patterns of integration and modularity in the hominoid wrist (MSc thesis). Arizona State University. Retrieved from https://scholarspace.library.gwu.edu/concern/gw_etds/ms35t8905.

Pena, A., Patel, B. A., Orr, C. M., Almecija, S. 2018. Patterns of integration in the hominoid skeleton: a case-study on the wrist. 87th Annual Meeting of the American Association of Physical Anthropologists, 11-14 April, Austin.

Pickford, M., Senut, B., Gommery, D., Treil, J., 2002. Bipedalism in *Orrorin tugenensis* revealed by its femora. Comptes Rendus Palevol. 1, 191–203.

Platzer, W., 2003. *Color Atlas and Textbook of Human Anatomy Vol 1. Locomotor System*. Thieme, Stuttgart and New york.

Pouydebat, E., Gorce, P., Coppens, Y., Bels, V., 2009. Biomechanical study of grasping according to the volume of the object: Human versus non-human primates. Journal of Biomechanics. 42, 266–272.

Pouydebat, E., Reghem, E., Borel, A., Gorce, P., 2011. Diversity of grip in adults and young humans and chimpanzees (*Pan troglodytes*). Behavioural Brain Research. 218, 21–28.

Pruetz, J.D., Bertolani, P., 2007. Savanna Chimpanzees, *Pan troglodytes verus*, hunt with tools. Current Biology. 17, 412–417.

Püschel, T.A., Marcé-nogué, J., Chamberlain, A.T., Yoxall, A., Sellers, W.I., 2020. The biomechanical importance of the scaphoid-centrale fusion during simulated knuckle-walking and its implications for human locomotor evolution. Scientific Reports. 10, 3526.

Rabey, K.N., Green, D.J., Taylor, A.B., Begun, D.R., Richmond, B.G., McFarlin, S.C., 2015. Locomotor activity influences muscle architecture and bone growth but not muscle attachment site morphology. Journal of Human Evolution. 78, 91–102.

Rein, T.R., 2011. The correspondence between proximal phalanx morphology and locomotion: Implications for inferring the locomotor behavior of fossil catarrhines. American Journal of Physical Anthropology. 146, 435–445.

Richmond, B.G., 2007. Biomechanics of phalangeal curvature. Journal of Human Evolution. 53, 678–690.

Richmond, B.G., Green, D.J., Lague, M.R., Chirchir, H., Behrensmeyer, A.K., 2020. The upper limb of *Paranthropus boisei* from Ileret, Kenya. Journal of Human Evolution. 141, 102727.

Richmond, B.G., Strait, D.S., 2000. Evidence that humans evolved from a knuckle-walking ancestor. Nature. 404, 382–385.

Ricklan, D.E., 1987. Functional anatomy of the hand of *Australopithecus africanus*. Journal of Human Evolution. 16, 643–664.

Robinson, J.T., 1972. *Early hominid posture and locomotion*. University of Chicago Press, Chicago.

Rolian, C., 2009. Integration and evolvability in primate hands and feet. Evolutionary Biology. 36, 100–117.

Rolian, C., Gordon, A.D., 2013. Reassessing manual proportions in *Australopithecus afarensis*. American Journal of Physical Anthropology. 152, 393–406.

Rolian, C., Lieberman, D.E., Hallgrímsson, B., 2010. The coevolution of human hands and feet. Evolution. 64, 1558–1568.

Rolian, C., Lieberman, D.E., Zermeno, J.P., 2011. Hand biomechanics during simulated stone tool use. Journal of Human Evolution. 61, 26–41.

Samuel, D.S., Nauwelaerts, S., Stevens, J.M.G., Kivell, T.L., 2018. Hand pressures during arboreal locomotion in captive bonobos (*Pan paniscus*). The Journal of Experimental Biology. 221, jeb170910.

Sanchez, S., Dupret, V., Tafforeau, P., Trinajstic, K.M., Ryll, B., Gouttenoire, P.J., Wretman, L., Zylberberg, L., Peyrin, F., Ahlberg, P.E., 2013. 3D microstructural architecture of muscle attachments in extant and fossil vertebrates revealed by synchrotron microtomography. PLoS ONE. 8, e56992.

Schilling, A.M., Tofanelli, S., Hublin, J.J., Kivell, T.L., 2014. Trabecular bone structure in the primate wrist. Journal of Morphology. 275, 572–585.

Seed, A., Byrne, R., 2010. Animal tool-use. Current Biology. 20, R1032–R1039.

Shrewsbury, M.M., Marzke, M.W., Linscheid, R.L., Reece, S.P., 2003. Comparative morphology of the pollical distal phalanx. American Journal of Physical Anthropology. 121, 30–47.

Skinner, M.M., Stephens, N.B., Tsegai, Z.J., Foote, A.C., Nguyen, N.H., Gross, T., Pahr, D.H., Hublin, J.-J., Kivell, T.L., 2015. Human-like hand use in *Australopithecus africanus*. Science. 347, 395–399.

Stephens, N.B., Kivell, T.L., Gross, T., Pahr, D.H., Lazenby, R.A., Hublin, J.J., Hershkovitz, I., Skinner, M.M., 2016. Trabecular architecture in the thumb of *Pan* and *Homo*: implications for

investigating hand use, loading, and hand preference in the fossil record. American Journal of Physical Anthropology. 161, 603–619.

Stephens, N.B., Kivell, T.L., Pahr, D.H., Hublin, J., Skinner, M.M., 2018. Trabecular bone patterning across the human hand. Journal of Human Evolution. 123, 1–23.

Straus, W.L., 1940. The posture of the great ape hand in locomotion, and its phylogenetic implications. American Journal of Physical Anthropology. 27, 199–207.

Straus, W.L., 1942. Rudimentary digits in primates. The Quarterly Review of Biology. 17, 228–243.

Susman, R., 1994. Fossil evidence for early hominid tool use. Science. 265, 1570–1573.

Susman, R.L., 1979. Comparative and functional morphology of hominoid fingers. American Journal of Physical Anthropology. 50, 215–236.

Susman, R.L., 1988. Hand of *Paranthropus robustus* from Member 1, Swartkrans: Fossil evidence for tool behavior. Science. 240, 781–784.

Susman, R.L., 1998. Hand function and tool behavior in early hominids. Journal of Human Evolution. 35, 23–46.

Susman, R.L., Creel, N., 1979. Functional and morphological affinities of the subadult hand (O.H. 7) from Olduvai Gorge. American Journal of Physical Anthropology. 51, 311–331.

Susman, R.L., De Ruiter, D., Brain, C.K., 2001. Recently identified postcranial remains of *Paranthropus* and early *Homo* from Swartkrans Cave, South Africa. Journal of Human Evolution. 41, 607–629.

Susman, R.L., Stern, J.T., 1979. Telemetered electromyography of flexor digitorum profundus and flexor digitorum superficialis in *Pan troglodytes* and implications for interpretation of the O.H. 7 hand. American Journal of Physical Anthropology. 50, 565–574.

Tocheri, M.W., Marzke, M.W., Liu, D., Bae, M., Jones, G.P., Williams, R.C., Razdan, A., 2003. Functional capabilities of modern and fossil hominid hands: Three-dimensional analysis of trapezia. American Journal of Physical Anthropology. 122, 101–112.

Tocheri, M.W., Orr, C.M., Jacofsky, M.C., Marzke, M.W., 2008. The evolutionary history of the hominin hand since the last common ancestor of *Pan* and *Homo*. Journal of Anatomy. 212, 544–562.

Tocheri, M.W., Razdan, A., Williams, R.C., Marzke, M.W., 2005. A 3D quantitative comparison of trapezium and trapezoid relative articular and nonarticular surface areas in modern humans and great apes. Journal of Human Evolution. 49, 570–586.

Toth, N., Schick, K.D., 2006. The Oldowan: Case studies into the earliest Stone Age. Stone Age Institute Press, Gosport.

Tsegai, Z.J., Kivell, T.L., Gross, T., Huynh Nguyen, N., Pahr, D.H., Smaers, J.B., Skinner, M.M., 2013. Trabecular bone structure correlates with hand posture and use in hominoids. PLoS ONE. 8, e78781.

Tuttle, R., Basmajian, J. V, Regenos, E., Shine, G., 1972. Electromyography of knuckle-walking:

Results of four experiments on the forearm of *Pan gorilla*. American Journal of Physical Anthropology. 37, 255–265.

Tuttle, R.H., 1969. Quantitative and functional studies on the hands of the Anthropoidea. Journal of Morphology. 128, 309–363.

Van Horn, R.N., 1972. Structural Adaptations to climbing in the gibbon hand. American Anthropologist. 74, 326–334.

Villotte, S., Castex, D., Couallier, V., Dutour, O., Knu, C.J., Henry-gambier, D., 2010. Enthesopathies as occupational stress markers: evidence from the upper limb. Journal of Physical Anthropology. 234, 224–234.

Visalberghi, E., Sirianni, G., Fragaszy, D., Boesch, C., 2015. Percussive tool use by Taï Western chimpanzees and Fazenda Boa Vista bearded capuchin monkeys: a comparison. Philosophical Transactions of the Royal Society B. 370, 20140351.

Ward, C., Leakey, M., Walker, A., 1999. The new hominid species *Australopithecus anamensis*. Evolutionary Anthropology. 7, 197–205.

Ward, C. V., Kimbel, W.H., Harmon, E.H., Johanson, D.C., 2012. New postcranial fossils of *Australopithecus afarensis* from Hadar, Ethiopia (1990-2007). Journal of Human Evolution. 63, 1–51.

White, T.D., Asfaw, B., Beyene, Y., Haile-Selassie, Y., Lovejoy, C.O., Suwa, G., Woldegabriel, G., 2009. *Ardipithecus ramidus* and the paleobiology of early hominids. Science. 326, 75–86.

Williams-Hatala, E.M., Hatala, K.G., Gordon, M., Key, A., Kasper, M., Kivell, T.L., 2018. The manual pressures of stone tool behaviors and their implications for the evolution of the human hand. Journal of Human Evolution. 119, 14–26.

Williams-Hatala, K.G., Hiles, S., Rabey, K.N., 2016. Morphology of muscle attachment sites in the modern human hand does not reflect muscle architecture. Scientific Reports. 6, 28353.

Williams, E.M., Gordon, A.D., Richmond, B.G., 2010. Upper limb kinematics and the role of the wrist during stone tool production. American Journal of Physical Anthropology. 143, 134–145.

Williams, E.M., Gordon, A.D., Richmond, B.G., 2012. Hand pressure distribution during Oldowan stone tool production. Journal of Human Evolution. 62, 520–532.

Williams, E.M., Gordon, A.D., Richmond, B.G., 2014. Biomechanical strategies for accuracy and force generation during stone tool production. Journal of Human Evolution. 72, 52–63.

Williams, S.A., 2010. Morphological integration and the evolution of knuckle-walking. Journal of Human Evolution. 58, 432–440.

Wolpoff, M. H., Senut, B., Pickford, M., Hawks, J., 2002. *Sahelanthropus* or '*sahelpithecus*'? Nature. 419, 581–582.

Wunderlich, R.E., Jungers, W.L., 2009. Manual digital pressures during knuckle-walking in chimpanzees (*Pan troglodytes*). American Journal of Physical Anthropology. 139, 394–403.

Wynn, T., Hernandez-Aguilar, R.A., Marchant, L.F., McGrew, W.C., 2011. "An ape's view of the

Oldowan" revisited. Evolutionary Anthropology. 20, 181–197.

Wynn, T., McGrew, W.C., 1989. An ape's view of the Oldowan. Man. 24, 383–398.

Young, N.M., Wagner, G.P., Hallgrimsson, B., 2010. Development and the evolvability of human limbs. Proceedings of the National Academy of Sciences. 107, 3400–3405.

Zollikofer, C.P.E., Ponce De León, M.S., Lieberman, D.E., Guy, F., Pilbeam, D., Likius, A., Mackaye, H.T., Vignaud, P., Brunet, M., 2005. Virtual cranial reconstruction of *Sahelanthropus tchadensis*. Nature. 434, 755–759.

Zumwalt, A., 2005. A new method for quantifying the complexity of muscle attachment sites. Anatomical Record. 286, 21–28.

Zumwalt, A., 2006. The effect of endurance exercise on the morphology of muscle attachment sites. Journal of Experimental Biology. 209, 444–454.

CHAPTER VIII

Appendix

8.1 Dissection database

Table S1 Sample information from dissected forearms.

Individual	Forearm[1]	Side	Age at death	Sex	HDS number[2]
1	1	Right	59	Male	55 M 17
1	2	Left	59	Male	55 M 17
2	3	Right	73	Female	46 F 17
2	4	Left	73	Female	46 F 17
3	5	Right	68	Female	53 M 17
4	6	Right	96	Female	55 F 17
5	7	Right	78	Female	44 F 17
5	8	Left	78	Female	44 F 17
6	9	Right	84	Male	39 M 17
6	10	Left	84	Male	39 M 17
7	11	Right	59	Female	65 F 17
8	12	Right	75	Female	61F17
9	13	Right	83	Female	64 F 17
10	14	Right	66	Female	63 F 17
11	15	Right	80	Female	45 F 17
11	16	Left	80	Female	45 F 17
12	17	Right	80	Female	27 F 18
13	18	Right	73	Male	19 M 18
13	19	Left	73	Male	19 M 18
14	20	Left	81	Male	17 M 18
15	21	Left	94	Female	26 F 18
16	22	Right	81	Female	21 F 18
17	23	Left	79	Female	66 F 17

[1]See Table S2 for details regarding muscle properties.
[2] HDS is the reference number of the individual at the Human Donation Service of the Universitat de Barcelona.

Table S2 Muscle properties (muscle and fiber length, mass and pennation angle) of the 23 dissected forearms. Details of individuals are in Table S1.

Forearm	Measurement[1]	Muscles[2]								
		APL	EPB	EPL	FPL	APB	AD	D1	FPB	OP
1	Muscle length 1 (mm)	132.4	100.0	120.8	141.4	67.0	68.4	57.2	59.9	54.8
	Muscle length 2 (mm)	130.8	99.2	125.7	142.3	66.7	68.6	56.3	60.1	52.6
	Muscle length 3 (mm)	134.2	101	123.8	140.8	66.6	66.1	54.9	61.0	52.1
	Pennation angle 1 (°)	1	8	0	10	4	9	6	0	10
	Pennation angle 2 (°)	5	5	0	22	3	16	6	1	5
	Pennation angle 3 (°)	2	10	0	28	5.5	10	6	6.	0
	Mass (g)	8.0	5.5	3.9	13.7	2.7	11.4	8.0	5.0	5.7
	Fiber length 1 (mm)	50.7	45.0	63.5	42.6	44.6	39.2	38.5	46.7	31.9
	Fiber length 2 (mm)	54.1	49.4	59.9	54.6	52.8	56.2	43.4	33.8	49.0
	Fiber length 3 (mm)	47.7	42.5	42.9	45.9	57.0	46.0	43.3	67.8	30.2
2	Muscle length 1 (mm)	148.0	87.9	131.5	142.0	54.0	65.4	59.0	56.0	51.0

	Muscle length 2 (mm)	149.5	88.4	131.1	143.5	54.6	65.0	58.0	56.8	51.5
	Muscle length 3 (mm)	149.8	89.0	135.4	142.6	55.8	67.0	57.6	56.1	49.0
	Pennation angle 1 (°)	2	20	3	2	0	12	2	9	6
	Pennation angle 2 (°)	5	6	0	17	0	9	7	5	5
	Pennation angle 3 (°)	10	5	5	35	5	5	5	5	5
	Mass (g)	9.2	4.5	4.0	13.4	2.6	11.8	8.1	4.0	2.1
	Fiber length 1 (mm)	38.9	50.1	51.4	13.5	42.4	44.5	29.8	46.3	31.6
	Fiber length 2 (mm)	50.5	53.0	44.1	68.0	48.8	49.0	40.6	31.4	46.1
	Fiber length 3 (mm)	24.0	45.7	47.3	44.4	38.5	48.8	42.8	30.3	28.0
3	Muscle length 1 (mm)	130.6	71.5	33.8	133.8	47.4	51.5	56.0	35.9	34.5
	Muscle length 2 (mm)	130.9	72.1	35.7	134.2	48.5	52.5	56.3	37.6	32.5
	Muscle length 3 (mm)	130.9	72.4	32.8	133.3	47.5	52.4	55.6	35.8	34.2
	Pennation angle 1 (°)	29	19	21	22	1	0	0	0	10
	Pennation angle 2 (°)	11	21	12	20	0	0	0	0	18
	Pennation angle 3 (°)	9	24	34	29	4	0	0	0	8
	Mass (g)	8.3	2.2	2.4	5.8	1.5	3.7	4.2	1.2	2.0
	Fiber length 1 (mm)	55.9	35.8	30.4	41.4	29.7	34.1	31.1	32.9	18.4
	Fiber length 2 (mm)	41.9	44.3	32.9	32.9	36.4	34.3	32.6	30.9	23.3
	Fiber length 3 (mm)	37.2	31.3	34.1	33.8	26.3	33.9	37.0	31.0	23.8
4	Muscle length 1 (mm)	124.8	114.2	147.4	127.6	51.7	51.5	54.9	40.4	37.0
	Muscle length 2 (mm)	125.0	116.9	149.9	124.2	48.9	52.1	53.6	41.8	38.8
	Muscle length 3 (mm)	125.5	116.2	149.2	127.9	50.2	52.2	53.6	41.9	38.3
	Pennation angle 1 (°)	14	-	4	12	0	15	11	1	0
	Pennation angle 2 (°)	22	5	15	17	0	10	10	4	1
	Pennation angle 3 (°)	22	24	12	19	0	25	7	4	2
	Mass (g)	7.0	2.5	3.7	6.6	2.0	44.1	3.4	1.4	2.1
	Fiber length 1 (mm)	39.6	44.5	52.5	73.0	36.4	36.3	41.4	37.9	31.6
	Fiber length 2 (mm)	44.0	42.4	61.7	93.7	49.8	35.0	41.4	39.6	31.7
	Fiber length 3 (mm)	42.8	30.0	64.7	62.6	37.1	32.9	39.4	35.0	32.4
5	Muscle length 1 (mm)	156.4	93.0	180.0	180.5	67.6	66.6	62.8	56.0	46.3
	Muscle length 2 (mm)	153.0	94.7	180.0	180.0	69.7	68.1	62.8	55.7	46.3
	Muscle length 3 (mm)	154.0	95.7	180.0	182.4	62.4	69.2	62.8	55.7	46.0
	Pennation angle 1 (°)	15	3	5	15	3	3	2	3	0
	Pennation angle 2 (°)	16	6	21	28	0	0	4	0	0
	Pennation angle 3 (°)	9	4	0	24	0	0	5	1	9
	Mass (g)	6.2	3.5	15.4	14.9	5.8	9.3	8.9	4.4	3.8
	Fiber length 1 (mm)	38.9	44.1	65.7	61.7	49.2	51.6	44.6	34.8	44.3
	Fiber length 2 (mm)	44.4	54.4	54.2	52.4	44.5	34.4	49.2	48.7	45.6

	Fiber length 3 (mm)	63.5	53.9	54.8	41.9	34.1	42.4	38.2	45.8	29.1
6	Muscle length 1 (mm)	110.9	106.9	117.1	147.8	55.9	54.3	47.5	50.3	48.1
	Muscle length 2 (mm)	114.8	108.3	118.4	148.2	55.8	52.8	46.0	51.4	46.7
	Muscle length 3 (mm)	113.3	107.8	117.5	147.2	58.0	53.1	46.9	49.6	49.0
	Pennation angle 1 (°)	15	6	3	0	0	11	20	0	0
	Pennation angle 2 (°)	22	6	14	16	0	20	9	0	5
	Pennation angle 3 (°)	22	3	8	17	0	30	0	0	7
	Mass (g)	3.3	2.4	2.9	4.6	1.8	4.0	1.7	1.8	1.5
	Fiber length 1 (mm)	40.7	41.4	48.2	28.2	33.7	30.2	39.6	30.9	26.0
	Fiber length 2 (mm)	36.8	45.6	33.9	36.4	43.3	39.9	36.3	40.6	35.0
	Fiber length 3 (mm)	38.8	39.6	34.7	41.5	38.7	39.0	34.4	26.8	27.3
7	Muscle length 1 (mm)	-	100.0	-	178.8	62.6	-	-	-	51.0
	Muscle length 2 (mm)	-	99.1	-	179	60.2	-	-	-	50.0
	Muscle length 3 (mm)	-	98.3	-	178.9	63.2	-	-	-	50.0
	Pennation angle 1 (°)	-	5	-	10	6	-	-	-	7
	Pennation angle 2 (°)	-	13	-	40	0	-	-	-	18
	Pennation angle 3 (°)	-	0	-	82	0	-	-	-	17
	Mass (g)	-	2.6	-	7.85	3.32	-	-	-	3.4
	Fiber length 1 (mm)	-	53	-	48.2	61.7	-	-	-	48.9
	Fiber length 2 (mm)	-	52.4	-	34.2	57.8	-	-	-	48
	Fiber length 3 (mm)	-	44.41	-	38.7	47	-	-	-	31.2
8	Muscle length 1 (mm)	149.8	63.9	171.8	163.1	60.7	69	55.4	57.9	53.6
	Muscle length 2 (mm)	151.4	62.7	169.3	162.4	60.8	67.5	56.5	58.2	52.1
	Muscle length 3 (mm)	148.9	64.5	-	160.7	61.7	68.6	56.9	59.1	55.0
	Pennation angle 1 (°)	5	11	0	17	10	0	12	3	0
	Pennation angle 2 (°)	28	22	14	28	4	0	5	4	0
	Pennation angle 3 (°)	16	29	11	34	0	0	0	0	3
	Mass (g)	6.8	0.85	3.2	8.6	3.2	7.6	3.34	2.86	2.31
	Fiber length 1 (mm)	49.3	46.3	56.6	60.5	43	44.5	35.6	39.6	34.2
	Fiber length 2 (mm)	63.3	46.8	49.6	59.7	43.5	55.8	46.8	42	43.1
	Fiber length 3 (mm)	73	-	50.35	61.26	45.6	52.5	36.6	33.2	39.6
9	Muscle length 1 (mm)	164.5	134.7	166.7	171.7	42.2	45.6	62.3	56.9	35.4
	Muscle length 2 (mm)	163.5	132.9	167.0	170.5	42.7	44.3	63.1	59.6	36.6
	Muscle length 3 (mm)	166.6	137.8	167.7	-	42.7	43.4	62.7	59.1	34.1
	Pennation angle 1 (°)	9	2	11	19	0	0	11	11	0
	Pennation angle 2 (°)	20	15	18	28	0	5	0	0	0
	Pennation angle 3 (°)	22	22	4	32	0	0	0	0	0

	Mass (g)	11.8	2.8	4.9	7.4	2.4	7.2	4.3	2.2	1.6
	Fiber length 1 (mm)	44.8	53.0	47.5	60.8	39.4	36.9	39.3	34.4	34.3
	Fiber length 2 (mm)	73.4	53.4	54.6	60.6	39.8	39.9	47.7	38.0	34.1
	Fiber length 3 (mm)	58.3	36.3	57.4	68.6	36.7	41.2	42.6	30.4	34.3
10	Muscle length 1 (mm)	152	-	-	-	-	-	60.6	-	70.1
	Muscle length 2 (mm)	152	-	-	-	-	-	61.6	-	68.8
	Muscle length 3 (mm)	152	-	-	-	-	-	61.6	-	68.0
	Pennation angle 1 (°)	0	-	-	-	-	-	4	-	0
	Pennation angle 2 (°)	11	-	-	-	-	-	0	-	4
	Pennation angle 3 (°)	3	-	-	-	-	-	15	-	4
	Mass (g)	16.2	-	-	-	-	-	3.6	-	6.9
	Fiber length 1 (mm)	79.1	-	-	-	-	-	43.7	-	40.1
	Fiber length 2 (mm)	80.3	-	-	-	-	-	35.5	-	46.8
	Fiber length 3 (mm)	96.4	-	-	-	-	-	-	-	44.8
11	Muscle length 1 (mm)	126.3	99.1	139.9	151.4	48.5	54.0	53.0	53.1	50.9
	Muscle length 2 (mm)	126.3	98.3	138.5	149.4	47.5	55.5	52.5	52.1	51.4
	Muscle length 3 (mm)	128.4	98.3	138.3	151.8	48.7	55.8	53.7	54.4	50.1
	Pennation angle 1 (°)	15	19	10	15	10	0	0	0	3
	Pennation angle 2 (°)	20	19	13	27	0	0	0	0	0
	Pennation angle 3 (°)	24	29	12	31	5	0	5	0	0
	Mass (g)	9.8	5.9	5.6	12.6	2.8	10.4	6.8	6.1	2.8
	Fiber length 1 (mm)	84.5	53.1	32.8	40.0	40.2	44.1	45.4	33.3	35.6
	Fiber length 2 (mm)	60.5	40.9	32.4	39.4	43.5	42.3	47.7	41.6	30.7
	Fiber length 3 (mm)	50.3	40.4	57.7	35.6	38.6	33.5	36.6	41.9	27.2
12	Muscle length 1 (mm)	144.8	78.7	151.8	142.6	50.3	62.0	50.2	48.6	45.6
	Muscle length 2 (mm)	145.5	76.2	151.9	143.9	50.1	61.9	50.8	48.6	46.6
	Muscle length 3 (mm)	144.3	77.9	151.9	144.9	50.9	61.5	50.7	49.1	46.4
	Pennation angle 1 (°)	15	30	10	6	0	10	0	0	0
	Pennation angle 2 (°)	11	14	14	11	0	14	0	0	0
	Pennation angle 3 (°)	10	26	8	21	0	6	0	0	0
	Mass (g)	6.8	1.3	4.1	10.3	2.5	4.0	4.4	2.6	1.7
	Fiber length 1 (mm)	65.4	45.8	47.3	46.7	39.2	42.1	38.5	37.5	35.6
	Fiber length 2 (mm)	57.0	49.3	50.7	63.7	43.2	36.3	33.9	45.6	32.6
	Fiber length 3 (mm)	56.9	47.0	69.2	66.3	50.4	38.9	44.1	42.8	33.3
13	Muscle length 1 (mm)	151.9	67.3	147.3	155.4	68.8	57.8	53.6	57.0	47.4
	Muscle length 2 (mm)	152.1	68.8	146.6	156.1	67.6	57.9	53.6	58.0	49.8
	Muscle length 3 (mm)	-	68.4	145.7	156.4	69.3	58.0	53.1	58.3	49.2

	Pennation angle 1 (°)	5	8	3	9	0	0	12	0	0
	Pennation angle 2 (°)	7	1	12	22	0	0	3	0	0
	Pennation angle 3 (°)	8	1	13	18	0	0	0	9	9
	Mass (g)	8.0	0.6	3.6	4.6	1.7	4.4	4.0	1.5	0.3
	Fiber length 1 (mm)	46.4	34.1	51.5	54.1	52.3	40.3	34.3	43.8	36.0
	Fiber length 2 (mm)	59.6	33.2	59.6	53.3	47.9	40.7	36.9	40.6	37.8
	Fiber length 3 (mm)	50.9	-	52.9	48.9	48.0	46.8	33.5	42.6	39.9
14	Muscle length 1 (mm)	145.4	95.4	148.7	159.5	53.1	59.6	62.1	51.3	45.7
	Muscle length 2 (mm)	143.8	96.4	148.3	160.0	54.1	61.1	62.2	52.0	46.0
	Muscle length 3 (mm)	143.8	97.6	147.8	160.0	54.1	61.0	62.2	51.1	46.9
	Pennation angle 1 (°)	25	8	10	11	7	3	11	0	0
	Pennation angle 2 (°)	10	10	13	22	0	0	15	0	0
	Pennation angle 3 (°)	20	9	11	21	0	0	9	0	0
	Mass (g)	8.6	1.2	4.0	8.5	2.8	6.3	4.1	2.0	2.5
	Fiber length 1 (mm)	60.2	39.2	57.7	48.9	43.6	39.8	38.5	43.3	36.2
	Fiber length 2 (mm)	61.0	51.4	59.0	48.9	47.2	45.0	35.9	44.5	39.9
	Fiber length 3 (mm)	64.7	40.4	64.1	45.7	53.3	40.7	34.7	41.0	30.9
15	Muscle length 1 (mm)	-	81.9	-	152.2	59.1	-	-	-	36.2
	Muscle length 2 (mm)	-	80.1	-	151.8	56.3	-	-	-	36.2
	Muscle length 3 (mm)	-	79.4	-	147.9	26.3	-	-	-	36.3
	Pennation angle 1 (°)	-	4	-	10	0	-	-	-	10
	Pennation angle 2 (°)	-	15	-	35	1	-	-	-	12
	Pennation angle 3 (°)	-	5	-	68	3	-	-	-	15
	Mass (g)	-	1.44	-	9.9	2.4	-	-	-	2.6
	Fiber length 1 (mm)	-	41.2	-	36.1	34	-	-	-	36.3
	Fiber length 2 (mm)	-	53.2	-	40.9	52.6	-	-	-	32.2
	Fiber length 3 (mm)	-	42.4	-	38.8	41.8	-	-	-	28.4
16	Muscle length 1 (mm)	-	-	-	-	-	-	-	-	-
	Muscle length 2 (mm)	-	-	-	-	-	-	-	-	-
	Muscle length 3 (mm)	-	66.7	-	156.6	56.4	-	-	-	48
	Pennation angle 1 (°)	-	1	-	25	15	-	-	-	1
	Pennation angle 2 (°)	-	4	-	28	0	-	-	-	6
	Pennation angle 3 (°)	-	3.5	-	19	0	-	-	-	9
	Mass (g)	-	0.7	-	9.4	2.4	-	-	-	3.3
	Fiber length 1 (mm)	-	3.9	-	4.8	4.5	-	-	-	3.9
	Fiber length 2 (mm)	-	-	-	-	-	-	-	-	-
	Fiber length 3 (mm)	-	-	-	-	-	-	-	-	-

17	Muscle length 1 (mm)	137.6	-	-	-	-	-	60.9	-	47.8
	Muscle length 2 (mm)	141.9	-	-	-	-	-	60.6	-	48.2
	Muscle length 3 (mm)	141.8	-	-	-	-	-	59.6	-	47.6
	Pennation angle 1 (°)	4.0	-	-	-	-	-	5.0	-	0.0
	Pennation angle 2 (°)	-	-	-	-	-	-	3.0	-	4.0
	Pennation angle 3 (°)	2.0	-	-	-	-	-	15.0	-	12.0
	Mass (g)	9.9	-	-	-	-	-	6.4	-	4.3
	Fiber length 1 (mm)	91.1	-	-	-	-	-	40.6	-	29.3
	Fiber length 2 (mm)	81.6	-	-	-	-	-	44.2	-	34.9
	Fiber length 3 (mm)	78.3	-	-	-	-	-	44.6	-	32.7
18	Muscle length 1 (mm)	149.2	-	-	-	-	-	60.2	-	54.5
	Muscle length 2 (mm)	146.8	-	-	-	-	-	63.2	-	57.7
	Muscle length 3 (mm)	147.6	-	-	-	-	-	63.4	-	56
	Pennation angle 1 (°)	3	-	-	-	-	-	0	-	0
	Pennation angle 2 (°)	0	-	-	-	-	-	22	-	0
	Pennation angle 3 (°)	10	-	-	-	-	-	5	-	3
	Mass (g)	9.05	-	-	-	-	-	6.3	-	3.4
	Fiber length 1 (mm)	67.7	-	-	-	-	-	31.1	-	37.5
	Fiber length 2 (mm)	66.6	-	-	-	-	-	34.4	-	39.9
	Fiber length 3 (mm)	83.3	-	-	-	-	-	39.8	-	35.4
19	Muscle length 1 (mm)	136.2	-	-	-	-	-	59.1	-	54.1
	Muscle length 2 (mm)	144.3	-	-	-	-	-	59.4	-	56.9
	Muscle length 3 (mm)	145.8	-	-	-	-	-	57.9	-	56.2
	Pennation angle 1 (°)	5	-	-	-	-	-	10	-	0
	Pennation angle 2 (°)	0	-	-	-	-	-	0	-	2
	Pennation angle 3 (°)	10	-	-	-	-	-	5	-	2
	Mass (g)	13.0	-	-	-	-	-	6.9	-	3.7
	Fiber length 1 (mm)	61.4	-	-	-	-	-	48	-	47.6
	Fiber length 2 (mm)	53.9	-	-	-	-	-	48.4	-	38.3
	Fiber length 3 (mm)	58.	-	-	-	-	-	41	-	42.5
20	Muscle length 1 (mm)	114.2	-	-	-	-	-	52.9	-	57.5
	Muscle length 2 (mm)	111.9	-	-	-	-	-	54.9	-	59.1
	Muscle length 3 (mm)	113.4	-	-	-	-	-	54.5	-	59.0
	Pennation angle 1 (°)	3.0	-	-	-	-	-	5.0	-	0.0
	Pennation angle 2 (°)	3.0	-	-	-	-	-	2.0	-	11.0
	Pennation angle 3 (°)	7.0	-	-	-	-	-	1.0	-	4.0
	Mass (g)	11.0	-	-	-	-	-	4.3	-	4.6
	Fiber length 1 (mm)	44.5	-	-	-	-	-	35.6	-	42.2

	Fiber length 2 (mm)	88.4	-	-	-	-	-	49.0	-	42.0
	Fiber length 3 (mm)	90.0	-	-	-	-	-	39.6	-	32.6
21	Muscle length 1 (mm)	103.4	-	-	-	-	-	46.7	-	46.2
	Muscle length 2 (mm)	108.6	-	-	-	-	-	51.4	-	46.5
	Muscle length 3 (mm)	108.9	-	-	-	-	-	51.8	-	45.9
	Pennation angle 1 (°)	10.0	-	-	-	-	-	10.0	-	10.0
	Pennation angle 2 (°)	12.0	-	-	-	-	-	0.0	-	5.0
	Pennation angle 3 (°)	0.0	-	-	-	-	-	0.0	-	0.0
	Mass (g)	4.2	-	-	-	-	-	4.1	-	2.3
	Fiber length 1 (mm)	69.4	-	-	-	-	-	43.8	-	33.7
	Fiber length 2 (mm)	60.4	-	-	-	-	-	44.3	-	34.3
	Fiber length 3 (mm)	61.1	-	-	-	-	-	40.7	-	37.5
22	Muscle length 1 (mm)	128.1	-	-	-	-	-	61.1	-	48.6
	Muscle length 2 (mm)	130.5	-	-	-	-	-	57.2	-	49.1
	Muscle length 3 (mm)	130.7	-	-	-	-	-	59.0	-	50.5
	Pennation angle 1 (°)	10.0	-	-	-	-	-	0.0	-	0.0
	Pennation angle 2 (°)	0.0	-	-	-	-	-	8.0	-	2.0
	Pennation angle 3 (°)	10.0	-	-	-	-	-	19.0	-	0.0
	Mass (g)	6.5	-	-	-	-	-	3.5	-	2.8
	Fiber length 1 (mm)	71.1	-	-	-	-	-	41.9	-	28.5
	Fiber length 2 (mm)	45.8	-	-	-	-	-	40.5	-	40.7
	Fiber length 3 (mm)	78.7	-	-	-	-	-	46.7	-	44.3
23	Muscle length 1 (mm)	141.7	-	-	-	-	-	53.6	-	53.5
	Muscle length 2 (mm)	140.8	-	-	-	-	-	49.2	-	54.6
	Muscle length 3 (mm)	143.8	-	-	-	-	-	52.3	-	53.4
	Pennation angle 1 (°)	5.0	-	-	-	-	-	0.0	-	0.0
	Pennation angle 2 (°)	0.0	-	-	-	-	-	5.0	-	4.0
	Pennation angle 3 (°)	18.0	-	-	-	-	-	2.0	-	0.0
	Mass (g)	4.1	-	-	-	-	-	3.7	-	2.1
	Fiber length 1 (mm)	63.7	-	-	-	-	-	38.3	-	47.9
	Fiber length 2 (mm)	67.3	-	-	-	-	-	36.6	-	32.7
	Fiber length 3 (mm)	58.9	-	-	-	-	-	42.2	-	29.8

[1]Muscle and fiber length are measured in millimeters (mm), Pennation angle in degrees (°) and mass in grams (g).
[2]Muscles: APL (*abductor pollicis longus*), EPB (*extensor pollicis brevis*), EPL (*extensor pollicis longus*), FPL (*flexor pollicis longus*), APB (*abductor pollicis brevis*), AD (*adductor pollicis*), D1 (*first dorsal interosseus*), FPB (*flexor pollicis brevis*) and OP (*opponens pollicis*).

8.2 Supplementary data for the paper Finite element analysis of the proximal phalanx of the thumb in Hominoidea during simulated stone tool use (Section 5.1).

Table S1 Loads applied to the models for each specimen under analysis and simulated loading scenarios (Sc).

Specimen	SC	HRF[a]		*FPB HS / FPB PT*[b]		AP *HS / AP PT*[b]		EPB *HS / EPB PT*[b]		ABP *HS / ABP PT*[b]		JRF_d[c]		JRF_{mc}[c]	
		N	Θ	N	Θ	N	Θ	N	Θ	N	Θ	N	Θ	N	Θ
Extant human	1	3.92	90	17.95/37.20	45	38.79/66.43	61.2	4.33/28.75	16.7	5.28/35.94	180	44.06/ 89.27	180	38.81/ 114.1	180
	2	7.65	90	13.49/27.95	45	29.15/49.91	61.2	2.74/18.18	16.7	3.34/22.72	180	28.26/61.46	180	28.02/ 78.76	180
	3	3.92	45	17.95/37.20	45	38.79/66.43	61.2	4.33/28.75	16.7	5.28/35.94	180	45.21/90.33	180	37.96/ 113.3	180
	4	7.65	45	13.49/27.95	45	29.15/49.91	61.2	2.74/18.18	16.7	3.34/22.72	180	30.70/63.62	180	26.36/ 77.14	180
Neanderthal	1	3.92	90	14.47/29.99	45	31.28/53.56	61.2	3.49/23.18	16.7	4.26/28.98	180	35.55/72.02	180	30.75/ 91.35	180
	2	7.65	90	10.87/22.54	45	23.50/40.24	61.2	2.21/14.66	16.7	2.69/18.32	180	22.79/49.58	180	22.36/ 63.11	180
	3	3.92	45	14.47/29.99	45	31.28/53.56	61.2	3.49/23.18	16.7	4.26/28.98	180	36.46/72.85	180	30.27/ 90.88	180
	4	7.65	45	10.87/22.54	45	23.50/40.24	61.2	2.21/14.66	16.7	2.69/22.72	180	24.75/51.29	180	21.41/ 62.18	180
Chimpanzee	1	3.92	90	18.34/38.01	45	39.64/67.88	61.2	-	-	5.39/36.72	180	43.78/ 82.63	180	35.51/ 90.61	180
	2	7.65	90	13.78/28.56	45	29.78/51.00	61.2	-	-	3.41/23.22	180	28.05/57.36	180	26.15/ 64.17	180
	3	3.92	45	18.34/38.01	45	39.64/67.88	61.2	-	-	5.39/36.76	180	45.11/83.92	180	35.78/ 90.89	180
	4	7.65	45	13.78/28.56	45	29.78/51.00	61.2	-	-	3.41/23.22	180	30.92/60.02	180	26.7/ 64.7	180
Gorilla	1	3.92	90	24.78/51.36	45	53.55/91.71	61.2	5.97/39.69	16.7	7.29/49.61	180	61.17/125.1	180	49.14/ 144.11	180
	2	7.65	90	18.62/38.59	45	40.24/68.91	61.2	3.78/25.10	16.7	4.61/31.37	180	39.33/86.13	180	35.31/ 99.38	180
	3	3.92	45	24.78/51.36	45	53.55/91.71	61.2	5.97/39.69	16.7	7.29/49.61	180	64.27/128.2	180	49.57/ 144.53	180
	4	7.65	45	18.62/38.36	45	40.24/68.91	61.2	3.78/25.10	16.7	4.61/31.37	180	45.94/92.39	180	36.15/ 100.2	180
Orangutan	1	3.92	90	19.74/40.91	45	42.66/73.06	61.2	-	-	5.80/39.52	180	47.62/89.76	180	47.85/ 117.2	180
	2	7.65	90	14.83/30.74	45	32.06/54.90	61.2	-	-	3.67/24.99	180	30.56/62.34	180	34.51/ 82.77	180
	3	3.92	45	19.74/40.91	45	42.66/73.06	61.2	-	-	5.80/39.52	180	49.01/91.09	180	50.55/ 119.84	180
	4	7.65	45	14.83/30.74	45	32.06/54.90	61.2	-	-	3.67/24.99	180	33.44/65.02	180	39.78/ 87.92	180
Gibbon	1	3.92	90	7.0814.66	45	15.29/26.1	61.2	-	-	2.08/14.17	180	17.75/32.87	180	19.08/ 45.46	180
	2	7.65	90	5.32/11.02	45	11.49/19.68	61.2	-	-	1.32/8.96	180	11.25/22.87	180	13.75/ 32.18	180
	3	3.92	45	7.08/14.66	45	15.29/26.19	61.2	-	-	2.08/14.17	180	17.88/33.25	180	19.64/ 46.00	180
	4	7.65	45	5.32/11.02	45	11.49/19.68	61.2	-	-	1.32/8.96	180	12.1/ 23.65	180	14.84/ 33.24	180

[a] Forces (N) and angles (θ) relative to the longitudinal axes of the bone.
[b] Muscle Forces for the human and chimpanzee reference models, respectively, are separate by a slash.
[c] Force reactions in the proximal and distal joints were scaled to remove size effects when computing stress distributions.

Table S2 Number of elements (N elements), mesh-weighted arithmetic mean (MWAM), mesh-weighted median (MWM), quartiles values (Q25, 50, 75 and 95), percentage error of the arithmetic mean (PEofAM) and percentage error of the median (PeofM) for each specimen and loading scenario, under human-scaled conditions.

Specimen	Scenario	N elements	MWAM	MWM	Q25	Q50	Q75	M95	PEofAM	PEofM
Extant human	1	225689	3.7540	2.6128	1.3997	2.6690	5.6844	10.0261	0.7130	2.1509
	2	225729	2.5238	1.7800	0.9680	1.8227	3.8100	6.6442	0.7309	2.3997
	3	225689	3.8349	2.6530	1.4269	2.7080	5.8135	10.2790	0.7100	2.0714
	4	225710	2.6876	1.8662	1.0241	1.9051	4.0670	7.1455	0.7225	2.0867
Neanderthal	1	240478	3.7401	2.7851	1.5604	2.8336	5.3814	9.6489	1.6161	1.7432
	2	240469	2.5277	1.8985	1.0995	1.9326	3.6118	6.4210	1.5858	1.7975
	3	240469	3.8275	2.8449	1.6271	2.8931	5.4883	9.8692	1.6163	1.6943
	4	240471	2.6708	1.9879	1.1443	2.0203	3.8108	6.8892	1.6184	1.6299
Chimpanzee	1	160103	4.1812	3.9750	2.2535	4.0610	5.9939	7.6454	0.0015	2.1631
	2	160104	2.8698	2.7413	1.5694	2.8039	4.0960	5.1944	0.0004	2.2836
	3	160046	4.2475	4.0192	2.2864	4.1141	6.0832	7.7941	0.0148	2.3599
	4	160104	3.0042	2.8468	1.6410	2.9113	4.2753	5.4869	0.0164	2.2646
Gorilla	1	225710	2.6876	1.8662	1.0241	1.9051	4.0670	7.1455	0.7225	2.0867
	2	327267	2.4440	2.1049	1.3316	2.1522	3.1882	5.1728	0.1482	2.2471
	3	327267	3.7738	3.1737	1.9572	3.2548	5.0131	8.1784	0.1610	2.5570
	4	327267	2.6870	2.2688	1.3987	2.3215	3.5807	5.7799	0.1603	2.3228
Orangutan	1	199857	4.0409	3.3878	2.1630	3.4804	5.2597	9.1689	0.6450	2.7344
	2	199857	2.7519	2.3201	1.5089	2.3899	3.5526	6.1413	0.6300	3.0085
	3	199813	4.1216	3.4543	2.2075	3.5543	5.3691	9.3611	0.6596	2.8941
	4	199813	2.9129	2.4571	1.5893	2.5330	3.7670	6.5330	0.6369	3.0885
Gibbon	1	311431	6.3313	5.4576	3.2272	5.5294	8.5269	14.0750	0.1785	1.3156
	2	311442	4.3431	3.7514	2.2259	3.8016	5.8425	9.6143	0.1738	1.3370
	3	311442	6.4105	5.5281	3.2583	5.6069	8.6284	14.2694	0.1767	1.4247
	4	311442	4.5087	3.9023	2.3007	3.9605	6.0438	10.0180	0.1783	1.4927

Table S3 Number of elements (N elements), mesh-weighted arithmetic mean (MWAM), mesh-weighted median (MWM), quartiles values (Q25, 50, 75 and 95), percentage error of the arithmetic mean (PEofAM) and percentage error of the median (PeofM) for each specimen and loading scenario, under chimpanzee-scaled conditions.

Specimen	Scenario	N elements	MWAM	MWM	Q25	Q50	Q75	M95	PEofAM	PEofM
Chimpanzee	1	160104	8.0122	7.6599	4.2909	7.8345	11.4830	14.6530	0.0387	2.2794
	2	160104	5.7312	5.4881	3.0880	5.6170	8.2101	10.4363	0.0341	2.3483
	3	160104	8.0771	7.7090	4.3233	7.8865	11.5780	14.7960	0.0417	2.3024
	4	160104	5.8607	5.5899	3.1557	5.7215	8.3844	10.7170	0.0419	2.3534
Extant human	1	225743	7.5983	5.4469	3.0316	5.5620	11.3770	19.8150	0.7364	2.1135
	2	225743	5.3623	3.8494	2.1389	3.9323	8.0325	13.9420	0.7334	2.1536
	3	225720	7.6821	5.4907	3.0617	5.6072	11.4980	20.0690	0.7328	2.1222
	4	225689	5.5209	3.9340	2.1951	4.0167	8.2813	14.4290	0.7156	2.1020
Neanderthal	1	240469	7.5408	5.7398	3.1415	5.8463	10.7260	19.1300	1.6003	1.8559
	2	240461	5.3229	4.0535	2.2448	4.1316	7.5691	13.4480	1.5817	1.9264
	3	240469	7.6103	5.7887	3.1663	5.8917	10.8170	19.3540	1.6076	1.7799
	4	240460	5.4615	4.1433	2.2936	4.2210	7.7516	13.9010	1.6017	1.8739
Gorilla	1	327267	7.5848	6.5180	4.1315	6.6614	10.0078	15.9652	0.1499	2.2001
	2	327267	5.3112	4.5847	2.9071	4.6850	6.9811	11.1340	0.1473	2.1877
	3	327267	7.7032	6.5956	4.1665	6.7425	10.1980	16.2770	0.1521	2.2272
	4	327267	5.5459	4.7386	2.9746	4.8493	7.3571	11.7390	0.1536	2.3361
Orangutan	1	199857	7.9291	6.5783	4.2297	6.7471	10.3643	18.0617	0.6350	2.5660
	2	199857	5.6296	4.6925	3.0326	4.8168	7.3231	12.7377	0.6308	2.6495
	3	199782	8.0098	6.6472	4.2716	6.8239	10.4630	18.2554	0.6575	2.6582
	4	199782	5.7884	4.8286	3.1119	4.9592	7.5206	13.1060	0.6481	2.7040
Gibbon	1	311442	12.1044	10.4260	6.1984	10.5940	16.2630	26.8950	0.1734	1.6114
	2	311431	8.6667	7.4740	4.4483	7.5885	11.6390	19.2340	0.1762	1.5325
	3	311442	12.1825	10.4940	6.2322	10.6650	16.3650	27.0820	0.1744	1.6295
	4	311442	8.8241	7.6109	4.5179	7.7380	11.8330	19.6238	0.1753	1.6704

8.3 Supplementary data for the paper Modularity of the wrist in extant hominids (Section 5.2).

Table S1 Dataset for the study (available at https://www.preprints.org/manuscript/202004.0474/v1).

Table S2 Effect sizes for the covariance ratio (Z_{CR}) for the modular hypotheses in the wrist of humans, chimpanzees and gorillas. All CR values were significant at $p<0.01$.

	Humans	Chimpanzees	Gorillas	All
H15	0	0	0	0
H1	-8.6	-8.5	-8.3	-8.9
H2	-9.1	-6.9	-7.3	-7.4
H3	-5.4	-5.6	-7.2	-5.8
H4	-5.9	-7.4	-7.2	-5.9
H5	-6.3	-5.8	-5.3	-5.2
H6	-6.2	-5.2	-3.9	-8.1
H7	-5.1	-5.2	-7.7	-4.9
H8	-5.7	-6.1	-6.7	-4.5
H9	-7.7	-7.6	-8.6	-6.6
H10	-7.6	-7.3	-6.7	-7.9
H11	-7.1	-7.3	-7.3	-8.4
H12	-7.6	-7.4	-7.4	-6.2
H13	-7.1	-7.5	-8.1	-6.5
H14	-7.8	-7.2	-6	-8.4

Table S3 Matrix of pairwise differences in effect sizes (Z_{12}) (lower left triangle) between the modular hypotheses in humans, and their associated p-values (upper right triangle). Significant values are in bold.

	H15	H1	H2	H3	H4	H5	H6	H7	H8	H9	H10	H11	H12	H13	H14
H15		**<0.01**	**<0.01**	**<0.01**	**<0.01**	**<0.01**	**<0.01**	**<0.01**	**<0.01**	**<0.01**	**<0.01**	**<0.01**	**<0.01**	**<0.01**	**<0.01**
H1	8.97		0.53	**<0.01**	**<0.01**	0.33	0.29	**0.05**	0.10	0.66	0.53	0.34	0.55	0.35	0.63
H2	9.56	0.63		**0.01**	**0.01**	0.64	0.58	0.14	0.24	0.89	0.96	0.68	0.98	0.69	0.92
H3	5.55	3.20	2.81		0.87	0.06	0.07	0.38	0.21	**0.01**	**0.01**	**0.04**	**0.01**	**0.03**	**0.01**
H4	6.00	3.11	2.70	0.16		0.07	0.09	0.45	0.26	**0.01**	**0.02**	**0.05**	**0.02**	**0.04**	**0.01**
H5	6.49	0.98	0.47	1.90	1.79		0.93	0.37	0.54	0.58	0.70	0.94	0.69	0.93	0.61
H6	6.32	1.06	0.56	1.79	1.68	0.08		0.42	0.60	0.53	0.64	0.87	0.62	0.86	0.55
H7	5.19	1.93	1.48	0.87	0.75	0.90	0.81		0.76	0.14	0.19	0.31	0.18	0.30	0.14
H8	5.82	1.64	1.17	1.24	1.12	0.61	0.52	0.31		0.23	0.30	0.48	0.29	0.47	0.24
H9	8.00	0.44	0.14	2.65	2.55	0.55	0.64	1.49	1.19		0.86	0.62	0.88	0.63	0.97
H10	7.79	0.62	0.05	2.47	2.36	0.38	0.47	1.32	1.03	0.18		0.74	0.98	0.76	0.89
H11	7.29	0.95	0.41	2.10	1.99	0.07	0.16	1.01	0.71	0.50	0.33		0.73	0.99	0.64
H12	7.82	0.60	0.03	2.49	2.38	0.40	0.49	1.35	1.05	0.16	0.02	0.3		0.74	0.91
H13	7.32	0.94	0.39	2.12	2.01	0.09	0.18	1.03	0.73	0.49	0.31	0.0	0.3		0.65
H14	8.05	0.48	0.10	2.63	2.53	0.52	0.60	1.46	1.17	0.04	0.14	0.5	0.1	0.45	

Table S4 Matrix of pairwise differences in effect sizes (Z_{12}) (lower left triangle) between the modular hypotheses in chimpanzees, and their associated p-values (upper right triangle). Significant values are in bold.

	H15	H1	H2	H3	H4	H5	H6	H7	H8	H9	H10	H11	H12	H13	H14
H15		**<0.01**	**<0.01**	**<0.01**	**<0.01**	**<0.01**	**<0.01**	**<0.01**	**<0.01**	**<0.01**	**<0.01**	**<0.01**	**<0.01**	**<0.01**	**<0.01**
H1	8.89		**0.03**	**<0.01**	0.11	0.17	0.07	0.29	0.26	0.68	0.39	0.51	0.62	0.52	0.37
H2	7.03	2.21		0.42	0.55	0.58	0.95	0.38	0.41	0.09	0.21	0.15	0.11	0.14	0.23
H3	5.70	2.92	0.81		0.17	0.22	0.46	0.13	0.14	**0.02**	**0.05**	**0.03**	**0.02**	**0.03**	0.06
H4	7.59	1.62	0.60	1.38		0.97	0.65	0.72	0.77	0.26	0.49	0.38	0.30	0.37	0.53
H5	5.86	1.38	0.55	1.23	0.04		0.67	0.78	0.82	0.34	0.57	0.46	0.38	0.45	0.60
H6	5.25	1.84	0.06	0.74	0.45	0.43		0.48	0.51	0.16	0.31	0.23	0.19	0.22	0.33
H7	6.12	1.05	0.87	1.53	0.36	0.29	0.71		0.95	0.52	0.80	0.67	0.57	0.65	0.83
H8	6.22	1.14	0.82	1.49	0.29	0.23	0.66	0.06		0.47	0.74	0.61	0.52	0.60	0.78
H9	7.84	0.42	1.69	2.39	1.13	0.96	1.41	0.65	0.72		0.67	0.82	0.93	0.83	0.64
H10	7.48	0.86	1.25	1.97	0.69	0.57	1.02	0.26	0.33	0.43		0.85	0.74	0.83	0.96
H11	7.54	0.65	1.44	2.14	0.88	0.74	1.19	0.43	0.50	0.23	0.19		0.89	0.99	0.81
H12	7.63	0.50	1.59	2.28	1.03	0.87	1.32	0.56	0.64	0.09	0.34	0.14		0.90	0.70
H13	7.68	0.64	1.47	2.18	0.91	0.76	1.21	0.45	0.52	0.22	0.21	0.01	0.13		0.80
H14	7.35	0.91	1.20	1.91	0.63	0.52	0.98	0.21	0.28	0.47	0.05	0.24	0.38	0.26	

Table S5 Matrix of pairwise differences in effect sizes (Z_{12}) (lower left triangle) between the modular hypotheses in gorillas, and their associated p-values (upper right triangle). Significant values are in bold.

	H15	H1	H2	H3	H4	H5	H6	H7	H8	H9	H10	H11	H12	H13	H14
H15		**<0.01**	**<0.01**	**<0.01**	**<0.01**	**<0.01**	**<0.01**	**<0.01**	**<0.01**	**<0.01**	**<0.01**	**<0.01**	**<0.01**	**<0.01**	**<0.01**
H1	8.38		0.08	0.09	0.07	0.12	**0.01**	0.79	0.61	0.67	0.32	0.59	0.63	0.97	0.13
H2	7.31	1.73		0.97	0.94	0.94	0.22	0.06	0.29	**0.03**	0.54	0.27	0.24	0.08	0.95
H3	7.18	1.68	0.03		0.92	0.92	0.22	0.07	0.31	**0.03**	0.56	0.28	0.26	0.09	0.98
H4	7.19	1.79	0.07	0.10		0.99	0.25	**0.05**	0.27	**0.03**	0.50	0.24	0.22	0.07	0.90
H5	5.28	1.56	0.08	0.10	0.02		0.32	0.09	0.32	**0.05**	0.55	0.30	0.28	0.12	0.90
H6	3.86	2.62	1.22	1.23	1.16	1.00		**0.01**	**0.05**	**<0.01**	0.10	**0.04**	**0.03**	**0.01**	0.24
H7	7.68	0.27	1.88	1.84	1.94	1.72	2.72		0.46	0.89	0.23	0.44	0.47	0.82	0.09
H8	6.73	0.51	1.05	1.02	1.11	0.99	2.00	0.74		0.36	0.66	1.00	0.96	0.59	0.36
H9	8.66	0.43	2.16	2.11	2.22	1.94	2.98	0.14	0.91		0.16	0.34	0.37	0.70	0.06
H10	6.69	1.00	0.61	0.58	0.67	0.60	1.64	1.20	0.44	1.41		0.65	0.61	0.31	0.62
H11	7.34	0.54	1.11	1.07	1.18	1.04	2.08	0.77	0.00	0.95	0.46		0.96	0.57	0.34
H12	7.46	0.49	1.18	1.14	1.24	1.09	2.14	0.72	0.05	0.90	0.51	0.05		0.61	0.31
H13	8.12	0.04	1.73	1.69	1.80	1.57	2.62	0.23	0.54	0.39	1.02	0.56	0.51		0.13
H14	6.00	1.51	0.06	0.03	0.12	0.12	1.17	1.68	0.92	1.91	0.50	0.96	1.01	1.52	

Table S6 Matrix of pairwise differences in effect sizes (Z_{12}) (lower left triangle) between the modular hypotheses in hominids (genera pooled), and their associated p-values (upper right triangle). Significant values are in bold.

	H15	H1	H2	H3	H4	H5	H6	H7	H8	H9	H10	H11	H12	H13	H14
H15		**<0.01**	**<0.01**	**<0.01**	**<0.01**	**<0.01**	**<0.01**	**<0.01**	**<0.01**	**<0.01**	**<0.01**	**<0.01**	**<0.01**	**<0.01**	**<0.01**
H1	8.99		**0.01**	**<0.01**	**<0.01**	0.06	0.97	**0.03**	**0.01**	0.14	0.62	0.83	0.10	0.16	0.92
H2	7.60	2.51		0.29	0.30	0.85	**0.02**	0.87	0.44	0.46	0.06	**0.03**	0.54	0.39	**0.02**
H3	5.93	3.40	1.06		0.98	0.31	**<0.01**	0.49	0.93	0.11	**0.01**	**<0.01**	0.13	0.08	**<0.01**
H4	5.92	3.37	1.03	0.03		0.32	**<0.01**	0.51	0.95	0.11	**0.01**	**<0.01**	0.14	0.09	**<0.01**
H5	5.24	1.89	0.19	1.02	0.99		0.06	0.77	0.42	0.65	0.16	0.09	0.73	0.59	0.07
H6	8.40	0.03	2.43	3.29	3.26	1.87		**0.03**	**0.01**	0.14	0.61	0.81	0.11	0.16	0.90
H7	4.93	2.23	0.16	0.69	0.66	0.29	2.19		0.60	0.44	0.08	0.05	0.51	0.39	**0.03**
H8	4.24	2.79	0.77	0.09	0.07	0.81	2.73	0.52		0.19	**0.02**	**0.01**	0.23	0.16	**0.01**
H9	6.38	1.49	0.75	1.62	1.59	0.46	1.47	0.77	1.31		0.32	0.21	0.90	0.93	0.17
H10	8.06	0.49	1.91	2.80	2.77	1.42	0.51	1.74	2.30	0.99		0.78	0.26	0.36	0.69
H11	8.41	0.21	2.22	3.10	3.07	1.67	0.24	2.00	2.55	1.26	0.28		0.16	0.24	0.91
H12	6.36	1.64	0.61	1.50	1.47	0.34	1.62	0.65	1.20	0.13	1.14	1.41		0.83	0.12
H13	6.60	1.41	0.85	1.74	1.71	0.54	1.40	0.86	1.40	0.09	0.91	1.19	0.22		0.19
H14	8.73	0.10	2.38	3.27	3.23	1.79	0.13	2.12	2.68	1.39	0.39	0.11	1.54	1.31	

8.4 Supplementary data for the paper Insertion sites in manual proximal phalanges of African apes and modern humans (Section 5.3).

Table S1 Dataset for the study. This dataset includes the flexor ridge area (FR, mm²) and phalaneal total area (PTA, mm²) per proximal phalanges 2-5 (PP2-5). Sex and first metacarpal length (MC1_length) are also included.

Taxa	PTA PP2	FR PP2	PTA PP3	FR_PP3	PTA_PP4	FR_PP4	PTA_PP5	FR_PP5	Sex	MC1_length
Human	1497	57.57	1421	70.47	1389	66.68	1019	28.12	M	428
Human	1331	51.22	1561	74.45	1365	46.98	988.9	50.26	M	425
Human	1444	35.7	1622	119.28	1522	86.8	1071	65.01	M	411
Human	1344	39.03	1166	20.29	1113	35.7	NA	NA	F	400
Human	1260	NA	1594	48.97	1427	36.64	908.7	8.62	F	416
Human	1167	48.1	1377	54.51	1126	49.95	830	57.91	F	418
Human	1479	34.03	1740	48.4	1380	45.1	937.4	51.68	F	429.8
Human	1476	54.24	1701	75.03	1387	48.29	966	44.98	M	461.9
Human	NA	NA	1533	91	1240	65.48	888	38.57	F	385
Human	1606	49.72	1953	60.25	1659	68.68	1229	61.24	M	440
Human	1466	50.2	1717	67.48	1426	45.27	NA	NA	F	439
Human	1598	64.77	1853	80.03	1490	65.4	960	35.55	F	448.6
Human	1509	88.92	1588	93.01	1543	97.05	NA	NA	M	438.4
Human	1331	24.4	1486	39.26	1297	40.65	926	26.58	F	421.8
Human	1311	46.95	1574	65.9	1321	50.96	930	23.89	F	402.1
Human	1503	73.64	1701	112.22	1382	42.28	1062	52.06	M	422.6
Human	1658	33.12	1987	101.53	1730	87.56	1287	57.98	M	436.2
Human	1634	24.2	1926	76.35	1558	94.36	1178	54.98	M	480.1
Human	1146	32.08	1243	38.11	986	34.34	785	23.13	F	372.5
Human	1224	32.6	1376	51.03	1271	38.37	849	21.33	F	408.2
Human	1289	36.78	1447	57.87	1284	63.54	895	49.08	F	421.9

Human	1167	23.1	1280	29.81	1071	33.21	790	12.78	M	393.3
Human	1407	60.81	1594	76.84	1330	56.59	976	14.64	F	453.5
Human	1250	56.29	1526	63.7	1332	39.1	859	28.6	F	447.1
Human	1608	50.76	1794	81.87	1572	81.79	1142	50.55	M	461.7
Human	1375	37.74	1547	55.5	1417	58.67	1110	28.39	M	406
Human	1485	56.71	1807	97.13	1476	35.45	1078	37.45	M	445.4
Human	1400	35.87	1611	61.96	1286	47.72	893	16.32	F	414
Human	1460	48.9	1182	51.5	867	51.21	895	33.65	F	383
Human	1275	34.52	1589	69.99	1375	40.38	977	20.39	F	457.1
Human	1670	34.58	1842	44.22	1246	56.13	1246	23.63	M	451
Human	1510	65.23	1708	81.15	1445	83.74	1086	57.32	M	439
Human	1558	31.43	1887	52.77	1206	NA	1203	52.99	M	468.4
Human	1133	25.99	1348	34.85	1078	31.12	793	7.1	F	391.5
Human	1488	69.58	1616	89.59	1340	69.68	1068	59.75	M	458.8
Human	1448	54.38	1703	41.48	1460	51.3	1073	43.95	M	434.3
Gorilla	NA	NA	4104	298.8	3624	352	NA	NA	M	510
Gorilla	2570	140.81	3391	289	3094	216.48	2296	142.63	M	498
Gorilla	1467	80.49	2531	259.55	2177	139.92	1341	76.48	M	402
Gorilla	2214	132.52	3648	224.3	3316	192.41	2826	236.38	M	522
Gorilla	4063	296.7	3750	280.92	3757	258.31	3176	317.98	M	466
Gorilla	2098	120.2	2949	232.1	2281	186.49	1602	81.14	F	386
Gorilla	3184	190.71	3544	352	3357	299	2709	200.5	M	471
Gorilla	2710	209.78	3475	272	3240	235	2305	129.17	M	497
Gorilla	2874	204.92	3634	223.5	3553	302	2636	154.7	M	493
Gorilla	2106	103.12	2729	181.07	2320	147.52	1778	89.78	F	396
Gorilla	2796	185.7	3726	270.7	3223	258.9	2533	NA	M	466
Gorilla	2865	217.13	3498	279.86	2980	221	1528	128.12	M	470
Gorilla	2756	242.5	3471	444.05	3286	476.1	2465	192.23	M	456
Gorilla	2188	197.77	2640	180.95	2412	178.72	1664	95.84	F	456

Gorilla	2919	250.92	3800	397.51	3241	292.41	2706	207.75	M	457
Gorilla	2659	185.25	2634	186.93	2433	215.47	1899	148.78	F	423
Gorilla	2045	127.64	2414	188.02	2089	149.3	NA	NA	F	379
Gorilla	1367	86.76	2145	87.5	2132	166.53	1996	159.13	F	416
Gorilla	1732	102.74	NA	NA	2262	135.2	2617	192.13	F	382
Gorilla	2002	149.43	3585	253.84	2164	150.07	1705	118.01	F	418
Gorilla	2220	159.49	2305	316.13	2509	341.54	1573	158.58	F	395
Gorilla	3681	302.2	4186	424.1	3483	291.44	2373	138.01	M	520
Gorilla	3339	409.25	4510	572.7	3748	447.18	2691	188.61	M	525
Gorilla	2512	248.75	2740	238.9	2068	227.68	2063	190.14	F	392
Gorilla	2791	237.8	3208	290.1	3118	257.25	NA	NA	F	420
Gorilla	1914	154.22	2466	236.73	1975	198.51	1426	92.88	F	378
Gorilla	3721	202.23	4721	405.83	4164	365.8	2775	176.83	M	507
Gorilla	2249	141.03	2715	189.99	2402	142.57	1577	100.54	F	465
Gorilla	3151	268.49	4448	301.86	3921	286.75	2594	158.86	M	472
Chimpanzee	2994	148.67	4195	269.32	3287	148.15	1905	92.63	M	460
Chimpanzee	2064	124.55	3026	165.2	2585	132.56	1388	51.74	M	429
Chimpanzee	2380	134.4	3070	120.7	3167	NA	1668	50.8	M	483
Chimpanzee	1591	44	2241	85.7	1901	68.1	1040	41.3	F	411
Chimpanzee	1979	86.7	2533	105.1	NA	NA	1376	41.1	M	458
Chimpanzee	2509	73.5	2110	95.4	1356	53.54	865	20.39	F	447
Chimpanzee	1987	83.7	2731	90	1754	50.3	NA	NA	F	316
Chimpanzee	1583	58.19	2175	121.17	1913	79.76	1157	35.51	F	371
Chimpanzee	1896	84.39	2603	90.24	2013	89.87	1235	31.56	M	365
Chimpanzee	2611	126.6	3291	204.03	3065	217.84	1816	178.28	M	453
Chimpanzee	2728	133.65	2677	149.69	2311	115.11	1461	30.05	F	431
Chimpanzee	1813	101.81	2795	99.53	2650	91.47	1846	42.42	UNK	453
Chimpanzee	1620	51.46	2129	88.03	1853	81.57	1118	10.96	M	389
Chimpanzee	2486	135.68	2894	84.19	2579	126.95	1574	42.89	UNK	426

Chimpanzee	1670	45.04	2219	88.8	1903	72.28	1400	12.54	M	397
Chimpanzee	2482	120.48	3271	155.2	2816	136.97	1297	4.01	M	467
Chimpanzee	2407	106.4	2647	71.84	2342	90.64	1770	69.73	UNK	418
Chimpanzee	1771	175.45	NA	NA	2742	213.46	NA	NA	F	405
Chimpanzee	2232	42.42	3196	120.91	2535	132.32	1000	39.34	F	421
Chimpanzee	1810	83.99	2532	115.33	2142	120.29	NA	NA	UNK	395
Chimpanzee	2254	112.78	2891	244.8	2282	116.55	1290	42.84	UNK	412
Chimpanzee	1667	125.72	2410	112.24	1949	71.72	1084	28.82	F	391
Chimpanzee	2411	102.32	2673	86.57	2629	94.05	2125	66.7	M	420
Chimpanzee	1765	53.03	2642	113.84	2583	95.81	1349	55.1	M	392
Chimpanzee	2886	139.17	3798	186.64	3570	208.67	1821	90.69	M	470
Chimpanzee	NA	NA	2631	65.97	2122	111.7	1774	67.74	UNK	398
Chimpanzee	2854	113.06	3118	167.59	2353	103.74	1483	25.17	M	455
Chimpanzee	1713	54.21	2378	116.14	1882	34.35	1374	33.18	F	362
Chimpanzee	2347	105.79	3098	137.16	2381	96.31	1514	21.63	F	470
Chimpanzee	1963	96.94	2399	191.5	1712	94.05	1220	57.34	UNK	410

8.5 Poster presented at the 8th Annual ESHE meeting held at Faro, Portugal in 2018.

Stress distribution in the thumb proximal phalanx in Chimpanzee and *Homo* species during simulated stone-tool use

Ana Bucchi[1,2], Thomas Püschel[3], Carlos Lorenzo[1,2], Jordi Marcé-Nogué[4,5]

1 - Catalan Institute of Human Paleoecology and Social Evolution (IPHES), Tarragona, Spain.
2 - Àrea de Prehistòria, Facultat de Lletres, Universitat Rovira i Virgili, Tarragona, Spain.
3 - School of Earth and Environmental Sciences, The University of Manchester, Oxford Road, Manchester, M13 9PL, UK.
4 - Centrum für Naturkunde, Universität Hamburg, Hamburg, Germany.
5 - Institut Català de Paleontologia M. Crusafont, Universitat Autònoma de Barcelona, Cerdanyola del Vallès, Spain.

Introduction

Is the human hand the result of selective pressures related to tool behaviors? Most of the archaeological literature believes that this is the case, as humans display a unique configuration of anatomical traits that facilitate these activities. Biological causality is, however, a hard problem to address.

Here, we use **Finite Element Analysis (FEA)** to see if stress on the first phalange of the hand is, as expected, better distributed in humans than in chimpanzees. This result would be in line with the functional-adaptation hypothesis for the evolution of our hand.

FEA is a method imported from engineering that reconstructs stress in a digital structure (Rayfield (2007)). It is suitable for problems like hand evolution as allows researchers to control and repeat biomechanical scenarios under **manipulable conditions**.

The Simulation

- **Two loading scenarios** were simulated, which differ in terms of mass of the hammer (780 and 400 g).
- One CT scan of a phalanx for each species was used.
- Elastic, linear and homogeneous material properties were assumed for the bone.
- Muscle force (physiological cross-sectional area) was calculated from a cadaver of a 59 year-old-man.
- Information on muscle recruitment during the production of Oldowan tools was obtained from Marzke *et al.* (1998).
- The human model was used as a reference for scaling the forces in the chimpanzee while keeping the original size of the bones.
- We aimed to reproduce biological meaningful conditions to define the boundary constraints (figure on the right).
- We **compared the Von Mises stress distribution** in both scenarios and species.

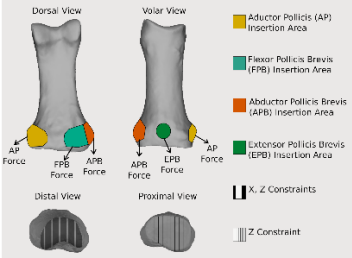

Homo-Chimpanzee Comparison

In the human (phalanges at the left), stress is concentrated in the center of the shaft, while in the chimpanzee the stress is **lower and better distributed** (phalages at the right), making the phalanx less prone to structural failure under these conditions.

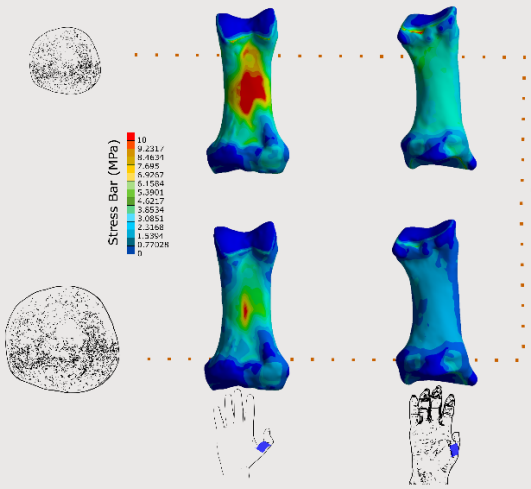

Scenarios Comparison

- Peak stresses values are higher when a small hammer is simulated.
- With the larger hammer, average stress decreased from 1.83 to 1.75 MPa for the human and from 1.71 to 1.62 MPa for the chimpanzee.
- The loading case that more efficiently distributes forces is the chimpanzee using the heavier hammer.
- **The loading case that less efficiently distributes forces is the human using the smaller hammer.**

Key Findings

- Contrary to our expectations, the **human phalanx is more fragile than the chimpanzee's**, in both scenarios. Therefore, from a load resistance point of view, humans are less efficient during strong precision pinch grips.
- Higher robusticity and cortical thickness of the chimpanzee bone may account for these results.
- Greater levels of muscle activity are needed when using a smaller hammer than with a larger hammer, and this explains the differences observed within each species.

Acknowledgements.
We are grateful to the Digital Morphology Museum, KUPRI, and Takaoka City Zoo for the chimpanzee material and to the Human Donation Service of the Universitat de Barcelona. This study was supported by the research grants CGL2015-65387-C3-1-P (MINECO/FEDER), with the financial support of the Generalitat de Catalunya, AGAUR agency, 2017 SGR 1040 Research Group, and with the URV project 2016PFR-URV-B2-17. A.B would like to acknowledge support from the Becas Chile Program (Conycit). J.M-N. was supported by the DFG German Research Foundation, KA 1525/9-2 and acknowledges the CERCA programme (Generalitat de Catalunya).

References
Marzke MW, Toth N, Schick K, Reece S (1998) EMG study of hand muscle recruitment during hard hammer percussion manufacture of Oldowan tools. *Am J Phys Anthropol* 105, 315-32
Rayfield E (2007) Virtual biomechanics: Basic concepts and technical aspects of the finite element analysis in vertebrate morphology. *Annu Rev Earth Planet* 35, 541-76
Poster style from Poster (presented by C. Funghi) on the International Ethological Conference, Lisbon, Portugal, 2017.

Poster presented at the 9th Annual ESHE meeting in Brussels, Belgium in 2019.

Patterns of insertion sites in proximal phalanges of African apes and modern humans

Ana Bucchi, Javier Luengo, Antonietta del Bove and Carlos Lorenzo

Catalan Institute of human palaeoecology and Social Evolution (IPHES) and University Rovira i Virgili

Background

We attempt to test the ability of flexor ridges to reveal information on the use of the hands in gorillas, chimpanzees and recent modern humans.

These ridges correspond to the insertion areas (entheses) of the annular ligaments of the fingers through which pass the tendons of both the flexor digitorum profundus and superficialis muscles, the main flexors of the fingers. During climbing and suspension both muscles are strongly recruited and are also slightly active during knuckle-walking [1].

Examining entheses in taxa with known behavioral repertoires (e.g. African apes) may help to elucidate the suitability of entheses to inform on the use of the hands in taxa with unknown activity patterns (past human populations), yet this kind of study is relatively scarce[e.g. 2].

Material

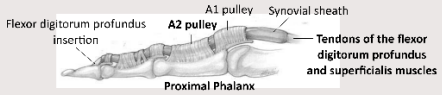

We analized 363 3D models of proximal phalanges 2-5 (PP2-5) from 30 gorilla hands (*Gorilla beringei* and *Gorilla gorilla*), 30 chimpanzee hands (*Pan troglodytes*) and 36 hands of recent modern humans from a medieval population. Entheseal areas (in mm^2) of the A2 pulley were quantified in Geomagic Studio®.

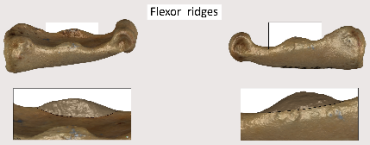

Results

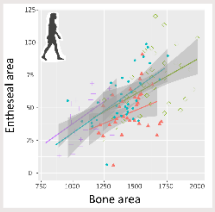

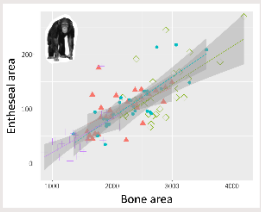

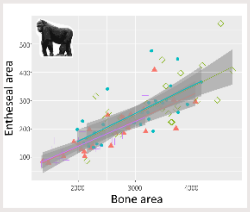

Bivariate plots of entheseal area vs bone area among the phalanges of humans, chimpanzees, and gorillas.

PP2
PP3
PP4
PP5

Slopes (as estimated by ANCOVA) are shown separately per each phalanx with a 95% confidence interval.

Question

The different way gorillas and chimpanzees load the hand during travel has been linked to the morphological differences in the hand; larger rays are subject to disproportionally larger biomechanical demands than the smallest rays [3],[4],[5]. **Can we see this in the patterns of the flexor ridges across digits?**

Each genus has a unique entheseal pattern across digits, with their variability being most homogeneous in gorillas, less so in humans, and least homogenous in chimpanzees. These patterns strongly corresponded to differences in phalangeal size across digits, but not to variations in biomechanical demands.

In gorillas the pattern for entheseal areas (as well as for phalangeal areas) is PP3= PP4> PP5, PP2= PP4 and = PP5.

In chimpanzees the pattern is PP3> PP4= PP2> PP5, both for entheseal areas and the size of the phalanges.

In humans, the gradient for entheseal areas is PP3> PP4> PP5, and PP2= PP4 and = PP5, while for phalangeal areas it is PP3> PP4= PP2> PP5.

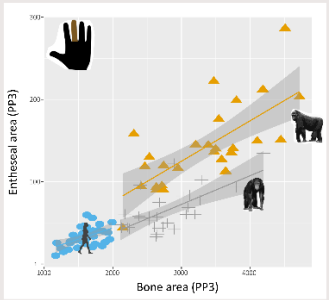

Bivariate plot of Entheseal area vs Bone area for PP3 of gorillas (▲), chimpanzees (+) and humans (●). Slopes (as estimated by ANCOVA) are shown separately per genera with 95% confidence interval.

ANCOVA results indicate that the adjusted means of Entheseal areas by Bone areas are significantly larger in gorillas, followed by chimpanzees, and are smallest in humans ($p<0.05$).

Chimpanzees are smaller in mean body size than humans, yet have relatively larger entheseal areas, which suggests that this reflects the greater biomechanical demands chimpanzees place on their hands compared to humans.

Chimpanzees exhibit more suspensory behavior than gorillas [6] (and thus higher activation of the flexor muscles), yet in this analysis they show smaller entheseal areas than gorillas. It is reasonable to think that although chimpanzees use more demanding locomotory modes than gorillas, this difference is masked in the flexor ridges by the gorillas' larger body size.

Conclusion

Large differences in behavior leave a skeletal trace, such as those found in this study between chimpanzees and humans, while smaller differences in biomechanical demands across digits are not reflected in the flexor ridges.

Acknowledgements

We are grateful to the institutions holding the material we analyzed: the Royal Museum for Central (Belgium), Museu de Ciències Naturals de Barcelona (Spain), Zoologische Staatssammlung München (Germany), Universidad de Burgos (Spain), and to the people who kindly helped us there, especially to Emmanuel Gilissen, Javier Quesada, Annelie L. van Heteren, Mikhail Lemeshev and José Miguel Carretero. To Juan Ignacio Morales, Valerie Deschênes and Alexandros Karakostis for the scanning of the human sample. This study was funded by the research projects AGAUR 2017 SGR 1040 and MINECO PGC2018-093925-B-C32. A.B. would like to acknowledge financial support from Becas Chile (Conicyt, Chile).

References

[1] Susman, R.L., Stern, J.T., 1979. Telemetered electromyography of flexor digitorum profundus and flexor digitorum superficialis in Pan troglodytes and implications for interpretation of the O. H. 7 hand. *American Journal of Physical Anthropology*, 50, 565–574.
[2] Dingwall, H. L. M. (2008). Chimpanzee bilateral asymmetry in humans and African apes. *HOMO-Journal of Comparative Human Biology*, 59, 93–109.
[3] Matarazzo, S., 2013. Manual pressure distribution patterns of knuckle-walking apes. *American Journal of Physical Anthropology*, 152, 41–50.
[4] Wunderlich, R.E., Jungers, W.L., 2009. Manual digital pressures during knuckle-walking in chimpanzees (Pan troglodytes). *American Journal of Physical Anthropology*, 139, 394–403.
[5] Inouye, S. E. (1991). Ontogeny of knuckle-walking hand postures in African apes. *Journal of Human Evolution*, 20, 459–485.
[6] Doran DM. 1996. Comparative positional behavior of the African apes. In: McGrew WC, Marchant LF and Nishida T, editors. Great ape societies. Cambridge: Cambridge University Press. p 213–224